The Role of Tepsin in Membrane Trafficking and Autophagy

By

Natalie Serina Wallace

Dissertation

Submitted to the Faculty of the

Graduate School of Vanderbilt University

in partial fulfillment of the requirements

for the degree of

DOCTOR OF PHILOSOPHY

in

Biological Sciences

May 12, 2023

Nashville, Tennessee

Approved:

Todd R. Graham, Ph.D.

Bruce D. Carter, Ph.D.

Irina N. Kaverina, Ph.D.

Lars Plate, Ph.D.

Lauren P. Jackson, Ph.D.

ACKNOWLEDGEMENTS

I would like to express my deepest gratitude to all the people that have supported me, and my academic endeavors, throughout my life. Thank you to all my mentors from Brentwood Middle/High School, Indiana University, and Vanderbilt University. I'd also like to extend my thanks to all my colleagues at Vanderbilt—in particular the Biological Sciences department and Center for Structural Biology—for creating a welcoming and collaborative research community.

To my advisor, Dr. Lauren Jackson, I deeply appreciate being accepted into your lab and your mentorship over the course of my PhD training. Thank you for always being available for scientific discussions and general advice. I'm so grateful that you acknowledge biology can be messy and "failed" experiments are not personal failures. You've helped me become a stronger, more resilient scientist and I will continue to be inspired by you.

I am incredibly fortunate to have spent my graduate career in the Jackson lab with fantastic colleagues that have also become the most incredible friends. Amy, thank you for always going above and beyond for us. All of my friends wish their lab had 'An Amy'. I can never thank you enough for all the time and energy you've put towards teaching and supporting me. John and Mintu: you've each been so encouraging and taught me so much about being a scientist. Meredith and Allie: the support you've provided me, even after leaving Vanderbilt, has been immense. I want to especially thank Betty for being by my side for the entirety of my PhD and keeping me going when my research was at its most frustrating. Cameron, I'm so inspired by you and beyond excited to see all the great

things you will accomplish in the future. It's also been my privilege to mentor several incredible undergraduates. Carli and Olivia, it's so exciting to see you both pursuing your own careers in science now.

Thank you to my committee: Dr. Bruce Carter, Dr. Irina Kaverina, Dr. Lars Plate, and my chair Dr. Todd Graham. You've all helped push me to be a stronger, more creative scientist and I appreciate all your support, ideas, and constructive criticism throughout the years. I've also received invaluable encouragement and validation from Dr. Walter Chazin, Dr. Cynthia Brame, Dr. Beth Bowman, Karen Davis and LaDonna Smith. I'd especially like to thank Kari Seedle in the Nikon Center of Excellence for helping me with image quantification and for helping build my confidence as a microscopist.

My friends are an extremely important part of my success and have been there for me in countless ways: hearing every frustration, celebrating every accomplishment, and helping me maintain something like a work-life balance. Gavin, Megan, Nicole, Nikki, Adam, Betty, Meredith, Allie, Esha, John, Jessie, Melanie, Shannon, and Cameron: I wouldn't be who I am without you all and you never let me doubt myself. I'd be remiss to not shout out Megan and all the time you spent helping me learn to write code. I'm not sure I would have made it through this without you.

Last, but far from least, I owe so much to my family. My parents have always encouraged me to be curious and to love learning. Thank you for always believing in me and for all your support of my education. Thank you to Luke, my brother, for always calling me a nerd, but meaning it with love. You inspire me to pursue what I want and to go outside my comfort zone. And my cousin (sister) Kristin, thank you for being the very best friend. There aren't enough words to express how much you've all helped me.

ACKNOWLEDGEMENT OF FUNDING

This work was supported by the Vanderbilt Molecular Biophysics Training Grant, NIH 5T32GM008320, trainee Natalie Wallace; NIH R35GM119525 to Lauren Jackson; and funding from the Pew Charitable Trusts to Lauren Jackson. Work in Chapter II was also supported by NIH 5T32GM008320, trainee Cameron Cohen; and Postdoctoral Program in Functional Neurogenomics NIH 5T32MH065215, trainee John Gadbery.

PUBLICATIONS

Work in Chapter II is submitted for review. Work in Chapter III is published under the same title in *Advances in Biological Regulation, 2022, 100945*. Reuse is permitted by the publisher. (Pembridge et al., 2022).

Additional publication:

Pathak, A., Stanley, E. M., Hickman, F. E., **Wallace, N.**, Brewer, B., Li, D., Gluska, S., Perlson, E., Fuhrmann, S., Akassoglou, K., Bronfman, F., Casaccia, P., Burnette, D. T., & Carter, B. D. (2018). Retrograde Degenerative Signaling Mediated by the p75 Neurotrophin Receptor Requires $p150^{Glued}$ Deacetylation by Axonal HDAC1. *Developmental Cell*, *46*(3), 376-387.e7. https://doi.org/10.1016/j.devcel.2018.07.001

TABLE OF CONTENTS

LIST OF TABLES

LIST OF FIGURES

LIST OF ABBREVIATIONS

2-AG	2-arachidonyl glycerol
AAGAB	Alpha- and gamma-adaptin-binding protein
AFold	AlphaFold
AP	Adaptor protein or assembly polypeptide
AP-1	Adaptor protein complex 1
AP-2	Adaptor protein complex 2
AP-3	Adaptor protein complex 3
AP-4	Adaptor protein complex 4
AP-5	Adaptor protein complex 5
AP180	Assembly protein 180
Arf1	ADP ribosylation factor 1
ATG	Autophagy related protein
CALM	Clathrin assembly lymphoid myeloid leukemia
CME	Clathrin-mediated endocytosis
COPI	Coat protein complex I
COPII	Coat protein complex II
CRISPR	Clustered regularly interspaced short palindromic repeats
DAGLB	Diacylglycerol lipase-beta
Dpf	days post fertilization
EBSS	Earle’s balanced salt solution
EEA1	Early endosome antigen-1

ENTH	Epsin N-terminal homology
ER	Endoplasmic reticulum
ERGIC	ER-Golgi intermediate compartment
FHF	FTS, Hook, and FHIP
FYVE	Fab 1, YOTB, Vac 1, EEA 1
GAK	Cyclin-G-associated kinase
GFP	Green fluorescent protein
GST	Glutathione S-transferase
GTP	Guanosine-5’-triphosphate
Hpf	Hours post fertilization
HRP	Horseradish peroxidase
HSP	Hereditary spastic paraplegia
HOPS	Homotypic fusion and vacuolar protein sorting
iPSC	Induced pluripotent stem cell
IP	Immunoprecipitation
ISCA1	Iron sulfur cluster assembly 1
ITC	Isothermal titration calorimetry
KO	Knockout
LAMP1	Lysosomal associated membrane protein-1
LDS	LIR docking site
LIR	LC3 interacting region
mTORC1	Mammalian target of rapamycin complex 1
mRFP	Monomeric red fluorescent protein

PAS	Pre-autophagic site
PDB	Protein data bank
PIP	Phosphatidylinositol phosphate
PI4P	Phosphatidylinositol 4 phosphate
PI3P	Phosphatidylinositol 3 phosphate
$PI(4,5)P_2$	Phosphatidylinositol-4,5-biphosphate
RT-qPCR	Reverse transcription quantitative polymerase chain reaction
RUSC1/2	RUN and SH3 domain-containing protein ½
sgRNA	small guide RNA
SNX	Sorting nexin
SPG	Spastic paraplegia gene
TGN	*trans*-Golgi network
Ub	Monoubiquitin
VHS	Vps27, Hrs, STAM
VPS35L	VPS35-like
WT	Wild-type

I. INTRODUCTION

The field of modern cell biology in part grew from the work of Albert Claude, Christian de Duve, and George Palade, who were awarded the 1974 Nobel Prize in Physiology or Medicine. Claude, de Duve, and Palade each led pioneering work uncovering the structural organization of cells. The advent of electron microscopy and development of cellular fractionation techniques allowed scientists to see beyond the limits of light microscopy for the first time. Early electron micrographs revealed a vast number of intracellular compartments (Figure 1-1), only some of which were previously identified by light microscopy. Research using these new "ultra-resolution" approaches characterized functions for mitochondria (Claude, 1946), ribosomes (Palade, 1955), and lysosomes (de Duve et al., 1955), to name a few key discoveries. From the work of Claude, Palade, and others we gained our first insights into the biosynthetic and secretory intracellular transport pathways (Jamieson and Palade, 1967; Palade and Porter, 1954; Porter, 1953; Porter et al., 1945). This work highlighted that these dynamic compartments have distinct functions while also acting as connected networks (Claude, 1975; de Duve, 1975; Palade, 1975).

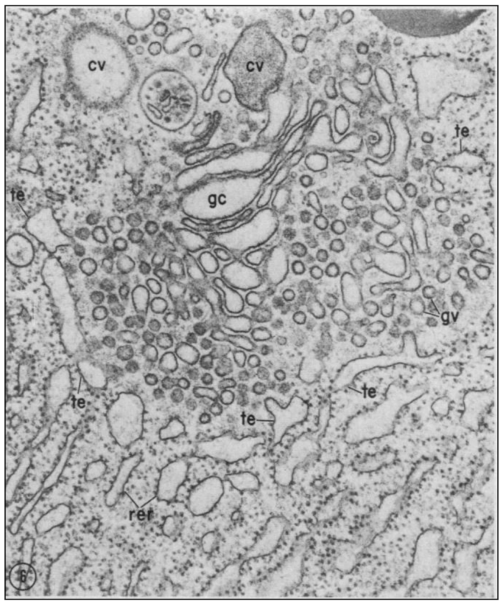

Figure 1-1: Intracellular compartments by electron micrograph. Electron micrograph depicting the rough endoplasmic reticulum (rer); transitional elements (te); Golgi cisternae (gc); Golgi vesicles (gv); and condensing vacuoles (cv). Adapted from Palade, 1975.

Building directly on these foundational discoveries, research led by James Rothman, Randy Schekman, and Thomas Sudhof—awarded the 2013 Nobel Prize in Physiology or Medicine—identified key proteins that mediate formation and fusion of intracellular transport carriers. This work emphasized the significance of complex, coordinated intracellular transport systems. Albert Claude titled his Nobel lecture “The Coming Age of the Cell” and now, after nearly 50 years, the complexity of the cellular environment is still emerging. With hindsight, Albert Claude and George Palade’s work understanding pathways of protein synthesis and secretion can be represented as a relatively simple diagram (Figure 1-2A) (Farquhar and Palade, 1981). Intracellular

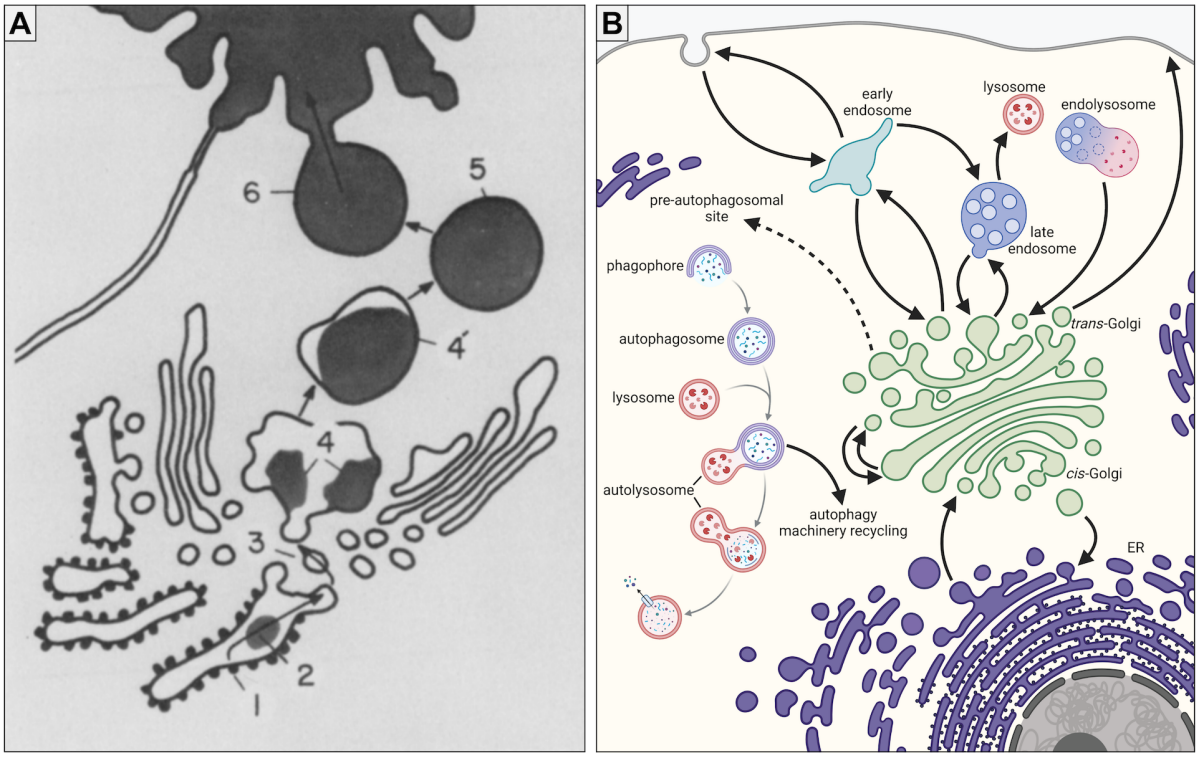

Figure 1-2: Overview of membrane trafficking pathways. (A) Early knowledge of trafficking pathways: digestive enzyme synthesis at the ER (steps 1 and 2) is followed by intracellular transport to the Golgi (step 3), concentration and storage in secretory granules (steps 4, 4’, and 5), and finally secretion by exocytosis (step 6). Adapted from Farquhar and Palade, 1981. (B) Established trafficking pathways to date, involving secretory, endocytic, endo-lysosomal, and autophagic cellular compartments. Dashed arrow indicates an emerging pathway investigated in this thesis work. Made in part with BioRender.

trafficking pathways are roughly divided into the secretory pathway, the endocytic pathway, and degradative pathways. Together these processes shape and maintain the intracellular environment through organized and directional membrane trafficking routes (Figure 1-2B).

MEMBRANE TRAFFICKING PATHWAYS

Early secretory pathway

The secretory pathway facilitates protein synthesis, folding, modification, and delivery via a system of membrane bound compartments and protein machinery. Protein biosynthesis begins at cytoplasmic free ribosomes before sorting signals initiate translocation to the endoplasmic reticulum (ER) membrane. Within the ER, protein folding and early post-translational modifications take place before proteins are packaged and delivered to the Golgi apparatus. Resident ER proteins and trafficking machinery are retrieved back to the ER maintaining relatively distinct molecular compositions of ER and Golgi compartments (Barlowe and Miller, 2013).

Anterograde vesicle trafficking out of the ER forms an ER-Golgi intermediate compartment (ERGIC) in mammalian cells. Stacked membrane cisternae compose the Golgi apparatus, responsible for further protein modification, protein sorting, and distribution to diverse cellular locations. Though still debated, prevailing theories indicate that Golgi cisternae act as anterograde carriers while retrograde vesicle trafficking

maintains molecularly distinct *cis*-, *medial*-, and *trans*-Golgi compartments (Barlowe and Miller, 2013; Bonifacino and Glick, 2004; Glick and Luini, 2011).

Endocytic pathway

Endocytosis refers to the internalization of extracellular materials and portions of the plasma membrane. Additionally, endocytic events help cells communicate with the extracellular environment by altering plasma membrane lipid and protein composition. Clathrin-mediated endocytosis (CME) is the most studied endocytic mechanism and perhaps best understood membrane trafficking mechanism altogether. Evidence of coated pits and vesicles in electron micrographs (Heuser and Reese, 1973; Roth and Porter, 1964) and the subsequent discovery and purification of clathrin by Barbara Pearse (Pearse, 1975) were landmark discoveries indicating formation of endocytic structures could be protein driven (reviewed by Robinson, 2015).

Following endocytosis, internalized material is sorted within endosome compartments which are a convergence point for the early secretory and endocytic pathways. This endosomal network is a highly dynamic series of compartments with distinct lumenal pH, protein, and phosphatidylinositol phospholipid compositions. Most endocytosed cargoes are recycled back to the plasma membrane either directly from endosomes or indirectly via the Golgi. Some endocytosed materials are instead targeted to lysosomes for degradation. The plasma membrane, endosomes, and lysosome are all important membrane platforms for cell signaling events. Trafficking between these compartments is important for modulating signaling cascades and cellular responses to

environmental stimuli (Elkin et al., 2016; Scott et al., 2014; Solinger and Spang, 2022; Wideman et al., 2014).

Degradative pathways and cellular homeostasis

Maintaining cellular health relies heavily on balancing biosynthetic (anabolic) and degradative (catabolic) pathways. Cells possess numerous cytosolic and organellar degradative pathways; of particular importance for this thesis are lysosomes and the autophagy pathway.

For a period following Christian de Duve's identification of lysosomes and initial characterization of their lytic properties, lysosomes were somewhat written off as a terminal, "garbage can" compartment of the cell. It is now well established that lysosomes function as nutrient-sensing signaling platforms. In nutrient-rich conditions, activated mammalian target of rapamycin complex 1 (mTORC1) localizes to lysosomal membranes, initiating signaling cascades to stimulate cell growth. When inactive (e.g. during nutrient-deprived conditions), lysosome biogenesis is increased allowing more macromolecule degradation to resupply cellular metabolites. As is the case for ER, Golgi, and endosomal compartments, lysosomes depend on membrane trafficking to maintain a functional composition of resident membrane-associated and lumenal proteins that define the molecular identity of these compartments (reviewed in Ballabio and Bonifacino, 2019; Patra et al., 2022).

Inactivation of mTORC1 also initiates the autophagy ("self-eating") pathway. Autophagy was first noted by identification of irregular, lysosome-like structures containing cytoplasmic material. Eventually, machinery essential for autophagy was

characterized in yeast; work for which Yoshinori Oshumi was awarded the 2016 Nobel Prize in Physiology or Medicine. Aligning with early observations, autophagy refers to a process of engulfing organelles and cytosolic contents into membrane-bound structures called autophagosomes (Figure 1-3). Subsequent autophagosome fusion with lysosomes recycles engulfed macromolecules (reviewed in Ohsumi, 2014).

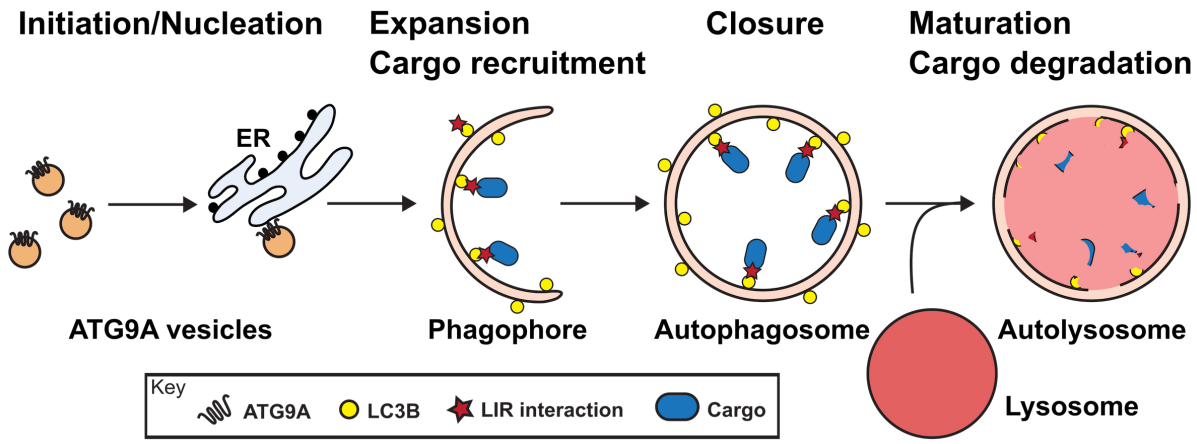

Figure 1-3: Overview of autophagy. ER membranes donate lipids to ATG9A vesicles serving as the seed membrane for early autophagy structures. ATG8 family proteins, including LC3B, recruit cargo receptors and autophagy machinery to expanding phagophores via LC3-interacting region (LIR) motifs. Cytosolic components are enclosed within the fully formed autophagosome and degraded following lysosome fusion in autolysosome structures.

Autophagy has historically been likened to organelle biogenesis more-so than membrane trafficking. However, many aspects of autophagosome formation are reminiscent of membrane trafficking mechanisms including cargo recruitment, membrane remodeling, and recycling of machinery components. Additionally, recruitment of cargo and autophagy machinery is commonly mediated by short peptide sequences, termed LC3-interacting region (LIR) motifs, in mammals (reviewed in Birgisdottir et al., 2013). In recent years, accumulating evidence has shown secretory and endocytic membrane trafficking components function in the autophagy pathway to mediate autophagosome closure, enable lysosome fusion, and recycle autophagy-related proteins (Jiang et al.,

2021; Ravussin et al., 2021; Tang, 2019; Zahoor and Farhan, 2018; Zhou et al., 2022).

MEMBRANE TRANSPORT MECHANISMS

Vesicle coats

Intracellular membrane transport requires precise packaging of contents into vesicle or tubule carriers. Cytoplasmic proteins that assemble on the membrane to guide vesicle formation are referred to as membrane coats. Examples of well characterized membrane coats include coat protein complex I (COPI), COPII, and clathrin coats. COPI functions in retrograde trafficking from endosomes to the *trans*-Golgi network (TGN), intra-Golgi transport, and transport from the Golgi to ER (Cosson and Letourneur, 1997; Popoff et al., 2011; Xu et al., 2017; Yang et al., 2011). COPII mediates ER export of newly synthesized proteins to the Golgi apparatus (Barlowe et al., 1994). Clathrin coats have spatially distinct functions in endocytosis and Golgi-endosome transport determined through association with distinct adaptor protein (AP) complexes, AP-1 and AP-2 (Keen et al., 1979; Pearse and Robinson, 1984; Robinson, 2015, 1987).

Structural and mechanistic similarities between COPI, COPII, and clathrin coats suggests they evolved from a common ancestral coat (Dacks and Robinson, 2017). Each of these coats is comprised of adaptor complexes and scaffolds (Figure 1-4). Adaptor complexes link scaffolds to the membrane and cargoes. COPII and clathrin coats both feature distinct inner coat adaptor layers and outer coat cage (scaffold) layers while COPI does not (Noble and Stagg, 2015). Nevertheless, both COPI and clathrin coats feature

heterotetrametric AP complexes. This organizational difference, in spite of structural similarities, indicates not all coats follow the convention set by discretely layered clathrin coats.

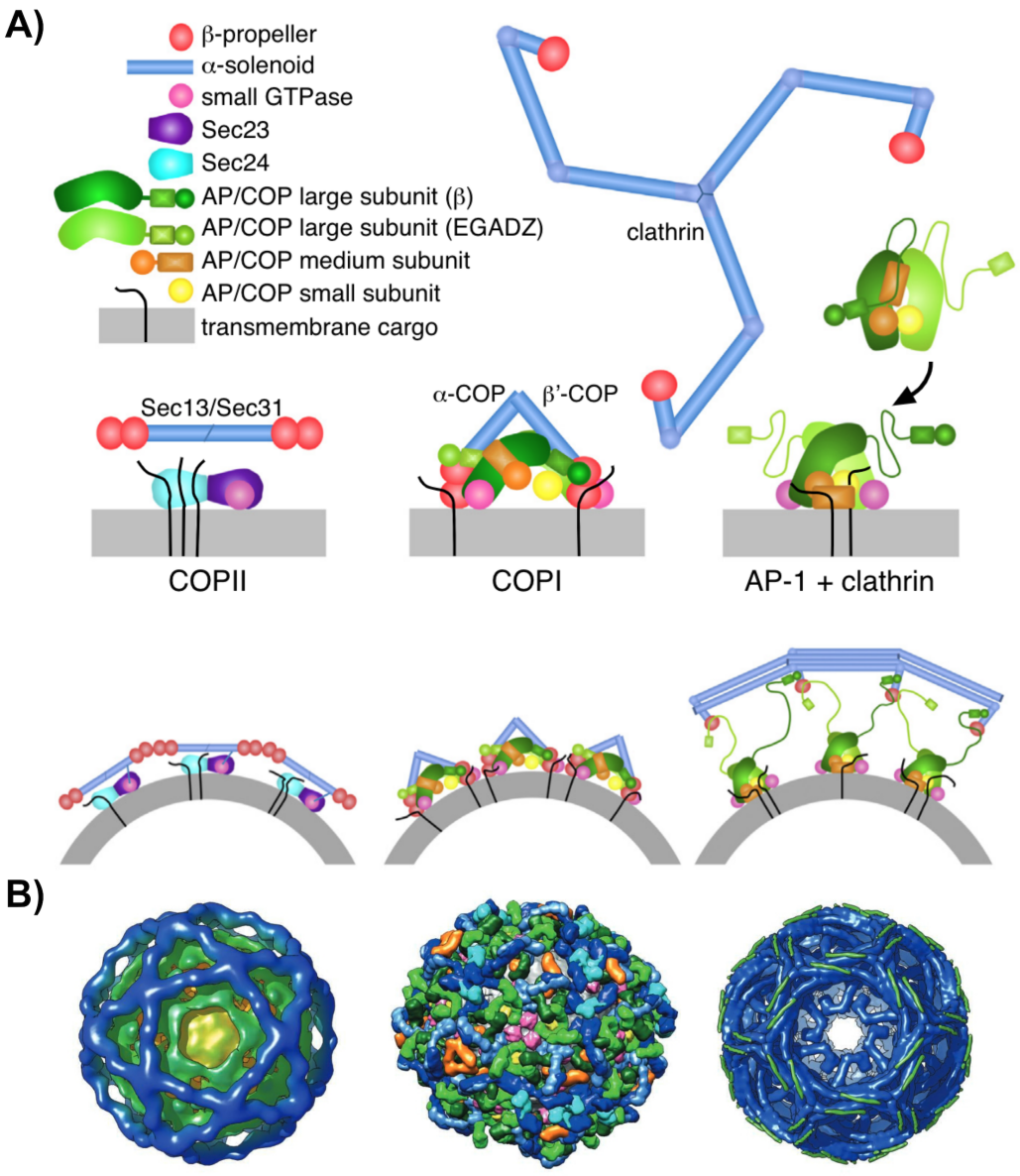

Figure 1-4: Three well-characterized coat architectures. (A) COPI, COPII, and clathrin coats exhibit several common structural elements. Inner coat components are recruited to membranes by lipids and/or small GTPases for subsequent cargo binding. Outer coat components commonly feature β-propeller and α-solenoid structural elements. Adapted from Dacks and Robinson, 2017 (B) For COPII and clathrin, the outer coat forms highly ordered geometric cages. COPI coats do not form distinct adaptor and cage layers. Adapted from Noble and Stagg, 2015.

Vesicle formation

Conventional vesicle formation models are based on common sequential steps that occur in COPI, COPII, and clathrin coat formation (Figure 1-5). Using clathrin-coated vesicles as a model, initiation of vesicle formation occurs at a donor membrane when cargo is present and recognized by coat components. Additionally, the appropriate v-SNARE (vesicle soluble N-ethylmaleimide-sensitive factor attachment protein receptor) must be packaged during vesicle formation to ensure delivery at target membranes in later steps. Accumulation of cargoes and SNAREs, along with the recruitment of additional coat components and clathrin, causes membrane deformation.

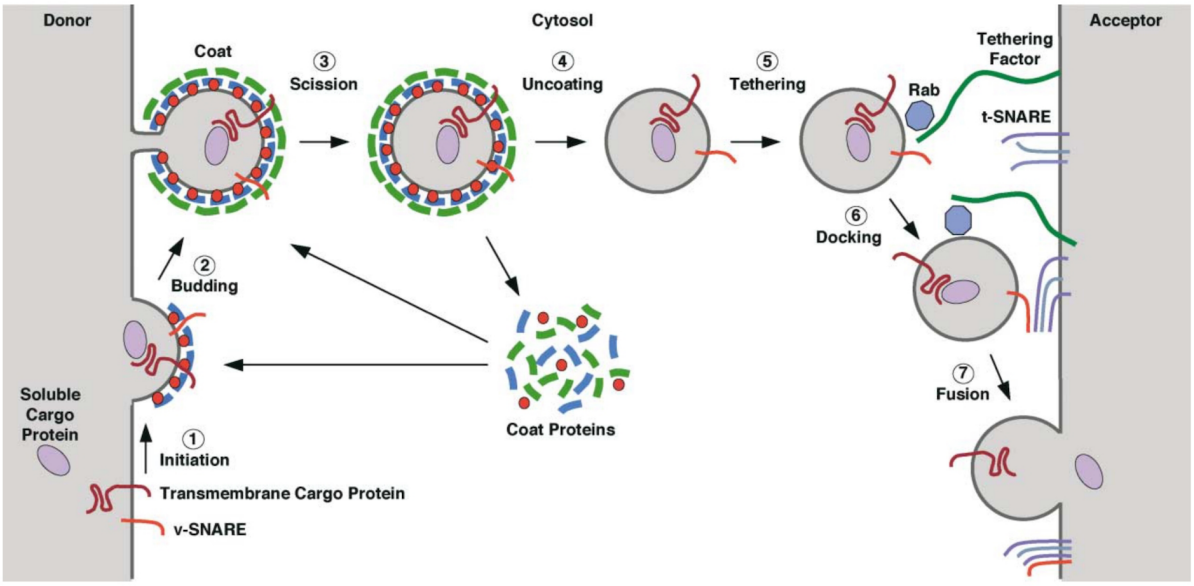

Figure 1-5: Steps of vesicle formation. (1) Initiation: membrane-proximal coat components (blue) are recruited by binding membrane-associated GTPases (red) or specific phosphoinositides. Transmembrane cargoes and SNAREs are sequestered by the assembling coat. (2) Budding: distal coat components (green) polymerize into an outer scaffold. Cargo become concentrated, contributing to increasing membrane curvature. (3) Scission: The neck between the forming vesicle and donor membrane compartments is severed by direct action of the membrane coat or accessory proteins. (4) Uncoating: soon after scission, various mechanisms promote dissociation of coat components for continued use at the donor membrane. (5) Tethering: vesicles move to the acceptor compartment, sometimes along the cytoskeleton. Rab GTPases and a tethering factor help position vesicles for delivery. (6) Docking: the v-SNARE and t-SNARE assemble into a four-helix bundle. (7) Fusion: the trans-SNARE complex promotes vesicle fusion, delivering cargo to the acceptor compartment. The v-SNARE will be recycled to the donor compartment. Adapted from Bonifacino and Glick, 2004.

Eventually, membrane buds are released as vesicles by membrane scission. Clathrin-coated vesicles undergo uncoating shortly after vesicle budding, recycling many cytosolic coat components. Uncoated vesicles are transported along the cytoskeleton to target membrane sites. Tethering factors and Rab GTPases recognize compatible incoming vesicles. Finally, t-SNAREs (target membrane SNARES) mediate vesicle docking and fusion (Bonifacino and Glick, 2004; Chen and Schmid, 2020; Kirchhausen et al., 2014).

ADAPTOR PROTEIN COMPLEXES

AP-1 and AP-2 were originally identified as "assembly polypeptides" that co-purified with clathrin-coated vesicles (Keen et al., 1979; Pearse and Robinson, 1984; Zaremba and Keen, 1983). The AP family currently consists of seven structurally and evolutionarily related complexes: APs 1-5, the COPI F-subcomplex, and TSET (Figure 1-6; Hirst et al., 2014, 2013; reviewed in Robinson, 2015). APs 1-5 and TSET function in post-

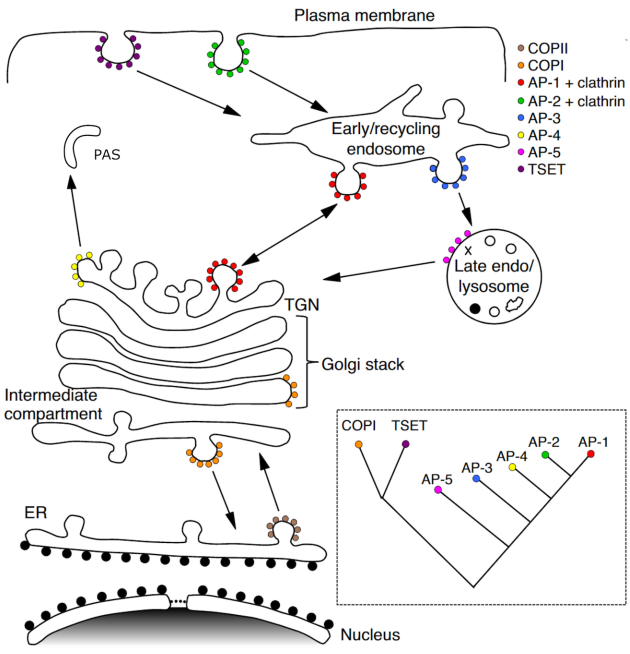

Figure 1-6: Intracellular trafficking by adaptor protein complexes. AP coats mediate vesicle budding for distinct trafficking pathways. COPII is also depicted. PAS refers to the pre-autophagosomal site. Inset represents known evolutionary relationships between the seven AP complexes. Adapted from Dacks and Robinson, 2017.

Golgi trafficking pathways. TSET is an ancestral complex to APs 1-5 and the proposed evolutionary link between COPI and the APs. AP-1, AP-2, and AP-3 are essential genes, conserved from yeast to human. AP-4 and AP-5 have been sporadically lost in several common eukaryotic model organisms including flies (*D. melanogaster*), worms (*C. elegans*), and budding yeast (*S. cerevisiae*; Hirst et al., 2013b). TSET has been lost in several eukaryotic lineages; animals and fungi retained only a partial domain from the TCUP subunit as the muniscin family of endocytic machinery (Hirst et al., 2014).

AP complexes are heterotetramers containing two large subunits (α/γ/δ/ε/ζ, β1-5), one medium (μ1-5), and one small (σ1-5) subunit (Hirst et al., 2011; Robinson and Bonifacino, 2001). While the APs are structurally homologous, they differ in lipid-binding specificity (Boehm et al., 2001; Hirst et al., 2021; Höning et al., 2005; Lefran et al., 2004; Ooi et al., 1998; Ren et al., 2013; Robinson, 1987; Robinson and Pearse, 1986; Schoppe et al., 2021; Seaman et al., 1996; Traub et al., 1993), cargo recognition (Aguilar et al., 2001; Burgos et al., 2010; Darsow et al., 1998; Höning et al., 2005; Kelly et al., 2008; Rapoport et al., 1998; Schoppe et al., 2021; Simmen et al., 2002), and clathrin binding (Dell'Angelica et al., 1999b; Hirst et al., 2013a, 2011, 1999; Pearse and Robinson, 1984; Robinson, 1987; Schoppe et al., 2020; Seaman et al., 1996) (summarized in Figure 1-7). AP-1 and AP-2 are clathrin-associated adaptors while AP-3, AP-4, and AP-5 are roughly grouped as non-clathrin-associated adaptors.

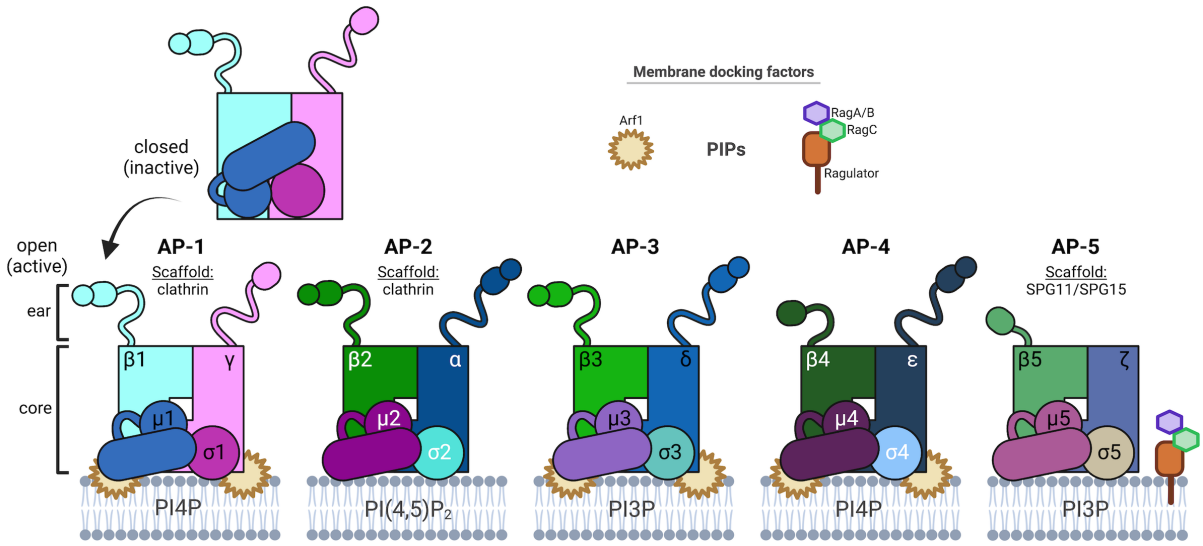

Figure 1-7: Schematic structures of AP complexes. Cytosolic AP complexes adopt a closed conformation. Binding phosphoinositides and/or small GTPases induces structural rearrangement to an open conformation. The AP core is comprised of two large subunit N-termini along with the μ and σ subunits. C-terminal appendage (ear) domains are connected to the core by flexible linkers. Made in BioRender.

Clathrin-associated APs

As previously discussed, adaptor proteins AP-1 and AP-2 were the first of the AP family identified because of their association with clathrin. Presently, AP-1 and AP-2 are also the best structurally characterized of the APs. Each large subunit (β1, β2, γ, α) contains a N-terminal trunk domain connect by a flexible linker to a C-terminal appendage domain. The core is formed from the two large subunit trunks (β1/γ; β2/α) with the medium (μ) and small (σ) subunits (Collins et al., 2002). Membrane-association is mediated by the core via interaction with phosphoinositides and/or small GTPases. These interactions drive conformational changes from a cytosolic “closed” form into a membrane-associated “open” form (Collins et al., 2002; Heldwein et al., 2004; Jackson et al., 2010; Ren et al., 2013).

The “open” forms of AP-1 and AP-2 are further stabilized by cargo binding

interactions. Two main cargo selection motifs have been well characterized: YXXΦ and [DE]XXL[L/I] (dileucine) motifs, where 'X' refers to any amino acid and Φ is a bulky hydrophobic residue (Boll et al., 1996; Ohno et al., 1996; Rapoport et al., 1998). Tyrosine-based (YXXΦ) motifs bind the μ subunit while dileucine motif binding is largely mediated by the small σ subunit (Kelly et al., 2008; Ohno et al., 1995; Owen and Evans, 1998). Clathrin binding is mediated by a conserved clathrin-box motif, LΦXΦ[D/E]. For AP-1, this motif resides in the γ appendage domain and for AP-2 the β2 appendage domain (reviewed in Dell'Angelica, 2001; Owen et al., 2004).

AP-1 transports material bi-directionally between endosomes and the TGN with additional pathways to specialized membrane domains in polarized neuronal and epithelial cells (Duncan, 2022). For membrane-association, AP-1 interacts with the small GTPase ADP-ribosylation factor 1 (Arf1) to enter an unlocked confirmation promoting phosphoinositide and cargo binding (Ren et al., 2013; Seaman et al., 1996; Stamnes and Rothman, 1993; Traub et al., 1993). Arf1 in an active, GTP-bound conformation features an exposed amphipathic helix. Insertion of this helix into the membrane, along with conformational accessibility of guanine nucleotide sensitive switch I/II regions, allows Arf1(GTP) to recruit AP-1 onto the membrane (Donaldson and Jackson, 2011; Ren et al., 2013). AP-1-Arf1 binding is likely cooperative with phosphatidylinositol 4 phosphate (PI4P) binding which is enriched in TGN and endosome membranes (Beacham et al., 2019; Ren et al., 2013). Together Arf1 and PI4P binding stabilize the "open" AP-1 complex which is able to bind cargo and initiate vesicle formation.

AP-2 membrane recruitment involves a series of allosterically regulated conformation changes as a result of phosphatidylinositol-4,5-biphosphate ($PI(4,5)P_2$) and

tyrosine-motif cargo binding (Kadlecova et al., 2017). AP-2 binding $PI(4,5)P_2$ at the plasma membrane induces a conformational change from the closed to open conformation (Collins et al., 2002; Gaidarov and Keen, 1999; Höning et al., 2005; Jackson et al., 2010). Ultimately, AP-1 and AP-2 clathrin coats exhibit similar spatial and temporal regulation during membrane recruitment and cargo selection. Though these mechanisms may differ slightly, there is a high degree of structural homology between the distinct conformations AP-1 and AP-2 adopt (Beacham et al., 2019).

Non-clathrin-associated APs

Compared with AP-1 and AP-2, coat assembly mechanisms for AP-3, AP-4, and AP-5 are less understood. The major AP-3 pathway in mammalian cells is important for biogenesis and maintenance of lysosome-related organelles (reviewed in Dell'Angelica, 2009). Whether or not AP-3 assembles into clathrin coats has been controversial. AP-3 was originally classified as a non-clathrin coat because AP-3 structures do not always localize with clathrin (Simpson et al., 1996). Additionally, AP-3 is barely detectable in clathrin coated vesicle purifications (Dell'Angelica et al., 1997). AP-3 can bind clathrin *in vitro* by a conserved clathrin-box motif (Drake et al., 2000); however, clathrin is not necessary for AP-3 function in yeast or mammalian cells (Black and Pelham, 2000; Zlatic et al., 2013).

Despite the evident lack of clathrin binding, there remain similarities between AP-3 and clathrin-associated family members. AP-3 also recognizes tyrosine- and dileucine-based cargo sorting motifs and its membrane recruitment is regulated by Arf1 (Cowles et al., 1997; Darsow et al., 1998; Lefran et al., 2004; Mardones et al., 2013; Ooi et al., 1998;

Sun et al., 2004). However, membrane association for AP-3 is primarily driven by cargo binding with secondary stabilization of an open conformation from Arf1 and PI4P binding, whereas Arf1 binding is the initial priming step for AP-1 (Schoppe et al., 2021).

An important question for non-clathrin coats is how potential lack of an outer cage layer affects vesicle formation. AP-1 and AP-2 vesicles undergo uncoating soon after vesicle budding to allow recycling of the coat machinery (reviewed in Kirchhausen et al., 2014). Recent work from the Ungermann lab shows AP-3 vesicles require an assembled coat for proper docking at target vacuolar membranes. An interaction between AP-3 and the HOPS (homotypic fusion and vacuolar protein sorting) complex mediates docking, subsequent uncoating allows SNARE assembly, and then finally vesicle fusion can occur (Schoppe et al., 2020). This late uncoating is reminiscent of COPI δ mediating a tethering interaction prior to uncoating (Andag and Schmitt, 2003; Zink et al., 2009).

Evolutionary analysis indicates AP-3, AP-4, and AP-5 diverged earliest making them more distantly related to AP-1 and AP-2 (Dacks and Robinson, 2017). This offers one explanation for several structural differences noted between AP-4/AP-5 and the other APs. Both AP-4 and AP-5 do not bind clathrin and in fact lack the clathrin-box motif entirely (Dell'Angelica et al., 1999a; Hirst et al., 2011, 1999). AP-4 β4 has a shortened linker between its trunk and appendage domain, which contains only a single lobe compared to the bi-lobal β1-3 appendages (Dell'Angelica et al., 1999a; Hirst et al., 1999). AP-5 ζ has no linker or appendage at all and the single lobe β5 appendage is proximal to the β5 trunk with only a minimal linker (Figure 1-7; Hirst et al., 2011).

AP-4 and AP-5 cargo binding and coat assembly mechanisms remain the least well understood of the APs. Structural prediction and evolutionary analysis indicate AP-5

along with two scaffold-like proteins, SPG11 and SPG15, likely form a heterohexameric complex similar to COPI (Dacks and Robinson, 2017; Hirst et al., 2013a, 2011). Recent work from the Robinson lab has begun to clarify a coincidence detection mechanism for AP-5 membrane recruitment. The FYVE domain in SPG15 binds PI3P; however, the majority of PI3P is present on early endosome compartments while AP-5 localizes to late endo-lysosomes. At minimum, a secondary interaction with Rag GTPases targets AP-5 specifically to a small pool of PI3P on late endo-lysosomes in a nutrient-sensitive manner, possibly indicating a role in lysosome reformation from autolysosomes (Hirst et al., 2021).

AP-4 vesicles presently have no candidate scaffold, tether, or SNARE proteins despite mass spectrometry analysis of AP-4 vesicles (Borner et al., 2012; Davies et al., 2018). Several *bona fide* and prospective cargoes have been identified for the AP-4 coat (Burgos et al., 2010; Davies et al., 2022, 2018; Ivankovic et al., 2020; Majumder et al., 2022; Matsuda et al., 2008a; Mattera et al., 2017; Simmen et al., 2002; Yap et al., 2003). Though the molecular basis of cargo binding remains poorly understood, AP-4 μ4 binds noncanonical tyrosine-based motifs at a novel interface compared to μ1, μ2, or μ3-YXXΦ interactions (Aguilar et al., 2001; Ross et al., 2014). AP-4 recruitment to TGN membranes requires Arf1 but little else is known about AP-4 coat formation (Boehm et al., 2001).

ACCESSORY PROTEINS OF VESICLE COATS

Accessory proteins in clathrin coats

AP-1 and AP-2 clathrin coats rely on a number of accessory proteins to assist in coat assembly, cargo recruitment, and coat disassembly. During clathrin-coated pit

initiation, early arriving accessory proteins such as CALM (AP180 in neurons) help stabilize the AP-2 open conformation, bind and polymerize clathrin, as well as recruit SNAREs (Maritzen et al., 2012). Epsins coordinate maturation of clathrin-coated pits by binding cargoes, adaptor proteins, and clathrin (Mettlen et al., 2018; Sen et al., 2012). Coat disassembly requires Hsc70 ATPase activity. Auxilin/GAK (cyclin-G-associated kinase) proteins function as clathrin assembly proteins and mediate the interaction with Hsc70 for uncoating (reviewed in Eisenberg and Greene, 2007). While these and many other accessory proteins are well characterized in clathrin coats, few accessory proteins have been identified or characterized for non-clathrin AP coats.

Divergent structure and evolution of the AP-4 accessory protein, tepsin

The first identified AP-4 accessory protein, tepsin, is a member of the epsin protein family characterized by an epsin N-terminal homology (ENTH) domain (Figure 1-8; Borner et al., 2012). Epsins 1-3 interact with AP-2, clathrin, Eps15, and ubiquitinated cargo through motifs in the unstructured C-terminus and with $PI(4,5)P_2$ via ENTH domains (Chen et al., 1998; Ford et al., 2002). Epsin-related protein (EpsinR) associates with AP-1 and clathrin but preferentially binds PI4P over $PI(4,5)P_2$ and lacks ubiquitin or Eps15 interacting motifs used by endocytic AP-2 coats (Hirst et al., 2003; Mills et al., 2003). Like other epsins, a largely unstructured C-terminus in tepsin harbors adapter protein interaction motifs; in the case of tepsin, the AP-4 β4 and ε appendage domains (Frazier et al., 2016; Mattera et al., 2015). As a non-clathrin accessory protein it is unsurprising that tepsin domain architecture differs from other epsins in a number of ways. Most

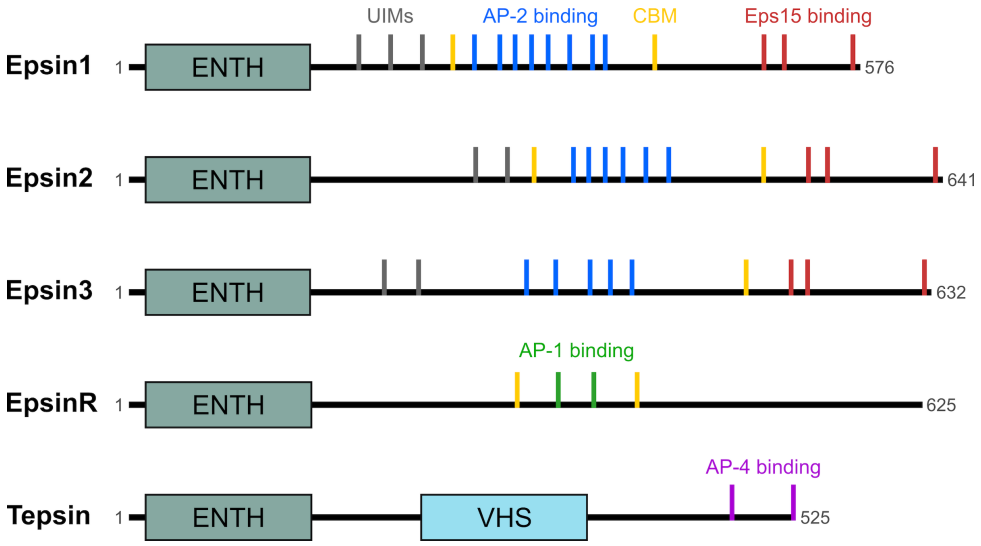

Figure 1-8: Epsin family protein domains and binding motifs. Epsins proteins all feature an epsin N-terminal homology (ENTH) domain. Epsin1/2/3 contain AP-2 and Eps15 binding motifs as well as 2-3 ubiquitin interacting motifs (UIMs). EpsinR binds AP-1 and thus lacks UIM and Eps15 motifs characteristic of Epsin1/2/3. Epsin1/2/3 and EpsinR all have clathrin-box motifs (CBM). Tepsin contains an additional VHS domain and presently only has AP-4 binding motifs characterized.

notably, tepsin features an internal VHS (for Vps27, Hrs, STAM) domain (Archuleta et al., 2017; Borner et al., 2012).

X-ray crystal structures of tepsin ENTH and VHS domains revealed they lack critical features for the canonical function of these domains. Tepsin ENTH does not bind phosphoinositides because it is missing amphipathic helix α0 which forms the necessary basic pocket (Archuleta et al., 2017). This also implies tepsin will require AP-4 binding for membrane recruitment. The VHS domain is atypical considering the superfamily of ENTH/ANTH/VHS domains usually reside at the very N-terminus. Structurally, the VHS domain lacks helices required for VHS binding to dileucine cargo and cannot accommodate ubiquitin binding either (Archuleta et al., 2017; Misra et al., 2002; Nielsen et al., 2001; Puertollano et al., 2001; Ren and Hurley, 2010; Takatsu et al., 2001).

It remains unclear what role tepsin ENTH and VHS domains will have in AP-4

trafficking. Concurrent loss of tepsin where AP-4 has been lost across eukaryotic lineages implies the function of tepsin is significantly linked to AP-4 (Hirst et al., 2013b, 1999). Evolutionary analysis indicates tepsin diverged early from other epsins, possibly to accommodate unique, non-clathrin associated features of the AP-4 coat (Archuleta et al., 2017).

CELLULAR FUNCTIONS OF AP-4

Bi-allelic loss-of-function mutation in any AP-4 subunit (β4/ε/μ4/σ4) results in hereditary spastic paraplegia (HSP) neurological disorders (Abou Jamra et al., 2011; Bauer et al., 2012; Ebrahimi-Fakhari et al., 2018; Moreno-De-Luca et al., 2011; Tessa et al., 2016; Verkerk et al., 2009). Shared clinical features of these AP-4 HSPs include: speech and motor developmental delay; progressive spasticity; microcephaly; thinning of the corpus callosum; and loss of white matter (Ebrahimi-Fakhari et al., 2020). Ubiquitous expression of AP-4 indicates importance for general cellular health but these neurological disease phenotypes suggest AP-4 is particularly important in polarized neuronal cells (Hirst et al., 2013b).

Trafficking in polarized cells

Cell polarity refers to asymmetric cell organization. Neurons, for example, organize into distinct regions (dendrites, soma, and axon) with unique signaling properties as well as protein synthesis and degradative needs (Bentley and Banker, 2016). Many APs are

known to perform critical functions in neurons to form and maintain this heterogeneous intracellular organization (reviewed in Guardia et al., 2018).

Prior to the identification of AP-4 deficiency in patients, AP-4 had already been linked to sorting in polarized cells. Epithelial cells maintain distinct apical and basolateral plasma membrane domains and loss of AP-4 results in the missorting of basolateral cargoes (Simmen et al., 2002). In neurons, AP-4 is implicated in proper somatodendritic sorting of AMPA and δ2 glutamate receptors (Matsuda et al., 2008a; Matsuda and Yuzaki, 2009; Yap et al., 2003). More recently, two new AP-4 cargoes have been identified with particular importance to neuronal function: diacylglycerol lipase-beta (DAGLB), a key enzyme for endocannabinoid synthesis, and the autophagy lipid scramblase, ATG9A (Davies et al., 2022, 2018; Ivankovic et al., 2020; Mattera et al., 2017). Mislocalization of both ATG9A and DAGLB offers an initial understanding of the molecular basis for AP-4 deficiency syndrome (Figure 1-9).

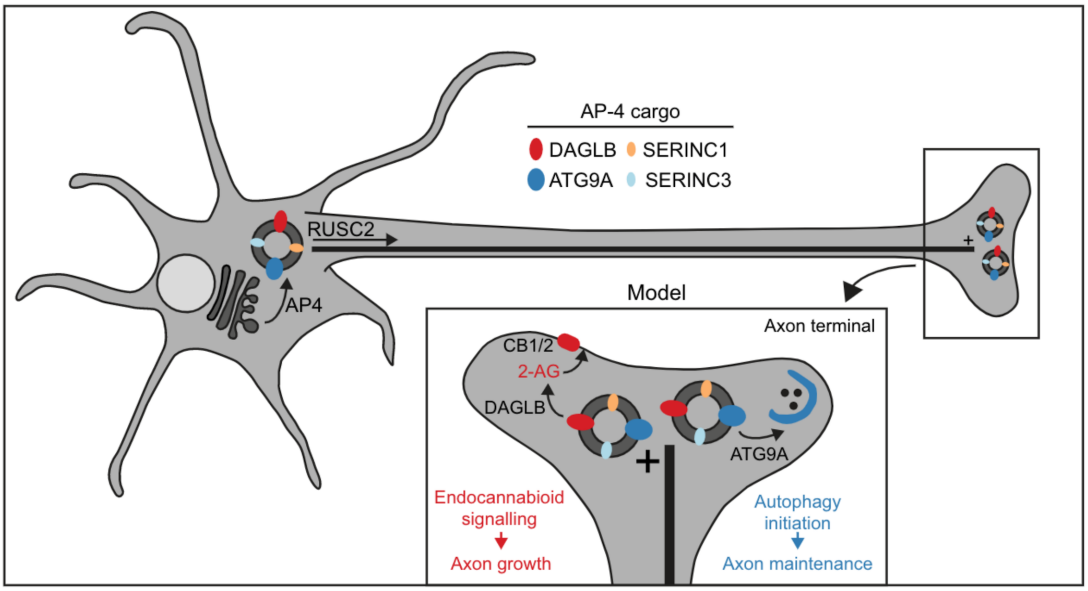

Figure 1-9: AP-4 trafficking pathways in neurons. AP-4 packages cargo proteins, including DAGLB and ATG9A, at the TGN. An AP-4 accessory protein, RUSC2, mediates anterograde axonal transport. At the axon terminal, DAGLB functions in endocannabinoid signaling to promote axon growth during neuronal development. ATG9A vesicles are essential for autophagy initiation which contributes to axon maintenance by sequestering dysfunction organelles and aggregated proteins. Figure and legend adapted from Davies et al., 2022.

Defects in endocannabinoid synthesis

Endocannabinoid signaling modulates many aspects of central and peripheral nervous system activity including axonal pathfinding and synaptic plasticity. Spatial coordination of cannabinoid receptors and endocannabinoid synthesis enzymes is paramount in highly polarized neuronal cells (Gorzkiewicz and Szemraj, 2018; Oudin et al., 2011; Zou and Kumar, 2018). The two principal endocannabinoid ligands, anandamide and 2-arachidonyl glycerol (2-AG), are synthesized on demand from lipid metabolites by lipases (reviewed in Kilaru and Chapma, 2020).

DAGLB, a lipase for generating 2-AG, was recently identified by mass spectrometry as a candidate cargo for AP-4. Loss of AP-4 in cultured HeLa, SH-SY5Y, and patient-derived induced pluripotent stem cells (iPSC) robustly traps DAGLB at the TGN. Furthermore, less DAGLB localized to iPSC axons and deficient DAGLB trafficking resulted in lower 2-AG levels in these cells. Accumulating 2-AG by blocking its downstream metabolism rescued neurite outgrowth defects (Davies et al., 2022). Together these data suggest transport of DAGLB via AP-4 contributes to spatial regulation of 2-AG endocannabinoid signaling, possibly impacting neuronal development.

Dysregulation of autophagy

Neurons rely heavily on degradative pathways during neuronal development and for prolonged cellular health as terminally differentiated cells. Metabolically demanding dendritic and axonal functions are also occurring far from the cell body. Managing the stress placed on the cell, particularly in these distal compartments, requires robust clearance of protein aggregates and dysfunctional organelles. Bulk autophagy is a critical

degradative pathway for neuronal development and homeostasis (Stavoe and Holzbaur, 2019).

AP-4 was indirectly connected to neuronal autophagy early on with the discovery of AMPA receptors accumulated in axonal autophagosome swellings of *AP4B1* knockout mice (Matsuda et al., 2008a). Now, the essential autophagy lipid scramblase, ATG9A, is an established AP-4 cargo. Similar to DAGLB, ATG9A is retained at the TGN when AP-4 is lost in several cultured cells, including patient-derived cells and neurons from *AP4E1* or *AP4B1* knockout mice (Behne et al., 2020; Davies et al., 2018; de Pace et al., 2018; Ivankovic et al., 2020; Mattera et al., 2017; Scarrott et al., 2023). Structural and biochemical studies recently confirmed ATG9A acts as a lipid scramblase in concert with ATG2, an ER-resident lipid flippase, to modulate lipid composition during autophagosome formation (Guardia et al., 2020b; Maeda et al., 2020b; Matoba et al., 2020; Noda, 2021). Furthermore, ATG9A vesicles possibly act as the seed membrane for autophagosome biogenesis (Olivas et al., 2022; Sawa-Makarska et al., 2020).

Several AP-4 accessory proteins have also been linked to ATG9A trafficking. RUN and SH3 domain-containing protein 1 and 2 (RUSC1 and RUSC2) mediate kinesin-dependent anterograde transport of ATG9A to the cell periphery (Davies et al., 2018). Hook1 and Hook2, as part of the FHF (FTS, Hook, and FHIP) complex, mediate retrograde transport of AP-4 and ATG9A (Mattera et al., 2020b). These complementary anterograde and retrograde events possibly regulate the spatial distribution of ATG9A for autophagy (Guardia et al., 2021; Mattera et al., 2020b).

RESEARCH OBJECTIVES

This research investigates the role of tepsin in AP-4-mediated autophagy phenotypes to characterize a function for tepsin in AP-4 coat biology. Chapter II details work identifying a functional LIR motif in tepsin that binds LC3B to regulate ATG9A subcellular distribution. Pulldown assays, ITC (isothermal titration calorimetry), and structural modelling characterize the molecular basis for the tepsin-LC3B interaction *in vitro*. Immunofluorescence imaging of tepsin-depleted cells establish the tepsin-LC3B interaction helps regulate autophagy dynamics via ATG9A vesicle trafficking to the cell periphery. This work presents the first identified functional role for tepsin beyond AP-4 binding. Chapter III focuses on generating CRISPR-edited zebrafish knockouts for each AP-4 gene and tepsin to explore their role during early embryo development. Chapter IV describes a prospective secondary binding site in tepsin for LC3B in vitro. Structural models identify a prospective motif which may mediate this interaction. Chapter V contains preliminary data where tepsin- or AP-4-loss dysregulates lysosome positioning and nutrient sensing. Additionally, tepsin is detectable in subcellular fractions with lipidated LC3B which may directly link AP-4-derived ATG9A vesicles to autophagosome biogenesis. Chapter VI discusses implications of this work on models of AP-4 trafficking as well as future directions for investigating tepsin in the AP-4 coat.

II. TEPSIN BINDS LC3B TO PROMOTE ATG9A EXPORT AND DELIVERY AT THE CELL PERIPHERY

Natalie S. Wallace[1,2], John E. Gadbery[1,2], Cameron I. Cohen[1,2], Amy K. Kendall[1,2], Lauren P. Jackson[1,2,3*]

[1]Department of Biological Sciences, Vanderbilt University, Nashville, TN, USA

[2]Center for Structural Biology, Vanderbilt University, Nashville, TN, USA

[3]Department of Biochemistry, Vanderbilt University, Nashville, TN, USA

*Correspondence to lauren.p.jackson@vanderbilt.edu

Work in this chapter is being submitted for review under the same title and is included here with permission from all co-authors.

ABSTRACT

Tepsin is an established accessory protein found in Adaptor Protein 4 (AP-4) coated vesicles, but the biological role of tepsin remains unknown. AP-4 vesicles originate at the *trans*-Golgi network (TGN) and target the delivery of ATG9A, a scramblase required for autophagosome biogenesis, to the cell periphery. Using *in silico* methods, we identified a putative LC3-Interacting Region (LIR) motif in tepsin. Biochemical experiments using purified recombinant proteins indicate tepsin directly binds LC3B, but not other members, of the mammalian ATG8 family. Calorimetry and structural modeling data indicate this interaction occurs with micromolar affinity using the established LC3B LIR docking site. Loss of tepsin in cultured cells dysregulates ATG9A export from the TGN as well as ATG9A distribution at the cell periphery. Tepsin depletion in mRFP-GFP-LC3B HeLa cells using siRNA knockdown increases autophagosome volume and number, but does not appear to affect flux through the autophagic pathway. Re-introduction of wild-type tepsin rescues ATG9A cargo trafficking defects. In contrast, re-introducing tepsin with a mutated LIR motif does not fully rescue altered ATG9A subcellular distribution. Together, these data suggest roles for tepsin in cargo export from the TGN; delivery of ATG9A-positive vesicles at the cell periphery; and in overall maintenance of autophagosome structure.

INTRODUCTION

Membrane trafficking pathways are fundamental for diverse cellular and physiological functions. The assembly of cytosolic coat protein complexes carefully regulates vesicle and tubule transport between compartments in the secretory and post-Golgi trafficking networks (Dacks and Robinson, 2017). Mammalian AP (Assembly Polypeptide) complexes 1-5 are a family of structurally homologous heterotetramers that drive vesicle coat formation at various organelle membranes (Sanger et al., 2019). The structures, mechanisms, and functions of coat formation are well understood for clathrin-associated complexes AP-1 and AP-2 (Robinson, 2015). In contrast, non-clathrin-associated AP coats are less well understood, with some exhibiting unique compositions (AP-5) and different assembly mechanisms (Hirst et al., 2021; Schoppe et al., 2021, 2020). The AP-4 complex ($\varepsilon/\beta4/\mu4/\sigma4$ subunits) is recruited to the *trans*-Golgi network (TGN) by Arf1 (Boehm et al., 2001). AP-4 does not interact with clathrin (Dell'Angelica et al., 1999a; Hirst et al., 1999) and no scaffold proteins have been identified in AP-4 coated vesicles. AP-4 is ubiquitously expressed but appears particularly important in neurons and neuronal tissues. AP-4 loss in humans results in a complex neurological disorder termed AP-4-deficiency syndrome (Abdollahpour et al., 2014; Abou Jamra et al., 2011; Bauer et al., 2012; Ebrahimi-Fakhari et al., 1993; Hardies et al., 2015; Jameel et al., 2014; Tessa et al., 2016).

Biochemical approaches including proteomics have identified AP-4 coat accessory proteins: tepsin (Borner et al., 2012; Frazier et al., 2016; Mattera et al., 2015); RUSC1 and RUSC2 (Davies et al., 2018); and Hook1 and Hook2 (Mattera et al., 2020b). These

recent studies also identified several AP-4 transmembrane protein cargoes: ATG9A (Davies et al., 2018; Ivankovic et al., 2020; Mattera et al., 2017), SERINC1 and SERINC3 (Davies et al., 2018), and diacylglycerol lipase β, or DAGLB (Davies et al., 2022). ATG9A mistrafficking has been identified as a diagnostic marker of AP-4-deficiency syndrome to aid development of therapeutics (Behne et al., 2020). This discovery highlights the importance of revealing the molecular mechanisms of AP-4 biology. Loss of AP-4 in many cell types, including patient-derived cells (Behne et al., 2020; Davies et al., 2018), results in retention of ATG9A in the TGN (Ivankovic et al., 2020; Mattera et al., 2017). ATG9A is a lipid scramblase (Guardia et al., 2020b; Maeda et al., 2020b; Matoba et al., 2020) important in early steps of autophagosome biogenesis (Noda et al., 2000; Young et al., 2006). Aberrant autophagosome formation has been observed in cellular models of AP-4 deficiency (Davies et al., 2018; Mattera et al., 2017) as well as in the axons of neurons in *AP4B1* (Matsuda et al., 2008a) and *AP4E1* (Ivankovic et al., 2020) knockout mouse models. The RUSC accessory proteins coordinate anterograde transport of ATG9A, SERINC1/3, and DAGLB toward the cell periphery in AP-4-derived vesicles (Davies et al., 2022, 2018). Conversely, Hook1 and Hook2 act as part of the FHF (FTS, Hook, and FHIP) complex thought to mediate retrograde trafficking of AP-4-coated and ATG9A-containing vesicles. This latter interaction is proposed to maintain a functional distribution of these proteins throughout the cytoplasm (Mattera et al., 2020b). Despite being the first identified AP-4 accessory protein (Borner et al., 2012), the role of tepsin within the AP-4 coat has remained unclear.

Tepsin is a member of the epsin family of adaptor proteins (Borner et al., 2012), but structural and evolutionary evidence indicate it has functionally diverged (Archuleta

et al., 2017). The tepsin unstructured C-terminus contains two conserved motifs for binding AP-4 appendage domains (Figure 2-1A; Frazier et al., 2016; Mattera et al., 2015). Tepsin contains two structured domains: an epsin N-terminal homology (ENTH) and VHS domains (Figure 2-1A; Frazier et al., 2016; Archuleta et al., 2017). X-ray crystallography structures of both domains revealed they lack critical features observed in other epsins that promote either phosphoinositide binding to ENTH domains or ubiquitin binding to VHS domains (Archuleta et al., 2017; Zouhar and Sauer, 2014). Tepsin has yet to be directly implicated in phenotypes associated with deficiencies in AP-4- trafficking or autophagy.

Autophagy regulates cellular homeostasis by engulfing cytosolic material and dysfunctional organelles into autophagosomes that fuse with lysosomes for degradation and to promote macromolecule recycling within cells. Many essential autophagy genes are conserved from yeast to humans, though higher eukaryotes possess an expanded number of autophagy-related proteins. This is exemplified by a key yeast autophagy protein, ATG8 (Feng et al., 2014). Mammals contain multiple ATG8 orthologs referred to as the mammalian ATG8 (mATG8) family. These proteins are further divided into two subfamilies: the LC3 (LC3A/B/C) and GABARAP (GABARAP and GABARAPL1, and GABARAPL2; Shpilka et al., 2011) families. The independent function of each mATG8 protein is not completely understood. They appear to have distinct roles at various stages of autophagy, from phagophore expansion and recruitment of autophagosome contents to maturation and closure of the autophagosome membrane (Lee and Lee, 2016). Thus far, biochemical analysis of both yeast and mammalian ATG8 proteins reveals many protein-protein interactions are mediated through short peptide motifs, commonly termed

LIR motifs (LC3 Interacting Region) in mammals (Birgisdottir et al., 2013).

In this study, we have identified a role for tepsin and AP-4 in regulating autophagy dynamics beyond export of ATG9A from the TGN. We demonstrate that tepsin directly interacts with LC3B *in vitro* and in cultured cell lines. The tepsin/LC3 interaction occurs between a LIR motif in tepsin's first unstructured region (Figure 2-1A) and the LIR docking site on the surface of LC3B. Biochemical data and AlphaFold modeling suggest how the tepsin LIR motif conveys specificity for LC3 over other mATG8 proteins. Tepsin depletion in cells drives partial accumulation of ATG9A at the TGN and promotes accumulation of ATG9A at the cell periphery. Tepsin depletion also dysregulates the morphology of autophagosomes and autolysosomes. The effect of tepsin depletion is distinct from AP-4 depletion providing evidence for a distinct function for tepsin in AP-4 coated vesicles. Finally, we tested the functional relevance of the tepsin LIR motif in ATG9A trafficking. While wild-type tepsin can rescue ATG9A trafficking defects, a tepsin LIR mutant cannot rescue ATG9A subcellular distribution to the wild-type pattern. Together, these data suggest tepsin is important for ATG9A-containing AP-4 vesicle formation and the tepsin/LC3B interaction contributes to the spatial organization of ATG9A in cells.

RESULTS

Tepsin directly and specifically binds LC3B in vitro

The *in silico* iLIR database (Jacomin et al., 2016) identified a strongly predicted LIR motif in tepsin (Figure 2-1A). LIR motifs commonly contain the sequence

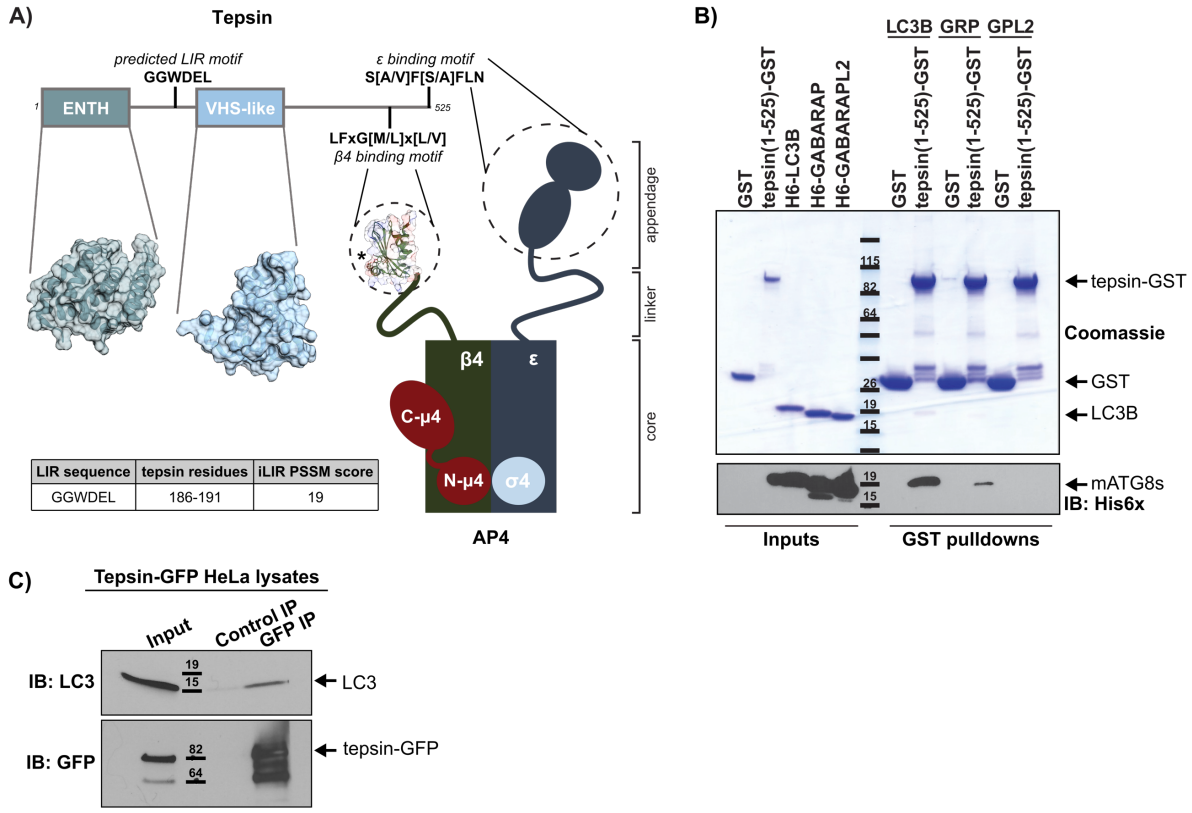

Figure 2-1: Tepsin directly and specifically binds LC3B *in vitro*. (A) Schematic diagrams of tepsin and AP-4 depicting the structural basis for the AP-4/tepsin interaction (PDB: 2MJ7); the predicted LIR motif (iLIR database; Jacomin et al., 2016) lies in the unstructured region between the tepsin ENTH (PDB: 5WF9) and VHS-like domains (PDB: 5WF2). (B) Coomassie-stained SDS-PAGE gel and Western blot (α-His; Abcam ab184607) of GST pulldowns using recombinant full-length tepsin-GST (residues 1-525) with His6x-LC3B, His6x-GABARAP (GRP), or His6x-GABARAPL2 (GPL2). Experiments show tepsin binds LC3B and weakly binds GABARAP; free GST was used as a negative control. (C) LC3 co-immunoprecipitates with tepsin from HeLa cells stably expressing tepsin-GFP detected by Western blot (α-LC3B: Abcam ab48394; α-GFP: Abcam ab6663). B and C: representatives of three independent experiments.

[W/F/Y]xx[V/I/L], where critical hydrophobic residues are buried into corresponding hydrophobic pockets on the surface of mATG8 proteins (Popelka and Klionsky, 2015). The putative tepsin LIR motif fits the canonical sequence (GGWDEL). Two glycine residues immediately preceding the WDEL sequence in tepsin were also highlighted in the iLIR result, based on common sequences found in annotated functional LIR motifs (Jacomin et al., 2016). As is common for LIR motifs (Popelka and Klionsky, 2015), this motif lies in an unstructured region located between the tepsin ENTH and VHS domains

(Figure 2-1A). The mATG8 subfamilies are partially distinguished by varying preferences for the specific sequence of LIR motifs (Rogov et al., 2017; Wirth et al., 2019). We tested whether tepsin could bind three distinct mATG8 members. We purified full length tepsin (residues 1-525) as a Glutathione S-Transferase (GST)-fusion protein. GST pulldown assays using recombinant purified tepsin-GST with His-tagged LC3B, GABARAP, or GABARAPL2 show tepsin preferentially binds to LC3B *in vitro* (Figure 2-1B). The tepsin/LC3 interaction is faintly visible by Coomassie staining on an SDS-PAGE gel and further confirmed by probing 6x-histidine-tags on mATG8 proteins by Western blot. Tepsin-GST weakly bound GABARAP and showed no detectable binding at either Coomassie or Western blot level to GABARAPL2 *in vitro*.

Based on biochemical and cell biological data, tepsin likely requires AP-4 binding to become membrane-associated (Archuleta et al., 2017; Borner et al., 2012; Frazier et al., 2016; Mattera et al., 2015). Like yeast ATG8, all mATG8 proteins are conjugated to a phosphatidylethanolamine through a ubiquitination-like cascade upon induction of autophagy (Shpilka et al., 2011). With this lipid modification, ATG8 proteins can be incorporated into the forming phagophore membrane to regulate autophagy. We tested whether AP-4 binding to tepsin affects the ability of tepsin to interact with LC3B using a tripartite GST pulldown assay. Tepsin-GST binding to the AP-4 β4 appendage domain does not significantly alter tepsin binding to LC3B *in vitro* (Figure A1-1).

We next tested whether tepsin interacts with LC3B in cultured cells. Using an established HeLa cell line stably expressing tepsin-GFP (Borner et al., 2012), co-immunoprecipitation experiments show enrichment for endogenous LC3 (Figure 2-1C). Together, these data suggest an interaction between tepsin and LC3B occurs in cells,

while the *in vitro* data using purified proteins suggests this is a direct interaction.

The tepsin LIR motif binds the hydrophobic pocket on LC3

The critical aromatic residues in a LIR motif interact with LC3B using two hydrophobic pockets termed the LIR docking site (LDS). Using AlphaFold Multimer, we modeled binding between LC3B and a peptide containing the tepsin LIR motif (residues 185-193). The tepsin/LIR motif interaction was superposed over an experimentally determined structure of LC3B bound to a p62 LIR motif (PDB: 2ZJD). As observed in p62, the critical tryptophan and leucine residues are positioned in the hydrophobic pockets of the LC3 LDS (Figure 2-2A). Additionally, the LDS region contains corresponding basic

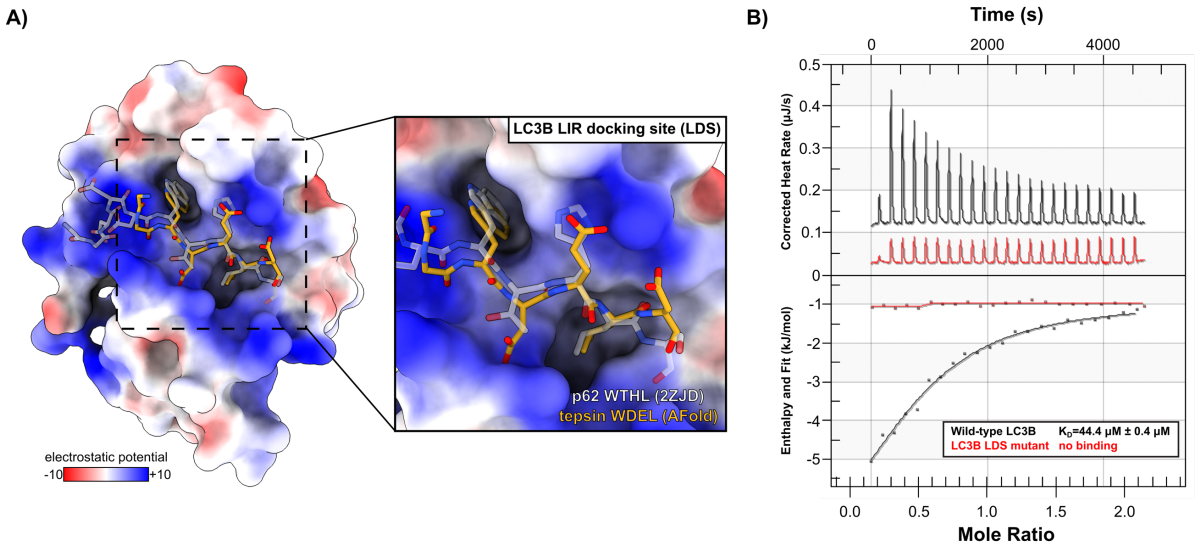

Figure 2-2: The tepsin LIR motif binds the established binding pocket on LC3B *in vitro*. (A) Electrostatic surface representation of LC3B (PDB: 2ZJD) indicating the LIR Docking Site (LDS; shown in inset) bound to the LIR peptide in p62. A model generated in AlphaFold Multimer shows the tepsin LIR motif peptide superposed (yellow) with the Trp and Leu residues occupying established hydrophobic pockets on the LC3B surface. (B) Representative isothermal titration calorimetry (ITC) experiments. Purified recombinant LC3B proteins and tepsin LIR motif peptide were used in ITC experiments to quantify binding affinities. The tepsin LIR motif peptide (residues 185-193) binds wild-type LC3B with a K_D of 44.4 µM ± 0.4 µM by ITC (n= 3 independent experiments). The tepsin LIR peptide shows no detectable binding to the LC3B LDS binding mutant (F52A/L53A). K_D values are represented as average ± standard deviation. ITC data are summarized in Table A1-1.

patches to accommodate the acidic aspartate and glutamate residues of the tepsin LIR motif (WDEL).

We used isothermal titration calorimetry (ITC) to quantify tepsin LIR motif binding to LC3B *in vitro*. Purified recombinant LC3B (residues 1-120) binds a synthesized tepsin LIR peptide (SGGGWDELDS, underlined residues 185-193) with micromolar affinity (K_D = 44.4 μM ± 0.4 μM). Mutant LC3B containing point mutations in the LDS (F52A/L53A; Behrends et al., 2010; Marshall et al., 2019; Noda et al., 2008) exhibits no detectable binding to the tepsin LIR peptide (KD > 300 μM; Figure 2-2B). In the context of full length recombinant tepsin, pulldowns reveal mutation of either the tepsin LIR motif or the LC3B LDS abrogates binding at both Coomassie and Western blot detection levels (Figure A1-2A). Together, these biochemical data indicate the tepsin LIR motif mediates an interaction between tepsin and LC3B in the established LIR binding site (Noda et al., 2008).

To better understand the selectivity of the tepsin LIR motif for LC3B over other mATG8 proteins (Figure 2-1B), we used AlphaFold to generate models of tepsin LIR peptides bound to LC3A, GABARAP, and GABARAPL2. These models were then superposed with experimentally determined structures of each mATG8 bound to a LIR motif. Models of LC3A show tepsin LIR residues W188 and L191 fit well into the corresponding hydrophobic pockets (Figure A1-2B), as observed for LC3B models. The LC3A LDS also contains basic patches that could accommodate the acidic Asp and Glu residues in tepsin. The GABARAP model shows tepsin LIR residues W188 and L191 dock well into hydrophobic pockets (Figure A1-2C). The reduced binding potential observed biochemically for GABARAP may instead be explained by two acidic residues

(D189 and E190) since the region between the hydrophobic pockets has a greatly reduced electrostatic potential compared to LC3A and LC3B. Finally, the GABARAPL2 model clearly exhibits a clash with the critical tepsin LIR W188 residue (Figure A1-2D). Together these models support our biochemical data (Figure 2-1B) indicating the tepsin LIR motif selectively binds LC3 over GABARAP proteins.

ATG9A accumulates near the cell periphery in cells acutely depleted of tepsin

We next sought to test the impact of tepsin knockdown in the context of established AP-4-deficiency phenotypes. Given the emerging links between AP-4 trafficking and autophagy (Davies et al., 2018; de Pace et al., 2018; Guardia et al., 2021; Ivankovic et al., 2020; Matsuda et al., 2008a; Mattera et al., 2020b, 2017), we used a well-established autophagy reporter line overexpressing a mRFP-GFP-LC3B fusion construct (Kimura et al., 2007; Sarkar et al., 2009). We acutely depleted these cells for tepsin or AP-4 using siRNA-mediated knockdown (Figure A1-3B). Whole lysate characterization of these cells showed tepsin-depletion drives increased expression of ATG9A by Western blot (Figure A1-4A).

We tested whether and how the subcellular distribution of ATG9A might be altered upon tepsin knockdown by co-immunostaining for ATG9A and the trans-Golgi marker, TGN46 (Figure 2-3A). Tepsin-depleted cells exhibit decreased co-localization of ATG9A with the TGN marker as quantified by Manders' overlap coefficient (Figure 2-3C). To further analyze this change to ATG9A subcellular localization, cells were segmented using the TGN46 marker into trans-Golgi ATG9A and non-Golgi ATG9A signal (representative enlargements in Figure 2-3B). In tepsin-depleted cells, isolated instances

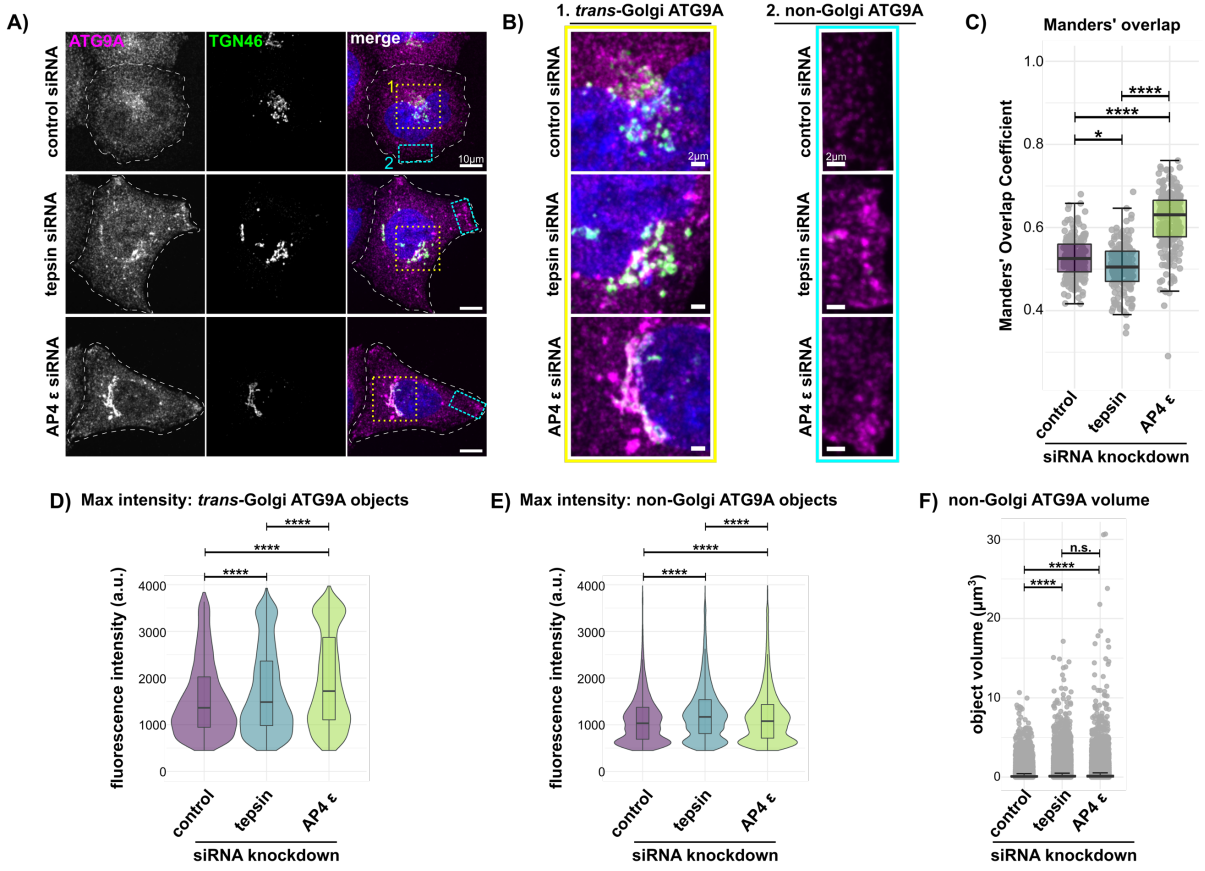

Figure 2-3: Tepsin depletion drives ATG9A accumulation at the cell periphery. (A) Representative maximum intensity projection confocal images of quenched mRFP-GFP-LC3B HeLa cells immunostained for ATG9A (α-ATG9A Abcam ab108338; secondary α-Rabbit-647 Thermo Fisher Scientific A32733) and TGN46 (α-TGN46 Bio-Rad AHP500GT; secondary α-Sheep-488 Thermo Fisher Scientific A11015). Cells were treated with control, non-targeting siRNA or tepsin siRNA. Scale bar: 10 μm. (B) Tepsin depletion results in ATG9A accumulation at the *trans*-Golgi (B.1; yellow boxes, A) and at the cell periphery (B.2;cyan boxes, A); Scale bar: 2 μm. (C) Manders' overlap coefficient indicates less ATG9A resides in the TGN after tepsin depletion. ATG9A is enriched in the TGN in AP-4-depleted cells. (D-F) Quantification of high intensity ATG9A objects (details in Methods). (D) Tepsin-depleted cells exhibit increased intensity of ATG9A signal accumulation at the TGN, at lower levels to those observed in AP-4-depleted cells. (E) The maximum intensity of ATG9A objects is significantly increased in tepsin-depleted cells compared to both control and AP-4-depleted cells. (F) AP-4- or tepsin-depleted cells exhibit enlarged ATG9A object volumes (μm^3). Quantification of four independent experiments with at least 175 total cells per condition; each dot represents an individual cell (C) or ATG9A object (F). Statistical results from Kruskal-Wallis test, Dunn test with Bonferroni correction; *p≤0.05, **p≤0.01, ***p≤0.001, ****p≤0.0001.

of ATG9A accumulation at the TGN were observed (Figure 2-3B.1; Figure 2-3D), but ATG9A largely redistributed to the cell periphery as judged by enlarged accumulations with high fluorescence intensity (Figure 2-3B.2; Figure 2-3E and 2-3F). Some peripheral accumulations of ATG9A were also observed upon AP-4 knockdown (Figure 2-3B.2). However, fluorescence intensity measurements indicate tepsin-depleted cells exhibit more apparent ATG9A in these peripheral structures than do AP-4-depleted cells (Figure 2-3E). The majority of ATG9A remains trapped in the TGN following AP-4 knockdown (Figure 2-3C, A1-4B, and A1-4C), as observed in multiple systems (Behne et al., 2020; Davies et al., 2018; de Pace et al., 2018; Ivankovic et al., 2020; Mattera et al., 2017; Scarrott et al., 2023). These data implicate tepsin in the ATG9A trafficking and export at the TGN, although it remains possible tepsin may also function in targeting these ATG9A-positive vesicles to their destination (next section; Discussion).

Tepsin-depleted cells exhibit dysregulated autophagosomes and autolysosomes

The biochemical and cellular data presented thus far suggest there are additional functions for the AP-4 coat in regulating autophagy dynamics via the accessory protein, tepsin. We next used the mRFP-GFP-LC3B cell line to assay flux through the autophagic pathway (Figure 2-4A). Coincident red and green structures positive for mRFP-GFP-LC3 are identified as yellow autophagosomes (or early autophagic structures). Lysosome fusion with autophagosomes quenches GFP fluorescence, so red (mRFP-only) LC3 structures are classified as autolysosomes. We visualized autophagosome and autolysosome structures in tepsin-depleted or AP-4-depleted cells under basal or

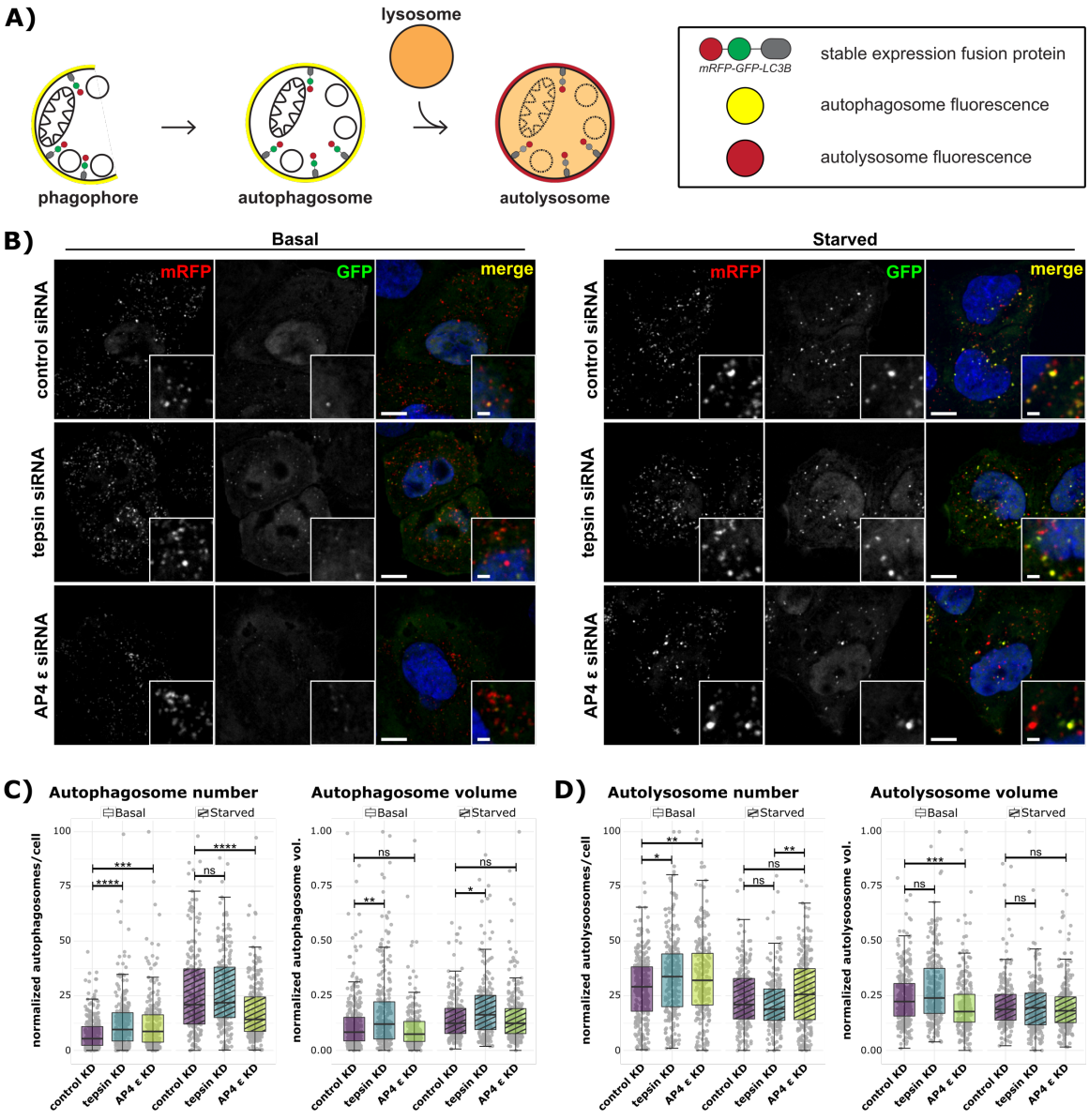

Figure 2-4: Acute tepsin depletion increases autophagosome number and volume under basal nutrient conditions. (A) Schematic of autophagy assay in HeLa cells stably expressing mRFP-GFP-LC3B. Coincident green and red fluorescence marks autophagosomes in yellow, while acidification of autolysosomes quenches GFP and leaves only red (RFP) signal. (B) Representative single plane confocal images of mRFP-GFP-LC3B HeLa cells cultured in either complete media (basal) or starved for 2 hours in EBSS. Cells were treated with control (non-targeting) siRNA, tepsin siRNA, or AP-4 ε siRNA. Scale bar: 10 μm; inset scale bar: 2 μm. (C-D) Quantification of 3 independent experiments with at least 200 total cells per condition. (C) Tepsin-depleted cells under basal conditions contain more autophagosomes with greater apparent autophagosome volume (μm^3) under both basal and starved conditions. AP-4 depleted cells contain more autophagosomes under basal conditions but fewer autophagosomes in starved conditions. (D) Tepsin-depleted cells under basal conditions contain more autolysosomes but no apparent difference in autolysosome volume. AP-4-depleted cells under basal and starved conditions contain increased autolysosome number but decreased apparent autolysosome volume only under basal conditions. Plots for C and D depict individual cell averages for each metric overlayed with box-and-whisker plots of the distribution where each point represents one cell. Statistical results from Kruskal-Wallis test, Dunn test with Bonferroni correction. All data was subject to min-max normalization; *p≤0.05, **p≤0.01, ***p≤0.001, ****p≤0.0001.

starvation (amino acid- and serum-free) conditions (Figure 2-4B). Knockdown efficiency and autophagy induction were confirmed by Western blot (Figure A1-5A).

Under basal conditions, both AP-4- and tepsin-depleted cells contain more autophagosomes (Figure 2-4C). Following starvation and induction of bulk autophagy, the number of autophagosomes in tepsin-depleted cells does not differ from the control treatment. However, AP-4-depleted cells contain fewer autophagosomes compared to control cells (Figure 2-4C). The apparent volume of autophagosomes in tepsin-depleted cells was increased under both basal and starvation conditions but was not significantly different from control in AP-4-depleted cells (Figure 2-4C). These data suggest tepsin-depletion results in the aberrant formation and growth of autophagosomes, while AP-4 acute depletion primarily affects the formation of early autophagosomes.

Tepsin or AP-4 depletion results in a greater number of autolysosomes in cells under basal conditions (Figure 2-4D). Autophagic flux is not drastically altered by tepsin depletion: starved cells show no significant change to the number of autolysosomes, and neither basal nor starved cells show changes to the apparent volume of autolysosomes. AP-4-depleted cells contain more autolysosomes compared to tepsin-depleted cells, but the number is not significantly different from control cells. Apparent autolysosome volume is decreased in AP-4-depleted cells under basal conditions compared to control cells (Figure 2-4D).

We further utilized the GFP tag in this reporter line to assay for an interaction with endogenous tepsin. GFP immunoprecipitations from mRFP-GFP-LC3B cells are enriched for endogenous tepsin and the AP-4 ε subunit by Western blot (Figure A1-5B). These data further indicate that tepsin interacts with LC3B in this cell line, and AP-4 is also

present. Overall tepsin loss dysregulates autophagosome and autolysosome morphology without blocking autophagic flux. The effect of acute tepsin depletion is distinct from acute AP-4 depletion, suggesting a separate, or an additional, function for tepsin in autophagosomes biogenesis.

The tepsin/LC3 interaction modulates AP-4-dependent ATG9A trafficking

Our data indicate tepsin loss impairs ATG9A trafficking and dysregulates autophagosome and autolysosome morphology. ATG9A peripheral accumulation when tepsin is lost suggests tepsin may target ATG9A-containing AP-4 vesicles for their use in autophagy. We generated an siRNA-resistant, myc-tagged construct of wild-type tepsin to test whether ATG9A accumulation was specific to tepsin loss. Tepsin-myc expression level was similar between control and tepsin-siRNA treatments confirming siRNA resistance (Figure A1-6, WT tepsin). We monitored the colocalization of ATG9A with the TGN46 marker in the quenched mRFP-GFP-LC3B cell line. Untransfected cells depleted for tepsin exhibited decreased ATG9A signal at the TGN (Figure 2-5A and 2-5C). However, re-introduction of wild-type tepsin rescues high-intensity ATG9A accumulations and restores ATG9A intracellular distribution (as measured by TGN46 co-localization) to levels similar to those observed in control cells (Figure 2-5B and 2-5D). These data indicate ATG9A mis-trafficking (Figure 2-3) was specific to the loss of tepsin.

Based on the *in vitro* characterization of the tepsin-LC3B interaction, we specifically tested the role of the tepsin LIR motif in ATG9A cargo trafficking. We generated siRNA-resistant myc-tagged constructs of LIR mutant tepsin (WDEL→SSSS) and a truncated tepsin containing only the C-terminal tail (ΔN-term tepsin; residues 360-

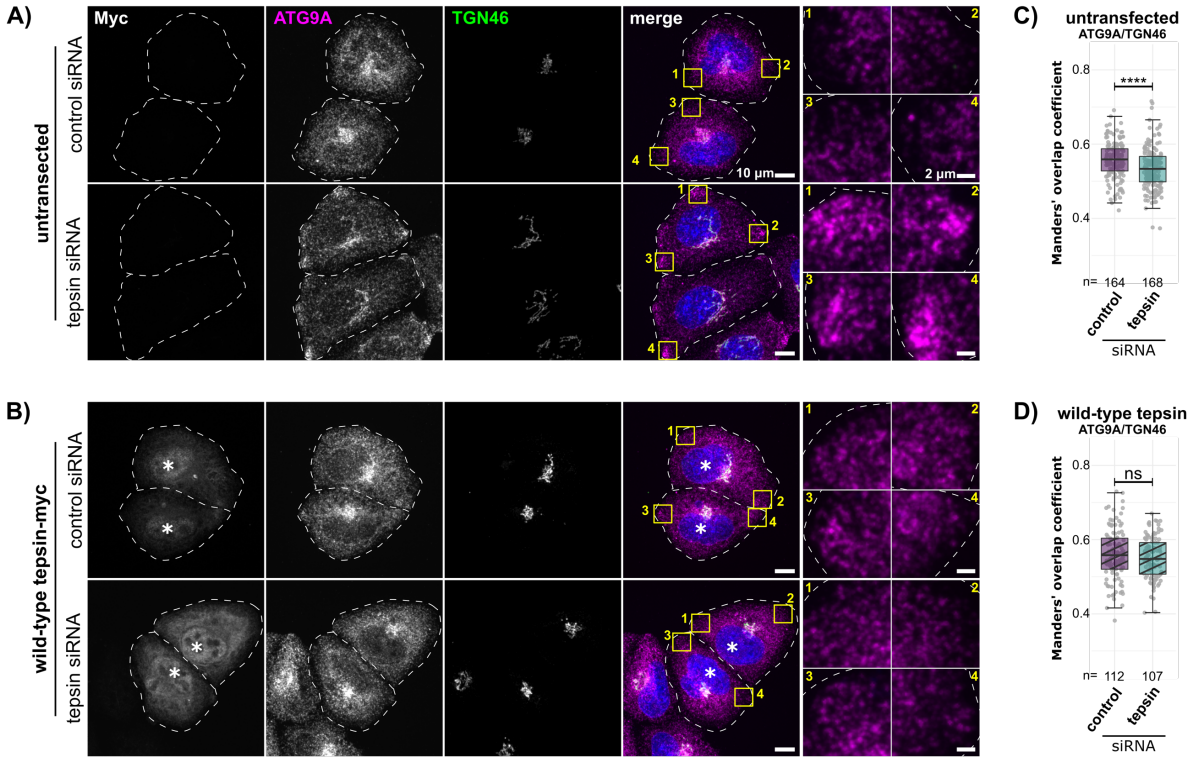

Figure 2-5: Re-introduction of wild-type tepsin restores ATG9A cellular distribution in tepsin-depleted cells. (A-B) Representative maximum intensity projection confocal images of quenched mRFP-GFP-LC3B HeLa cells immunostained for ATG9A (α-ATG9A Abcam ab108338; secondary α-Rabbit-647 Thermo Fisher Scientific A32733), TGN46 (α-TGN46 Bio-Rad AHP500GT; secondary α-Sheep-488 Thermo Fisher Scientific A11015), and myc-tag (α-myc-tag Cell Signaling Technology 2276; secondary goat α-Mouse-555 Thermo Fisher Scientific A32727). Cells were treated with non-targeting siRNA (control) or tepsin siRNA. Cells in B were subsequently transfected with wild-type siRNA resistant tepsin; transfected cells (anti-myc stained) are marked by asterisks (*). ATG9A accumulates at the cell periphery to a greater extent in tepsin-depleted cells (A; yellow inset boxes) compared to cells rescued with wild-type tepsin (B; yellow inset boxes). Scale bar: 10 µm; inset scale bar: 2 µm. (C) Manders' overlap coefficient indicates less ATG9A resides within the *trans*-Golgi of tepsin-depleted cells. (D) ATG9A subcellular distribution is restored following re-introduction of wild-type tepsin. Quantification of 3 independent experiments (n = total cell number). Plots for C and D depict box-and-whisker plots of the distribution where each point represents one cell. Statistical results from Kruskal-Wallis test, Dunn test with Bonferroni correction; *p≤0.05, **p≤0.01, ***p≤0.001, ****p≤0.0001.

525). Each construct transfected at similar efficiency and exhibited resistance to tepsin siRNA treatments (Figure A1-6, ΔN-term and LIR mutant). Expression of LIR mutant tepsin failed to rescue ATG9A cellular distribution in tepsin-depleted cells (Figure 2-6A and 2-6C). Interestingly, instead of the TGN and peripheral accumulations previously observed, ATG9A is more diffusely distributed throughout the cell. We also tested the ΔN-term tepsin mutant, which contains only tepsin C-terminal tail harboring established AP-

4 binding motifs (Frazier et al., 2016; Mattera et al., 2015). Expression of the ΔN-term tepsin mutant gives a dominant negative phenotype, in which ATG9A co-localization with the TGN46 marker is decreased in both control siRNA-treated and tepsin-depleted cells (Figure 2-6B and 2-6D).

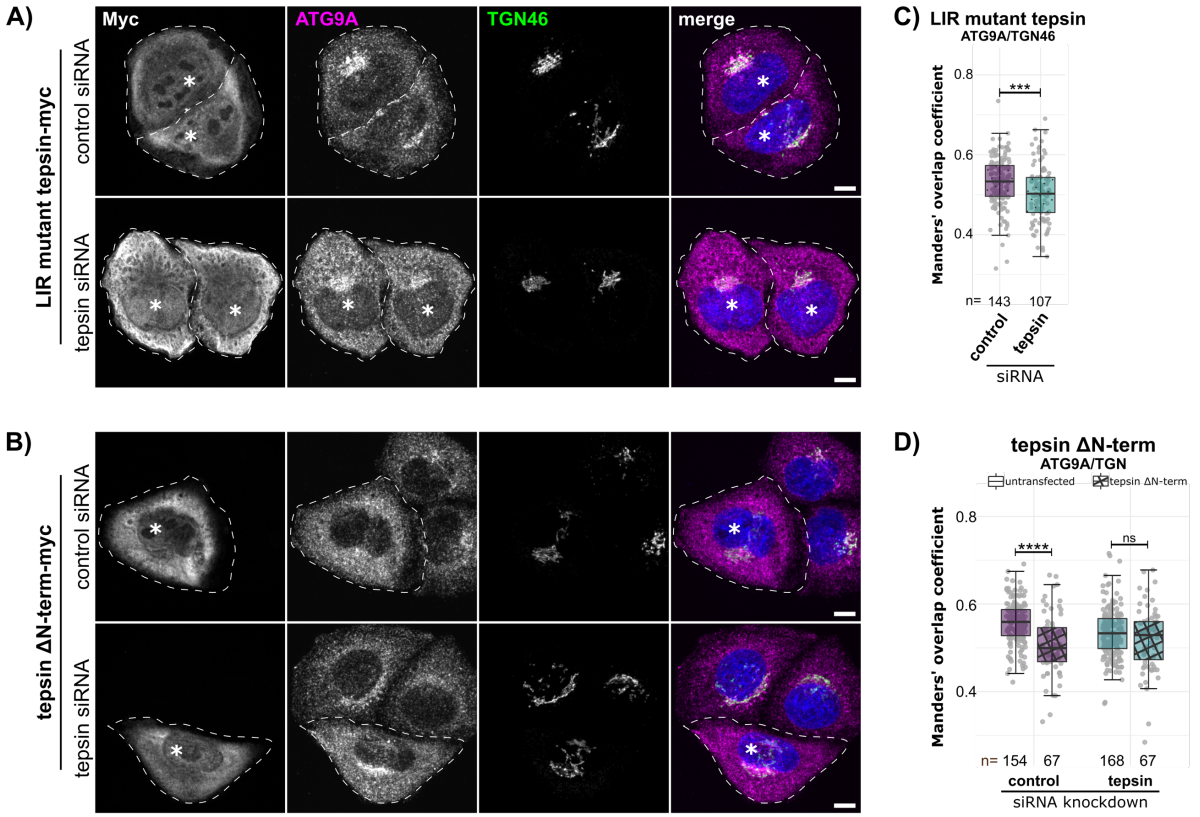

Figure 2-6: The tepsin LIR motif is required to maintain ATG9A cellular distribution. (A-B) Representative maximum intensity projection confocal images of quenched mRFP-GFP-LC3B HeLa cells immunostained for ATG9A (α-ATG9A Abcam ab108338; secondary α-Rabbit-647 Thermo Fisher Scientific A32733), TGN46 (α-TGN46 Bio-Rad AHP500GT; secondary α-Sheep-488 Thermo Fisher Scientific A11015), and myc-tag (α-myc-tag Cell Signaling Technology 2276; secondary goat α-Mouse-555 Thermo Fisher Scientific A32727). Cells were treated with non-targeting siRNA (control) or tepsin siRNA. Cells were subsequently transfected with LIR mutant tepsin (WDEL/SSSS) or tepsin ΔN-terminus (residues 360-525; ΔN-term); transfected cells are marked by asterisks (*). Targeted mutation of the LIR motif (A) or loss via N-terminus truncation (B) results in dispersed ATG9A accumulation outside of the *trans*-Golgi. Scale bar: 10 μm. (C) Introducing LIR-mutant tepsin in tepsin-depleted cells fails to restore ATG9A cellular distribution measured by Manders' overlap coefficient for ATG9A signal at the TGN. (D) Tepsin ΔN-term acts as a dominant negative by dysregulating ATG9A colocalization at the TGN in control siRNA- and tepsin siRNA-treated cells. Quantification of 3 independent experiments (n = total cell number). Statistical results from Kruskal-Wallis test, Dunn test with Bonferroni correction in C and Mann-Whitney U-test in D; *p≤0.05, **p≤0.01, ***p≤0.001, ****p≤0.0001.

Both the tepsin LIR mutant and ΔN-term tepsin constructs exhibited increased cytotoxicity (based on viability during sample preparation) and more variability in expression level for individual cells when visualized by immunofluorescence imaging. As a result, expression levels for both constructs appears higher than for wild-type tepsin in most cells (represented in Figure 2-5A and 2-5B; 2-6A and 2-6B). However, for each construct, exogenous expression levels were comparable between control and tepsin-depleted cells. Increased toxicity and dominant negative effects following ΔN-term tepsin transfection could indicate the tepsin N-terminus performs several important functions (see Discussion). Though both the LIR mutant and ΔN-term tepsin constructs retain AP-4 binding motifs, they fail to rescue ATG9A cellular distribution phenotypes. Together with the *in vitro* data, this suggests cells need a functional tepsin N-terminus and a direct interaction between tepsin and LC3B to mediate AP-4-dependent trafficking of ATG9A vesicles for their intended function during autophagy.

DISCUSSION

Summary

Published work from multiple groups has characterized the molecular interaction of tepsin with AP-4 (Borner et al., 2012; Frazier et al., 2016; Mattera et al., 2015) and determined X-ray structures of the tepsin ENTH and VHS domains (Archuleta et al., 2017). Despite these data, the function for tepsin in AP-4 coats has remained elusive. Data presented here provide multiple new mechanistic insights into tepsin function in AP-

4-mediated trafficking. Using *in silico* and biochemical methods together with fluorescence imaging, we have identified and characterized a functional LIR motif in tepsin that interacts with LC3B *in vitro* and in cultured cells. Tepsin depletion in cells induces partial ATG9A accumulation at the TGN and enrichment at the cell periphery. Re-introduction of tepsin constructs with a mutated LIR motif or lacking the N-terminus are unable to rescue ATG9A trafficking defects. These data suggest tepsin may play roles in AP-4 vesicle formation and possibly in cargo delivery or recycling of ATG9A-positive vesicles (Figure 2-7).

Molecular characterization of the tepsin LIR motif

Emerging models of AP-4-deficiency syndrome highlight a dysregulation of autophagy resulting from retention of ATG9A, the essential autophagy lipid scramblase (Guardia et al., 2020b; Maeda et al., 2020b; Matoba et al., 2020; Noda et al., 2000; Young et al., 2006), at the TGN (Behne et al., 2020; Davies et al., 2018; Ivankovic et al., 2020; Mattera et al., 2017). Identification and characterization of a LIR motif within tepsin further links AP-4 coats to autophagy and maintenance of cellular homeostasis. The tepsin LIR motif (WDEL) fits an established consensus sequence (WxxL) for binding ATG8 proteins (Noda et al., 2008). Computational structural modeling and *in vitro* biochemical data provide strong evidence that tepsin interacts with LC3B with low micromolar affinity using the LIR docking site (LDS). LIR interaction affinities exhibit a large range (K_D values from sub-micromolar to ~100 μM), usually because mATG8 family proteins exhibit selectivity (reviewed Wesch et al., 2020). While most interactions with autophagy cargo receptors

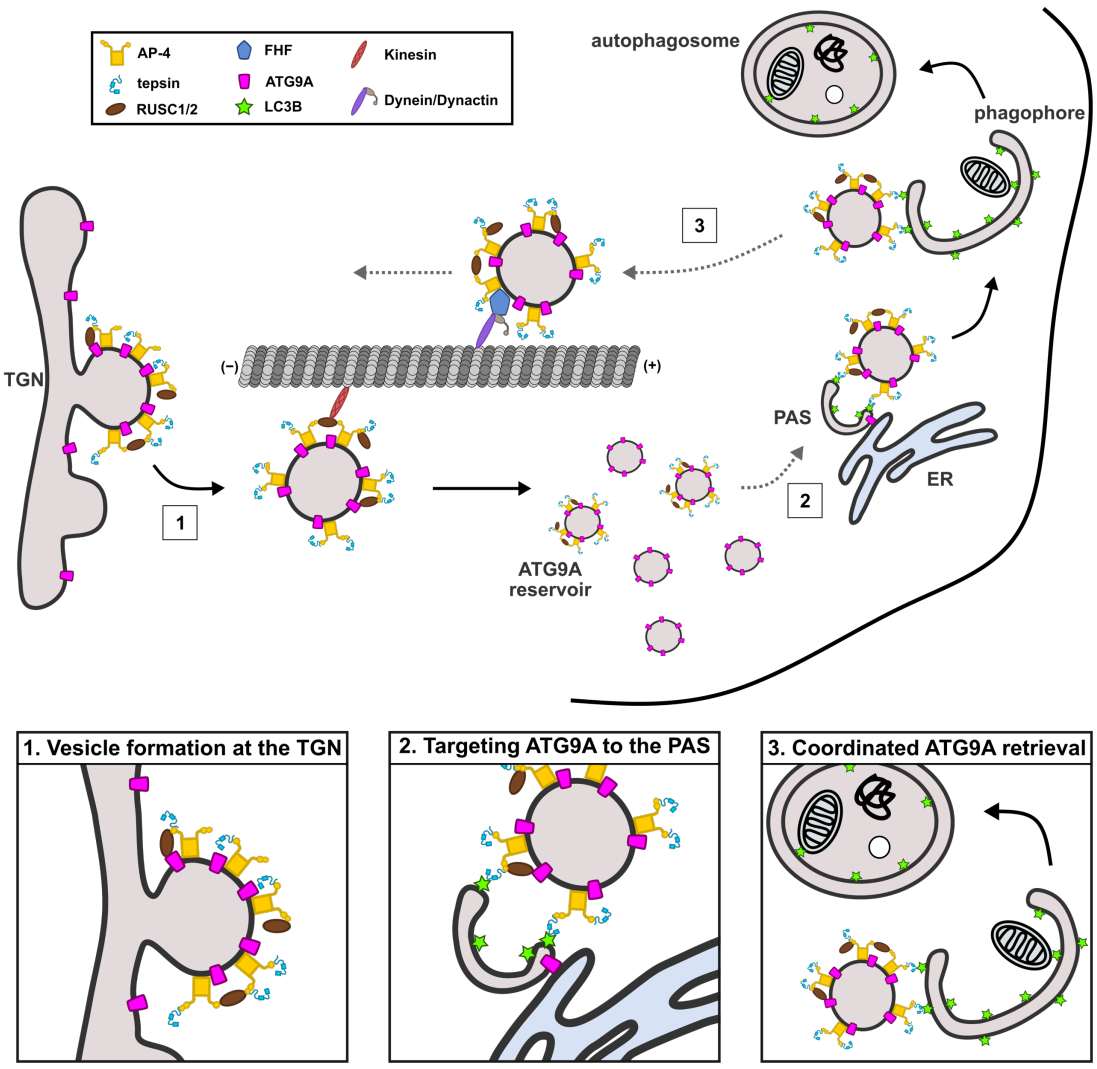

Figure 2-7: Models for tepsin function in AP-4 trafficking and autophagy. AP-4 coats containing tepsin assemble at the TGN, packaging ATG9A into vesicles. AP-4- and ATG9A-containing vesicles undergo anterograde (Davies et al., 2018) and retrograde (Mattera et al., 2020b) transport to maintain ATG9A distribution. Tepsin depletion leads to peripheral ATG9A accumulation which may suggest AP-4 vesicles remain coated and function in ATG9A delivery. Together, published data and new data presented here lend themselves to three possible interpretations, that are not mutually exclusive. (1) Tepsin and AP-4 are required for efficient packaging of ATG9A into AP-4-coated vesicles exiting the TGN. (2) The tepsin/LC3B interaction may be required for targeting ATG9A to the PAS. (3) Alternatively, tepsin may coordinate retrieval of ATG9A from maturing autophagosomes.

are high affinity, the broad affinity range reflects the diverse functional roles of mATG8/LIR interactions (Birgisdottir et al., 2013).

The tepsin LIR motif shows partial specificity for LC3 over GABARAP proteins *in vitro* (Figure 2-1B). AlphaFold modelling indicates selectivity may be conferred by the

tepsin acidic aspartate and glutamate residues (WDEL) which are better accommodated in the basic patch located between hydrophobic pockets in the LDS region of LC3 proteins (Figures 2-2A and A1-2). Furthermore, an alternative consensus sequence has been proposed as a GABARAP interaction motif (GIM), which displays a preference for aliphatic residues in the first variable position: [W/F]-[V/I]-X-V (Rogov et al., 2017). In cells, endogenous LC3B co-immunoprecipitates with tepsin-GFP (Figure 2-1C), and conversely, endogenous tepsin and AP-4 ε co-immunoprecipitate with mRFP-GFP-LC3B (Figure A1-5B). The micromolar affinity of this interaction *in vitro*, as well as weak detection by traditional immunoprecipitation methods, suggest the tepsin interaction with LC3B occurs transiently in cells.

The major question arising from the identification of the LIR motif is where in the cell do tepsin and LC3 interact? Both tepsin and LC3 cycle between cytosolic and membrane-associated states, with tepsin primarily localized at Golgi membranes during steady-state (Borner et al., 2012) while LC3 is found at autophagosomal membranes following lipid conjugation (Ichimura et al., 2000; Kabeya et al., 2000; Kirisako et al., 2000). LC3 is not enriched in AP-4 vesicle proteomic datasets which identified several AP-4 cargo and accessory proteins (Borner et al., 2012; Davies et al., 2022, 2018). Proteomic vesicle profiling is imperfect for identifying prospective cargoes; however, LC3 lipid conjugation occurs via a ubiquitination-like cascade and seems to be targeted to sites of autophagosome biogenesis (Fracchiolla et al., 2016; Kabeya et al., 2004, 2000; Maruyama et al., 2021; Nath et al., 2014). It therefore seems unlikely LC3 is brought as a cargo by AP-4 vesicles, and instead supports the idea that tepsin transiently interacts with LC3B, likely at the autophagosomal membrane.

LC3 conjugation begins early in autophagosome biogenesis; increases as the phagophore expands; and, following autophagosome closure, cytosolic-facing LC3 is deconjugated to its cytosolic form (Kirisako et al., 2000; Landajuela et al., 2016; Nair et al., 2012; Weidberg et al., 2010). Tepsin-LC3B interactions at phagophore membranes would likely be regulated by avidity effects dependent on protein density on the membrane. Autophagosome maturation and eventual deconjugation of LC3 could also temporally regulate the tepsin/LC3B interaction. It is also possible that other AP-4 coat components interact with autophagy machinery. The iLIR database (Jacomin et al., 2016) identifies multiple LIR motifs in another AP-4 accessory protein, RUSC2 (Davies et al., 2018). In the future, it will be interesting to explore functionality of putative RUSC2 LIR motifs and whether they affect ATG9A trafficking.

The tepsin/LC3B interaction affects ATG9A cellular distribution

Impaired export of ATG9A from the TGN is now established as a hallmark of AP-4-deficiency syndrome (Behne et al., 2020). AP-4 knockout in cultured cells (Davies et al., 2018; Mattera et al., 2017), fibroblasts from AP-4-deficient patients (Davies et al., 2018; de Pace et al., 2018), AP-4 ε or β4 knockout mice neurons (de Pace et al., 2018; Ivankovic et al., 2020; Scarrott et al., 2023), and the acute AP-4 depletion shown here (Figure 2-3C-D) robustly traps ATG9A at the TGN. Tepsin knockout HAP1 cells did not accumulate ATG9A at the TGN (Mattera et al., 2017), but the role of tepsin in ATG9A trafficking was largely unexplored. Data shown here, using acute depletion methods, offers compelling evidence that tepsin is required for efficient formation of AP-4 coated vesicles and/or delivery of ATG9A-positive vesicles. The discrepancy between tepsin

knockout data (Mattera et al., 2017) and our acute depletion system may indicate compensation by other identified ATG9A trafficking or recycling events (Campisi et al., 2022; Imai et al., 2016; Jia et al., 2017; Ravussin et al., 2021; Young et al., 2006; Zhou et al., 2022).

Acute tepsin depletion has two distinct effects on ATG9A trafficking: it drives partial ATG9A accumulation at the TGN (Figure 2-3D) and promotes ATG9A accumulation at the cell periphery (Figure 2-3E-F). Re-introducing wild-type tepsin rescues both phenotypes (Figure 2-5). Whole cell lysates also exhibit increased ATG9A expression upon tepsin loss (Figure A1-4A). Similarly, ATG9A expression levels are increased in patient-derived cells (Davies et al., 2018), presumably as cells attempt to compensate for failed TGN export of ATG9A. In this work, acute tepsin-depletion led to higher ATG9A expression levels than did AP-4-depletion. Compensatory ATG9A overexpression in tepsin-depleted cells may be more effective, since ATG9A export is not blocked as significantly.

ATG9A has a well-documented role during autophagy, so we used an established mRFP-GFP-LC3B reporter (Sarkar et al., 2009) to assay flux through the autophagy pathway following acute depletion of tepsin or AP-4. Autophagic flux seemed largely unaffected by tepsin- or AP-4 depletion (Figure 2-4). However, formation and morphology of autophagosome and autolysosome structures were differentially affected by these depletions, suggesting some separation of function between tepsin and AP-4. We note AP-4 depleted cells form more autophagosomes under basal conditions but appear to have fewer autophagosomes than do control cells following autophagy induction (Figure 2-4C). This assay cannot distinguish between early phagophore structures and maturing

autophagosomes, so this may indicate AP-4 loss hinders proper formation of early autophagic structures. ATG9A is critical for early nucleation of the phagophore (Noda et al., 2000; Sawa-Makarska et al., 2020; Yamamoto et al., 2012; Young et al., 2006), and AP-4 trafficking of ATG9A is thought to contribute to maintenance of an ATG9A vesicle pool used in these nucleation steps (Davies et al., 2018). Altered formation of autophagosomes without a total block in autophagy supports the idea that AP-4-derived ATG9A vesicles partially contribute to this pool.

Conversely, tepsin depletion primarily appears to affect morphology of autophagosomes which have larger apparent volume under basal or starved cell conditions (Figure 2-4C). A greater number of autophagosomes and autolysosomes form in tepsin-depleted cells, suggesting dysregulation of autophagy even under fed cell conditions (Figure 2-4C and 2-4D). If tepsin was solely involved in formation of AP-4 coated vesicles at the TGN, we would expect tepsin depletion to have the same effect on autophagy dynamics as AP-4-depletion because of failed ATG9A export. We observe increased ATG9A expression in tepsin-depleted cells (Figure A1-4A), which could partially compensate for inefficient ATG9A export (Figure 2-7.1). The different effect of AP-4 or tepsin depletion on autophagosome morphology presented here (Figure 2-4) may reflect a secondary role for tepsin during autophagy.

The tepsin LIR motif binding to LC3B hints tepsin can mediate an interaction between AP-4 vesicles and autophagic membranes. Expressing tepsin with a mutated LIR motif failed to restore ATG9A subcellular distribution in tepsin-depleted cells. In fact, expression of the LIR mutant tepsin seems to drive diffuse distribution of ATG9A throughout the cell (Figure 2-6A and 2-6C). Similarly, expressing the ΔN-term tepsin

fragment acts as a dominant negative, where ATG9A is expressed more diffusely throughout the cell in control cells (Figure 2-6B and 2-6D). The tepsin LIR mutant and ΔN-term retain established AP-4 binding motifs (Frazier et al., 2016; Mattera et al., 2015), so these results likely reflect specific contributions from the tepsin LIR motif and N-terminus.

These data together suggest the tepsin LIR motif helps coordinate localization of ATG9A-positive vesicles to pre-autophagic sites (Figure 2-7.2). AP-4 trafficking is also implicated in retrograde transport of ATG9A (Mattera et al., 2020b), so it remains possible that tepsin coordinates ATG9A retrieval (Figure 2-7.3). It will be important for future work to establish whether AP-4 vesicles remain coated to mediate effects at the periphery. Considering morphological defects of early autophagosomes (Figure 2-4C), the tepsin LIR interaction with LC3B may contribute to ATG9A function or delivery for development and growth of autophagy membrane structures. It may be particularly interesting to explore avidity effects on the tepsin-LC3B interaction given that maturation of autophagosome structures coincides with LC3 protein density at the membrane (Kabeya et al., 2000; Nath et al., 2014). Together these data identify the first functional role of tepsin and further develop our understanding of AP-4 trafficking and autophagy.

MATERIALS AND METHODS

Reagents

Unless otherwise noted, all chemicals were purchased from Sigma.

The following antibodies were used in this study: rabbit anti-AP-4 epsilon 1:400 for Western blots (612019; BD Transduction Labs); rabbit anti-ATG9A 1:200 for immunofluorescence and 1:1000 for Western blots (ab108338; Abcam); rabbit anti-LC3B 1:3000 for Western blots (ab48394; Abcam); HRP-conjugated anti-GFP 1:2000 for Western blots (ab6663; Abcam); rabbit anti-tepsin 1:500 (in-house; Genscript) and 1:1000 (Robinson Lab, Cambridge) for Western blots; sheep anti-TGN46 1:1000 for immunofluorescence (AHP500GT; Bio-Rad); mouse anti-alpha tubulin 1:3000 for Western blots (66031; Proteintech); mouse anti-Myc-tag 1:8000 for immunofluorescence and 1:6000 for Western blots (2276; Cell Signaling Technology); HRP-conjugated anti-6X His tag 1:8000 for Western blots (ab184607; Abcam); HRP-conjugated secondaries for Western blots, 1:5000: Pierce goat anti-rabbit IgG (31460; Thermo Fisher Scientific); Pierce goat anti-mouse IgG (31430; Thermo Fisher Scientific); Fluorescent secondary antibodies for immunofluorescence, 1:500: goat anti-Rabbit 647 (A32733; Thermo Fisher Scientific), goat anti-Mouse 555 (A32727; Thermo Fisher Scientific), donkey anti-Sheep 488 (A11015; Thermo Fisher Scientific).

Molecular biology and cloning

For biochemical analysis, full-length tepsin (Borner et al., 2012) was subcloned using *Nde*I/*Bam*HI sites into in-house vector pMW172 (Owen and Evans, 1998) modified to

incorporate a C-terminal, thrombin cleavable GST tag. Full-length constructs of LC3B (residues 1-125), GABARAP (residues 1-117), and GABARAPL2 (residues 1-117) were subcloned by Genscript into pGEX-6P-1 using *Bam*HI/*Sal*I sites to generate N-terminal GST-fusion protein; an additional His6x-tag was added to the N-terminus of each protein sequence. The GST-fusion AP-4 β4 appendage (residues 615-739) was cloned previously (Frazier et al., 2016). A two-stage mutagenesis protocol (Frazier et al., 2016) was used to truncate full-length LC3B into the mature isoform (residues 1-120) and make the following mutations to tepsin and LC3B constructs: LC3B LIR docking site (LDS) mutant (F52A/L53A); LIR mutant tepsin (W188S, D189S, E190S, L191S); and tepsin siRNA target site silent mutations (nucleotides G1329A, A1335G, T1338C, A1341G, G1344A).

To generate constructs for tepsin rescue experiments, full-length tepsin was subcloned into pcDNA3.1 vector (Thermo Fisher Scientific) using *Bam*HI/*Xho*I sites. A C-terminal myc-tag (EQKLISEEDL) was included in the 3' primer to generate tepsin-myc constructs. This construct was subjected to mutagenesis as described above to confer siRNA resistance and mutate the tepsin LIR motif. A truncated construct of the tepsin C-terminal tail (residues 360-525 with myc-tag) was subcloned from the siRNA-resistant tepsin-myc using *Bam*HI/*Sal*I sites into the pcDNA3.1 backbone. The sequences of all constructs described above were verified by Sanger DNA sequencing (Azenta). Oligonucleotides used in this study may be found in Table 2.

Protein expression and purification

Constructs were expressed in BL21(DE3)pLysS cells (Invitrogen) for 16-20 hours at 22ºC after induction with 0.4 mM Isopropyl β-D-1-thiogalactopyranoside (IPTG). All tepsin constructs were purified in 20 mM Tris (pH 8.5), 200 mM NaCl and 2 mM βME. Wild-type β4 appendage domain and all mammalian ATG8 proteins (mATG8; LC3B, GABARAP, and GABARAPL2) were purified in 20 mM HEPES (pH 7.5), 200 mM NaCl and 2mM βME. Cells were lysed by a disruptor (Constant Systems Limited) and proteins were affinity purified using glutathione sepharose (GE Healthcare) in purification buffer. GST-tagged mATG8 constructs were cleaved overnight with recombinant 3C protease at 4^{o}C and eluted in batch. All proteins were further purified by gel filtration on preparative Superdex HiLoad 26/600 or analytical (Superdex 200 10/300) columns (GE Healthcare).

Tepsin antibody production

The tepsin ENTH domain was expressed and purified as described previously (Archuleta et al., 2017). Protein was provided to Genscript to raise an antibody in New Zealand rabbits through three rounds of immunization followed by affinity purification. This tepsin antibody was tested on lysates generated from commercially available HAP1 AP-4 ε (gene: *AP4E1*) and tepsin (gene: *ENTHD2*) KO cell lines (Horizon Discovery) and compared to a published tepsin antibody (Figure A1-3A) provided by the Robinson lab (Borner et al., 2012).

iLIR

Putative LIR motifs discussed in this paper were identified using the iLIR *in silico* resource (https://ilir.warwick.ac.uk/kwresult.php; Jacomin et al., 2016). The putative tepsin LIR motif is found in the list of identified putative LIR motif-containing proteins found searching by gene name (*ENTHD2*). It is also predicted when given the fasta sequence of full-length tepsin.

Structure representation and modeling

Models of tepsin LIR motif interactions with mammalian ATG8 proteins were generated using AlphaFold 2.2 Multimer (Jumper et al., 2021b, 2021a). Models were validated by visualization of peptide residues docked into hydrophobic pockets on the modeled mATG8 surfaces. Each model docked critical LIR motif residues (Trp188 and Leu191) into hydrophobic pockets without major clashes. The models were compared to experimental mATG8-LIR structures by superposition. ChimeraX MatchMaker was used to superpose AlphaFold2 models with experimental structures deposited in the Protein Data Bank. All structural figures were generated in ChimeraX.

GST-pulldown assays

GST or tepsin-GST fusion proteins (50 µg) and indicated prey proteins at a 5X molar excess to tepsin (mATG8 and/or AP-4 β4 appendage) were incubated with glutathione sepharose resin (GE Healthcare) for 2 hours at 4ºC in 20 mM HEPES (pH 7.5), 100 mM NaCl, 0.5% NP-40 and 2 mM DTT. Resin was washed three times with the same buffer. Proteins were eluted from the resin using the wash buffer plus 30 mM

reduced glutathione. Elution buffer was incubated with resin for 20 min on ice with gentle agitation every 2 minutes. Gel samples were prepared from the supernatant following elution with glutathione, and the assay was analyzed by Coomassie staining and Western blotting of SDS-PAGE gels. When further analyzed by Western blot, His-tagged prey protein were detected using anti-His6-HRP conjugated primary antibody (Abcam, ab184607). Uncropped gels and films are displayed in Figure A1-7.

Isothermal titration calorimetry

Isothermal titration calorimetry (ITC) experiments were conducted on a NanoITC instrument (TA Instruments) at 25^{o}C. Molar peptide concentration in the syringe was at least 6.5 times that of protein in the cell; 0.13 mM LC3B was placed in the cell and 0.845 mM tepsin LIR peptide was placed in the syringe. The tepsin LIR peptide was synthesized (Genscript) with the native tepsin sequence (residues 185-192; SGGGWDELS) and an additional serine added for solubility (underlined). All experiments were carried out in 20 mM HEPES (pH 7.5), 100mM NaCl and 0.5 mM TCEP, filtered and degassed. Incremental titrations were performed with an initial baseline of 120 seconds and injection intervals of 200 seconds. Titration data were analyzed in NANOANALYZE (TA Instruments) to obtain a fit and values for stoichiometry (n) and equilibrium association (K_a). K_D values were calculated from the association constant.

Tissue culture

HAP1 cell lines (Horizon Discovery; *AP4E1* KO: HZGHC000768c003; *ENTHD2* (tepsin) KO: HZGHC000845c002; Parental HAP1: C631) were maintained in IMDM

(Gibco) supplemented with 10% v/v fetal bovine serum (FBS; R&D Systems). Stable tepsin-GFP (Borner et al., 2012) and mRFP-GFP-LC3B (Sarkar et al., 2009) HeLa cell lines were obtained as gifts from the Robinson and Rubinsztein labs (Cambridge Institute for Medical Research), respectively. Cells were maintained in MEM-alpha (Gibco), supplemented with 10% v/v fetal bovine serum and 600 µg/mL G418 (Corning) at 37ºC in a 5% CO_2 atmosphere. Cell lines were routinely monitored for mycoplasma contamination using DAPI to stain DNA. For starvation during autophagy assays, cells were washed twice with Earle's balanced salt solution (EBSS; Gibco) and incubated with EBSS for 2 hours. Basal cells were concurrently given fresh complete media for the same duration. Where indicated, cells were treated with 100 nM Bafilomycin A1 (Millipore-Sigma) in either EBSS or complete cell media for 2 hours.

Western blotting

Cells were resuspended and lysed in NP-40 lysis buffer (10 mM HEPES [pH 7.5], 150 mM NaCl, 0.5 mM ethylenediaminetetraacetic acid (EDTA), 1% NP-40, and 1 cOmplete Mini EDTA-free Protease Inhibitor Cocktail (Roche). Cell slurry was vortexed briefly then incubated on ice for 30 minutes. The cell slurry was then centrifuged at 20,500 x RCF for 30 minutes. The soluble fraction (lysate) was reserved, and total protein concentration was measured using Precision Red (Cytoskeleton). Normalized samples were denatured with SDS loading buffer (250mM Tris [pH 6.8], 50 mM DTT, 10% v/v SDS, 20% v/v glycerol, 0.5% w/v bromophenol blue) and boiled for 1 min at 95ºC. Samples were subjected to SDS-PAGE using 4-20% gels (Bio-Rad) and transferred to PVDF membranes (Immobilon-P; Millipore). Blots were incubated with indicated primary and

HRP-conjugated secondary antibodies then detected using Amersham ECL Western blotting reagents (GE Healthcare). All uncropped blots are shown in Figure A1-7. Where indicated, Western blot results were quantified using the ImageStudio lite software (LI-COR). Statistical significance was analyzed using R (R Core Team, 2021) with scripts written in RStudio to run one-way ANOVA with Tukey post-hoc test or Student's t-tests as appropriate. The following packages were used in R for data management, statistical testing, and data visualization: tidyverse (Wickham et al., 2019); rstatix (Kassambara, 2021); and viridis (Garnier et al., 2021).

GFP immunoprecipitation assays

Cell lysates from tepsin-GFP or mRFP-GFP-LC3B HeLa cells were prepared as described above. Lysate was incubated with unconjugated agarose (control) resin (Chromotek) for 30 min at 4^{o}C to reduce background binding. This pre-cleared lysate was divided equally among GFP-trap resin (Chromotek) and fresh control resin for co-immunoprecipitation (IP) experiments. An equal volume of dilution buffer (20 mM HEPES [pH 7.5], 150mM NaCl, 0.5 mM EDTA, 1 cOmplete Mini EDTA-free Protease Inhibitor Cocktail tablet per 20 mL) to lysate was added to each sample then IPs were incubated 1 h at 4^{o}C followed by three washes with dilution buffer. IPs were eluted by adding SDS loading buffer to the washed resin pellet and boiling for 5 minutes at 95^{o}C.

siRNA knockdown and DNA transfection

Cells were seeded on 6 well plates and used in knockdown assays the following day. AP-4 knockdown was achieved using ON-TARGETplus AP4E1 siRNA (J-021474-

05; Dharmacon) and tepsin knockdown was achieved using ON-TARGETplus C17orf56 siRNA (J-015821-17; Dharmacon). Control cells were treated with ON-TARGETplus non-targeting siRNA (D-001810-01; Dharmacon). Transfections of siRNA were carried out with Oligofectamine (Thermo Fisher Scientific) with a final siRNA concentration of 7.5 nM (for each AP-4, tepsin, and control siRNA treatment) in complete culture media and assayed 48 hours after transfection. Cells were re-seeded 24 hours after siRNA treatment to a lower cell density on 6 well plates (with or without coverslips) for Western blotting and immunofluorescence assays. For rescue experiments, cells were subjected to an additional transfection step. Transfection with siRNA was conducted as described above, but cells were seeded into and maintained throughout the experiment in antibiotic-free media (MEM-alpha with 10% FBS, no G418). 4 hours after incubation with siRNA treatment, wild-type and mutant tepsin-myc constructs were transfected using Fugene 4K (Promega) at 1.5:1 Fugene:DNA ratio following manufacturer protocol. Replating and a total time course of 48 hours from initial siRNA knockdown were maintained as described above.

Fluorescence microscopy

Cells were seeded onto 12 mm #1.5 glass coverslips (Fisher Scientific) coated with Histogrip (Invitrogen). Coverslips were imaged with a Nikon Spinning Disk confocal microscope equipped with a Photometrics Prime 95B sCMOS monochrome camera; Plan Apo Lambda Oil 60x 1.40 NA WD 0.13mm objective; 405, 488, 561, and 647 nm excitation lasers. Image analysis was conducted using Nikon's NIS Elements AR Analysis software GA3 pipelines.

For autophagic flux assays: mRFP-GFP-LC3B cells were fixed in 3% paraformaldehyde (Electron Microscopy Sciences) in PBS-CM (1X PBS with 0.1 mM $CaCl_2$, 1 mM $MgCl_2$) at room temperature for 20 minutes. Residual paraformaldehyde was quenched by incubating with 50 mM NH_4Cl for 10 minutes. Coverslips were washed three times in PBS-CM with a final wash in Milli-Q H_2O (Millipore Sigma). To preserve fluorophore signal, coverslips were kept in a dark box during all incubations. Coverslips were mounted in Prolong Diamond with DAPI (Invitrogen). Quantification of autophagic flux was performed using spinning disk confocal z-stack images. Individual cell regions of interest (ROIs) were generated using the “grow objects” function on the DAPI [excitation: 405 nm] signal. Punctate structures corresponding to autophagosomes (defined as having mRFP [excitation: 561 nm] and GFP [excitation: 488 nm] signal) or autolysosomes (mRFP signal only) were segmented using the “threshold” function then subjected to 3D analysis functions to obtain object counts and measure object volume. Data from each replicate was transformed using min-max normalization and individual data points from all replicates were combined for statistical analysis and data visualization.

For immunofluorescence assays: mRFP-GFP-LC3B cells were either fixed and permeabilized in ice-cold methanol for 10 minutes at -20ºC (tepsin-myc rescue experiments) or fixed in 3% paraformaldehyde PBS-CM followed by 5 min permeabilization with ice cold methanol at -20ºC. Coverslips were washed three times with PBS-CM then blocked for 1 hour in 1% bovine serum albumin (BSA) in PBS-CM. Primary antibody incubations were conducted overnight at 4ºC. The next day, coverslips were washed 3 times (10 minutes each) with BSA blocking buffer. Fluorescent secondaries were diluted in BSA blocking buffer and incubated for 2 hours at room

temperature protected from light. Coverslips were then washed two times with BSA block, once with PBS-CM, and once with dH_2O before being mounted in Prolong Diamond with DAPI. Fixation effectively quenched exogenous mRFP-GFP-LC3B signal confirmed by comparing secondary antibody-only control cells to immuno-stained cells (Figure A1-3C). Quantification of ATG9A object measurements and colocalization with TGN46 was performed using spinning disk confocal z-stack images. Individual cell ROIs were generated using the 3D segmentation "OR" function to combine two ROIs (ROI-A and ROI-B) resulting in more precise cell segmentation. ROI-A was defined by the DAPI [excitation: 405 nm] signal subjected to the "grow objects" function and ROI-B was defined by the ATG9A channel [excitation: 647 nm] subjected to the "fast smooth" function (sigma=25 or sigma=18 [rescue experiments]). Combined ROIs were subjected to the "separate objects" function to generate final individual cell ROIs. ATG9A and TGN46 channels were background subtracted using the "detect regional maxima" function. The TGN was segmented using an intensity threshold on the TGN46 channel [excitation: 488 nm]. ATG9A objects within the TGN segmented area were defined as "*trans*-Golgi ATG9A" and ATG9A objects outside the TGN area were defined as "non-Golgi ATG9A". The two populations of ATG9A objects were subjected to 3D measurement functions "max object intensity" and "object volume". For Manders' colocalization analysis, max intensity projections were generated for the ATG9A and TGN46 channels followed by background subtraction by the "detect regional maxima" function. For tepsin-myc rescue experiments, the mean intensity of the myc channel in each cell area was measured and used to subset the dataset in RStudio to specifically analyze transfected cells. Data across all replicates was combined for statistical analysis and data visualization.

All statistical significance was analyzed using R with scripts written in RStudio and packages described above. Normalcy was assessed based on box-and-whisker plots for all data. These data did not exhibit a normal Gaussian distribution, so non-parametric tests were used. Nonparametric analysis of variance was assessed by the Kruskal-Wallis test and significant results were followed by a Dunn test with Bonferroni correction. When appropriate, two independent samples were compared using the Mann-Whitney U test. Data was graphed using ggplot2 functions in RStudio.

ACKNOWLEDGEMENTS

We sincerely thank Margaret Robinson (Cambridge Institute for Medical Research) for providing the tepsin-GFP HeLa cell line and David Rubinsztein (Cambridge Institute for Medical Research) for providing the mRFP-GFP-LC3B HeLa cell line. We also thank members of the Jackson lab for helpful discussion and critical reading of the manuscript. NSW, JEG, CIC, and LPJ are supported by NIH R35GM119525. LPJ is a Pew Scholar in the Biomedical Sciences, supported by the Pew Charitable Trusts. NSW and CIC were partly supported by the Molecular Biophysics Training Grant NIH 5T32GM008320. JEG was partly supported by the Postdoctoral Program in Functional Neurogenomics NIH 5T32MH065215. Imaging and image analysis was performed in part using the Vanderbilt Cell Imaging Shared Resource (supported by NIH grants CA68485, DK20593, DK58404, DK59637 and EY08126).

III. AP-4 LOSS IN CRISPR-EDITED ZEBRAFISH AFFECTS EARLY EMBRYO DEVELOPMENT

Olivia G. Pembridge[1†], Natalie S. Wallace[1,2†], Thomas P. Clements[1], Lauren P. Jackson[1,2,3*]

[1]Department of Biological Sciences, Vanderbilt University, Nashville, TN, USA

[2]Center for Structural Biology, Vanderbilt University, Nashville, TN, USA

[3]Department of Biochemistry, Vanderbilt University, Nashville, TN, USA

† OGP and NSW contributed equally to this work

*Correspondence to lauren.p.jackson@vanderbilt.edu

Division of work: In this co-first author paper, Olivia Pembridge performed CRISPR-editing and characterized AP-4 or tepsin knockout zebrafish. Natalie Wallace and Olivia Pembridge performed quantitative gene expression experiments with statistical analysis by Natalie Wallace. Natalie Wallace drafted the original manuscript.

This article has been published under the same title in *Advances in Biological Regulation*, 2022, 100945 and is reproduced here with permission from all co-authors.

ABSTRACT

Mutations in the heterotetrametric adaptor protein 4 (AP-4; ε/β4/μ4/σ4 subunits) membrane trafficking coat complex lead to complex neurological disorders characterized by spastic paraplegia, microcephaly, and intellectual disabilities. Understanding molecular mechanisms underlying these disorders continues to emerge with recent identification of an essential autophagy protein, ATG9A, as an AP-4 cargo. Significant progress has been made uncovering AP-4 function in cell culture and patient-derived cell lines, and ATG9A trafficking by AP-4 is considered a potential target for gene therapy approaches. In contrast, understanding how AP-4 trafficking affects development and function at the organismal level has long been hindered by loss of conserved AP-4 genes in key model systems (*S. cerevisiae*, *C. elegans*, *D. melanogaster*). However, zebrafish (*Danio rerio*) have retained AP-4 and can serve as an important model system for studying both the nervous system and overall development. We undertook gene editing in zebrafish using a CRISPR-ExoCas9 knockout system to determine how loss of single AP-4, or its accessory protein tepsin, genes affect embryo development 24 hours post-fertilization (hpf). Single gene-edited embryos display abnormal head morphology. We further conducted the first exploration of how AP-4 single gene knockouts in zebrafish embryos affect expression levels and patterns of two autophagy genes, *atg9a* and *map1lc3b*. This work suggests zebrafish may be further adapted and developed as a tool to uncover AP-4 function in membrane trafficking and autophagy in the context of a model organism.

INTRODUCTION

Large multi-subunit coat protein complexes are essential for the movement of transmembrane protein cargoes and lipids to distinct membrane-bound organelles within cells. Disruption or loss of trafficking coat complexes is often severely detrimental to human health (reviewed Sanger et al., 2019). Mutations in the adaptor protein 4 (AP-4; ε/β4/μ4/σ4 subunits) heterotetrametric complex in humans result in a family of neurological disorders called AP-4-deficiency syndrome (Ebrahimi-Fakhari et al., 2020) characterized by spastic paraplegia, microcephaly, and intellectual disability (Abdollahpour et al., 2014; Abou Jamra et al., 2011; Bauer et al., 2012; Ebrahimi-Fakhari et al., 2018; Hardies et al., 2015; Jameel et al., 2014; Tessa et al., 2016).

AP-4 is recruited to the *trans*-Golgi network (TGN) by the small GTPase, Arf1 (Boehm et al., 2001), where it forms a coat and recognizes specific transmembrane protein cargoes (Burgos et al., 2010; Simmen et al., 2002; Yap et al., 2003). Molecular mechanisms underlying AP-4-deficiency syndrome in human patients have recently emerged with identification of new cargo proteins. Both ATG9A (Davies et al., 2018; Ivankovic et al., 2020; Mattera et al., 2017) and diacylglycerol lipase β, or DAGLB (Davies et al., 2022), are now established to be proteins sorted out of the TGN by AP-4. In addition, several accessory proteins have been identified in trafficking AP-4 cargoes (Davies et al., 2022, 2018; Mattera et al., 2020b). Accessory proteins in trafficking coats perform diverse functions regulating vesicle formation, scission, targeting, or uncoating (Merrifield and Kaksonen, 2014; Zouhar and Sauer, 2014). ATG9A export from the TGN and anterograde transport towards the cell periphery depends on RUSC1 and RUSC2

(Davies et al., 2018; Guardia et al., 2021). Regulation of ATG9A subcellular distribution is also partially regulated by Hook1 and Hook2, which coordinate retrograde trafficking as part of the FHF (FTS, Hook, and FHIP) complex (Mattera et al., 2020b). Tepsin was the first identified accessory protein in AP-4 coats (Borner et al., 2012), but its molecular role within the coat remains unclear. Tepsin is considered a member of the epsin family (Rosenthal et al., 1999) because it contains an Epsin N-Terminal Homology (ENTH) domain. However, multiple lines of evidence, including X-ray structural and biochemical data, suggest tepsin has functionally diverged from other epsin family members (Archuleta et al., 2017; Frazier et al., 2016; Mattera et al., 2015). While no pathogenic mutations have been identified, tepsin loss-of-function studies would greatly contribute to our understanding of AP-4 coat function and biology.

Emerging data on both AP-4 and its accessory proteins have significantly improved understanding of AP-4-deficiency syndrome at the cellular level, and loss of ATG9A export from the TGN can be used as a diagnostic marker of AP-4 related disorders in patient classification (Behne et al., 2020; Ebrahimi-Fakhari et al., 2021). ATG9A is an essential autophagy protein (Noda et al., 2000; Young et al., 2006) and has recently emerged as a lipid scramblase (Guardia et al., 2020a; Maeda et al., 2020a; Matoba et al., 2020) during early stages of autophagy (Orsi et al., 2012; Yamamoto et al., 2012). Experiments in mammalian cell culture suggest AP-4 impacts ATG9A sorting to the cell periphery (Davies et al., 2018; Mattera et al., 2020b), which links AP-4 trafficking indirectly to regulation of cellular homeostasis through the autophagy pathway (reviewed in Galluzzi et al., 2017). However, it remains unclear why the severe phenotypes associated with

these disorders appear to be specific to the nervous system since AP-4 proteins are ubiquitously expressed.

Study of AP-4 trafficking pathways and deficiencies in organisms has been impacted by loss of conserved AP-4 genes across many common model organisms including budding and fission yeast (*S. cerevisiae* and *S. pombe*), worms (*C. elegans*), and fruit flies (*D. melanogaster*) (Hirst et al., 2013b). Two knockout mouse models targeting the large subunits ε (gene: *AP4E1*) (de Pace et al., 2018) and β4 (gene: *AP4B1*) (Matsuda et al., 2008b) have reported phenotypes linked to trafficking and autophagy defects, but mouse models have only partly recapitulated human disease. *AP4B1* knockout mice present no gross motor or cognitive deficits. *AP4E1* knockout mice display impaired performance in motor function tests and exhibit neuroanatomical abnormalities similar to those observed in human patients, though only partially model the severity of motor and cognitive phenotypes typical of AP-4-deficiency disorders. It remains very beneficial to establish a model system like zebrafish, because organisms having a shorter life span and well-established suite of tools will allow researchers to study a time-course of organismal development with a large sample size. One study has reported how a morpholino knockdown of *ap4s1* gene (AP4 σ4 subunit) yields embryos with altered neural development including small head size, irregular eye development, and locomotor deficits (D'Amore et al., 2020).

In this study, we generated CRISPR gene-edited F0 knockout zebrafish containing single gene deletions of individual AP-4 (*ap4e1, ap4b1, ap4m1, ap4s1*) subunits or the accessory protein, tepsin (*enthd2)*. We utilized an established CRISPR-ExoCas9 approach to produce larger deletions at an increased hit rate (Clements et al., 2017). We

characterized phenotypes at 24 hours post-fertilization (hpf) and found all gene-edited embryos consistently display developmental defects characterized by abnormal head shape, enlarged yolk sacs, and neural tissue malformation. We monitored autophagy gene expression in knockout embryos using reverse transcription quantitative PCR (RT-qPCR) on two genes: *atg9a*, an essential scramblase, and *map1lc3b*, (LC3B; reviewed in Wesch et al., 2020), an autophagy marker used in cultured cells and organisms (Klionsky et al., 2021). CRISPR-edited tepsin knockout embryos showed a trend towards increased *atg9a* expression. Finally, *in situ* hybridization data suggest both genes display altered patterns early in zebrafish development. Together, these data suggest loss of single AP-4 or tepsin genes gives a consistent phenotype in zebrafish and suggests either AP-4 or tepsin loss may yield trafficking or autophagy defects.

RESULTS

CRISPR-edited zebrafish lacking AP-4 or tepsin genes exhibit morphological defects

We investigated whether *Danio rerio* could be used as a model system for understanding and exploring AP-4 trafficking. We generated single gene knockout models using a modified CRISPR technology referred to as CRISPR-ExoCas9, in which fusion of an exonuclease (Exo1) to the Cas9 protein improves overall hit rate and produces larger deletions (summarized in Figure A2-1A) (Clements et al., 2017). This approach and overall ExoCas9 efficiency were confirmed by recapitulating pigment loss in the eye of tyrosinase CRISPR-edited knockout (KO) embryos (Figure A2-1B) in line with published

data (Clements et al., 2017). This control also established injection trauma is not likely to explain phenotypes described below for single gene AP-4 or tepsin knockouts. We individually targeted genes corresponding to each AP-4 subunit (*ap4b1*, *ap4e1*, *ap4m1*, and *ap4s1*) and tepsin (*enthd2*). For clarity, we will describe knockout embryos using standard zebrafish gene nomenclature. Following injection of both ExoCas9 and small guide RNAs (sgRNAs), embryos were initially monitored over a period of three days post-fertilization (dpf), and recurring phenotypic variations from wild-type embryos of the same clutch were noted. A preliminary characterization revealed greater than 90% of injected embryos died (Table 3-1) by 3 dpf. Phenotypes were instead scored at 24 hours post-fertilization (hpf) in the F0 generation, and representative phenotypic classes for each gene knockout are shown in Figure A2-2).

Gene & sgRNA	Injected embryos (N)	Embryos surviving (3 dpf)
ap4b1 sgRNA-1	128	3
ap4b1 sgRNA-2	31	0
ap4e1 sgRNA-1	66	6
ap4m1 sgRNA-1	51	4
ap4s1 sgRNA-1	55	2
enthd2 sgRNA-1	28	2

Table 3-1: Preliminary characterization of AP-4 subunit and *enthd2* single gene knockout phenotypes. Total number of embryos injected with individual sgRNAs (N) and the number of surviving phenotypic embryos observed at 3 days post-fertilization (dpf).

A consensus phenotype emerged across *ap4b1*, *ap4e1*, *ap4m1*, *ap4s1*, and *enthd2* single gene KO embryos. Each knockout model exhibited stunted head development, sometimes lacking a defined head region while still retaining a distinct tail region with somites (Figure 3-1; columns 1 & 2). At 24 hpf, single gene knockout embryos

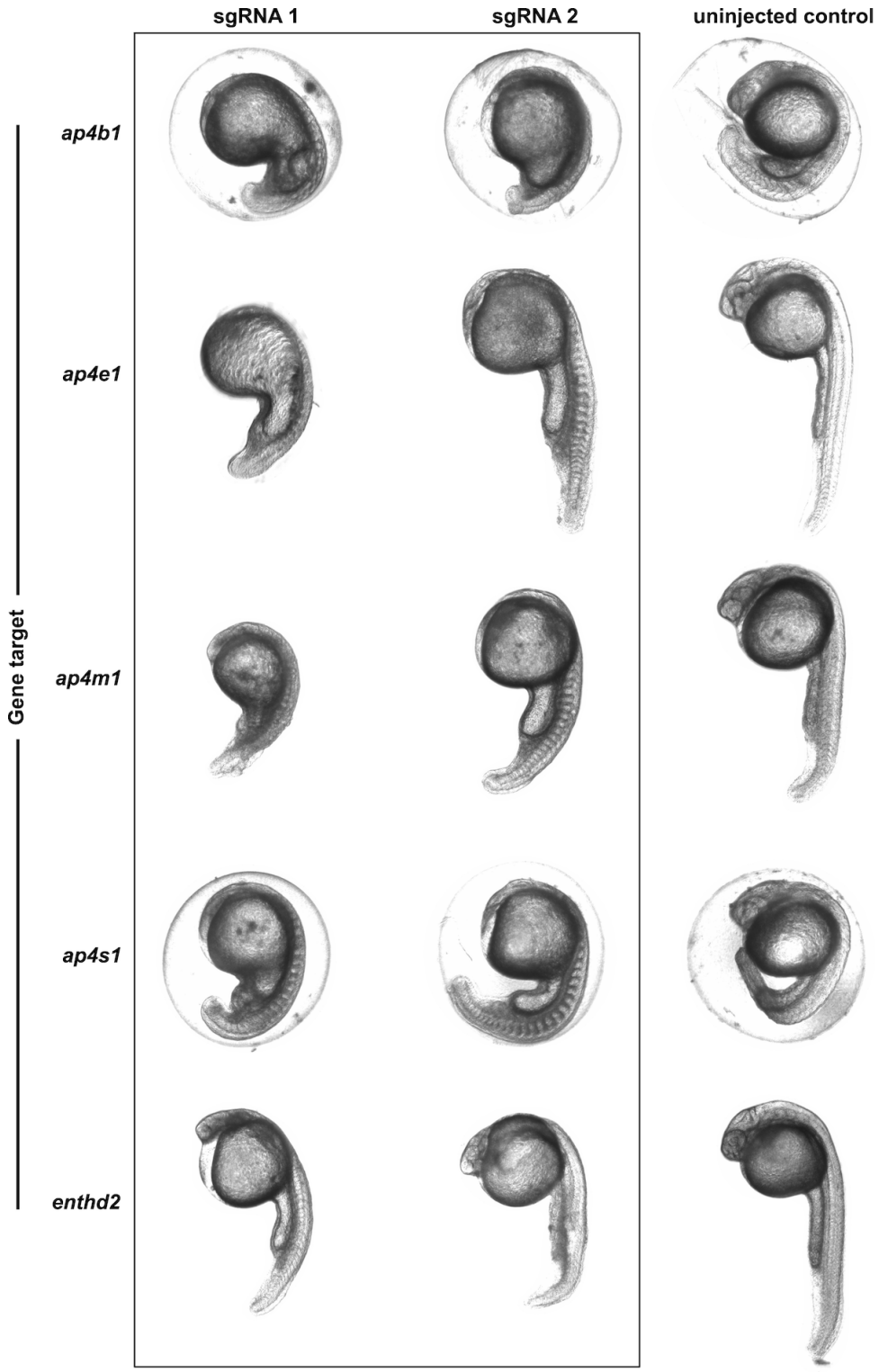

Figure 3-1: AP-4 or tepsin gene loss causes irregular head size and neural necrosis in zebrafish. Representative intermediate knockout phenotypes of each AP-4 subunit or tepsin gene at 24 hours post-fertilization (hpf). Rows depict gene target, and columns depict injection condition. Knockout embryos display irregularly small heads with neural necrosis compared to the uninjected (wild-type) control. This phenotype is consistent across all guide RNAs for all five KO genes (N values; Table 3-2). Uninjected 24 hpf embryos are from the pair-matched clutch for each of the knockout embryos.

exhibited a global developmental delay with enlarged yolk sac and shorter length. These embryos contained fewer somites than expected at 24 hpf and looked more reminiscent of earlier developmental stages (e.g. 15-somite to 25-somite stages; Kimmel et al., 1995). These phenotypes were not observed in uninjected wild-type embryos from the same clutch (Figure 3-1; column 3, “uninjected control”). *Ap4b1*, *ap4e1*, *ap4m1*, and *ap4s1* KO embryos using two independent sgRNA targeting different sites produced similar phenotypic ratios (Table 3-2); approximately 50-60% of injected AP-4 gene knockout embryos displayed phenotypic traits characterized as intermediate or severe (Table 3-2).

sgRNA	% None	% Intermediate	% Severe	Total embryos (N)
ap4b1 sgRNA-1	36	46	18	124
ap4b1 sgRNA-2	41	44	14	63
ap4e1 sgRNA-1	53	40	7	75
ap4e1 sgRNA-2	43	52	5	98
ap4m1 sgRNA-1	52	43	5	95
ap4m1 sgRNA-2	47	47	6	144
ap4s1 sgRNA-1	55	38	8	88
ap4s1 sgRNA-2	51	39	10	89
enthd2 sgRNA-1	72	24	4	82
enthd2 sgRNA-2	91	7	1	140
enthd2 sgRNA-3	68	31	2	124

Table 3-2: Classification of AP-4 subunit and *enthd2* single gene knockout embryos. Percentages of embryos scored into each of three phenotypic scoring categories. Percentages calculated from total number of replicates (N) for each knockout type and rounded to the nearest whole percent.

Three sgRNAs were utilized for *enthd2* knockouts because one sgRNA (“sgRNA-2”, Table 3-2) demonstrated low hit rates and thus lower phenotypic ratios. However, *enthd2* sgRNA-1 and sgRNA-3 independently gave hit rates near 30%, suggesting it may be

more difficult to target tepsin than single AP-4 genes. The consistency across multiple guide RNAs and across all four AP-4 genes suggests these phenotypic effects arise from AP-4 loss during early development.

We verified whether CRISPR-mediated gene editing was successful by sequencing embryos scored in the intermediate class (Figure 3-2; Figure A2-3). Representative reads for *ap4b1* (Figure 3-2A, 3-2B), *ap4e1* (Figure A2-3A, A2-3B), *ap4m1* (Figure A2-3C, A2-3D), *ap4s1* (Figure A2-3E, A2-3F), and *enthd2* (Figure 3-2C, 3-2D) indicate CRISPR-edited embryos for each single gene exhibited nucleotide insertions, deletions, or mutations in regions surrounding the sgRNA target sites. *Ap4b1* knockout occurred with the highest efficiency compared to other AP-4 genes (Figure 3-2A, percent reads), which is a notable result in the context of established patient mutations (see Discussion). Overall, sequencing data confirm successful CRISPR-mediated gene editing in zebrafish embryos for all genes, although tepsin (*enthd2*) knockouts exhibited lower efficiency.

Autophagy gene expression quantification in AP-4 zebrafish knockout models

We chose to follow up with two gene-edited knockout models to look at potential effects on autophagy genes. Published models of AP-4-deficiency syndrome in multiple cell lines focus on ATG9A export from the TGN to the cell periphery (Davies et al., 2018; Mattera et al., 2017). This suggests a link between AP-4 trafficking and autophagy, since ATG9A is both an essential autophagy protein (Noda et al., 2000; Young et al., 2006) and an AP-4 cargo. We selected *ap4b1* KO embryos for follow-up, because these embryos consistently yielded the largest percentage demonstrating intermediate or severe

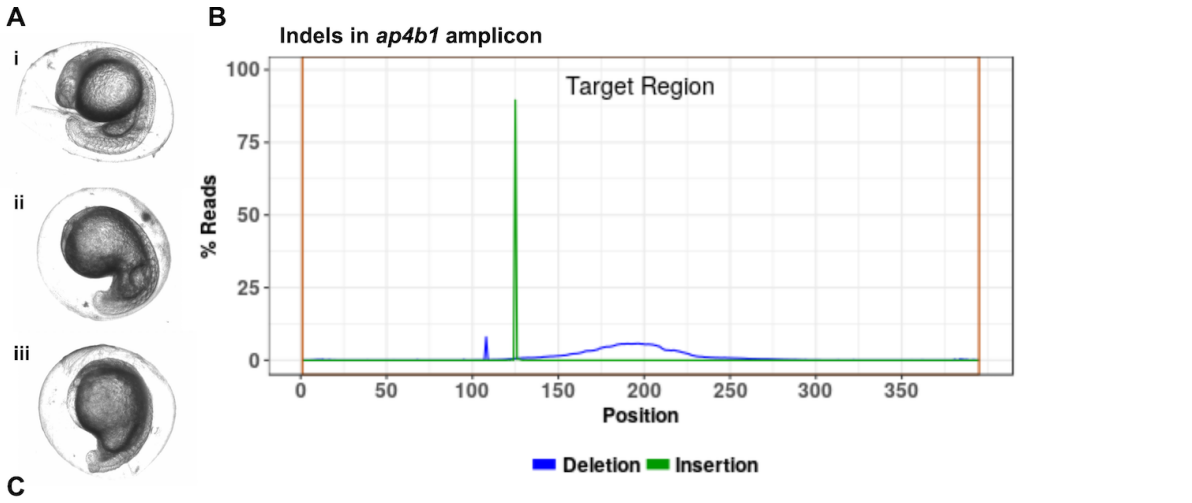

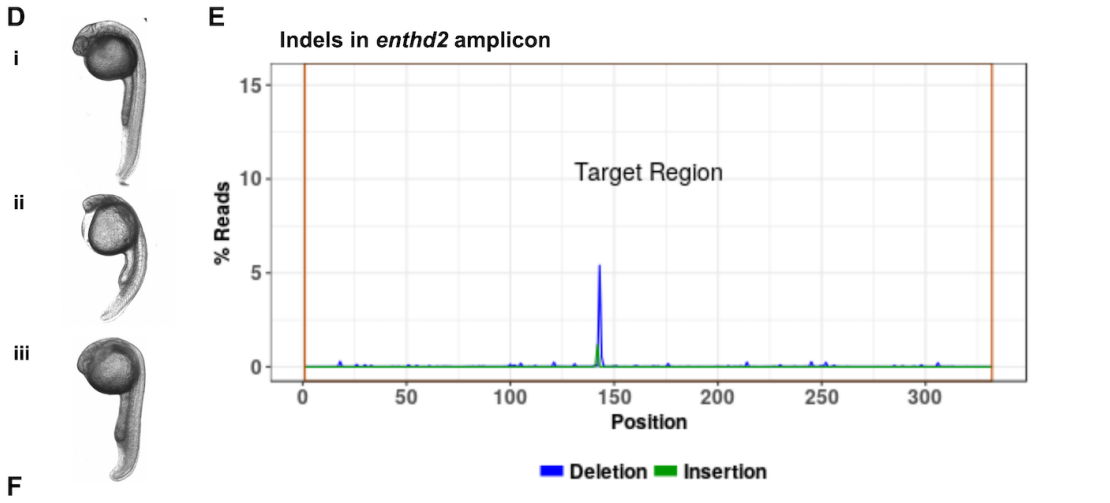

Figure 3-2: Sequencing validates successful *ap4b1* and *enthd2* single gene knockout zebrafish embryos. Embryos displaying intermediate phenotypes (Figure 1; Figure S2) were analyzed by Amplicon EZ deep sequencing (Azenta). Percentage of reads containing insertions (green) or deletions (blue) in the sgRNA target site (gray box) are displayed for representative *ap4b1* (A) and *enthd2* (C) KO embryos. Sequencing data were obtained from a single representative 24 hpf embryo in the intermediate phenotype category. (B, D) Three different representative reads (R1, R2, R3) from sequencing of the *ap4b1* (B) and *enthd2* (D) KO embryos are shown together with the WT sequence (underlined target site highlighted in gray with nucleotide numbers marked). Both point mutations (yellow) and deletions (dashes) are observed.

phenotypes (Figure 3-1; Figure A2-2; Table 3-2). Human patients also contain mutations in the β4 subunit with higher frequency than other subunits (Ebrahimi-Fakhari et al., 2020; Gadbery et al., 2020). We also selected *enthd2* KO embryos, because the function of tepsin within AP-4 coats remains elusive. We probed *atg9a* gene expression levels in both wild-type and knockout fish to establish whether *ap4b1* or *enthd2* loss affects *atg9a* expression. We also probed *map1lc3b* (LC3B). LC3B is a well-established autophagy marker in cultured cells and in model organisms from budding yeast to higher metazoans (reviewed in Klionsky et al., 2021) that influences autophagosome formation and expansion (Wesch et al., 2020; Xie et al., 2008).

We used reverse transcription quantitative PCR (RT-qPCR) to analyze *atg9a* gene expression in *ap4b1* and *enthd2* knockout embryos. We observed a trend towards elevated expression levels in tepsin (*enthd2*) knockout compared to wild-type embryos, but this result was not statistically significant likely due to variability across mosaic samples (Figure 3-3A). *Atg9a* expression in *ap4b1* knockout embryos was no different from levels observed in wild-type embryos (Figure 3-3A). *Map1lc3b* expression levels in both *ap4b1* and *enthd2* knockout embryos

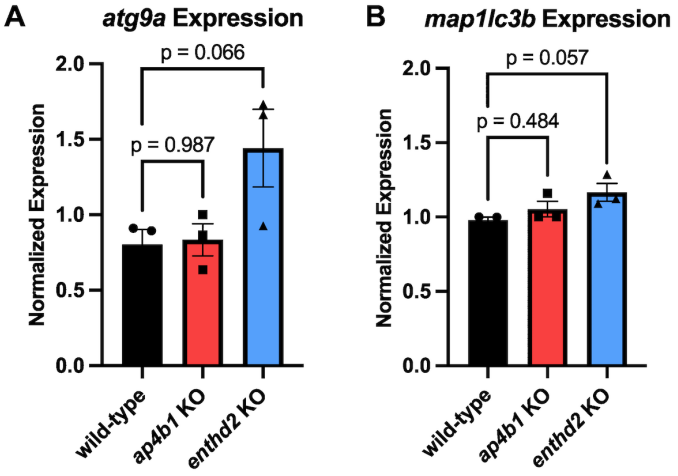

Figure 3-3: Autophagy gene expression levels in *ap4b1* and *enthd2* single gene knockout models. Autophagy gene expression at 24 hpf was assayed by RT-qPCR of pooled wild-type, *ap4b1*, or *enthd2* KO embryos. (A) Expression levels of *atg9a* were generally elevated in *enthd2* knockout embryos though not statistically significant. (B) *Map1lc3b* expression levels were not significantly different from WT. Each data point represents a pool of approximately 40 embryos from 3 independent injections. Normalized expression values (determined in Bio-Rad Maestro) were calculated using a control gene (*elfa*). Data are presented as the mean ± SEM with p-value from one-way ANOVA with Dunnett's multiple comparison post-hoc analysis.

were not statistically different from wild-type embryos (Figure 3-3B). In addition, we explored expression patterns of both autophagy genes using *in situ* hybridization. Wild-type *atg9a* (Figure A2-5A) or *map1lc3b* (Figure A2-5B) showed concentrated expression in the central nervous system, including the forebrain and notochord. There are no published reports of *atg9a* expression data in zebrafish embryos, but *map1lc3b* expression observed here is consistent with published data (B. Thisse & Thisse, 2004). Overall, we observed greater *atg9a* and *map1lc3b* staining in the tails of *ap4b1* and *enthd2* knockout embryos compared to wild-type embryos. While non-specific staining can be common in *in situ* hybridization experiments, we did not observe non-specific staining in wild-type embryos (Figure A2-5A, column 1). Additionally, knockout embryos show consistently darker staining for both *atg9a* and *map1lc3b*. This result partially supports the trend observed in RT-qPCR data indicating increased expression levels for *atg9a*. Overall, these data are worth further exploration, because they suggest both ATG9A and LC3B may either be slightly elevated or mis-localized during early development in zebrafish lacking AP-4 coat components.

DISCUSSION

Summary

Overall, this study suggests it is feasible to generate CRISPR-edited zebrafish lacking single genes associated with AP-4 coat components. Independently targeting single AP-4 subunit or tepsin (*enthd2)* genes yields embryos displaying similar gross

morphological phenotypes at 24 hpf, including abnormal head shape and stunted development. These models share some features with human patients, but they also exhibit limitations as tools for future study (discussed below).

Zebrafish models for studying AP-4 trafficking and deficiency

This study aimed to establish whether zebrafish could serve as a suitable model system for studying AP-4 during development or trafficking. The observed phenotypes for zebrafish embryos lacking either single AP-4 or tepsin genes include neural necrosis, stunted head development, and a global developmental delay. These traits are somewhat reminiscent of the microcephaly and altered neuronal development that characterize AP-4-deficiency syndrome in human patients (Abdollahpour et al., 2014; Abou Jamra et al., 2011; Bauer et al., 2012; Ebrahimi-Fakhari et al., 2018; Hardies et al., 2015; Jameel et al., 2014; Tessa et al., 2016). The characterized phenotypes observed in gene-edited zebrafish are broadly consistent with published *ap4s1* studies (D'Amore et al., 2020) in which the σ4 subunit was acutely depleted using morpholinos. Very few knockout embryos developed heads in this study, but in some cases, those with heads appeared to have irregular eye development (data not shown). Unfortunately, the very small sample size prevented assessment of eye development using the approach established for published *ap4s1* knockdown embryos (D'Amore et al., 2020).

The similarities between phenotypes observed here (Figure 3-4A) when single AP-4 genes are genetically removed from zebrafish using CRISPR and human AP-4-deficiency syndrome may suggest both orthologs function broadly in similar trafficking and autophagy pathways (Figure 3-4B) established in mammalian cell culture (Davies et

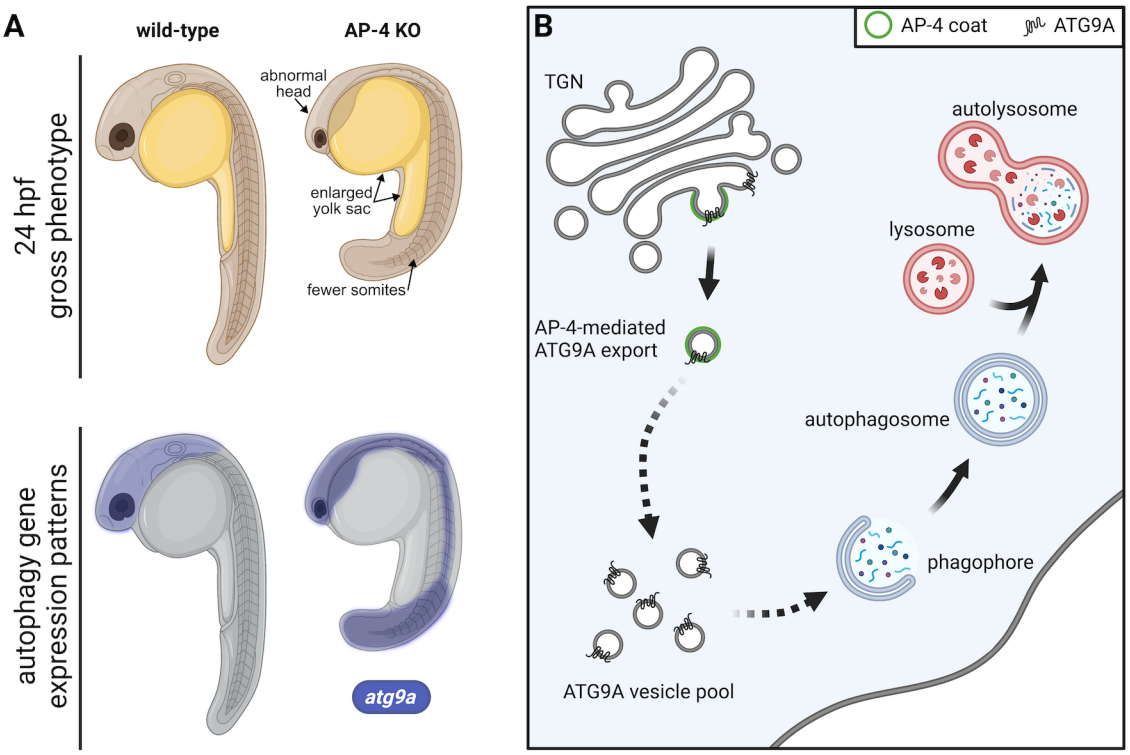

Figure 3-4: Insight into AP-4 loss using knockout zebrafish models. (A) AP-4 and *enthd2* single gene knockout embryos display abnormal head development, enlarged yolk sacs, and shortened tails containing fewer somites. Autophagy gene expression patterns (represented in blue by *atg9a*) exhibit darker staining patterns in the zebrafish brain, notochord, and tail. (B) At the cellular level, AP-4 mediates ATG9A export from the TGN. ATG9A is required for generation and maintenance of autophagosomes, suggests links between AP-4 trafficking and autophagy. CRISPR-edited AP-4 single gene knockout zebrafish models suggest AP-4 loss may be linked to trafficking or autophagy defects early in development. (Created using Biorender)

al., 2022, 2018; de Pace et al., 2018; Guardia et al., 2021; Ivankovic et al., 2020; Mattera et al., 2020b, 2017) and in human patients lacking AP-4 (Behne et al., 2020; Ebrahimi-Fakhari et al., 2021). Zebrafish are an established model organism for studying how proteins function in membrane trafficking (Cox et al., 2018; Edeling et al., 2009; Sarmah et al., 2010), as well as how protein function in the nervous system underlies the basis for complex disorders like hereditary spastic paraplegias (Naef et al., 2019). Since AP-4 genes are absent in other model organisms (Hirst et al., 2013b), using zebrafish as a tool to study AP-4 effects on trafficking or autophagy may be beneficial in the context of uncovering AP-4 biology at the organismal level. However, substantial limitations exist.

AP-4 single gene knockout embryos appear to have notably more severe phenotypes than those observed in human patients. It is possible that human embryos also exhibit high levels of lethality when AP-4 genes are lost or mutated early in human pregnancies, but we do not have a way to validate this. Few zebrafish embryos survive past 3 dpf, thus preventing observation at later developmental stages as well as generation of knockout lines. In addition, the mosaic nature inherent in F0 generation knockouts complicates a more thorough study of zebrafish physiology.

AP-4 is considered an obligate heterotetramer, with all four subunits required for the protein complex to fold and carry out cellular function. However, data presented here indicate *ap4b1* gene loss produced a higher percentage of severe phenotypes compared to other AP-4 genes. This trend is reminiscent of reported data highlighting genetic variation and pathogenicity observed in human populations and patients; published data report both predicted and observed pathogenic variants tend to cluster in the β4 and C-terminal μ4 subunits (Gadbery et al., 2020). This suggests the β4 subunit may be a genetic “hot spot” for viable mutations.

Unlike AP-4, tepsin loss has not been well-explored, particularly since there are no reported human patients with disease-causing mutations. The *enthd2* knockout zebrafish presented here offers an early glimpse into the importance of tepsin in AP-4 coats. Overall, *enthd2* knockout in this study resulted in less severe phenotypes than did AP-4 during early embryo development, but its loss nevertheless corresponded to a low frequency of intermediate and severe phenotypes displaying abnormal head development. Future studies are necessary to understand whether the malformed heads result from delayed development, neural necrosis, apoptosis, or decreased stem cell

proliferation. These data provide additional genetic evidence that tepsin and AP-4 occur in the same pathway, since tepsin loss in zebrafish phenocopies AP-4 loss, which is already well-established in cell culture (Borner et al., 2012; Davies et al., 2018; Frazier et al., 2016).

An emerging role for AP-4 and tepsin in autophagy?

Based on cell culture models, neurological symptoms observed in human patients are thought to arise partly from ATG9A mistrafficking (reviewed in Mattera, de Pace, et al., 2020). ATG9A protein expression is increased in patient-derived fibroblasts and other cell lines lacking AP-4 (Davies et al., 2018; Mattera et al., 2017). We explored whether expression differences occur at the transcriptional level in single gene knockout zebrafish models. Two independent pools of *enthd2* knockout embryos exhibited higher *atg9a* expression levels, but variability in the third replicate resulted in a statistically insignificant result. This is worth further exploration, because these data were obtained from pools of *enthd2* F0 generation embryos despite the *enthd2* sgRNAs exhibiting relatively low hit rates. Low hit rates suggest these embryos are highly mosaic, which could confound accurate determination of *atg9a* expression levels. In spite of this complexity, *enthd2* loss had a more pronounced effect on *atg9a* expression than did *ap4b1* loss. The role of tepsin in AP-4 coats thus remains a particularly interesting area of investigation.

The RT-qPCR results (Figure 3-3) can be further considered alongside *in situ* hybridization data (Figure A2-5). Immunostaining for either autophagy gene (*atg9a* or *map1lc3b*) suggests altered expression patterns in *ap4b1* or *enthd2* single gene knockout embryos compared to wild-type embryos. Together these data indicate loss of AP-4

genes may globally dysregulate autophagy in zebrafish. Future work should explore whether these differences in expression patterns are explained by trafficking defects. This may be challenging to address directly in gene-edited fish. CRISPR-editing can give rise to a complete genetic loss, and surviving fish likely will find ways to compensate. Acute depletion strategies using knockdown approaches may be more appropriate for follow-up in some cases because embryos will survive and can be monitored at relevant developmental stages.

MATERIALS AND METHODS

Zebrafish Care and Embryo Collection

Wild-type AB zebrafish were used for all experiments. Zebrafish were maintained on a 12h/12h light/dark cycle. At the end of the experiments, no longer than 3 dpf, embryos were euthanized. All procedures were conducted in accordance with the Institutional Animal Care and Use Committee (IACUC) at Vanderbilt University under protocol number M1800200-01 (PI: James Patton)

Reagents and Oligonucleotides

All chemicals were purchased from Sigma unless otherwise stated.

CRISPR injections

Zebrafish embryos were injected at the single cell stage (Gagnon et al., 2014) with

modifications for design of single guide RNAs (sgRNAs) and use of ExoCas9 (Clements et al., 2017). The ExoCas9 construct (Clements et al., 2017) was prepared according to published protocol. Two sgRNA target sites were selected for each AP-4 gene, and three were selected for *enthd2* (tepsin). All sgRNA target sequences are listed in Table 3-3.

sgRNA identifier	target sequence
ap4b1 sgRNA-1	GGTGAAAGCCAGTGCCACGG
ap4b1 sgRNA-2	GGACCCAGACCCAGTGGTGG
ap4e1 sgRNA-1	GGCATGGATGTAGCTGAAGG
ap4e1 sgRNA-2	GGCTGAGATGCCGCAGCTCG
ap4m1 sgRNA-1	GGGAAAGAATGAGATCTTTG
ap4m1 sgRNA-2	GAGGGGAATAACTGAAATGG
ap4s1 sgRNA-1	GGAGGAGGAATGGCCGCCCA
ap4s1 sgRNA-2	GGAAAGGGCGCATTGGGAAG
enthd2 sgRNA-1	GGTTGCGCCCTCTGCTGCTG
enthd2 sgRNA-2	GGCTGGGAGGAAACAGACAG
enthd2 sgRNA-3	GGCTGTCCTGGCTATCTCTTCG

Table 3-3: sgRNA target site sequences.

Oligonucleotides for sgRNAs were synthesized (Sigma). Final single guide RNAs were prepared according to published protocol (Clements et al., 2017).

Phenotype Identification and Scoring

Embryos were initially monitored twice daily following CRISPR injections. Embryos displaying divergent morphology were separated as “phenotypic” and surviving phenotypic embryos at 3 dpf were counted (Table 3-1). Subsequently, injected embryos were scored into three phenotypic classes under a dissecting microscope (Leica Zoom 2000) 24 hpf. Those with no apparent differences from wild-type embryos were scored into classification 1 (none). Those with abnormally small (or absent) heads and/or

abnormally shaped eyes were scored into classification 2 (intermediate). Those with morphological abnormalities that prevented head and tail from being clearly distinguished were scored into classification 3 (severe). Representative embryos from each class are displayed in Figure A2-2.

For phenotypic characterization, live embryos were mounted 24 hpf in E3 medium (0.17 mM KCl, 0.33 mM $CaCl_2$, 0.33 mM Mg SO_4, 5% Methylene Blue) on a glass slide (Corning) with no coverslip and photographed under transmitted light on an EVOS FL inverted microscope (Thermo Fisher Scientific). Representative embryos were selected for imaging from total injected embryos (Table 3-2; N) Images were taken both in and out of the chorion. Knockout embryos were always imaged in conjunction with wild-type embryos from the same clutch.

Deep Sequencing

Representative embryos scored in the intermediate classification were chosen for each single gene knockout, and genomic DNA was isolated from individual embryos according to published protocol (Xing et al., 2014). PCR primers (Table 3-4) were designed to amplify the region surrounding each target site (Geneious primer design; product size <500 bp) in the genomic DNA template based on gene transcript data (Ensembl). Following amplification, samples were purified using a QIAquick PCR purification kit (Qiagen) and resuspended in 30 µL sterile water. DNA concentration was determined using a NanoDrop spectrophotometer (Thermo Fisher Scientific) and the samples were diluted to 20 ng/µL. Samples were sequenced using amplicon EZ sequencing (Azenta). INDEL graphs were generated using the Azenta bioinformatics

pipeline.

Gene	5' Forward Primer	3' Reverse Primer
ap4b1	TCTTTGTACTGTGGTCTTCAGTGT	ACATGTTTCTCAGGGCCAGG
ap4e1	GCATGTGTCGACGCACTTAC	TGTTTTGGGAAGGCTCAGCA
ap4m1	AGCGTTTGGTCTTTGCATCT	GCACGGGGACAGTAATGGAA
ap4s1	GAAAACCACAACAGCCGCTC	AAAGCAACCGACGAGTTGTC
enthd2	CCACTGTGCCACCATCTTCA	GCCCACTGACTCATGGGAAA

Table 3-4: Deep sequencing primers to amplify near sgRNA target sites.

RNA extraction

RNA extractions were performed on 40-45 embryos using TRIzol (Thermo Fisher Scientific) after the manufacturer protocol. The resulting pellets were resuspended in 100 µL of sterile water. Samples were visualized on an agarose gel, and RNA yield was quantified using a NanoDrop spectrophotometer (Thermo Fisher Scientific). Where indicated, complementary DNA (cDNA) was generated from RNA using M-MLV Reverse Transcriptase (Promega) according to manufacturer protocol.

In situ hybridization

RNA probes for *in situ* hybridization were designed and prepared (Table 3-5; Thisse and Thisse, 2007) utilizing the two-step amplification method (Hua et al., 2018) with cDNA from pooled embryos (described above). Published primers were ordered for the control gene, *krt4* (Thisse et al., 2001). PCR products were purified using the QIAquick PCR purification kit (Qiagen).

In situ hybridization was modified after a published protocol (Thisse and Thisse,

2007). During the wash step (protocol step 40), embryos were washed twice for 30 minutes each in 0.2X Saline-Sodium Citrate (SSC) buffer (30 mM NaCl, 3 mM sodium citrate) and then washed for 5 minutes at room temperature with 1 mL 1X MAB buffer (100 mM maleic acid, 150 mM NaCl, pH adjusted to 7.5 with 10M NaOH) before being transferred directly to blocking buffer. Following this step, embryos were incubated overnight in 1:2000 anti-DIG Fab fragments (Sigma Aldrich 11093274910) in blocking buffer. Embryos were incubated at room temperature in the dark for 4-8 hours in 1 mL 1X MAB before moving directly to the alkaline buffer wash steps. Following staining, embryos were washed twice with PBST for 5 minutes each, followed by sterile water for 1 minute and stored for 5 days in a 50% benzylalcohol / 50% benzylbenzoate destaining solution. Representative embryos in the intermediate phenotypic category were mounted in glycerol on a bridge slide and imaged on a Nikon AZ 100M wide field microscope at 5X magnification.

Probe	Forward	Reverse	Forward T7	Reverse T7
map1lc3b	TCTGCCTACAA CAAACGTGT	AGCTTCGTGTT TGGGTAGCC	AAGGGAGAGA AGCAACTGCC	GCGCATGCTAATACGACTCACTAT AGGGACCAGCAGGAAGAAAGCCT
atg9a	CTTTCGGTTGC CTGTGTTGG	TGCATGAGCG ACAGTTCTGT	AGGGAATCGC TTGGAGTTGG	GCGCATGCTATACGACTCACTAG GATGACCAGTTGGCGGACAT

Table 3-5: *In situ* hybridization probe sequences.

Reverse transcription quantitative PCR

Reverse transcription quantitative PCR (RT-qPCR) was conducted using iTaq Universal SYBR Green Supermix (Bio-Rad) after manufacturer protocol using cDNA from pooled embryos (described above) and run on a CFX96 Thermocycler (Bio-Rad) in the

Vanderbilt Cell and Developmental Biology Resource Core. Primers for *atg9a* and *map1lc3b* (Table 3-6) were validated by assessing the derivative of a 65-95°C melting curve (Figure A2-4A-C). Normalized expression values were calculated using Bio-Rad Maestro 1.1 software by the ΔΔCq method (defined by the software) with the published control gene, *elfa* (McCurley and Callard, 2008) as a benchmark for normalization (Figure A2-4D). Statistical significance was analyzed using one-way ANOVA with Dunnett's multiple comparison post-hoc testing in GraphPad Prism 9 software.

Gene	Forward	Reverse
map1lc3b	AAGAGGTGCAGGCAAGGATC	CCAACACAGGCAACCGAAAG
atg9a	AAGGGAGAGAAGCAACTGCC	GACCAGCAGGAAGAAAGCCT

Table 3-6: qPCR primer sequences.

ACKNOWLEDGEMENTS

We sincerely thank James Patton for providing advice, zebrafish embryos, and access to the Vanderbilt University zebrafish facility. We thank Qiang Guan for his work maintaining zebrafish in the Vanderbilt University zebrafish facility and Carli Needle for preliminary *in situ* hybridization trials. OGP performed CRISPR injections, characterized phenotypes observed in knockout zebrafish models, and undertook *in situ* hybridization experiments. NSW and OGP conducted RT-qPCR experiments and analyzed data. NSW performed statistical analyses. NSW, OGP, and LPJ wrote the paper with input from all authors. TPC and LPJ conceived the project. OGP, NSW, and LPJ are supported by NIH R35GM119525. LPJ is a Pew Scholar in the Biomedical Sciences, supported by the Pew

Charitable Trusts. NSW was partly supported by the Molecular Biophysics Training Grant NIH 5T32GM008320. Zebrafish work was supervised by TPC and conducted under IACUC protocol M1800200-01 at Vanderbilt University (PI: Patton) using funds from Vanderbilt University and the Pew Charitable Trusts. Imaging was performed in part using the Vanderbilt Cell Imaging Shared Resource (supported by NIH grants CA68485, DK20593, DK58404, DK59637 and EY08126).

IV. THE TEPSIN VHS DOMAIN HARBORS A SECOND LC3B BINDING SITE

INTRODUCTION

While characterizing the tepsin LIR motif interaction with LC3B (see Chapter II), *in vitro* biochemical experiments indicated the tepsin VHS domain mediates a secondary LC3B binding interaction. Specific loss of the LIR motif in cells results in diffuse ATG9A subcellular distribution instead of peripheral accumulation, similar to distribution following tepsin depletion (Chapter II). This difference in phenotypes could be explained by a second LC3B binding site if both interactions are required for AP-4-mediated ATG9A trafficking, because mutating one will not emulate complete tepsin loss. This chapter details preliminary characterization of the VHS domain interaction with LC3B using purified protein in pulldown assays and ITC, as well as structural modeling to identify a candidate binding motif in tepsin.

RESULTS

The tepsin VHS domain binds LC3B in vitro

The tepsin LIR motif resides in a flexible linker between the tepsin ENTH and VHS domains (Chapter II). We purified a panel of tepsin N-terminal GST-fusion proteins intending to show the tepsin LIR/LC3B interaction was unaffected by either the ENTH or

VHS domains (Figure 4-1, left panel). GST-pulldown assays using His-tagged LC3B and either the ENTH domain with the flexible linker (ENTH-LIR; residues 1-220) or the flexible linker with the VHS domain (LIR-VHS; residues 135-356) show both are capable of binding LC3B (Figure 4-1). Binding was detectable by Coomassie staining on an SDS-PAGE gel and further confirmed by probing the 6x-His tag on LC3B by Western blot. Purified ENTH-GST (residues 1-136) or GST-VHS domain (residues 220-360) were used to test for binding in the absence of the LIR motif. Tepsin ENTH-GST showed no detectable binding to LC3B at either Coomassie or Western blot level. Unexpectedly, the

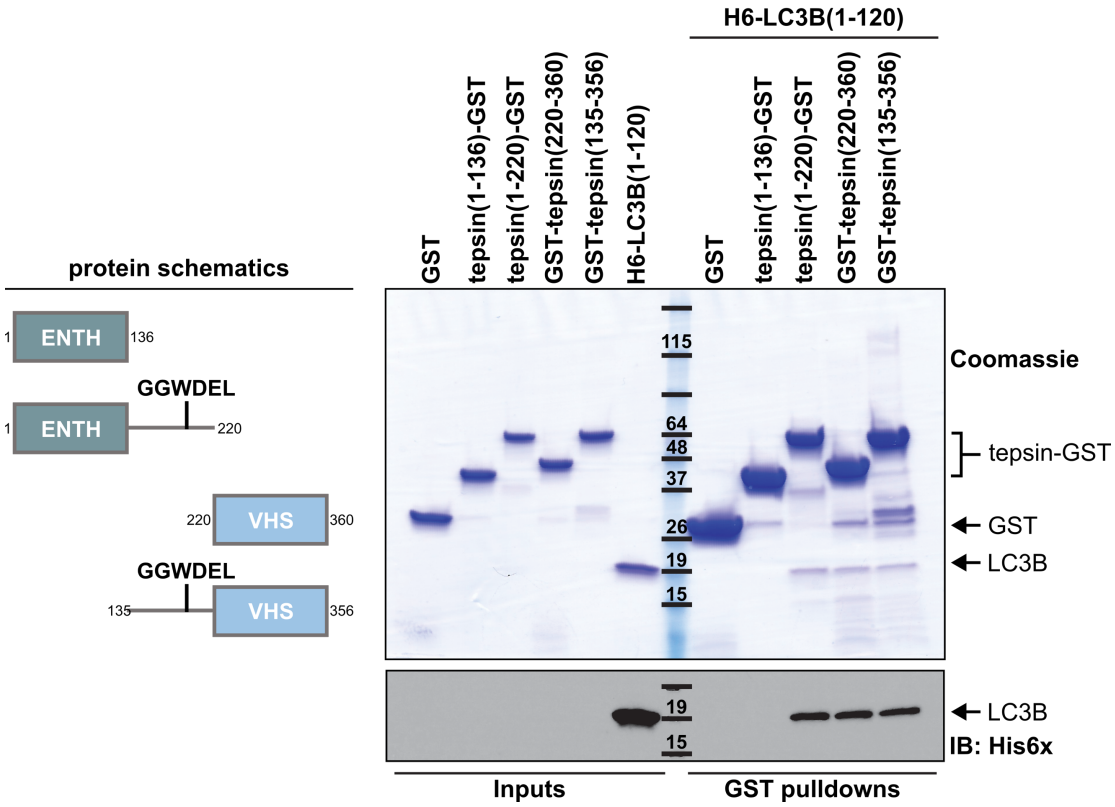

Figure 4-1: The tepsin VHS domain harbors a second LC3B binding site *in vitro*. Coomassie-stained SDS-PAGE gel and Western blot of GST pulldowns using recombinant GST-fusion tepsin proteins (left panel: schematic representations) ENTH (residues 1-136); ENTH-LIR (residues 1-220); VHS (residues 220-360); or LIR-VHS (residues 135-356) with His6x-LC3B (residues 1-120). ENTH-LIR and LIR-VHS both bind LC3B detectable by Coomassie stain and Western blot. The ENTH domain alone does not bind LC3B. The VHS domain alone binds LC3B with seemingly similar affinity to the ENTH-LIR or LIR-VHS proteins indicating the VHS domain may harbor a second LC3B binding site. Free GST was used as a negative control. Representative of three independent experiments.

tepsin VHS domain alone binds LC3B *in vitro,* detectable by Coomassie stain and Western blot (Figure 4-1). This indicates the tepsin VHS domain harbors a second LC3B binding site.

Recombinant LC3B appears to bind ENTH-LIR, LIR-VHS, or VHS proteins at similar levels by Coomassie stain or Western blot detection. This could indicate the VHS/LC3B and the LIR/LC3B interactions cannot occur simultaneously, and thus do not exhibit cooperative binding. To explore this, we used ITC to quantify ENTH-LIR or LIR-VHS binding to LC3B *in vitro* (Figure A3-1). Purified, untagged LIR-VHS (residues 135-356) binds LC3B with weak micromolar affinity (K_D = 262.9 μM ± 104.8 μM). ENTH-LIR (residues 1-220) binds LC3B with a similar weak micromolar affinity (K_D = 148.7 μM; one replicate). These affinities are nearing the range of detection for the instrument used (~300 μM), making it difficult to accurately calculate a binding affinity or to interpret these ITC data. However, the stoichiometry for LIR-VHS/LC3B was typically greater than one, indicating a single molecule of tepsin may be able to bind multiple LC3B molecules simultaneously (see Discussion).

Structural modelling identifies a prospective second LC3B binding motif

Using AlphaFold Multimer (Jumper et al., 2021b, 2021a), we modelled binding between the tepsin VHS domain (residues 220-360) and LC3B. AlphaFold predicts a short motif (ERVEV; residues 233-237) in tepsin binds LC3B (Figure 4-2A) in the LIR docking site (LDS) interface (Figure 4-2B). This motif is located prior to helix α1 observed in the x-ray crystal structure, but these residues were disordered. The ERVEV/LC3B model partially resembles LIR motif binding to LC3B (Figure 4-2C): Val237 docks into the

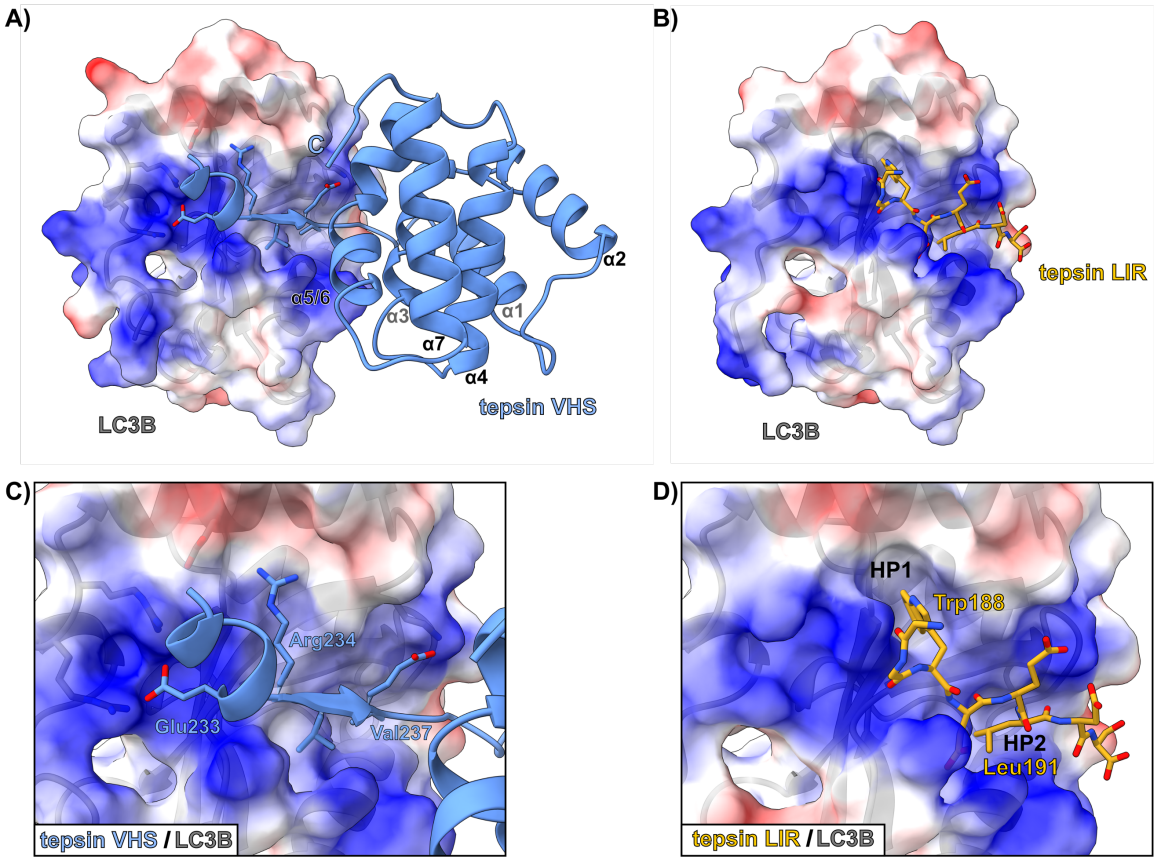

Figure 4-2: Computational modelling predicts tepsin VHS/LC3B binding in the LDS. AlphaFold Multimer models were generated using (A) tepsin VHS domain (residues 220-360) or (B) the tepsin LIR peptide with LC3B. (A) Upstream of VHS helix α1, a motif with the sequence ERVEV binds in the established LIR docking site (LDS). The LDS is enlarged in (C) to show positioning of ERVEV residues. For comparison, (B) shows a model of the tepsin LIR motif bound to the LDS. The LDS is enlarged in (D) with Trp188 in the first hydrophobic pocket (HP1) and Leu191 in the second hydrophobic pocket (HP2). The LC3B electrostatic surface representation shows several basic patches accommodate the ERVEV acidic glutamate residues and Val237 docks into LDS HP2.

second hydrophobic pocket of the established LDS (Noda et al., 2008); the space between the hydrophobic pockets can accommodate small hydrophobic or acidic residues (Birgisdottir et al., 2013); and Glu233 is positioned to bind a basic patch on LC3B that typically accommodates acidic residues upstream of the LIR hydrophobic residue docked into the first hydrophobic pocket (Birgisdottir et al., 2013; Wirth et al., 2019). The major distinguishing feature between the LIR and ERVEV motifs is Arg234 (Figure 4-2C) which takes the place of the critical tryptophan or phenylalanine residue in a LIR motif

(Figure 4-2D; Birgisdottir et al., 2013; Noda et al., 2008). The AlphaFold model predicts Arg234 can span across the first hydrophobic pocket to an acidic patch formed by an α-helix of LC3B.

Tepsin LIR and ERVEV motifs are conserved in vertebrates

We performed sequence alignments to examine conservation of the tepsin LIR and ERVEV motifs. Looking broadly across the eukaryotic super groups, neither the LIR nor ERVEV motifs are conserved (Figure 4-3A). However, both the LIR and ERVEV motifs are well conserved across representative vertebrate classes, which could indicate the function of these motifs is particularly important in vertebrates (Figure 4-3B; see Discussion). The LIR motif has a consensus sequence of GGW[D/E]EΨ, where Ψ

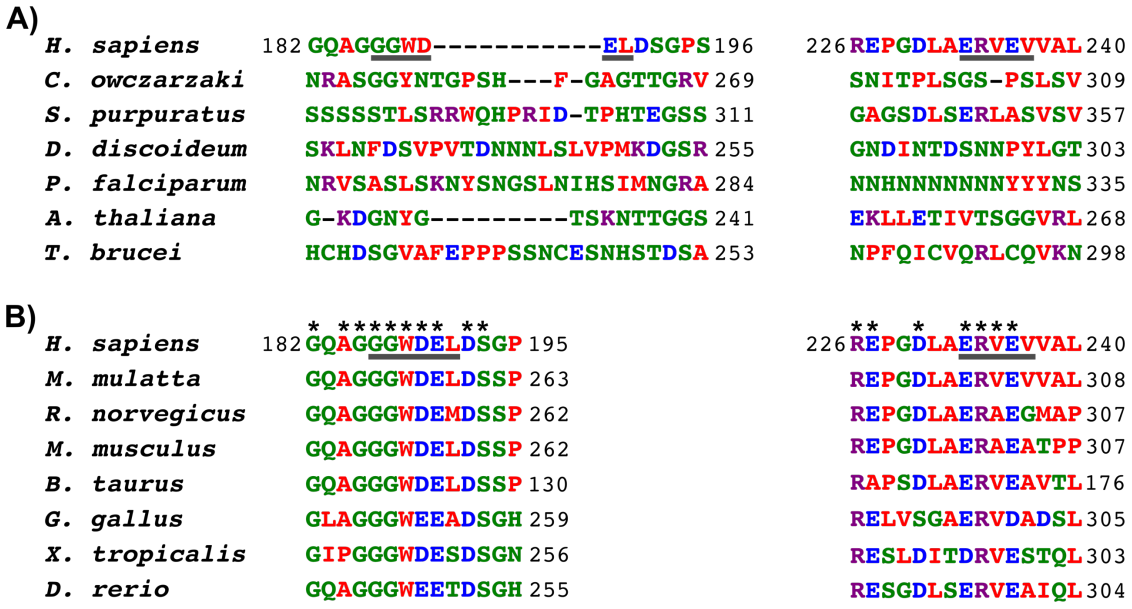

Figure 4-3: Tepsin LIR and ERVEV motifs emerged recently in evolution. Tepsin sequence alignments for (A) representative species from eukaryotic super groups or (B) vertebrates. Underlined sequences bind in the LDS and highly conserved residues are marked by asterisks (*). Coloring denotes amino acid properties; red: hydrophobic; green: hydrophilic; purple: basic (+); and blue: acidic (-). (A) Neither the tepsin LIR motif (GGWDEL, left) nor the ERVEV motif (right) are conserved across the eukaryotic super groups. (B) In vertebrates, the tepsin LIR motif is conserved as: GGW[D/E]EΨ, where Ψ represents an aliphatic residue. The ERVEV motif is also well conserved in vertebrates as: ER[V/A]E[V/A]. Upstream of the ERVEV motif, we noted three very well conserved charged residues: Arg226, Glu227, and Asp230.

represents an aliphatic residue. The ERVEV consensus sequence is ER[V/A]E[V/A] where the charged residues are highly conserved. We also noted several particularly well conserved charged residues upstream of the ERVEV sequence: Arg226, Glu227, and Asp230.

We looked at possible hydrogen bonding for these charged residues in the AlphaFold Multimer model (Figure 4-4A). Arg234 clearly distinguishes the ERVEV motif from a LIR motif by replacing a bulky hydrophobic residue with a basic residue (previous

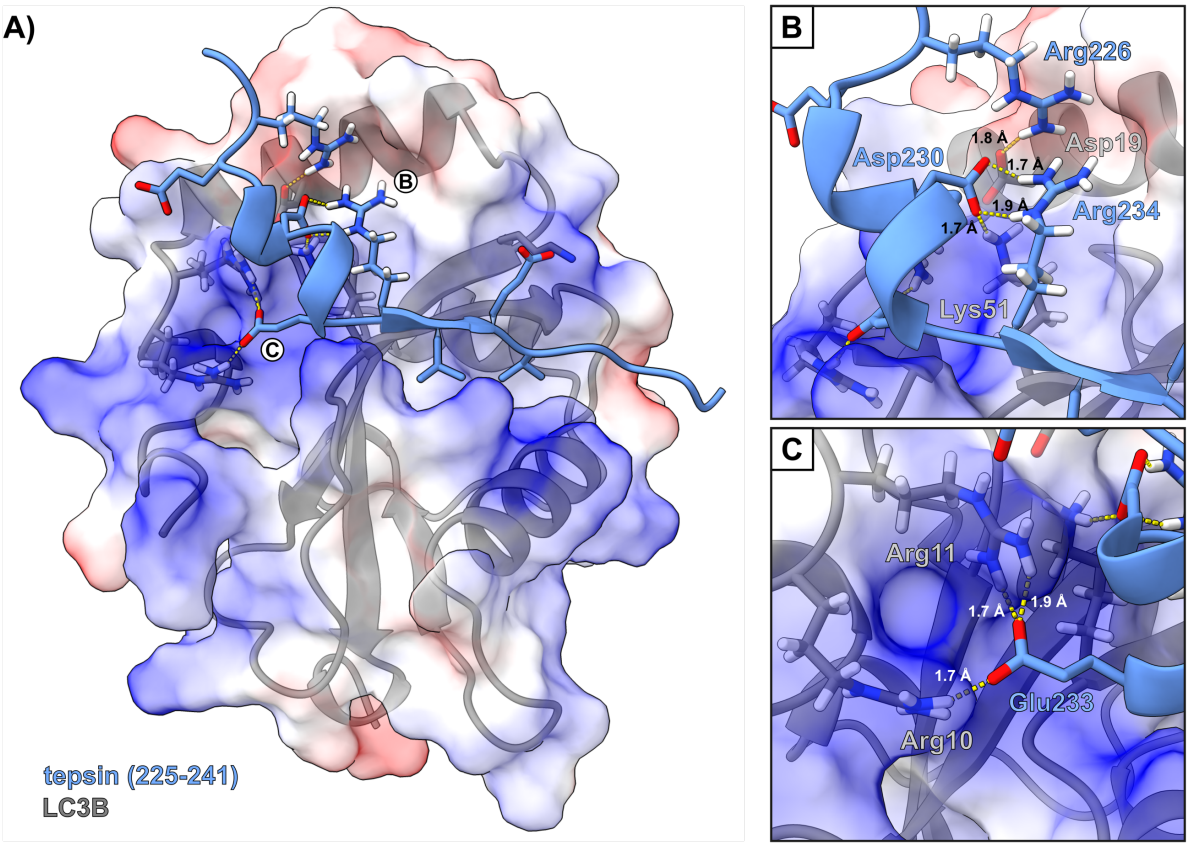

Figure 4-4: Hydrogen bond modelling for conserved ERVEV motif residues. (A) AlphaFold model of tepsin VHS (residues 220-360) bound to LC3B displaying only the region around the ERVEV motif (residues 225-241). Possible hydrogen bonds (yellow dashes) between tepsin and LC3B are shown in B and C with bond distances indicated. (B) Conserved tepsin residues Arg226, Asp230, and Arg234 may hydrogen bond with LC3B residues Asp19 and Lys51. Tepsin residue Arg234 spans across the first hydrophobic pocket of the LC3B LDS. This model indicates Asp230 in tepsin may help stabilize Arg234 instead. (C) Glu233 of the tepsin ERVEV motif may hydrogen bond with LC3B residues Arg10 and Arg11. These data indicate key residues that can be mutated to test and validate this binding motif in future studies.

section). The AlphaFold model shows extensive hydrogen bonding between Arg226, Asp230, Arg234, LC3B Asp19, and LC3B Lys51 (Figure 4-4B). The first conserved glutamate in the ERVEV motif, Glu233, may hydrogen bond with LC3B Arg10 and/or Arg11, similar to acidic residues upstream from LIR motifs (Figure 4-4C; Birgisdottir et al., 2013; Wirth et al., 2019). These conserved charged residues, proximal to the tepsin VHS domain, are strong candidates to probe the molecular basis of VHS domain binding to LC3B using structure-based mutagenesis.

DISCUSSION

Chapter II characterized the LIR interaction between tepsin and LC3B using *in vitro* biochemistry, structural modeling, and immunofluorescence in cultured cells. During the biochemical characterization of the tepsin LIR motif, we found the tepsin VHS domain could bind LC3B in absence of the LIR motif (Figure 4-1), indicating the VHS domain alone contains a LC3B binding site. The presence of both the LIR motif and the VHS domain did not substantially affect the strength of this interaction with LC3B in pulldowns (Figures 4-1) However, preliminary stoichiometry measurements from ITC do indicate more than one LC3B may be able to bind a single tepsin molecule (A3-1). These ITC data were analyzed using a single independent binding site model and should be reanalyzed using two binding site models. With the current data, it is not clear whether the two binding sites compete to bind LC3B or each motif can bind LC3B simultaneously.

Using AlphaFold Multimer to model the VHS/LC3B interaction, we identified a prospective binding motif (ERVEV) prior to VHS helix α1. The ERVEV motif resides in a flexible tail of residues unresolved in experimental x-ray crystal structures of the VHS domain (Figure 4-2; Archuleta et al., 2017). In this model, ERVEV binding to LC3B occurs at the established LDS but does not conform to the sequence of a LIR motif ([W/F]xx[I/V/L]) and does not follow conventions of LIR motif interactions at the LDS (Figures 4-2 and 4-4; Noda et al., 2008). Nevertheless, electrostatic interactions may mediate ERVEV binding at the LDS (Figure 4-4B and 4-4C). The key residues identified in the AlphaFold Multimer model are strong candidates to test using structure-based mutagenesis. Prior to the public release of AlphaFold, we attempted to identify key residues for the VHS/LC3B interaction by considering an experimentally determined VHS/ubiquitin interaction (Ren and Hurley, 2010). However, superposition models exhibit clashes between the tepsin VHS domain and LC3B (Figure A3-2).

Presently, it is unclear whether the VHS domain/LC3B interaction occurs in the context of full length tepsin. We would expect mutation of the LIR motif would not completely abolish binding to LC3B if there was a second LC3B binding site. Pulldown assays using purified full-length wild-type tepsin or LIR mutant tepsin (WDEL→SSSS) with LC3B indicate that LC3B binding is lost when the LIR motif is mutated (Chapter II). However, LC3B binding to full-length tepsin has been difficult to detect with pulldown assays at either Coomassie stain or Western blot level, so it's possible we weren't able to reliably observe residual binding with the LIR mutant tepsin due to weak signal.

Interestingly, the ERVEV motif and the LIR motif are poorly conserved across eukaryotic super groups but well conserved in vertebrates (Figure 4-3). The AP-4 ε

binding motif in tepsin is similarly only conserved in vertebrates (Mattera et al., 2015). This indicates the LIR and ERVEV motifs evolved in vertebrates to perform important functions. AP-4 traffics the essential autophagy lipid scramblase, ATG9A (Guardia et al., 2020b; Maeda et al., 2020b; Mari et al., 2010; Matoba et al., 2020; Yamamoto et al., 2012), from the TGN to the cell periphery (Davies et al., 2018; Ivankovic et al., 2020; Mattera et al., 2017). ATG9A trafficking links AP-4 to general cellular health, however AP-4 loss in humans results in severe neurological disorders (Abdollahpour et al., 2014; Abou Jamra et al., 2011; Bauer et al., 2012; Ebrahimi-Fakhari et al., 2020; Hardies et al., 2015; Jameel et al., 2014; Tessa et al., 2016; Tüysüz et al., 2014; Verkerk et al., 2009), suggesting particular importance in neuronal development and maintenance (Behne et al., 2020; Davies et al., 2018; de Pace et al., 2018; Guardia et al., 2021; Ivankovic et al., 2020; Matsuda et al., 2008a; Mattera et al., 2020b, 2017; Scarrott et al., 2023).

Work presented in Chapter III suggests loss of tepsin is detrimental to zebrafish embryonic development, though less severe than loss of AP-4. Chapter II indicates tepsin performs multiple functions in the AP-4 coat to help regulate autophagy via trafficking of ATG9A. Furthermore, the tepsin LIR motif is important for spatial regulation of AP-4-mediated ATG9A trafficking. It is possible the LIR motif evolved due to high demand for tightly coordinated autophagic processes in neuronal cells (reviewed in Stavoe and Holzbaur, 2019). Similarly, the prospective ERVEV motif may spatially or temporally coordinate distribution of ATG9A-containing AP-4 vesicles. LC3B and tepsin most likely interact at autophagic membranes which means either of these motifs could be further regulated by avidity effects from protein density on the membrane. Potential competition between LIR and ERVEV motif binding to LC3B could additionally act as a molecular

switch coordinating ATG9A trafficking. Alternatively, Alternatively, simultaneous binding of two LC3B molecules by each motif could increase the interaction avidity.

Future directions

The identified ERVEV motif is a strong candidate to explain VHS domain binding to LC3B *in vitro*. The AlphaFold Multimer model and sequence conservation indicate the ERVEV motif residues, along with several upstream residues, are major contributors to the interaction. We have an alternate VHS domain construct (residues 241-356) which excludes all the residues implicated in the AlphaFold Multimer model but retains the entire folded VHS domain. This truncated VHS construct in pulldown assays can be used to confirm residues 220-241 contain the second LC3B binding site. We could then make structure-based mutations to identified conserved residues for pulldown assays and design peptides to quantify binding affinities by ITC. Future studies may benefit from using biolayer interferometry instead of ITC to better quantify binding kinetics when both the LIR and ERVEV motifs are present.

If the ERVEV motif is validated as a second LC3B binding motif, it will be particularly interesting to see how mutation of key ERVEV residues affect ATG9A trafficking in cells. Comparing specific loss of ERVEV binding with loss of LIR motif binding on the ATG9A subcellular distribution may help clarify why introduction of LIR mutant tepsin does not phenocopy loss of endogenous tepsin in cells (Chapter II). It is also interesting to consider why and how two LC3B motifs could be differentially regulated. Tepsin most likely interacts with LC3B at autophagic membranes (see Chapter II Discussion) so the two motifs may be subject to avidity effects related to protein density

along the membrane. LC3B protein density on autophagic membranes increases as pre-autophagosome structures mature then decreases as LC3B is deconjugated and removed from the cytosolic face of the membrane (Fujita et al., 2009; Kabeya et al., 2000; Nath et al., 2014; Shpilka et al., 2011; Weidberg et al., 2011, 2010). Therefore, avidity effects could temporally coordinate tepsin/LC3B interactions during autophagy. Liposome pelleting experiments or biolayer interferometry could probe avidity by immobilizing LC3B to a surface and testing tepsin binding.

MATERIALS AND METHODS

Reagents

Unless otherwise noted, all chemicals were purchased from Sigma.

The following antibody was used in this study: HRP-conjugated anti-6X His tag 1:8000 for Western blots (ab184607; Abcam).

Molecular biology and cloning

For biochemical analysis, ENTH-LIR tepsin (residues 1-220) was subcloned from full-length tepsin (Borner et al., 2012) using *Nde*I/*Bam*HI sites into in-house vector pMW172 (Owen and Evans, 1998) modified to incorporate a C-terminal, thrombin cleavable GST tag. LIR-VHS tepsin (residues 135-356) was subcloned into pGEX-6P-1 (Amersham) using *Bam*HI/*Sal*I sites to generate N-terminal GST-fusion protein. Cloning of the ENTH (residues 1-136) and VHS (residues 220-360) domains was described

previously (Archuleta et al., 2017). Full-length LC3B (residues 1-125) was subcloned by Genscript into pGEX-6P-1 using *Bam*HI/*Sal*I sites. A two-stage mutagenesis protocol (Frazier et al., 2016) was used to truncate full-length LC3B into the mature isoform (residues 1-120). Oligonucleotides used in this study may be found in Table 4-1.

Protein	Sequence (5'-3')	Restriction site	Primer use
ENTH-LIR (aa1-220)	GGAGCACATATGATGGCTGCCGCGC	*Nde*I	5' human tepsin, starts at aa1
ENTH-LIR (aa1-220)	TGCTCCGGATCCGCTGTCGCTGCC	*BamH*I	3' human tepsin, stops at aa220, no stop codon
LIR-VHS (aa135-356)	GAGGCAGGATCCACCGTGTTGCCGCTGGCTCCC	*BamH*I	5' human tepsin, starts at aa135
LIR-VHS (aa135-356)	GTCTCCGTCGACCTAGGACAGCTGCCCACAGGA	*Sal*I	3' human tepsin, stops at aa356, with stop codon
LC3B (aa1-120)	CAGGAGACGTTCGGGTAAGTCGACTCGAGC	N/A	5' mutagenesis primer to remove aa121-125
LC3B (aa1-120)	GCTCGAGTCGACTTACCCGAACGTCTCCTG	N/A	3' mutagenesis primer to remove aa121-125

Table 4-1: Oligonucleotides used in Chapter IV study.

Protein expression and purification

Constructs were expressed in BL21(DE3)pLysS cells (Invitrogen) for 16-20 hours at 22ºC after induction with 0.4 mM Isopropyl β-D-1-thiogalactopyranoside (IPTG). All tepsin constructs were purified in 20 mM Tris (pH 8.5), 250 mM NaCl and 2 mM βME. LC3B (residues 1-120) was purified in 20 mM HEPES (pH 7.5), 200 mM NaCl and 2mM βME. Cells were lysed by a disruptor (Constant Systems Limited) and proteins were affinity purified using glutathione sepharose (GE Healthcare) in purification buffer. GST-tagged LC3B was cleaved overnight with recombinant 3C protease at 4ºC and eluted in batch. ENTH-LIR and LIR-VHS GST-fusion proteins were cleaved by this method for use

in ITC experiments. All proteins were further purified by gel filtration on preparative Superdex HiLoad 26/600 or analytical (Superdex 200 10/300) columns (GE Healthcare).

Structure representation and modeling

Models of tepsin LIR motif or tepsin VHS interactions with LC3B were generated using Alphafold 2.2 Multimer (Jumper et al., 2021b, 2021a). ChimeraX MatchMaker was used to superpose tepsin VHS domain and LC3B with experimental structures of a VHS-ubiquitin interaction deposited in the Protein Data Bank. All structural figures were generated in ChimeraX.

GST-pulldown assays

Tepsin GST-fusion proteins (50 µg) and LC3B, at a 5X molar excess to tepsin, were incubated with glutathione sepharose resin (GE Healthcare) for 2 hours at 4ºC in 20 mM HEPES (pH 7.5), 100 mM NaCl, 0.5% NP-40 and 2 mM DTT. Resin was washed three times with the same buffer. Proteins were eluted from the resin using the wash buffer plus 30 mM reduced glutathione. Elution buffer was incubated with resin for 20 min on ice with gentle agitation every 2 minutes. Gel samples were prepared from the supernatant following elution with glutathione, and the assay was analyzed by Coomassie staining and Western blotting of SDS-PAGE gels. When further analyzed by Western blot, His-tagged prey protein were detected using anti-His6-HRP conjugated primary antibody (Abcam, ab184607).

Isothermal titration calorimetry

Isothermal titration calorimetry (ITC) experiments were conducted on a NanoITC instrument (TA Instruments) at 30°C. Molar peptide concentration in the syringe was 9 times that of protein in the cell; 0.1 mM tepsin ENTH-LIR or LIR-VHS was placed in the cell and 0.9 mM LC3B was placed in the syringe. All experiments were carried out in 20 mM HEPES (pH 7.5), 100mM NaCl and 0.5 mM TCEP, filtered and degassed. Incremental titrations were performed with an initial baseline of 120 seconds and injection intervals of 200 seconds. Titration data were analyzed in NANOANALYZE (TA Instruments) to obtain a fit and values for stoichiometry (n) and equilibrium association (K_a). K_D values were calculated from the association constant.

ACKNOWLEDGMENTS

Thanks to Amy Kendall for generating tepsin and LC3B AlphaFold Multimer models and all members of the Jackson lab for helpful discussion of the ERVEV motif.

V. PROFILING TEPSIN PHENOTYPES IN CULTURED CELLS

INTRODUCTION

Over the course of my thesis research, I've employed several approaches to investigate tepsin binding partners and better understand the function of tepsin within cells. Following the identification of ATG9A as an AP-4 cargo (Davies et al., 2018; Ivankovic et al., 2020; Mattera et al., 2017), we considered implications for AP-4 trafficking in the regulation of autophagy. The work in Chapters II, III, and IV is expanded from this motivation. This chapter compiles exploration of prospective tepsin binding partners and additional preliminary data for cellular phenotypes following tepsin loss or depletion.

Prospective tepsin binding partners

The ENTH and VHS domains in tepsin lack structural features to perform their expected functions (see Chapter I and Archuleta et al., 2017). We moved on to investigating prospective binding partners for tepsin ENTH and VHS domains that were identified by commercial yeast two-hybrid screens (detailed in the thesis of Meredith Frazier; Frazier, 2018). Validation attempts by *in vitro* pulldown assays or immunoprecipitations from cell lysates were inconsistent dependent on tag placement and experimental conditions but we remain interested in two candidates: VPS35L and ISCA1.

VPS35L is a candidate binding partner for the tepsin ENTH domain (Frazier, 2018) and part of a heterotrimeric trafficking complex called ‘retriever’ (Mallam and Marcotte, 2017; McNally et al., 2017). Retriever is structurally similar to the retromer complex and both function in independent endosomal sorting pathways (Chen et al., 2019; Healy et al., 2022, 2018; Laulumaa and Varjosalo, 2021; Mallam and Marcotte, 2017; McNally et al., 2017). The core heterotrimer of retriever consists of VPS35L, VPS26C, and VPS29 (Mallam and Marcotte, 2017; McNally et al., 2017). Identification of VPS35L as a candidate binding partner for tepsin raises interesting questions about whether tepsin could participate in AP-4 independent trafficking pathways. Determining whether tepsin and VPS35L interact within cells could expand possible functional roles for tepsin in membrane trafficking. Although, concomitant loss of tepsin whenever AP-4 is lost hints that tepsin function may rely primarily on AP-4 (Borner et al., 2012; Hirst et al., 2013b).

The top candidate from VHS domain yeast two-hybrid screens is ISCA1 (Frazier, 2018). ISCA1 is a mitochondrial iron sulfur cluster assembly protein involved in the biogenesis and subsequent transfer of [4FE-4S] clusters to mitochondrial proteins (Kaut et al., 2000; Suraci et al., 2021). These iron sulfur clusters are important cofactors for various catalytic processes and particularly well characterized in the electron transport chain (reviewed in Read et al., 2021). The biological significance of a tepsin/ISCA1 interaction is not immediately clear considering ISCA1 localizes to the mitochondrial matrix while tepsin is cytosolic. However, we are able to detect VHS domain and ISCA1 binding by *in vitro* pulldown assays.

RESULTS AND DISCUSSION

Using cell fractionation to probe tepsin binding partners

Previous work in the lab to validate VPS35L or ISCA1 as tepsin binding partners was inconclusive. *In vitro* pulldown assays and immunoprecipitations from cell lysates gave variable results depending on experimental conditions. It is not clear why tepsin would interact with another trafficking complex or a mitochondrial matrix protein. We hypothesized that damaged mitochondria, subsequently degraded by autophagy, may transiently result in cytosolic ISCA1. I conducted mitochondrial fractionation experiments of basal or starved cells in an effort to probe for either ISCA1 in the cytosol or tepsin in mitochondrial fractions. However, characterization of the mitochondrial fraction determined it was really a crude organelle fraction (Figure 5-1). Lysosome, mitochondria, late endosome, and autophagosome markers were all present in the organellar fraction. Early endosome marker EEA1 was the only marker tested that remained in the cytosolic fraction.

At the time this experiment was conducted, I did not have access to optimal antibodies for Western blot detection of AP-4 or tepsin. The AP-4 β4 antibody prominently detected a band enriched in the organelle fraction, but the molecular weight (~120 kDa) is higher than expected for β4 (~83 kDa) (Figure 5-1). We also expected to visualize some AP-4 in the cytosolic fraction considering AP-4 cycles between being cytosolic or membrane-associated in an Arf1-dependent manner (Boehm et al., 2001; Dell'Angelica et al., 1999a; Hirst et al., 1999). Arf1 exhibits the expected fractionation to both the

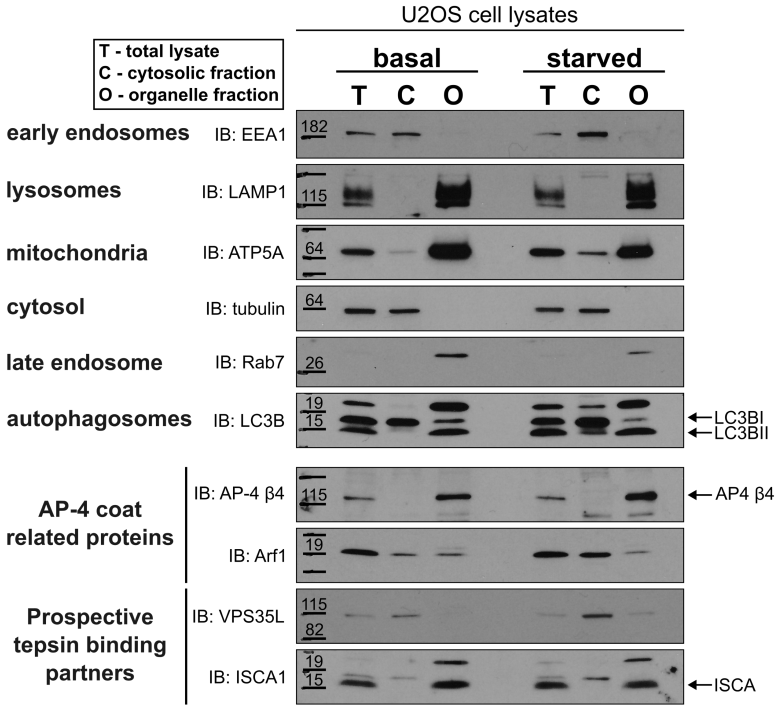

Figure 5-1: Using cell fractionation to study tepsin binding partners. U2OS cells were fractionated (see Methods) into an organelle and cytosolic fraction; a sample of total cell lysate was reserved for comparison. Cells in complete growth media (basal) were compared to cells starved for 2 hours in EBSS. The organelle fraction contains lysosomes (marker: LAMP1), mitochondria (marker: ATP5A), late endosomes (marker: Rab7), and autophagosomes (marker: LC3BII). Early endosomes (marker: EEA1) remain in the "cytosolic" fraction with tubulin and un-lipidated LC3B (LC3BI). AP-4 β4 resides in the organelle fraction. Arf1, which is required to recruit AP-4 to TGN membranes, exhibits an expected cytosolic and membrane-associated localization. We tested two prospective tepsin binding partners: VPS35L and ISCA1. ISCA1 fractionates cleanly into the organelle fraction. VPS35L is only faintly detected in the organelle fraction from starved cells.

cytosolic and membrane-enriched organelle fraction. I now have a validated tepsin antibody and preferred AP-4 ε antibody (Chapter II) which will improve visualization of AP-4 coat components following subcellular fractionation.

ISCA1 appears to selectively reside in the organelle fraction under both basal and starved conditions (Figure 5-1). Since this fraction contains many different membrane populations in addition to mitochondria, this alone does not clarify whether ISCA1 and tepsin are ever coincident in the cell. If tepsin and ISCA1 interact in cells, it seems likely to be a transient interaction or only occur between limited subpopulations of the two

proteins. Immunoprecipitations using this membrane enriched fraction may help assay the tepsin/ISCA1 interaction (see Future directions).

VPS35L resides in the cytosolic/early endosome fraction (Figure 5-1) which does correlate with retriever mediating endosomal recycling at EEA1-positive endosomes (McNally et al., 2017). In starved cells, VPS35L is faintly detectable in the organelle fraction where AP-4 appears enriched. Again, it may be beneficial to use the organelle fraction in immunoprecipitations to probe for a tepsin/VPS35L interaction. Cargo recognition for the retriever complex is mediated by SNX17 (Ghai et al., 2013, 2011; Healy et al., 2022; McNally et al., 2017). SNX17 was also recently identified, along with SNX4 and SNX5, as part of a complex called 'recycler' which mediates recycling of ATG9A and STX17 from autolysosomes (Ravussin et al., 2021; Zhou et al., 2022). This ATG9A and STX17 recycling was shown to occur independently from retriever trafficking (Zhou et al., 2022).

Disrupting recycler function does not inhibit autophagosome biogenesis (Zhou et al., 2022); this suggests compensatory autophagic component recycling pathways may exist to prevent complete accumulation of ATG9A at the autolysosome. AP-4 is implicated in retrograde transport of ATG9A (Mattera et al., 2020b) but it is unclear whether this is a retrieval from autophagic membranes or to regulate distribution of ATG9A vesicles for autophagosome biogenesis. It may be interesting to explore recycler function in the context of tepsin depletion to understand whether the tepsin LIR motif coordinates ATG9A delivery or retrieval at autophagic membranes (Chapter II). It's also possible tepsin helps coordinate a "hand-off" of ATG9A to recycler during autophagosome maturation.

Tepsin knockout cell morphology

At the initiation of my thesis work, three papers were published linking AP-4 more clearly to autophagy via the trafficking of ATG9A (Davies et al., 2018; Ivankovic et al., 2020; Mattera et al., 2017). In these studies, disruption of AP-4 trafficking also dysregulated autophagosome morphology in various cultured cells and primary mouse neurons (Davies et al., 2018; Ivankovic et al., 2020; Mattera et al., 2017).

The role of tepsin in these phenotypes was only partially explored by one group, showing that HAP1 tepsin knockout cells did not drastically accumulate ATG9A at the TGN, as AP-4 knockout does (Mattera et al., 2017). No further analysis of tepsin in AP-4 mediated autophagy phenotypes was done. We broadly surveyed for aberrant autophagy in tepsin knockout HAP1 cells by thin cell section transmission electron microscopy. Cells maintained in complete nutrient conditions (basal) were compared with cells starved for amino acids and serum (starved). Tepsin knockout cells contained numerous enlarged membrane-bound structures resembling multivesicular bodies or degradative organelles under basal conditions (Figure 5-2).

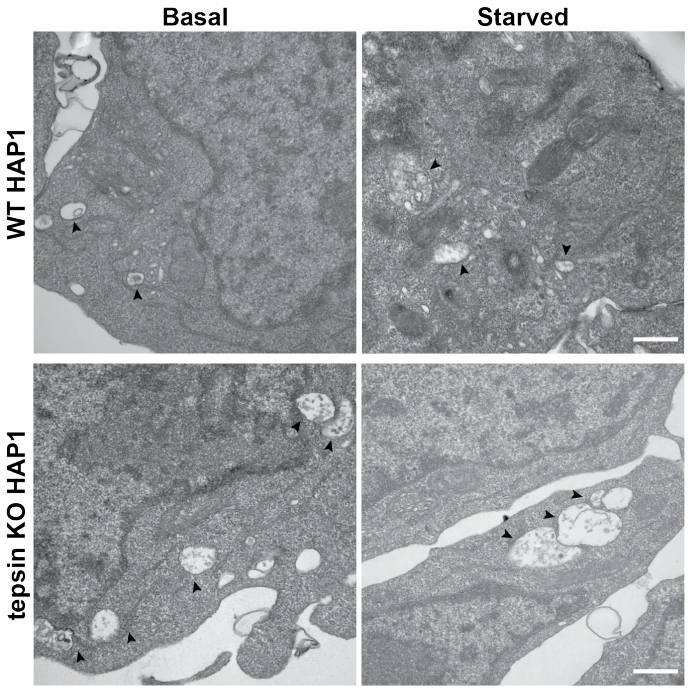

Figure 5-2: Tepsin knockout HAP1 cells accumulate enlarged multivesicular bodies. Wild-type (WT) or tepsin knockout (KO) HAP1 cells were cultured in complete cell media (basal) or starved for 2 hours in EBSS. In basal conditions, tepsin KO cells exhibit more, and enlarged, membrane-bound structures resembling multivesicular bodies (arrowheads) compared to WT HAP1 cells. Apparent size of these structures was further increased in starved cells. Scale bar is 500 nm

The size of these structures was further increased following nutrient starvation. Wild-type HAP1 cells, in basal or starved conditions, did contain similar structures but fewer per cell and the structures were smaller (Figure 5-2). Without specific protein markers, we could not definitively identify these structures; however, we hypothesized they were dysregulated autophagy structures or lysosomes.

Tepsin or AP-4 ε knockout HAP1 cells were immunostained for LC3, a common autophagosome marker (Klionsky et al., 2021), to observe the morphology of autophagy structures. Preliminary data show tepsin or AP-4 knockout cells exhibit increased accumulation of LC3-positive structures in basal and starved cells (Figure 5-3). HAP1 cells grow in tight clumps and are relatively small, with little distance between the nucleus and cell periphery. This made it difficult to segment cells for analysis. It is also worth noting, I later switched my preferred LC3 antibody to obtain better signal to noise ratio

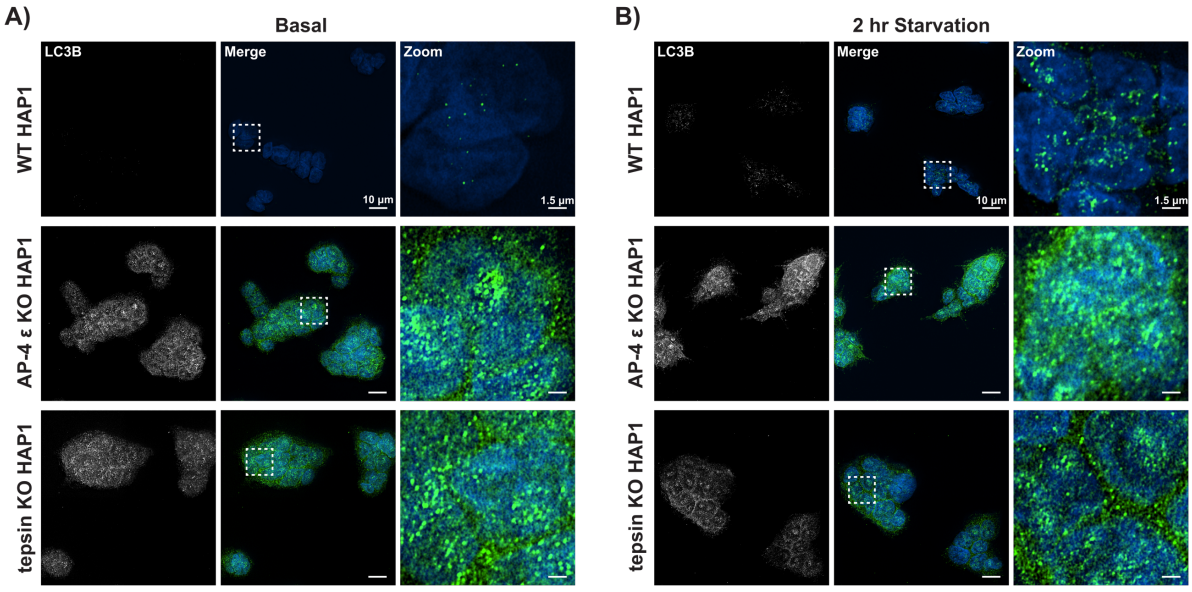

Figure 5-3: Tepsin knockout HAP1 cells accumulate LC3-positive structures. HAP1 cells were cultured in complete media (basal; A) or starved in EBSS for 2 hours (B) then immunostained for autophagy marker, LC3 (NanoTools). Tepsin or AP-4 knockout results in accumulation of LC3 signal above wild-type cells. Small cell size and tendency for cell clumping hindered analysis. Scale bar is 10 µm and zoom scale bar is 1.5 µm

(preferred: LC3 from Molecular Biology Laboratory). Instead, I pursued acute tepsin depletion by siRNA knockdown. Knockdown is an important complement to knockout studies, which may be complicated by upregulation of compensatory pathways or emergence of indirect phenotypes. Acute depletion can help visualize phenotypes before other pathways compensate.

We assayed autophagy in tepsin or AP-4 depleted HeLa cells by immunostaining for endogenous LC3 and quantifying LC3-positive, autophagosome structures (Figure A4-1A). Tepsin depletion dysregulated autophagy with trends toward increased autophagosome number and volume in basal conditions (Figure A4-1B-H). Statistical analysis for these experiments was complicated by heterogeneity in the sample population. Using total LC3 puncta intensity per cell as a metric sensitive to both size and volume of LC3-positive structures, we saw significant differences between tepsin-depleted and both wild-type or control cells (Figure A4-1H). Heterogeneity could be related to knockdown efficiency (typically > 75%) and/or asynchronous autophagy levels across the population of cells. However, the trends are in general agreement with the preliminary HAP1 tepsin knockout cells (Figure 5-3) and data in Chapter II. It may be worth returning to tepsin knockout HAP1 cells using my improved methodologies and reagents (see Future directions).

Defects in nutrient sensing following tepsin depletion

The enlarged degradative structures in tepsin knockout HAP1 cells (Figure 5-2) could also indicate dysregulated lysosomes. Primary neurons from AP-4 ε knockout mice or induced pluripotent stem cells exhibit axonal swellings independently characterized to

contain: ER (Ivankovic et al., 2020); lysosomes (de Pace et al., 2018; Majumder et al., 2022); LC3B (de Pace et al., 2018); or ATG9A (Majumder et al., 2022). Lysosomes are heavily involved in the autophagy process. In late-stage autophagy, autophagosomes fuse with the lysosome allowing recycling of macromolecules during starvation conditions (Rabanal-Ruiz et al., 2018). In nutrient-rich conditions, activated mTORC1 at lysosomal membranes inhibits autophagy induction and autophagy-related gene expression, while inactivation of mTORC1 in nutrient-starved conditions leads to autophagy induction (Mercer et al., 2018).

To probe lysosomal morphology, I immunostained basal and starved HeLa cells for the lysosomal marker, LAMP1. In starvation conditions, lysosomes redistribute from the cell periphery to the perinuclear region, so accumulation of juxtanuclear LAMP1 signal is expected in nutrient-depleted conditions (Korolchuk et al., 2011). Accumulation of LAMP1 signal during starvation is coincident with autolysosome formation before autophagic component recycling and autophagic lysosome reformation (Yu et al., 2010; Zhou et al., 2022).

Following starvation, wild-type and control siRNA treated cells exhibit accumulation of LAMP1-positive structures in the juxtanuclear region (Figure 5-4A) measured both by the average LAMP1 object intensity and the total LAMP1 intensity per cell (Figure 5-4B and 5-4C). AP-4-depleted cells exhibit similar starvation-induced LAMP1 accumulation, though basal accumulation appears higher than wild-type or control siRNA-treated cells (Figure 5-4B and 5-4C). Following starvation, tepsin-depleted cells show a less robust increase in the mean intensity of LAMP1 objects and no significant increase in the total LAMP1 object intensity per cell (Figure 5-4B and 5-4C). Both tepsin- and AP-

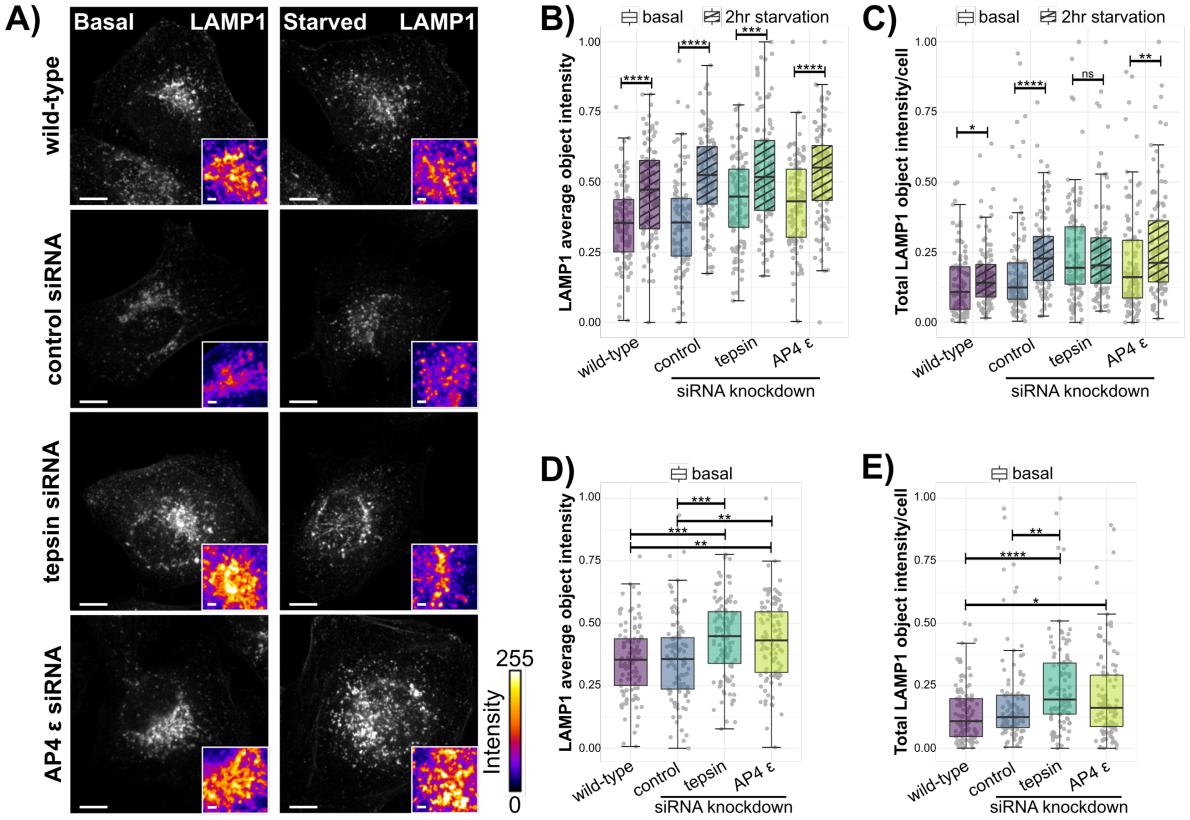

Figure 5-4: Tepsin depletion dysregulates lysosome morphology in HeLa cells. HeLa cells were cultured in complete media (basal) or starved in EBSS for 2 hours then immunostained for lysosomal marker, LAMP1. (A) Representative single-plane confocal images of wild-type and control (non-targeting) siRNA-, tepsin siRNA-, or AP-4 ε siRNA-treated HeLa cells. Inset is depicted using the Fire look-up table (FIJI) with intensity scale as shown. Scale bar: 10 μm, inset scale bar: 2 μm. (B-C) Comparison of LAMP1 objects following starvation: LAMP1-positive objects were quantified by (B) average object signal intensity per cell or (C) total signal intensity for all LAMP1 objects per cell. (B) Average LAMP1 object intensity increases in all conditions following starvation. (C)Tepsin-depleted cells accumulate more LAMP1 signal in basal conditions, without significant change following starvation. Statistical results in B and C are from Mann-Whitney U test. (D-E) Comparing LAMP1 signal intensity in basal conditions following tepsin or AP-4 depletion: (D) tepsin or AP-4 depleted cells accumulate higher intensity LAMP1 objects in basal conditions compared to WT or control siRNA-treated cells. (E) Tepsin depleted cells accumulate more total LAMP1 signal compared to WT and control siRNA-treated cells. Statistical results from Kruskal-Wallis test, Dunn test with Bonferroni correction. Quantification (B-E): data from three independent biological replicates each with 35 cells per condition was subject to min/max normalization; each data point on the box-and-whisker plots corresponds to one cell; *p≤0.05, **p≤0.01, ***p≤0.001, ****p≤0.0001.

4-depleted cells have significantly brighter LAMP1 accumulations in basal conditions (Figure 5-4D). Tepsin-depleted cells also show significantly higher total LAMP1 signal intensity per cell (Figure 5-4E). These data, together with dysregulated autophagy occur in nutrient-rich conditions (Chapter II, Figure 5-3, Figure A4-1), which suggests tepsin and AP-4 depletion may somehow hinder nutrient sensing.

Starving cells followed by addition of essential amino acids to the media should activate mTORC1 signaling (Hesketh et al., 2018). Tepsin or AP-4 depletion appears to suppress mTORC1 activation, indicated by lower levels of phosphorylated p70 S6K relative to total p70 S6K (Figure 5-5). Forcing juxtanuclear lysosome positioning is known to suppress mTORC1 activation and induce autophagy; conversely, forcing peripheral lysosome localization increases mTORC1 activity (Korolchuk et al., 2011). AP-4 ε knockout neurons accumulate endo-lysosome organelles in axonal swellings (de Pace et al., 2018; Majumder et al., 2022) which could indicate a role for AP-4 in lysosome distribution. However, the axonal swellings appear to be heterogenous as independent groups have shown they contain: lysosomes (de Pace et al., 2018; Majumder et al., 2022); LC3B (de Pace et al., 2018); ATG9A (Majumder et al., 2022); ER (Ivankovic et al., 2020); neurofilament H (de Pace et al., 2018); or mutant Huntingtin aggregates (de Pace et al., 2018). Axonal swellings are also observed in AP-4 β4 knockout mice (Matsuda et al., 2008a; Scarrott et al., 2023) but the only molecular marker tested was LC3, indicating accumulated autophagy structures (Matsuda et al., 2008a).

Future studies are necessary to understand how AP-4 trafficking relates to lysosome positioning but if lysosomes are forced to the juxtanuclear region following tepsin or AP-4 depletion, this could explain the diminished mTORC1 activity and formation of aberrant autophagy structures in basal conditions (Figure 5-5). There is some evidence that AP-4 is important for neuronal lysosome biogenesis and function (Majumder et al., 2022); additionally, AP-4 μ4 can weakly bind YXXΦE sorting signals in lysosomal proteins LAMP1, LAMP2, and CD63 but the relevance of these interactions in cells remains unclear (Aguilar et al., 2001; Stephens and Banting, 1998).

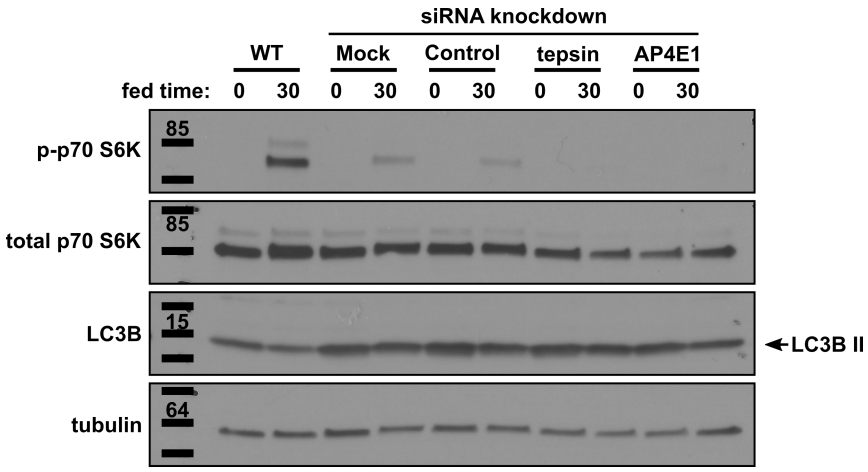

Figure 5-5: mTORC1 activation is suppressed following tepsin or AP-4 depletion in HeLa cells. HeLa cells depleted for tepsin or AP-4 ε (gene: AP4E1) show no detectable mTORC1 activation, monitored by p-p70 S6K compared to total p70 S6K. Cells were starved for amino-acid free media then fed essential amino acids for 30 minutes. Control (non-targeting) siRNA treatment and mock treatment with only transfection reagents also inhibited mTORC1 activation in this preliminary experiment. These data indicate tepsin or AP-4 depletion may hinder nutrient sensing; however experimental procedures need optimization.

Interestingly, I found that cells starved for two hours then re-fed with complete nutrient media for 1 hour exhibit synchronized basal autophagy (Figure 5-6). After 2 hours in complete media, tepsin-depleted cells began accumulating more autophagosomes and this trend continues at 6 hours in complete media; although, control cells also began accumulating autophagosomes by this time point (Figure 5-6). These preliminary data indicate tepsin or AP-4 depletion does not completely inhibit nutrient sensing, since autophagosome numbers decrease when nutrients are initially restored. Instead, it seems like tepsin-depleted cells become desensitized to nutrients more quickly. A more extensive re-feeding time course will be necessary to understand this phenotype.

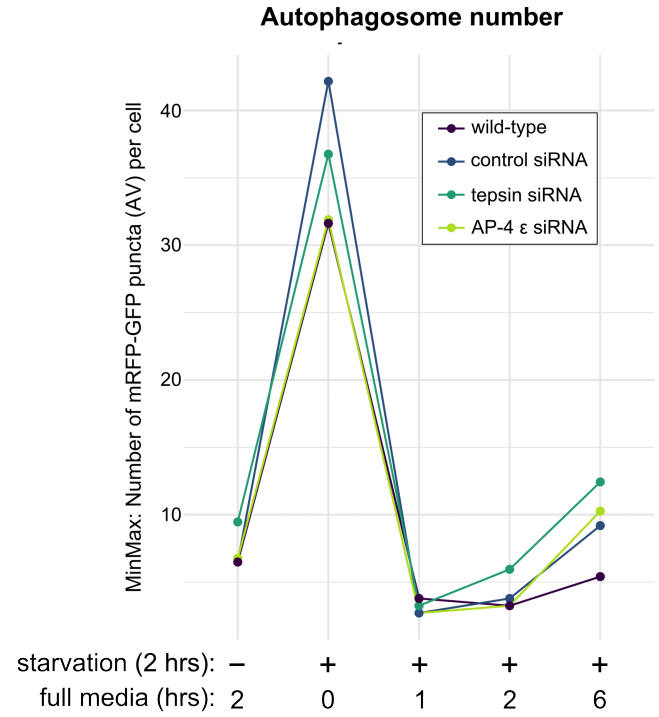

Figure 5-6: Basal autophagy induction in synchronized tepsin-depleted mRFP-GFP-LC3B HeLa cells. Starved mRFP-GFP-LC3B HeLa cells were starved for 2 hours in EBSS and then re-fed with complete media for the indicated period of time; for comparison, basal cells were given 2 hours of fresh complete media and never grown in starvation media. (A) Starvation for 2 hours in EBSS followed by 1 hour in complete media synchronizes autophagosome number across wild-type (WT), control siRNA-, tepsin siRNA-, or AP-4 ε siRNA-treated cells. Tepsin depletion drives increased autophagosome formation after 2 hours in fed conditions. Autophagosomes are defined as coincident mRFP-GFP, yellow, structures. Data are from one biological replicate with at least 50 cells per condition and subjected to min-max normalization.

FUTURE DIRECTIONS

AP-4-mediated ATG9A trafficking implicates AP-4 in the maintenance of cellular homeostasis via the autophagy pathway. Tepsin contributes to vesicle formation at the TGN and additionally regulates ATG9A trafficking via a LIR motif interaction with LC3 (Chapter II). Acute tepsin depletion also dysregulates lysosomes, resulting in their accumulation in the juxtanuclear region (Figure 5-4). Future experiments are necessary

to understand whether this is a direct effect on lysosome function or a secondary effect of dysregulated ATG9A trafficking. Initial experiments to tease apart these phenomenon in tepsin-depleted cells should further test mTORC1 activity and visualize lysosome positioning dynamics.

The preliminary mTORC1 activity assay tested cells after 30 minutes in fed conditions, and no mTORC1 activity was detectable in tepsin-depleted cells (Figure 5-5). However, these cells exhibit reduced autophagy levels in response to nutrient feeding, measured by autophagosome number after one hour in complete nutrient media (Figure 5-6). Conducting a time-course for mTORC1 activation, instead of one static time point, will more thoroughly test effects on nutrient signaling. Based on the rate of autophagy down regulation (Figure 5-6), expanding the time course to measure every 10 minutes across 1 hour of feeding may capture a better dynamic range.

To investigate lysosome positioning, live-cell imaging with an acidic organelle marker (e.g. LysoTracker, Thermo Fisher) would visualize dynamic transport between the cell periphery and the perinuclear region. In wild-type cells, starvation should induce retrograde lysosome transport and nutrient feeding should promote anterograde transport toward the cell periphery (Korolchuk et al., 2011; Pu et al., 2016). Considering juxtanuclear LAMP1 accumulations occur in basal conditions (Figure 5-4) it may be most beneficial to observe starved cells after nutrient re-feeding. If tepsin-depleted cells accumulate LAMP1 signal due to defects in nutrient sensing, we would expect that re-feeding nutrients would not induce anterograde transport of lysosomes toward the periphery. We could also test for dysregulation of lysosome transport machinery by co-

localizing anterograde or retrograde transport effectors with LAMP1 (Pu et al., 2017, 2016, 2015).

It may also be worth returning to tepsin knockout HAP1 cells to look for lysosome and ATG9A phenotypes, characterized for acute tepsin depletion (Figure 5-4, Chapter II), using my improved methodologies. Enlarged degradative organelles were observed by electron micrograpy in tepsin knockout cells (Figure 5-2) suggesting that autophagosome or lysosome morphology is altered. Having phenotypes established in a tepsin knockout system could be very beneficial in teasing apart mechanistic details of tepsin function.

Lastly, crude membrane fractionation (Figure 5-1) approaches may help probe tepsin binding partners, particularly for transient interactions. Co-immunoprecipitations from the membrane enriched fraction could help determine whether tepsin interacts with an LC3B population that is coincident with early autophagic machinery or machinery for autophagic component recycling. This will be an important next step in understanding the mechanistic role of tepsin/LC3B interactions. Similarly, using membrane enriched fractions in co-immunoprecipitations may help validate VPS35L and ISCA1 as tepsin binding partners. From a structural perspective, implementing AlphaFold Multimer to model tepsin interactions with VPS35L or ISCA1 may help clarify how these proteins could interact. Efforts with AlphaFold Multimer are already underway in the lab using computational structural models to inform *in vitro* pulldown experiments.

MATERIALS AND METHODS

Reagents

All reagents were purchased from Sigma unless otherwise noted.

The following antibodies were used in this study: rabbit anti-Phospho-p70S6K 1:1000 for Western blot (9234; Cell Signaling Technology); rabbit anti-p70 S6K 1:1000 for Western blot (2708; Cell Signaling Technology); rabbit anti-LC3B 1:3000 for Western blots (ab48394; Abcam); mouse anti-LC3 1:400 for immunofluorescence (M152-3; Molecular Biology Laboratory); mouse anti-LC3 1:20 for immunofluorescence in HAP1 cells (0231-100/LC3-5F10; NanoTools); mouse anti-alpha tubulin 1:3000 for Western blots (66031; Proteintech); rabbit anti-LAMP1 1:700 for Western blots and 1:1000 for immunofluorescence (ab24170; Abcam); rabbit anti-EEA1 1:1000 for Western blots (ab2900; Abcam); mouse anti-ATP5A 1:3000 (ab14748; Abcam); mouse anti-Rab7 1:2000 for Western blot (ab50533; Abcam); rabbit anti-AP4B1(AP-4 β4) 1:1000 for Western blot (ab130589; Abcam); mouse anti-Arf1 1:5000 for Western blots (ab191376; Abcam); rabbit anti-C16orf62(VPS35L) 1:1500 for Western blots (ab97889; Abcam); rabbit anti-ISCA1 1:100 (PA5-60121; Thermo Fisher Scientific); HRP-conjugated secondaries for Western blots, 1:5000: Pierce goat anti-rabbit IgG (31460; Thermo Fisher Scientific); Pierce goat anti-mouse IgG (31430; Thermo Fisher Scientific); Fluorescent secondary antibodies for immunofluorescence, 1:500: goat anti-Rabbit 594 (A32740; Thermo Fisher Scientific); goat anti-Mouse 488 (A32723; Thermo Fisher Scientific).

Tissue culture

HAP1 cell lines (*ENTHD2* (tepsin) KO: HZGHC000845c002; Parental HAP1: C631) were maintained in IMDM (Gibco) supplemented with 10% v/v fetal bovine serum (FBS; R&D Systems). U-2 OS cells (ATCC; HTB-96) were maintained in McCoy's 5A (modified) media (Thermo Fisher Scientific) supplemented with 10% v/v fetal bovine serum (FBS; R&D Systems). mRFP-GFP-LC3B (Sarkar et al., 2009) HeLa cells were obtained as a gift from the Rubinsztein lab (Cambridge Institute for Medical Research) and maintained in MEM-alpha (Gibco), supplemented with 10% v/v fetal bovine serum and 600 µg/mL G418 (Corning). Wild-type HeLa cells (ATCC; CCL-2) were maintained in MEM-alpha (Gibco), supplemented with 10% v/v fetal bovine serum. All cell lines were cultured at 37ºC in a 5% CO_2 atmosphere. Cell lines were routinely monitored for mycoplasma contamination using DAPI to stain DNA. For starvation during autophagy assays, cells were washed twice with Earle's balanced salt solution (EBSS; Gibco) and incubated with EBSS for 2 hours. Basal cells were concurrently given fresh complete media for the same duration.

siRNA knockdown and DNA transfection

Cells were seeded on 6 well plates and used in knockdown assays the following day. AP-4 knockdown was achieved using ON-TARGETplus AP4E1 siRNA (J-021474-05; Dharmacon) and tepsin knockdown was achieved using ON-TARGETplus C17orf56 siRNA (J-015821-17; Dharmacon). Control cells were treated with ON-TARGETplus non-targeting siRNA (D-001810-01; Dharmacon). Transfections of siRNA were carried out with Oligofectamine (Thermo Fisher Scientific) with a final siRNA concentration of 7.5 nM

(for each AP-4, tepsin, and control siRNA treatment) in complete culture media and assayed 48 hours after transfection. Cells were re-seeded 24 hours after siRNA treatment to a lower cell density on 6 well plates (with or without coverslips) for Western blotting and immunofluorescence assays.

Western blotting

To obtain total cell lysates, cells were resuspended and lysed in NP-40 lysis buffer (10 mM HEPES [pH 7.5], 150 mM NaCl, 0.5 mM EDTA, 1% NP-40, and 1 cOmplete Mini EDTA-free Protease Inhibitor Cocktail tablet (Roche) per 20 mLs. Cell slurry was vortexed briefly then incubated on ice for 30 minutes. The cell slurry was then centrifuged at 20,500 x RCF for 30 minutes. The soluble fraction (lysate) was reserved, and total protein concentration was measured using Precision Red (Cytoskeleton).

Normalized samples were denatured with SDS loading buffer (250mM Tris [pH 6.8], 50 mM DTT, 10% v/v SDS, 20% v/v glycerol, 0.5% w/v bromophenol blue) and boiled for 1 min at 95ºC. Samples were subjected to SDS-PAGE using 4-20% gels (Bio-Rad) and transferred to PVDF membranes (Immobilon-P; Millipore). Blots were incubated with indicated primary and HRP-conjugated secondary antibodies then detected using Amersham ECL Western blotting reagents (GE Healthcare).

mTORC1 activation assay

Cells were seeded on 6 well plates and subsequently subjected to siRNA knockdown as described above. Cells were grown for 48 hours following siRNA transfection. Amino-acid free DMEM (US Biological) without serum was used as

starvation media. Cells were washed once with amino-acid free DMEM then incubated in this media for 2 hours. At 2 hours, 50X MEM amino acid solution (Thermo Fisher Scientific) was added to a final concentration of 1X and incubated for 30 minutes. Cells were lysed in 2% sodium dodecyl sulfate, 50 mM Tris pH 7.5, 150 mM NaCl, 0.5 mM ethylenediaminetetraacetic acid (EDTA), and 1 cOmplete Mini EDTA-free Protease Inhibitor Cocktail tablet (Roche) per 20 mLs. Lysate was applied to a QIAShredder column (Qiagen) and centrifuged for 1 min at 13,000 x RCF. Samples were denatured with SDS loading buffer (250mM Tris [pH 6.8], 50 mM DTT, 10% v/v SDS, 20% v/v glycerol, 0.5% w/v bromophenol blue) and boiled for 1 min at 95ºC then used for Western blotting.

Cell fractionation

Cell fractionation experiments used a published mitochondrial fractionation protocol (Schmucker et al., 2008). Following fractionation samples were normalized by Precision Red and prepared for Western blotting. We probed additional organelle markers to characterize the “mitochondrial” fraction. We detected multiple membrane bound organelles and thus renamed this an organelle fraction.

Transmission electron microscopy

HAP1 cells were culture in complete media (basal) or starved in EBSS. Cells were fixed with 2.5% glutaraldehyde in 0.1 M cacodylate, mechanically lifted from the culture dishes and post-fixed in 1% OsO4 in 0.1 M cacodylate. The samples were dehydrated through a graded ethanol series and infiltrated with Epon-812 (Electron Microscopy Sciences) using propylene oxide as a transition solvent. The resin was polymerized at

60° C for 48 hours. Ultrathin sections with a nominal thickness of 70 nm were taken on a Leica UC7 Ultramicrotome and collected onto 300 mesh copper grids. The sections were stained with 2% uranyl acetate and lead citrate. Transmission electron microscopy was performed using an FEI Tecnai T12 operating at 100 keV using a side mount AMT CMOS camera.

Fluorescence microscopy

Cells were seeded onto 12 mm #1.5 glass coverslips (Fisher Scientific) coated with Histogrip (Invitrogen). Coverslips were imaged with a Nikon Spinning Disk confocal microscope equipped with a Photometrics Prime 95B sCMOS monochrome camera; Plan Apo Lambda Oil 60x 1.40 NA WD 0.13mm objective; 405, 488, 561, and 647 nm excitation lasers. Image analysis was conducted using Nikon's NIS Elements AR Analysis software GA3 pipelines.

mRFP-GFP-LC3B cells were fixed in 3% paraformaldehyde (Electron Microscopy Sciences) in PBS-CM (1X PBS with 0.1 mM $CaCl_2$, 1 mM $MgCl_2$) at room temperature for 20 minutes. Residual paraformaldehyde was quenched by incubating with 50 mM NH_4Cl for 10 minutes. Coverslips were washed three times in PBS-CM with a final wash in dH_2O. To preserve fluorophore signal, coverslips were kept in a dark box during all incubations. Coverslips were mounted in Prolong Diamond with DAPI (Invitrogen). Quantification was performed using spinning disk confocal z-stack images. Individual cell regions of interest (ROIs) were generated using the "grow objects" function on the DAPI [excitation: 405 nm] signal. Punctate structures corresponding to autophagosomes (defined as having mRFP [excitation: 561 nm] and GFP [excitation: 488 nm] signal) or autolysosomes (mRFP signal

only) were segmented using the “threshold” function then subjected to 3D analysis functions to obtain object counts and measure object volume. Data from each replicate was transformed using min-max normalization.

For immunofluorescence assays: Cells were fixed in 3% paraformaldehyde PBS-CM followed by 5 min permeabilization with ice cold methanol at -20ºC. Coverslips were washed three times with PBS-CM then blocked for 1 hour in 1% bovine serum albumin (BSA) in PBS-CM. Primary antibody incubations were conducted overnight at 4ºC. The next day, coverslips were washed 3 times (10 minutes each) with BSA blocking buffer. Fluorescent secondaries were diluted in BSA blocking buffer and incubated for 2 hours at room temperature protected from light. Coverslips were then washed two times with BSA block, once with PBS-CM, and once with dH_2O before being mounted in Prolong Diamond with DAPI. HeLa cell data: quantification of LC3-positive or LAMP1-positive objects performed using spinning disk confocal z-stack images. Individual cell regions of interest (ROIs) were generated using the “grow objects” function on the DAPI [excitation: 405 nm] signal. LC3-positive punctate structures [excitation: 488 nm] or LAMP1-positive objects [excitation: 561 nm] signal) were segmented using the “threshold” function then subjected to 3D analysis functions to obtain measurements. LC3-positive object measurements: object counts per cell, individual object volume; individual mean object intensity [excitation: 488 nm signal], individual object sum intensity [excitation: 488 nm signal]. LAMP1-positive object measurements: individual object volume; individual mean object intensity [excitation: 561 nm signal], individual object sum intensity [excitation: 561 nm signal]. Data from each replicate was transformed using min-max normalization and

individual data points from all replicates were combined for statistical analysis and data visualization.

All statistical significance was analyzed using R (R Core Team, 2021) with scripts written in RStudio and the following packages for data management, statistical testing, and data visualization: tidyverse (Wickham et al., 2019); rstatix (Kassambara, 2021); and viridis (Garnier et al., 2021). Normalcy was assessed based on box-and-whisker plots for all data. These data did not exhibit a normal Gaussian distribution, so non-parametric tests were used. Nonparametric analysis of variance was assessed by the Kruskal-Wallis test and significant results were followed by a Dunn test with Bonferroni correction. When appropriate, two independent samples were compared using the Mann-Whitney U test. Data was graphed using ggplot2 functions in RStudio.

ACKNOWLEDGEMENTS

We sincerely thank David Rubinsztein (Cambridge Institute for Medical Research) for providing the mRFP-GFP-LC3B HeLa cell line. Sincere thanks to Janice Williams (Vanderbilt Cell Imaging Shared Resource EM core, previously) and Amy Kendall for assistance imaging thin cell sections by electron microscopy. Imaging and image analysis was performed in part using the Vanderbilt Cell Imaging Shared Resource (supported by NIH grants CA68485, DK20593, DK58404, DK59637 and EY08126). Special thanks to Kari Seedle in the Nikon Center of Excellence for helping troubleshoot image analysis.

VI. DISCUSSION AND FUTURE DIRECTIONS

It is now well established that AP-4 mediates ATG9A export from the TGN (Chapter II, Behne et al., 2020; Davies et al., 2018; de Pace et al., 2018; Ivankovic et al., 2020; Majumder et al., 2022; Mattera et al., 2017; Scarrott et al., 2023). AP-4-derived ATG9A-containing vesicles are transported toward the cell periphery via RUSC2 interaction with kinesin-1 (Davies et al., 2018; Guardia et al., 2021). AP-4 is also implicated in retrograde ATG9A transport via the FHF complex coupling to dynein-dynactin (Mattera et al., 2020b). Anterograde transport of AP-4-derived ATG9A vesicles has been proposed to partially supply ATG9A vesicle reservoirs (Davies et al., 2018). The function of retrograde ATG9A transport is less clear, but possibly counters RUSC2 anterograde transport to maintain a functional cellular distribution of ATG9A (Mattera et al., 2020b).

Despite being the first identified AP-4 accessory protein (Borner et al., 2012), the function of tepsin is poorly understood. My thesis work has investigated the role of tepsin in the AP-4 coat and how tepsin loss impacts cellular phenotypes. We took two approaches in this work—tepsin knockdown in cultured cells and tepsin knockout in embryonic zebrafish. On the cellular level, we found tepsin is required for efficient ATG9A trafficking and proper function of the autophagy pathway (Chapter II). Our tepsin knockout zebrafish model offers the first characterization of tepsin loss on an organismal scale and indicates tepsin significantly contributes to AP-4 function (Chapter III).

Our data implicate tepsin in coated vesicle formation at the TGN, in line with previous data that AP-4 recruits tepsin to the TGN (Borner et al., 2012; Dell'Angelica et al., 1999a; Frazier et al., 2016; Hirst et al., 1999; Mattera et al., 2015). We looked directly at the trafficking of an AP-4 cargo, ATG9A, to better understand tepsin function at the TGN. Using acute depletion in HeLa cells, we found tepsin is required for proper transport but its loss does not trap ATG9A at the TGN to the same extent as AP-4 (Chapter II). Only one other study has investigated the role of tepsin during AP-4 cargo sorting and found ATG9A export at the TGN was unaffected in tepsin knockout HAP1 cells (Mattera et al., 2017). This difference may arise from the use of knockdown versus knockout techniques. Alternate pathways often compensate for genetic loss, masking cellular phenotypes (Damke et al., 1995; Dell'Angelica et al., 1999b; Hirst et al., 2018; Robinson et al., 2010). Knockout techniques assay protein function after prolonged periods of time, allowing cells to adapt. Acute depletion shortens the time between loss of protein function and experimental observation, meaning there may be less compensation relative to knockout studies. Tepsin depletion does drive increased ATG9A expression levels in cells, which may be an effort to compensate for inefficient ATG9A export at the TGN (Chapter II).

We were able to specifically rescue ATG9A accumulation at the TGN by re-introducing either wild-type or LIR mutant tepsin to cells (Chapter II). These data have raised several interesting questions about the AP-4 coat, especially about possible roles for tepsin in AP-4 coat assembly and vesicle delivery. No scaffold protein has been

identified for the AP-4 coat; it may instead rely on cargo sequestration and accessory proteins to nucleate vesicle formation. Epsins and epsinR are required for AP-1 and AP-2 coat formation, functioning in cargo binding, membrane curvature, and oligomerization of coat components (Chen et al., 1998; Ford et al., 2002; Hirst et al., 2004, 2003; Mills et al., 2003; Sen et al., 2012). We know the tepsin ENTH domain lacks the amphipathic helix other ENTH domains use to induce membrane curvature (Archuleta et al., 2017; Ford et al., 2002; Koshiba et al., 2002). However, tepsin may bind cargo or AP-4 coat components to aide in vesicle formation.

Tepsin may contribute to nucleation by bridging two AP-4 complexes via its β4 and ε binding motifs. Testing this will likely require structural studies of AP-4 with tepsin. Past attempts to purify AP-4 complex in our lab have been unsuccessful. However, AAGAB was recently shown to act as a chaperone for the ε/σ4 heterodimer in cells and loss of AAGAB traps ATG9A at the TGN, akin to AP-4 knockout (Mattera et al., 2022). Future attempts could try co-expression with AAGAB to facilitate AP-4 complex formation, as has been done for AP-1 and AP-2 (Wang et al., 2022). Since loss of epsins results in abortive clathrin coated pit formation (Mettlen et al., 2009), it could also be interesting to explore the ultrastructure of ATG9A accumulations at the TGN to better understand when tepsin is required during coat formation. It is currently unclear whether ATG9A accumulation at the TGN results from malformed vesicle buds or unstable, stalled vesicles that do not efficiently traffic away from the TGN. Fluorophore-ATG9A fusion proteins have been used in several studies to assay ATG9A function during autophagy (Judith et al., 2019; Karanasios et al., 2016; Orsi et al., 2012). With tagged ATG9A, we

could use correlative light electron microscopy to visualize the ultrastructure of ATG9A TGN accumulations.

We can also specifically test the role of tepsin/AP-4 binding in coat formation by mutating the AP-4 binding sites and looking at ATG9A by immunofluorescence. We expect tepsin/AP-4 binding mutants would partially accumulate ATG9A at the TGN similar to tepsin depletion (Chapter II). If tepsin bridges two AP-4 molecules by binding the β4 and ε appendages, mutating only one of the appendage-binding motifs may be sufficient to destabilize coat formation. It may also be beneficial to explore the effect of tepsin depletion on other AP-4 cargoes and accessory proteins to expand our analysis of tepsin function in AP-4 coat formation. Proteomic analyses of tepsin-GFP immunoprecipitations detect several established AP-4 cargoes (Davies et al., 2018): ATG9A, SERINC1, SERINC3, and DAGLB (Davies et al., 2022, 2018; Ivankovic et al., 2020; Mattera et al., 2017). This proteomic dataset is also enriched for the AP-4 accessory protein, Hook1, and assembly chaperone, AAGAB (Davies et al., 2018; Mattera et al., 2022, 2020b).

Detection of all these AP-4-related proteins in tepsin immunoprecipitations strengthens the evidence that tepsin is a major component of AP-4 coated vesicles, as has been previously suggested (Borner et al., 2012). We expect other cargoes will exhibit defects in TGN export following tepsin depletion, similar to ATG9A (Chapter II). DAGLB antibodies are commercially available and suitable for immunofluorescence studies in tepsin-depleted cells. Notably, work currently in pre-print suggests SERINC3 and SERINC5 are lipid scramblases (Leonhardt et al., 2022). This implicates AP-4 in the trafficking of three lipid scramblases, though scramblase activity of SERINC1 and

SERINC3 needs additional biochemical validation. The functional implication of AP-4 as a lipid scramblase transport pathway is a particularly interesting avenue for future studies.

TEPSIN IN AUTOPHAGY

Cellular phenotypes

Similar to AP-4 knockout systems (Davies et al., 2018; de Pace et al., 2018; Ivankovic et al., 2020; Matsuda et al., 2008a; Mattera et al., 2017), autophagy is dysregulated following AP-4 or tepsin acute depletion (Chapter II). Interestingly, we saw different effects for AP-4 and tepsin depletion using an established mRFP-GFP-LC3B reporter to distinguish autophagosome structures from autolysosomes (Sarkar et al., 2009). AP-4 depletion traps ATG9A at the TGN, likely preventing formation of productive early autophagosome structures (Chapter II; Ivankovic et al., 2020). Conversely, tepsin-depleted cells exhibit many, enlarged autophagosomes which mature into autolysosomes (Chapter II). Differences between AP-4 depletion and tepsin depletion likely correspond to differences in ATG9A trafficking defects. Tepsin-depleted cells exhibit increased peripheral ATG9A accumulation, possibly driving increased autophagosome initiation or expansion (Chapter II).

Re-introducing LIR mutant or ΔN-term tepsin resulted in highly dispersed ATG9A throughout the cell instead of clustered accumulations (Chapter II). While this suggests the tepsin LIR/LC3B interaction is important for ATG9A spatial coordination, it's not clear why loss of the LIR motif did not replicate the peripheral ATG9A accumulations observed

after full-length tepsin depletion. We did identify a second LC3B binding interaction *in vitro* (Chapter IV) and, if this interaction occurs in cells, it would presumably be functional in LIR mutant tepsin. Therefore, the ATG9A dispersal may represent a more specific phenotype of the tepsin LIR/LC3B interaction.

Despite the recent characterization of multiple new AP-4 accessory proteins and cargoes, it is still unclear where AP-4 vesicles are targeted and how they are received at those destinations (Davies et al., 2022, 2018; Guardia et al., 2021; Ivankovic et al., 2020; Mattera et al., 2022, 2020b, 2017). In conventional AP trafficking paradigms, tethers on target membranes recognize components on the vesicle to facilitate docking and then SNAREs mediate membrane fusion (Bonifacino and Glick, 2004). Our leading hypothesis to explain the functional role of the tepsin/LC3B interaction suggests tepsin aides in target membrane recognition for AP-4 coated ATG9A vesicles during autophagy.

Knockout phenotypes in embryonic zebrafish

We used CRISPR-editing to knockout tepsin in embryonic zebrafish. We found tepsin knockout phenocopies loss of AP-4 in embryonic zebrafish, resulting in stunted head development and general developmental delays; though, tepsin knockout phenotype severity was diminished compared to AP-4 knockout (Chapter III). Strong similarity between tepsin and AP-4 knockout embryos suggests tepsin and AP-4 are in the same genetic pathway; this is in line with previous data indicating tepsin is a major component of AP-4 vesicles (Borner et al., 2012). ATG9A mRNA expression levels were elevated in tepsin knockout embryos (Chapter III), reminiscent of increased ATG9A protein expression in tepsin-depleted HeLa cells (Chapter II). In both cases, tepsin loss

resulted in higher ATG9A expression than did AP-4 loss. These data hint that autophagy dysregulation partially contributes to tepsin knockout embryo phenotypes (Chapter III).

It's important for future work to consider that neuronal autophagosomes and lysosomes are under additional spatial regulation due to neuronal polarization (Lie and Nixon, 2019; Stavoe and Holzbaur, 2019; Yap et al., 2022). While tepsin or AP-4 loss appears to globally dysregulate lysosome position and nutrient sensing in HeLa cells (Chapter V), neurons may have phenotypes in specific cellular regions. Stalled LC3 structures and axon swellings occur at the distal axon tip in AP-4 ε knockout mice (de Pace et al., 2018; Ivankovic et al., 2020) and may indicate accumulation of immature autophagosomes. Exploring tepsin depletion in neurons could greatly improve our understanding of dysregulated autophagosome morphology considering the unique spatial coordination.

ATG9A SPATIAL OR TEMPORAL COORDINATION VIA TEPSIN/LC3B INTERACTIONS

Emerging evidence implicates ATG9A vesicles as seed membranes for autophagosome biogenesis; as a result, ATG9A is a minor component in mature autophagosomes and difficult to detect (Olivas et al., 2022; Sawa-Makarska et al., 2020). ATG9A, a lipid scramblase, interacts with ATG2, a lipid transferase, to expand the phagophore membrane (Guardia et al., 2020b; Maeda et al., 2020b; Matoba et al., 2020; Noda, 2021; Osawa et al., 2019). LC3/GABARAP proteins also mediate membrane tethering and fusion, contributing to pre-autophagosome structure formation and later to

phagophore membrane expansion (Landajuela et al., 2016; Weidberg et al., 2011, 2010; Yamamoto et al., 2012).

We identified a second LC3B binding site in the tepsin VHS domain region (residues 220-360; Chapter IV). AlphaFold Multimer modelling predicts a motif, with the core sequence ERVEV, which binds at the LC3B LDS. While this prospective motif needs further validation, it is interesting to speculate how the LIR motif and ERVEV motif could each contribute to tepsin/LC3B interactions. It seems most likely for tepsin to interact with LC3B at autophagic membranes (Chapter II). Sharing a common interface, the LIR and ERVEV motifs may compete to bind a single LC3B molecule (Figure 6-1A). Alternatively, a single molecule of tepsin could utilize both motifs (41 residues apart; approximately 102 Å) and interact with two LC3B molecules, dependent on the LC3B spacing along autophagic membranes (Figure 6-1B). Our *in vitro* pulldown experiments do not indicate an additive effect from having both motifs but preliminary ITC experiments using a tepsin construct with both motifs does exhibit 2:1 stoichiometry (Chapter IV). These data were originally analyzed

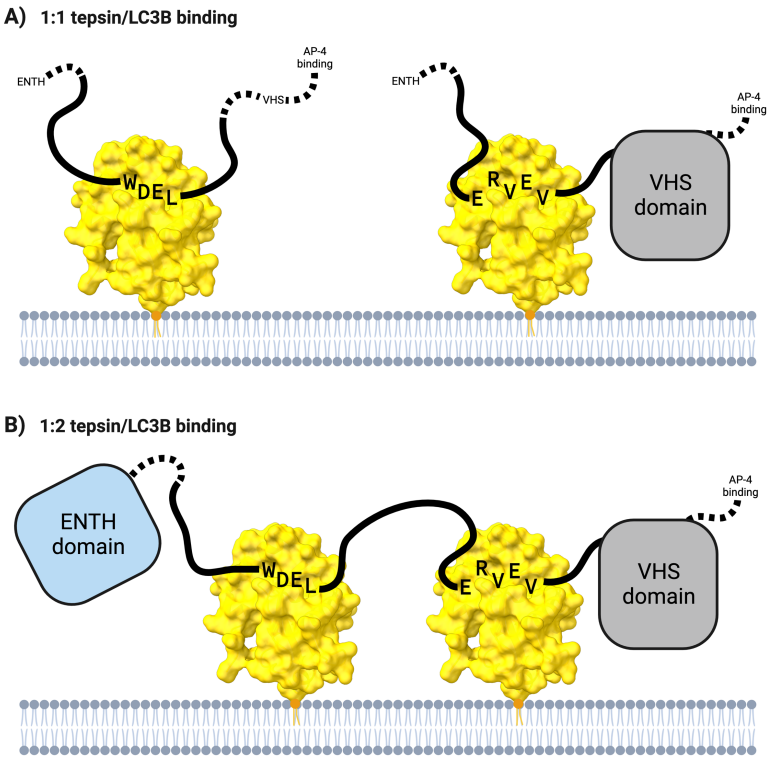

Figure 6-1: Models for tepsin/LC3B binding. (A) Tepsin binds LC3B with 1:1 stoichiometry using either the LIR motif or the ERVEV motif. (B) Tepsin binds LC3B with 1:2 stoichiometry using both the LIR motif and the ERVEV motif to bind two LC3B molecules. LC3B is modeled from PDB: 2ZJD. Made in part with BioRender.

assuming an independent binding site and should be re-analyzed with a two binding-site model.

We determined the tepsin LIR motif binds LC3B in solution with micromolar affinity (Chapter II). LC3B protein density on autophagic membranes increases during early phagophore nucleation and expansion then decreases as de-lipidation machinery removes LC3B from the cytosolic face of mature autophagosomes/autolysosomes (Abreu et al., 2017; Agrotis et al., 2019; Kirisako et al., 2000; Landajuela et al., 2016; Nair et al., 2012; Weidberg et al., 2010). Avidity effects may therefore allow temporal regulation by LIR- and/or ERVEV-LC3B interactions during autophagosome maturation. LC3B is sufficient to tether and fuse liposomes *in vitro* and contributes to nucleation and expansion of the phagophore in cells (Moreau et al., 2011; Weidberg et al., 2011). However, it's possible other interactions in cells are necessary to help specify which membranes LC3B will tether or fuse. With this in mind, LIR mutant tepsin may drive highly diffuse ATG9A distribution because the cells are trying to compensate for ineffective targeting to the PAS. Interestingly, two LC3B arginine residues (Arg10 and Arg11) significantly contribute to LC3B-mediated membrane fusion *in vitro* and in cells, promoting autophagosome biogenesis and expansion (Weidberg et al., 2011, 2010). These same residues are implicated in ERVEV/LC3B binding but not LIR/LC3B binding (Chapter IV). Increased LC3B membrane density could allow for high avidity ERVEV-LC3B interactions that reduce LC3B-mediated membrane expansion. In this scenario, loss of ERVEV binding could cause enlarged autophagosomes due to unregulated LC3B-mediated expansion.

Biochemically, it is important to validate the ERVEV AlphaFold Multimer model *in vitro* and in cells. From the model, we will test structure-based mutations to determine

which residues are essential for LC3B-binding. Biolayer interferometry can be used to probe the effect of avidity on LIR or ERVEV binding. We can also use this technique to measure kinetics when both motifs are present versus only one or the other. Following molecular characterization of the ERVEV motif, we can compare the independent effect of ERVEV mutant versus LIR mutant tepsin on ATG9A trafficking and autophagy in cells. Together, these data will provide additional insight into the ways tepsin may regulate these processes.

MODELS FOR TEPSIN IN ATG9A AVAILABILITY DURING AUTOPHAGY

Altogether, these data suggest tepsin, as a part of the AP-4 coat, can modulate autophagy. Two important questions remain. Where does the tepsin/LC3B interaction occur and how does its loss dysregulate autophagosome expansion? Our favored models propose that tepsin either regulates ATG9A targeting to the PAS for early nucleation (Figure 6-2A) or mediates retrieval of ATG9A to limit phagophore expansion (Figure 6-2B).

We know tepsin requires AP-4 for its membrane recruitment at the TGN (Archuleta et al., 2017; Borner et al., 2012; Frazier et al., 2016; Mattera et al., 2015). For these models, AP-4-derived vesicles would need to remain coated at the cell periphery. Clathrin cage disassembly, as well as AP-1 and AP-2 membrane dissociation, occur shortly after vesicle budding (Barouch et al., 1994; Beacham et al., 2019; Ghosh and Kornfeld, 2003; Prasad et al., 1993; Robinson and Pearse, 1986; Rothnie et al., 2011; Schuermann et al.,

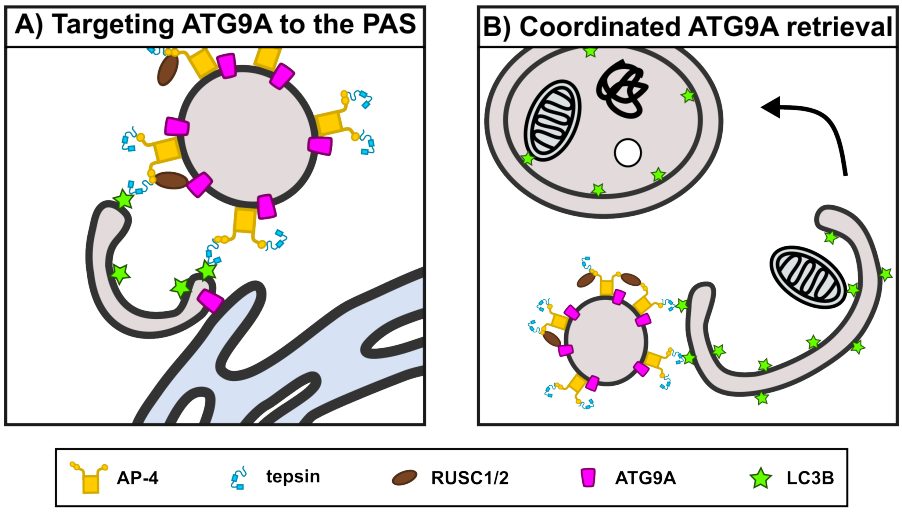

Figure 6-2: Models for tepsin/LC3B interaction in ATG9A delivery or retrieval. (A) Tepsin/LC3B interaction mediates recognition of target membranes for ATG9A delivery to pre-autophagosome sites (PAS). (B) Tepsin/LC3B interaction coordinates ATG9A retrieval during autophagosome maturation, dependent on LC3B protein density.

2008). However, non-clathrin AP coats may form and function differently from AP-1 and AP-2 clathrin coats (Hirst et al., 2021, 2013a; Schoppe et al., 2021, 2020). δ-COPI binds the Dsl1 tethering complex, and additional interactions between Dsl1 and COPI subunits mediate uncoating to allow vesicle fusion (Andag and Schmitt, 2003; Suckling et al., 2015; Travis et al., 2020, 2019; Zink et al., 2009). AP-3 also mediates its own tethering interaction and only afterward does AP-3 uncoat from vesicles to allow vesicle fusion (Darsow et al., 2001; Schoppe et al., 2020). There is also evidence of punctate tepsin structures moving between the perinuclear region and cell periphery in live cell imaging (Borner et al., 2012). AP-4 recruits accessory proteins RUSC2 or Hook1/Hook2 for anterograde or retrograde transport, respectively (Davies et al., 2018; Guardia et al., 2021; Mattera et al., 2020b). These data indicate AP-4 vesicles may remain coated, at least during microtubule transport.

Does tepsin target ATG9A vesicles to the PAS?

Multiple trafficking pathways via the TGN, endosomes, and plasma membrane are proposed contributors to ATG9A reservoirs for autophagosome biogenesis (Davies et al., 2018; Imai et al., 2016; Mari et al., 2010; Orsi et al., 2012; Singh et al., 2019; Søreng et al., 2018; Yamamoto et al., 2012). However, Golgi-derived ATG9A vesicles are believed to be the primary source in yeast as well as metazoans (Mari et al., 2010; Yamamoto et al., 2012). If tepsin mediates ATG9A targeting to the PAS, we would expect to see accumulation in ATG9A reservoirs following tepsin depletion.

Instead, our rescue experiments show introducing LIR mutant tepsin resulted in highly dispersed ATG9A. We saw similar ATG9A dispersal after introducing ΔN-term tepsin, which lacks the ENTH and VHS domains, as well as both the LIR and ERVEV motifs. The ΔN-term tepsin construct acted as a dominant negative, causing diffuse ATG9A distribution even in control cells and hinting at the importance of the entire tepsin N-terminus (Chapter II). These phenotypes most closely resemble depletion of the FHF complex and thus disruption of retrograde AP-4 vesicle trafficking. AP-4 μ4 interacts with Hook1/Hook2 to coordinate this retrograde transport. Depletion of FHF components results in dispersed AP-4 and ATG9A as well as enlarged LC3B-positive autophagosomes (Mattera et al., 2020b).

Balance between anterograde and retrograde ATG9A transport is believed to maintain a functional distribution of ATG9A throughout the cell. Perhaps this also involves some tethering of AP-4 coated vesicles at the PAS to “drop off” ATG9A-positive vesicles. Without the tepsin LIR/LC3B interaction, it is possible ATG9A-containing AP-4 vesicles essentially get stuck moving between the perinuclear region and the cell periphery (Figure

6-3). In this context, peripheral accumulation observed following tepsin depletion could instead represent de-stabilized AP-4 coats that irregularly distribute ATG9A, since tepsin is necessary for efficient AP-4 coat formation.

These ATG9A accumulations may still be competent for autophagy initiation but result in aberrant autophagosome morphology (Chapter II). LC3 and GABARAP proteins are present early on in autophagosome biogenesis, incorporated at high curvature membranes (Alemu et al., 2012; Nath et al., 2014; Weidberg et al., 2010). ATG9A vesicles

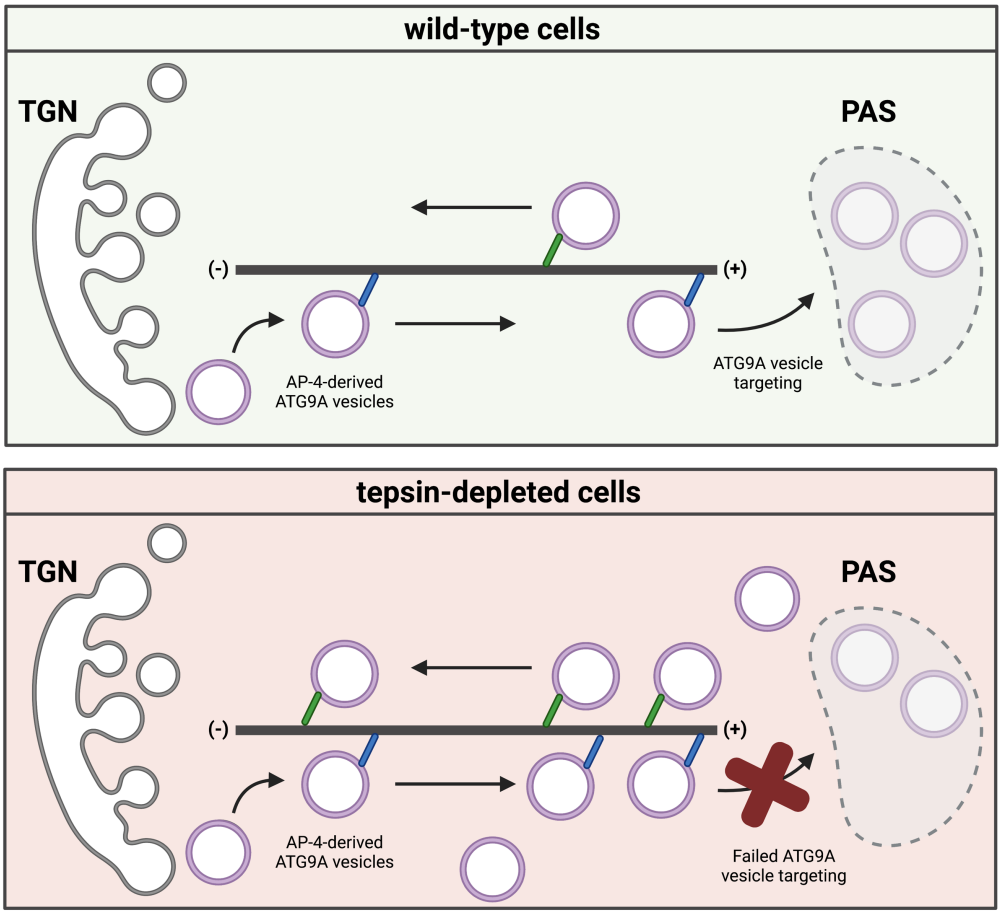

Figure 6-3: Model for tepsin in ATG9A vesicle delivery. In wild-type cells, anterograde and retrograde transport distributes AP-4 vesicles containing ATG9A throughout the cell. Tepsin mediates the delivery of ATG9A vesicles to the PAS via interaction with LC3B. In tepsin-depleted cells, ATG9A vesicles are not properly targeted to the PAS and as a result accumulate throughout the cell. Compensatory increases in ATG9A expression levels may also contribute to this diffuse accumulation and allow some ATG9A to end up at the PAS, in spite of AP-4 trafficking defects. Made in Biorender.

are implicated as seed membranes for autophagosomes that expand via the ATG9/ATG2 lipid transfer system with ER membranes (Noda, 2021; Olivas et al., 2022; Sawa-Makarska et al., 2020). There is also evidence that ATG9A vesicles undergo early homotypic fusion events combining multiple ATG9A vesicles to nucleate pre-autophagosome structures (Yamamoto et al., 2012). mATG8 proteins are sufficient to fuse liposomes *in vitro* (Weidberg et al., 2011), so it's possible accumulated ATG9A vesicles fuse and, with more ATG9A incorporated, exhibit increased phagophore expansion.

Could tepsin mediate ATG9A retrieval from the cell periphery?

Alternatively, AP-4 retrograde transport of ATG9A may mediate retrieval of some ATG9A from autophagy structures (Mattera et al., 2017). Recent work characterized a pathway that recycles autophagy proteins, ATG9A and STX17, from autolysosomes by SNX4, SNX5, and SNX17, together called 'recycler' (Ravussin et al., 2021; Zhou et al., 2022). Blocking recycler function did not impair autophagosome biogenesis, suggesting ATG9A is not terminally accumulated on autolysosomes and may have other recycling mechanisms (Zhou et al., 2022).

Retrograde ATG9A transport by AP-4 could be an alternate mechanism to recycler for ATG9A retrieval (Figure 6-4). Temporal coordination of ATG9A retrieval could be conferred by tepsin/LC3B interaction avidity, and we would expect peripheral accumulations when ATG9A was not properly retrieved. Furthermore, prolonged residency of ATG9A in phagophore membranes may increase autophagosome size. However, it is difficult to conceptualize how loss of an LC3B interaction would induce

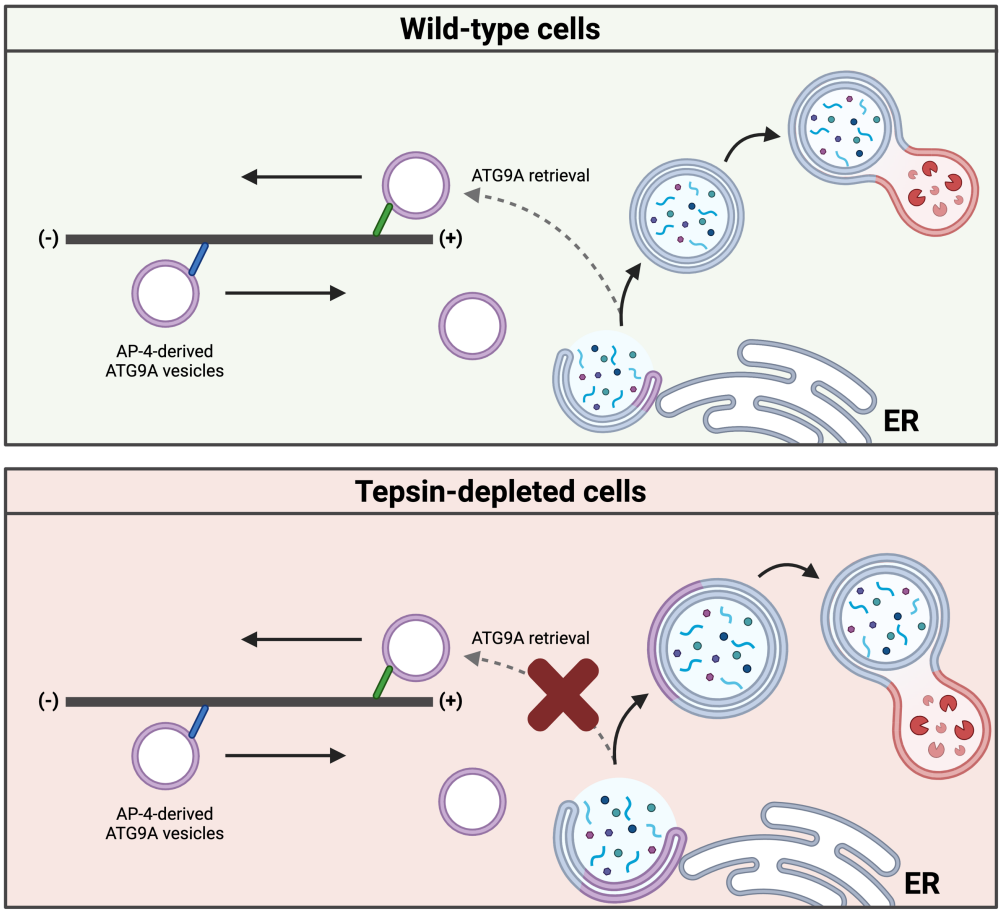

Figure 6-4: Model for tepsin in ATG9A retrieval. In wild-type cells, ATG9A vesicles are seed membranes for autophagosomes. As autophagosomes mature, tepsin coordinates retrieval of ATG9A from autophagosomes for AP-4-mediated retrograde transport. In tepsin-depleted cells, ATG9A accumulates along autophagosomes, increasing ATG9A-driven phagophore expansion. Made in BioRender.

retrograde transport; especially if the tepsin/LC3B interaction do not target ATG9A delivery in the first place. Would this mean AP-4-coated vesicles develop into autophagosomes? How would ATG9A vesicles reform to bud off mature autophagosomes? Perhaps AP-4 could hand-off ATG9A to the recycler complex and tepsin/LC3B interaction helps temporally coordinate recycling indirectly. The retriever subunit, VPS35L, is a prospective tepsin binding partner (Chapter V) and SNX17 associates with the retriever and recycler complexes (McNally et al., 2017; Zhou et al.,

2022). It would be particularly interesting to explore a tepsin and SNX17 interaction. Ultimately, a recycling model seems less likely than a role for tepsin/LC3B interaction in targeting to the PAS; however, future experiments will need to improve our molecular understanding of the tepsin/LC3B interaction in cells. It is important to understand where tepsin/LC3B interaction occurs and what other autophagic machinery is coincident at the time of interaction.

Future directions for distinguishing ATG9A delivery and recycling models

To differentiate between the delivery and retrieval models, we must determine the location of tepsin/LC3B interactions. If the ATG9A accumulations occur due to a block in retrieval, ATG9A accumulations should co-localize with LC3B on autophagosome or autolysosomes. Profiling co-localization with other autophagy machinery is limited by compatibility of the available antibodies, but we can co-stain ATG9A with either LC3B or WIPI2, a marker for early autophagy structures (Wan and Liu, 2019). CLEM analysis of ATG9A peripheral accumulations could also help clarify whether these accumulations are ATG9A vesicle pools or ATG9A accumulations on autophagosomes.

Co-immunoprecipitation experiments from tepsin-GFP HeLa cells can look for coincidence of tepsin with autophagy initiation components (i.e. ATG2 and WIPI2) or recycler trafficking proteins (SNX4, SNX5, SNX17). Since this is likely to occur with only a transient protein population, using the membrane-enriched fraction from subcellular fractionations (Chapter V) in co-immunoprecipitations may improve detection. Alternatively, since the ΔN-term tepsin construct functions as a dominant negative, we may be able to use the myc-tag in this construct to enrich for defective AP-4 vesicles. Our

ATG9A targeting model suggests the dispersed ATG9A signal may represent an accumulation of AP-4 coated, ATG9A-containing vesicles. Similar accumulations of coated vesicles are observed when mutations block COPI tethering (Zink et al., 2009). Myc immunoprecipitations from ΔN-term tepsin-myc transfected lysates should exhibit reduced coincidence with autophagy machinery compared to wild-type tepsin-myc.

FUNCTIONAL LINKS BETWEEN ATG9A TRAFFICKING AND LYSOSOMES

While characterizing autophagy in AP-4 or tepsin-depleted cells, I also identified defects in lysosomal morphology and mTORC1 signaling (Chapter V). Following tepsin or AP-4 depletion, LAMP1-positive late endosome/lysosomes accumulate in the perinuclear area. mTORC1 activation, in response to nutrient feeding, was also diminished in cells depleted for AP-4 or tepsin (Chapter V). Disruption of lysosome function and transport was partially corroborated by a recent study using iPSC-derived AP-4 ε knockout neurons. Majumder *et al.* found AP-4 loss disrupted lysosomal composition and axonal transport (Majumder et al., 2022). This study, and others using AP-4 β4 or ε knockout mice, have commonly found axonal swellings containing varying combinations of autophagosomes, lysosomes, protein aggregates, and ER (de Pace et al., 2018; Ivankovic et al., 2020; Majumder et al., 2022; Matsuda et al., 2008a; Scarrott et al., 2023). It remains unclear whether AP-4 dysfunction directly causes lysosomal phenotypes or whether they represent indirect phenotypes resulting from AP-4 loss.

Lysosomes are linked to the autophagy pathway as the terminal fusion step to

generate autolysosomes (Yu et al., 2010; Zhao and Zhang, 2019). Activated mTORC1 also uses lysosomes as a signaling platform during nutrient-rich conditions to negatively regulate autophagy induction (Hesketh et al., 2018; Rabanal-Ruiz et al., 2018). Interestingly, ATG9A has also been linked to lysosomal hydrolase transport through a direct interaction with AP-1 that promotes AP-1 interaction with the cation independent mannose-6-phosphate receptor (CIMPR) (Jia et al., 2017). Disrupting the AP-1/ATG9A interaction resulted in defective maturation of cathepsin L, reduced lysosomal degradation, but no change in lysosome acidification (Jia et al., 2017). Interestingly, these same lysosomal phenotypes were reported following AP-4 knockout (Majumder et al., 2022).

ATG9A steady state localization is dispersed between the TGN, endosomes, plasma membrane, and ATG9 vesicle “reservoirs” with many membrane trafficking proteins implicated in maintaining ATG9A cellular distribution (Campisi et al., 2022; Davies et al., 2018; Imai et al., 2016; Judith et al., 2019; Mari et al., 2010; Popovic and Dikic, 2014; Søreng et al., 2018; Yamamoto et al., 2012; Young et al., 2006). ATG9A trafficking is highly dynamic and it’s important to remember that ATG9A has some identified functions independent of autophagy. It would be interesting to test lysosome composition in tepsin-depleted cells to see whether tepsin depletion replicates AP-4 knockout results (Majumder et al., 2022). Preliminary staining conducted with LysoTracker dye does suggest LAMP1 structures are properly acidified (high degree of LAMP1/LysoTracker colocalization; data not shown). However, tepsin or AP-4 depletion may inadvertently disrupt the cellular availability for other ATG9A pathways, such as ATG9A/AP-1-mediated hydrolase trafficking. It will be important to separate secondary

effects of AP-4 or tepsin depletion from direct AP-4 trafficking defects. It may be interesting to see whether re-introducing LIR mutant tepsin can rescue lysosomal phenotypes. If lysosomal phenotypes arise in tepsin-depleted cells due to disrupted coat formation and inefficient ATG9A trafficking, introducing LIR mutant tepsin should partially rescue AP-4-cargo trafficking defects that are independent of autophagy. However, if lysosomal phenotypes persist with LIR mutant tepsin this indicates lysosomes are disrupted by effects downstream of AP-4-mediated ATG9A trafficking.

TEPSIN FUNCTION IN NEURONS AND AP-4 HEREDITARY SPASTIC PARAPLEGIAS

Autophagy is particularly important for the maintenance of long-lived neuronal cells (Ebrahimi-Fakhari et al., 2016; Stavoe and Holzbaur, 2019). Loss of AP-4 reduces axonal transport of ATG9A, diminishing its availability for autophagy induction at the axon terminal (Behne et al., 2020; De Pace et al., 2018; Ivankovic et al., 2020; Scarrott et al., 2023). Autophagosome formation and maturation are subjected to unique spatial coordination within polarized neurons as autophagosomes mature into autolysosomes while being transported from the distal axon to the soma (Fu et al., 2014; Maday et al., 2012). AP-4 knockout neurons accumulate autophagosomes in the distal axon, suggesting retrograde autophagosome transport is blocked (De Pace et al., 2018; Ivankovic et al., 2020; Matsuda et al., 2008; Scarrott et al., 2023). These accumulations form during impaired axon outgrowth and may explain white matter loss in AP-4 HSP patients (Ebrahimi-Fakhari et al., 2020; Ivankovic et al., 2020).

Beyond export of ATG9A from the TGN, the data presented here link AP-4 more directly to the autophagy pathway via the interaction of tepsin and LC3B (Chapters II and IV). Visualizing axonal autophagosome transport in neurons lacking tepsin may clarify the role of tepsin/LC3B interactions during autophagy. We hypothesize tepsin/LC3 interaction impacts ATG9A availability for neuronal autophagy and tepsin loss would dysregulate autophagosome form and function. Therefore, tepsin loss would decrease retrograde autophagosome transport, resulting in similar axonal autophagosome accumulations to those observed in AP-4 knockout neurons. On the organismal level, we expect defective autophagy, from either tepsin or AP-4 knockout, would result in similar anatomical abnormalities, such as loss of white matter. In fact, tepsin knockout zebrafish exhibit malformed heads similar to AP-4 knockout zebrafish (Chapter III), which may partially arise from deficits in neuronal autophagy and neuronal development.

CONCLUDING REMARKS

This work provides the first direct evidence of tepsin functions in AP-4 coat formation, ATG9A trafficking, and autophagy. These discoveries expand our understanding of non-clathrin AP coats and how they compare to AP-1 and AP-2 coat paradigms. The tepsin/LC3B interaction we characterized suggests AP-4 trafficking directly intersects with autophagosome biogenesis. Many trafficking mechanisms maintain organelle identities through the movement of proteins and lipids, but the

recycling of autophagy machinery was only recently identified. Our work further implicates AP-4 in the maintenance of readily accessible ATG9A seed membranes, driven in part by tepsin/LC3B interactions. In addition to recycling from autophagosomes, future work should consider how cells maintain ATG9A availability for rapid autophagosome biogenesis and ultimately cellular homeostasis.

BIBLIOGRAPHY

Abdollahpour, H., Alawi, M., Kortüm, F., Beckstette, M., Seemanova, E., Komárek, V., Rosenberger, G., Kutsche, K., 2014. An AP4B1 frameshift mutation in siblings with intellectual disability and spastic tetraplegia further delineates the AP-4 deficiency syndrome. European Journal of Human Genetics 2015 23:2 23, 256–259.

Abou Jamra, R., Philippe, O., Raas-Rothschild, A., Eck, S.H., Graf, E., Buchert, R., Borck, G., Ekici, A., Brockschmidt, F.F., Nöthen, M.M., Munnich, A., Strom, T.M., Reis, A., Colleaux, L., 2011. Adaptor protein complex 4 deficiency causes severe autosomal-recessive intellectual disability, progressive spastic paraplegia, shy character, and short stature. Am J Hum Genet 88, 788–795.

Abreu, S., Kriegenburg, F., Gómez-Sánchez, R., Mari, M., Sánchez-Wandelmer, J., Rasmussen, M.S., Guimarães, R.S., Zens, B., Schuschnig, M., Hardenberg, R., Peter, M., Johansen, T., Kraft, C., Martens, S., Reggiori, F., 2017. Conserved Atg8 recognition sites mediate Atg4 association with autophagosomal membranes and Atg8 deconjugation. EMBO Rep 18, 765–780.

Agrotis, A., Pengo, N., Burden, J.J., Ketteler, R., 2019. Redundancy of human ATG4 protease isoforms in autophagy and LC3/GABARAP processing revealed in cells. Autophagy 15, 976–997.

Aguilar, R.C., Boehm, M., Gorshkova, I., Crouch, R.J., Tomita, K., Saito, T., Ohno, H., Bonifacino, J.S., 2001. Signal-binding Specificity of the μ4 Subunit of the Adaptor Protein Complex AP-4. Journal of Biological Chemistry 276, 13145–13152.

Alemu, E.A., Lamark, T., Torgersen, K.M., Birgisdottir, A.B., Larsen, K.B., Jain, A., Olsvik, H., Øvervatn, A., Kirkin, V., Johansen, T., 2012. ATG8 family proteins act as scaffolds for assembly of the ULK complex: Sequence requirements for LC3-interacting region (LIR) motifs. Journal of Biological Chemistry 287, 39275–39290.

Andag, U., Schmitt, H.D., 2003. Dsl1p, an Essential Component of the Golgi-Endoplasmic Reticulum Retrieval System in Yeast, Uses the Same Sequence Motif to Interact with Different Subunits of the COPI Vesicle Coat. Journal of Biological Chemistry 278, 51722–51734.

Archuleta, T.L., Frazier, M.N., Monken, A.E., Kendall, A.K., Harp, J., McCoy, A.J., Creanza, N., Jackson, L.P., 2017. Structure and evolution of ENTH and VHS/ENTH-like domains in tepsin. Traffic 18, 590–603.

Ballabio, A., Bonifacino, J.S., 2019. Lysosomes as dynamic regulators of cell and organismal homeostasis. Nature Reviews Molecular Cell Biology 2019 21:2 21, 101–118.

Barlowe, C., Orci, L., Yeung, T., Hosobuchi, M., Hamamoto, S., Salama, N., Rexach, M.F., Ravazzola, M., Amherdt, M., Schekman, R., 1994. COPII: A membrane coat formed by Sec proteins that drive vesicle budding from the endoplasmic reticulum. Cell 77, 895–907.

Barlowe, C.K., Miller, E.A., 2013. Secretory Protein Biogenesis and Traffic in the Early Secretory Pathway. Genetics 193, 383–410.

Barouch, W., Prasad, K., Greene, L.E., Eisenberg, E., 1994. ATPase Activity Associated with the Uncoating of Clathrin Baskets by Hsp70*. Journal of Biological Chemistry 269, 28563–28568.

Bauer, P., Leshinsky-Silver, E., Blumkin, L., Schlipf, N., Schröder, C., Schicks, J., Lev, D., Riess, O., Lerman-Sagie, T., Schöls, L., 2012. Mutation in the AP4B1 gene cause hereditary spastic paraplegia type 47 (SPG47). Neurogenetics 13, 73–76.

Beacham, G.M., Partlow, E.A., Hollopeter, G., 2019. Conformational regulation of AP1 and AP2 clathrin adaptor complexes. Traffic 20, 741–751.

Behne, R., Teinert, J., Wimmer, M., D'Amore, A., Davies, A.K., Scarrott, J.M., Eberhardt, K., Brechmann, B., Chen, I.P.F., Buttermore, E.D., Barrett, L., Dwyer, S., Chen, T., Hirst, J., Wiesener, A., Segal, D., Martinuzzi, A., Duarte, S.T., Bennett, J.T., Bourinaris, T., Houlden, H., Roubertie, A., Santorelli, F.M., Robinson, M., Azzouz, M., Lipton, J.O., Borner, G.H.H., Sahin, M., Ebrahimi-Fakhari, D., 2020. Adaptor protein complex 4 deficiency: a paradigm of childhood-onset hereditary spastic paraplegia caused by defective protein trafficking. Hum Mol Genet 29, 320–334.

Behrends, C., Sowa, M.E., Gygi, S.P., Harper, J.W., 2010. Network organization of the human autophagy system. Nature 466, 68–76.

Bentley, M., Banker, G., 2016. The cellular mechanisms that maintain neuronal polarity. Nature Reviews Neuroscience 2016 17:10 17, 611–622.

Birgisdottir, Å.B., Lamark, T., Johansen, T., 2013. The LIR motif - crucial for selective autophagy. J Cell Sci 126, 3237–3247.

Black, M.W., Pelham, H.R.B., 2000. A Selective Transport Route from Golgi to Late Endosomes That Requires the Yeast Gga Proteins. Journal of Cell Biology 151, 587–600.

Boehm, M., Aguilar, R.C., Bonifacino, J.S., 2001. Functional and physical interactions of the adaptor protein complex AP-4 with ADP-ribosylation factors (ARFs). EMBO Journal 20, 6265–6276.

Boll, W., Ohno, H., Songyang, Z., Rapoport, I., Cantley, L.C., Bonifacino, J.S., Kirchhausen, T., 1996. Sequence requirements for the recognition of tyrosine-based endocytic signals by clathrin AP-2 complexes. EMBO J 15, 5789–5795.

Bonifacino, J.S., Glick, B.S., 2004. The Mechanisms of Vesicle Budding and Fusion. Cell 116, 153–166.

Borner, G.H.H., Antrobus, R., Hirst, J., Bhumbra, G.S., Kozik, P., Jackson, L.P., Sahlender, D.A., Robinson, M.S., 2012. Multivariate proteomic profiling identifies novel accessory proteins of coated vesicles. Journal of Cell Biology 197, 141–160.

Burgos, P. v., Mardones, G.A., Rojas, A.L., daSilva, L.L.P., Prabhu, Y., Hurley, J.H., Bonifacino, J.S., 2010. Sorting of the Alzheimer's Disease Amyloid Precursor Protein Mediated by the AP-4 Complex. Dev Cell 18, 425–436.

Campisi, D., Desrues, L., Dembélé, K.P., Mutel, A., Parment, R., Gandolfo, P., Castel, H., Morin, F., 2022. The core autophagy protein ATG9A controls dynamics of cell protrusions and directed migration. Journal of Cell Biology 221.

Chen, H., Fre, S., Slepnev, V.I., Capua, M.R., Takei, K., Butler, M.H., di Fiore, P.P., de Camilli, P., 1998. Epsin is an EH-domain-binding protein implicated in clathrin-mediated endocytosis. Nature 1998 394:6695 394, 793–797.

Chen, K.E., Healy, M.D., Collins, B.M., 2019. Towards a molecular understanding of endosomal trafficking by Retromer and Retriever. Traffic 20, 465–478.

Chen, Z., Schmid, S.L., 2020. Evolving models for assembling and shaping clathrin-coated pits. J Cell Biol 219.

Claude, A., 1946. FRACTIONATION OF MAMMALIAN LIVER CELLS BY DIFFERENTIAL CENTRIFUGATION : II. EXPERIMENTAL PROCEDURES AND RESULTS. J Exp Med 84, 61.

Claude, A., 1975. The coming of age of the cell. Science (1979) 189, 433–435.

Clements, T.P., Tandon, B., Lintel, H.A., McCarty, J.H., Wagner, D.S., 2017. RICE CRISPR: Rapidly Increased Cut Ends by an Exonuclease Cas9 Fusion in Zebrafish. Genesis 55.

Collins, B.M., McCoy, A.J., Kent, H.M., Evans, P.R., Owen, D.J., 2002. Molecular Architecture and Functional Model of the Endocytic AP2 Complex. Cell 109, 523–535.

Cosson, P., Letourneur, F., 1997. Coatomer (COPI)-coated vesicles: role in intracellular transport and protein sorting. Curr Opin Cell Biol 9, 484–487.

Cowles, C.R., Odorizzi, G., Payne, G.S., Emr, S.D., 1997. The AP-3 Adaptor Complex Is Essential for Cargo-Selective Transport to the Yeast Vacuole. Cell 91, 109–118.

Cox, N.J., Unlu, G., Bisnett, B.J., Meister, T.R., Condon, B.M., Luo, P.M., Smith, T.J., Hanna, M., Chhetri, A., Soderblom, E.J., Audhya, A., Knapik, E.W., Boyce, M., 2018. Dynamic glycosylation governs the vertebrate COPII protein trafficking pathway. Biochemistry 57, 91.

Dacks, J.B., Robinson, M.S., 2017. Outerwear through the ages: evolutionary cell biology of vesicle coats. Curr Opin Cell Biol 47, 108–116.

Damke, H., Baba, T., van der Bliek, A.M., Schmid, S.L., 1995. Clathrin-independent pinocytosis is induced in cells overexpressing a temperature-sensitive mutant of dynamin. Journal of Cell Biology 131, 69–80.

D'Amore, A., Tessa, A., Naef, V., Bassi, M.T., Citterio, A., Romaniello, R., Fichi, G., Galatolo, D., Mero, S., Battini, R., Bertocci, G., Baldacci, J., Sicca, F., Gemignani, F., Ricca, I., Rubegni, A., Hirst, J., Marchese, M., Sahin, M., Ebrahimi-Fakhari, D., Santorelli, F.M., 2020. Loss of ap4s1 in zebrafish leads to neurodevelopmental defects resembling spastic paraplegia 52. Ann Clin Transl Neurol 7, 584–589.

Darsow, T., Burd, C.G., Emr, S.D., 1998. Acidic Di-leucine Motif Essential for AP-3–dependent Sorting and Restriction of the Functional Specificity of the Vam3p Vacuolar t-SNARE. J Cell Biol 142, 913.

Darsow, T., Katzmann, D.J., Cowles, C.R., Emr, S.D., 2001. Vps41p function in the alkaline phosphatase pathway requires homo-oligomerization and interaction with AP-3 through two distinct domains. Mol Biol Cell 12, 37–51.

Davies, A.K., Alecu, J.E., Ziegler, M., Vasilopoulou, C.G., Merciai, F., Jumo, H., Afshar-Saber, W., Sahin, M., Ebrahimi-Fakhari, D., Borner, G.H.H., 2022. AP-4-mediated axonal transport controls endocannabinoid production in neurons. Nat Commun 13.

Davies, A.K., Itzhak, D.N., Edgar, J.R., Archuleta, T.L., Hirst, J., Jackson, L.P., Robinson, M.S., Borner, G.H.H., 2018. AP-4 vesicles contribute to spatial control of autophagy via RUSC-dependent peripheral delivery of ATG9A. Nat Commun 9.

de Duve, C., 1975. Exploring cells with a centrifuge. Science (1979) 189, 186–194.

de Duve, C., Pressman, B.C., Gianetto, R., Wattiaux, R., Appelmans, F., 1955. Tissue fractionation studies. 6. Intracellular distribution patterns of enzymes in rat-liver tissue. Biochemical Journal 60, 604.

de Pace, R., Skirzewski, M., Damme, M., Mattera, R., Mercurio, J., Foster, A.M., Cuitino, L., Jarnik, M., Hoffmann, V., Morris, H.D., Han, T.U., Mancini, G.M.S., Buonanno, A., Bonifacino, J.S., 2018. Altered distribution of ATG9A and accumulation of axonal aggregates in neurons from a mouse model of AP-4 deficiency syndrome. PLoS Genet 14, e1007363.

Dell'Angelica, E.C., 2001. Clathrin-binding proteins: Got a motif? Join the network! Trends Cell Biol 11, 315–318.

Dell'Angelica, E.C., 2009. AP-3-dependent trafficking and disease: the first decade. Curr Opin Cell Biol 21, 552–559.

Dell'Angelica, E.C., Mullins, C., Bonifacino, J.S., 1999a. AP-4, a novel protein complex related to clathrin adaptors. J Biol Chem 274, 7278–85.

Dell'Angelica, E.C., Ohno, H., Ooi, C.E., Rabinovich, E., Roche, K.W., Bonifacino, J.S., 1997. AP-3: an adaptor-like protein complex with ubiquitous expression. EMBO J 16, 917–928.

Dell'Angelica, E.C., Shotelersuk, V., Aguilar, R.C., Gahl, W.A., Bonifacino, J.S., 1999b. Altered trafficking of lysosomal proteins in Hermansky-Pudlak syndrome due to mutations in the β3A subunit of the AP-3 adaptor. Mol Cell 3, 11–21.

Donaldson, J.G., Jackson, C.L., 2011. ARF family G proteins and their regulators: roles in membrane transport, development and disease. Nature Reviews Molecular Cell Biology 2011 12:6 12, 362–375.

Drake, M.T., Zhu, Y., Kornfeld, S., 2000. The assembly of AP-3 adaptor complex-containing clathrin-coated vesicles on synthetic liposomes. Mol Biol Cell 11, 3723–3736.

Duncan, M.C., 2022. New directions for the clathrin adaptor AP-1 in cell biology and human disease. Curr Opin Cell Biol 76, 102079.

Ebrahimi-Fakhari, D., Alecu, J.E., Brechmann, B., Ziegler, M., Eberhardt, K., Jumo, H., D'Amore, A., Habibzadeh, P., Faghihi, M.A., de Bleecker, J.L., Vuillaumier-Barrot, S., Auvin, S., Santorelli, F.M., Neuser, S., Popp, B., Yang, E., Barrett, L., Davies, A.K., Saffari, A., Hirst, J., Sahin, M., 2021. High-throughput imaging of ATG9A distribution as a diagnostic functional assay for adaptor protein complex 4-associated hereditary spastic paraplegia. Brain Commun 3.

Ebrahimi-Fakhari, D., Behne, R., Davies, A.K., Hirst, J., 2018. AP-4-Associated Hereditary Spastic Paraplegia, GeneReviews®.

Ebrahimi-Fakhari, D., Cheng, C., Dies, K., Diplock, A., Pier, D.B., Ryan, C.S., Lanpher, B.C., Hirst, J., Chung, W.K., Sahin, M., Rosser, E., Darras, B., Bennett, J.T., 2018. Clinical and genetic characterization of AP4B1-associated SPG47. Am J Med Genet A 176, 311–318.

Ebrahimi-Fakhari, D., Saffari, A., Wahlster, L., Lu, J., Byrne, S., Hoffmann, G.F., Jungbluth, H., Sahin, M., 2016. Congenital disorders of autophagy: An emerging novel class of inborn errors of neuro-metabolism. Brain 139, 317–337.

Ebrahimi-Fakhari, Darius, Teinert, J., Behne, R., Wimmer, M., D'Amore, A., Eberhardt, K., Brechmann, B., Ziegler, M., Jensen, D.M., Nagabhyrava, P., Geisel, G., Carmody, E., Shamshad, U., Dies, K.A., Yuskaitis, C.J., Salussolia, C.L., Ebrahimi-Fakhari, Daniel, Pearson, T.S., Saffari, A., Ziegler, A., Kölker, S., Volkmann, J., Wiesener, A., Bearden, D.R., Lakhani, S., Segal, D., Udwadia-Hegde, A., Martinuzzi, A., Hirst, J., Perlman, S., Takiyama, Y., Xiromerisiou, G., Vill, K., Walker, W.O., Shukla, A., Dubey Gupta, R., Dahl, N., Aksoy, A., Verhelst, H., Delgado, M.R., Kremlikova Pourova, R., Sadek, A.A., Elkhateeb, N.M., Blumkin, L., Brea-Fernández, A.J., Dacruz-Álvarez, D., Smol, T., Ghoumid, J., Miguel, D., Heine, C., Schlump, J.U., Langen, H., Baets, J., Bulk, S., Darvish, H., Bakhtiari, S., Kruer, M.C., Lim-Melia, E., Aydinli, N., Alanay, Y., El-Rashidy, O., Nampoothiri, S., Patel, C., Beetz, C., Bauer, P., Yoon, G., Guillot, M., Miller, S.P., Bourinaris, T., Houlden, H., Robelin, L., Anheim, M., Alamri, A.S., Mahmoud, A.A.H., Inaloo, S., Habibzadeh, P., Faghihi, M.A., Jansen, A.C., Brock, S., Roubertie, A., Darras, B.T., Agrawal, P.B., Santorelli, F.M., Gleeson, J., Zaki, M.S., Sheikh, S.I., Bennett, J.T., Sahin, M., 2020. Defining the clinical, molecular and imaging spectrum of adaptor protein complex 4-associated hereditary spastic paraplegia. Brain 143, 2929–2944.

Edeling, M.A., Sanker, S., Shima, T., Umasankar, P.K., Höning, S., Kim, H.Y., Davidson, L.A., Watkins, S.C., Tsang, M., Owen, D.J., Traub, L.M., 2009. Structural Requirements for PACSIN/Syndapin Operation during Zebrafish Embryonic Notochord Development. PLoS One 4, 8150.

Eisenberg, E., Greene, L.E., 2007. Multiple Roles of Auxilin and Hsc70 in Clathrin-Mediated Endocytosis. Traffic 8, 640–646.

Elkin, S.R., Lakoduk, A.M., Schmid, S.L., 2016. Endocytic Pathways and Endosomal Trafficking: A Primer. Wien Med Wochenschr 166, 196.

Farquhar, M.G., Palade, G.E., 1981. The Golgi apparatus (complex)-(1954-1981)-from artifact to center stage. Journal of Cell Biology 91, 77s–103s.

Feng, Y., He, D., Yao, Z., Klionsky, D.J., 2014. The machinery of macroautophagy. Cell Res.

Ford, M.G.J., Mills, I.G., Peter, B.J., Vallis, Y., Praefcke, G.J.K., Evans, P.R., McMahon, H.T., 2002. Curvature of clathrin-coated pits driven by epsin. Nature 2002 419:6905 419, 361–366.

Fracchiolla, D., Sawa-Makarska, J., Zens, B., de Ruiter, A., Zaffagnini, G., Brezovich, A., Romanov, J., Runggatscher, K., Kraft, C., Zagrovic, B., Martens, S., 2016. Mechanism of cargo-directed Atg8 conjugation during selective autophagy. Elife 13, 978–979.

Frazier, M.N., 2018. Structural and Functional Studies of AP4 and its Accessory Protein Tepsin (Ph.D. Thesis). Vanderbilt University, Nashville.

Frazier, M.N., Davies, A.K., Voehler, M., Kendall, A.K., Borner, G.H.H., Chazin, W.J., Robinson, M.S., Jackson, L.P., 2016. Molecular Basis for the Interaction Between AP4 β4 and its Accessory Protein, Tepsin. Traffic 17, 400–415.

Fu, M. meng, Nirschl, J.J., Holzbaur, E.L.F., 2014. LC3 Binding to the scaffolding protein jip1 regulates processive dynein-driven transport of autophagosomes. Dev Cell 29, 577–590.

Fujita, N., Noda, T., Yoshimori, T., 2009. An ATG4B mutant hampers the lipidation of LC3 paralogues and causes defects in autophagosome closure. Autophagy 5, 88–89.

Gadbery, J.E., Abraham, A., Needle, C.D., Moth, C., Sheehan, J., Capra, J.A., Jackson, L.P., Lauren Jackson, C.P., 2020. Integrating structural and evolutionary data to interpret variation and pathogenicity in adapter protein complex 4.

Gagnon, J.A., Valen, E., Thyme, S.B., Huang, P., Ahkmetova, L., Pauli, A., Montague, T.G., Zimmerman, S., Richter, C., Schier, A.F., 2014. Efficient Mutagenesis by Cas9 Protein-Mediated Oligonucleotide Insertion and Large-Scale Assessment of Single-Guide RNAs. PLoS One 9.

Gaidarov, I., Keen, J.H., 1999. Phosphoinositide–Ap-2 Interactions Required for Targeting to Plasma Membrane Clathrin-Coated Pits. Journal of Cell Biology 146, 755–764.

Galluzzi, L., Baehrecke, E.H., Ballabio, A., Boya, P., Bravo-San Pedro, J.M., Cecconi, F., Choi, A.M., Chu, C.T., Codogno, P., Colombo, M.I., Cuervo, A.M., Debnath, J., Deretic, V., Dikic, I., Eskelinen, E., Fimia, G.M., Fulda, S., Gewirtz, D.A., Green, D.R., Hansen, M., Harper, J.W., Jäättelä, M., Johansen, T., Juhasz, G., Kimmelman, A.C., Kraft, C., Ktistakis, N.T., Kumar, S., Levine, B., Lopez-Otin, C., Madeo, F., Martens, S., Martinez, J., Melendez, A., Mizushima, N., Münz, C., Murphy, L.O., Penninger, J.M., Piacentini, M., Reggiori, F., Rubinsztein, D.C., Ryan, K.M., Santambrogio, L., Scorrano, L., Simon, A.K., Simon, H., Simonsen, A., Tavernarakis, N., Tooze, S.A., Yoshimori, T., Yuan, J., Yue, Z., Zhong, Q., Kroemer, G., 2017. Molecular definitions of autophagy and related processes. EMBO J 36, 1811–1836.

Garnier, S., Ross, N., Rudis, R., Camargo, A.P., Sciaini, M., Scherer, C., 2021. viridis - Colorblind-Friendly Color Maps for R.

Ghai, R., Bugarcic, A., Liu, H., Norwood, S.J., Skeldal, S., Coulson, E.J., Li, S.S.C., Teasdale, R.D., Collins, B.M., 2013. Structural basis for endosomal trafficking of diverse transmembrane cargos by PX-FERM proteins. Proc Natl Acad Sci U S A 110, E643–E652.

Ghai, R., Mobli, M., Norwood, S.J., Bugarcic, A., Teasdale, R.D., King, G.F., Collins, B.M., 2011. Phox homology band 4.1/ezrin/radixin/moesin-like proteins function as molecular scaffolds that interact with cargo receptors and Ras GTPases. Proc Natl Acad Sci U S A 108, 7763–7768.

Ghosh, P., Kornfeld, S., 2003. AP-1 binding to sorting signals and release from clathrin-coated vesicles is regulated by phosphorylation. Journal of Cell Biology 160, 699–708.

Glick, B.S., Luini, A., 2011. Models for Golgi Traffic: A Critical Assessment. Cold Spring Harb Perspect Biol 3.

Gorzkiewicz, A., Szemraj, J., 2018. Brain endocannabinoid signaling exhibits remarkable complexity. Brain Res Bull 142, 33–46.

Guardia, C.M., de Pace, R., Mattera, R., Bonifacino, J.S., 2018. Neuronal functions of adaptor complexes involved in protein sorting. Curr Opin Neurobiol 51, 103–110.

Guardia, C.M., Jain, A., Mattera, R., Friefeld, A., Li, Y., Bonifacino, J.S., 2021. RUSC2 and WDR47 oppositely regulate kinesin- 1-dependent distribution of ATG9A to the cell periphery. Mol Biol Cell 32.

Guardia, C.M., Tan, X.-F., Lian, T., Bonifacino, J.S., Jiang, J., Banerjee, A., Rana, M.S., Zhou, W., Christenson, E.T., Lowry, A.J., Faraldo-Gó, J.D., 2020a. Structure of Human ATG9A, the Only Transmembrane Protein of the Core Autophagy Machinery. CellReports 31, 107837.

Guardia, C.M., Tan, X.-F., Lian, T., Rana, M.S., Zhou, W., Christenson, E.T., Lowry, A.J., Faraldo-Gómez, J.D., Bonifacino, J.S., Jiang, J., Banerjee, A., Supervision, A.J.L.;, Writing -Original, A.B.;, Draft, C.M.G., 2020b. Structure of Human ATG9A, the Only Transmembrane Protein of the Core Autophagy Machinery. Cell Rep 31, 107837.

Hardies, K., May, P., Djémié, T., Tarta-Arsene, O., Deconinck, T., Craiu, D., Helbig, I., Suls, A., Balling, R., Weckhuysen, S., de Jonghe, P., Hirst, J., Afawi, Z., Barisic, N., Baulac, S., Caglayan, H., Depienne, C., de Kovel, C.G.F., Dimova, P., Guerrero-López, R., Guerrini, R., Hjalgrim, H., Hoffman-Zacharska, D., Jahn, J., Klein, K.M., Koeleman, B.P.C., Leguern, E., Lehesjoki, A.E., Lemke, J., Lerche, H., Marini, C., Muhle, H., Rosenow, F., Serratosa, J.M., Møller, R.S., Stephani, U., Striano, P., Talvik, T., von Spiczak, S., Weber, Y., Zara, F., 2015. Recessive loss-of-function mutations in AP4S1 cause mild fever-sensitive seizures, developmental delay and spastic paraplegia through loss of AP-4 complex assembly. Hum Mol Genet 24, 2218–2227.

Healy, M.D., Hospenthal, M.K., Hall, R.J., Chandra, M., Chilton, M., Tillu, V., Chen, K.E., Celligoi, D.J., McDonald, F.J., Cullen, P.J., Lott, J.S., Collins, B.M., Ghai, R., 2018. Structural insights into the architecture and membrane interactions of the conserved COMMD proteins. Elife 7.

Healy, M.D., Sacharz, J., McNally, K.E., McConville, C., Tillu, V.A., Hall, R.J., Chilton, M., Cullen, P.J., Mobli, M., Ghai, R., Stroud, D.A., Collins, B.M., 2022. Proteomic identification and structural basis for the interaction between sorting nexin SNX17 and PDLIM family proteins. Structure 30, 1590-1602.e6.

Heldwein, E.E., Macia, E., Wang, J., Yin, H.L., Kirchhausen, T., Harrison, S.C., 2004. Crystal structure of the clathrin adaptor protein 1 core. Proc Natl Acad Sci U S A 101, 14108–14113.

Hesketh, G.G., Wartosch, L., Davis, L.J., Bright, N.A., Luzio, J.P., 2018. The Lysosome and Intracellular Signalling. Prog Mol Subcell Biol 57, 151–180.

Heuser, J.E., Reese, T.S., 1973. Evidence for recycling of synaptic vesicle membrane during transmitter release at the frog neuromuscular junction. J Cell Biol 57, 315.

Hirst, J., Borner, G.H.H., Edgar, J., Hein, M.Y., Mann, M., Buchholz, F., Antrobus, R., Robinson, M.S., 2013a. Interaction between AP-5 and the hereditary spastic paraplegia proteins SPG11 and SPG15. Mol Biol Cell 24, 2558–69.

Hirst, J., Bright, N.A., Rous, B., Robinson, M.S., 1999. Characterization of a Fourth Adaptor-related Protein Complex. Mol Biol Cell 10, 2787–2802.

Hirst, J., D. Barlow, L., Francisco, G.C., Sahlender, D.A., Seaman, M.N.J., Dacks, J.B., Robinson, M.S., 2011. The Fifth Adaptor Protein Complex. PLoS Biol 9, e1001170.

Hirst, J., Hesketh, G.G., Gingras, A.C., Robinson, M.S., 2021. Rag GTPases and phosphatidylinositol 3-phosphate mediate recruitment of the AP-5/SPG11/SPG15 complex. Journal of Cell Biology 220.

Hirst, J., Irving, C., Borner, G.H.H., 2013b. Adaptor Protein Complexes AP-4 and AP-5: New Players in Endosomal Trafficking and Progressive Spastic Paraplegia. Traffic 14, 153–164.

Hirst, J., Itzhak, D.N., Antrobus, R., Borner, G.H.H., Robinson, M.S., 2018. Role of the AP-5 adaptor protein complex in late endosome-to-Golgi retrieval. PLoS Biol 16, e2004411.

Hirst, J., Miller, S.E., Taylor, M.J., von Mollard, G.F., Robinson, M.S., 2004. EpsinR is an adaptor for the SNARE protein Vti1b. Mol Biol Cell 15, 5593–5602.

Hirst, J., Motley, A., Harasaki, K., Chew, S.Y.P., Robinson, M.S., 2003. EpsinR: An ENTH domain-containing protein that interacts with AP-1. Mol Biol Cell 14, 625–641.

Hirst, J., Schlacht, A., Norcott, J.P., Traynor, D., Bloomfield, G., Antrobus, R., Kay, R.R., Dacks, J.B., Robinson, M.S., 2014. Characterization of TSET, an ancient and widespread membrane trafficking complex. Elife 2014.

Höning, S., Ricotta, D., Krauss, M., Späte, K., Spolaore, B., Motley, A., Robinson, M., Robinson, C., Haucke, V., Owen, D.J., 2005. Phosphatidylinositol-(4,5)-bisphosphate regulates sorting signal recognition by the clathrin-associated adaptor complex AP2. Mol Cell 18, 519–531.

Hua, R., Yu, S., Liu, M., Li, H., 2018. A PCR-based method for RNA probes and applications in neuroscience. Front Neurosci 12, 266.

Ichimura, Y., Kirisako, T., Takao, T., Satomi, Y., Shimonishi, Y., Ishihara, N., Mizushima, N., Tanida, I., Kominami, E., Ohsumi, M., Noda, T., Ohsumi, Y., 2000. A ubiquitin-like system mediates protein lipidation. Nature 408, 488–492.

Imai, K., Hao, F., Fujita, N., Tsuji, Y., Oe, Y., Araki, Y., Hamasaki, M., Noda, T., Yoshimori, T., 2016. Atg9A trafficking through the recycling endosomes is required for autophagosome formation. J Cell Sci 129, 3781–3791.

Ivankovic, D., Drew, J., Lesept, F., White, I.J., López Doménech, G., Tooze, S.A., Kittler, J.T., 2020. Axonal autophagosome maturation defect through failure of ATG9A sorting underpins pathology in AP-4 deficiency syndrome. Autophagy 16, 391–407.

Jackson, L.P., Kelly, B.T., McCoy, A.J., Gaffry, T., James, L.C., Collins, B.M., Höning, S., Evans, P.R., Owen, D.J., 2010. A large-scale conformational change couples membrane recruitment to cargo binding in the AP2 clathrin adaptor complex. Cell 141, 1220–1229.

Jacomin, A.-C., Samavedam, S., Promponas, V., Nezis, I.P., 2016. iLIR database: A web resource for LIR motif-containing proteins in eukaryotes. Autophagy 12, 1945–1953.

Jameel, M., Klar, J., Tariq, M., Moawia, A., Altaf Malik, N., Seema Waseem, S., Abdullah, U., Naeem Khan, T., Raininko, R., Baig, S.M., Dahl, N., 2014. A novel AP4M1 mutation in autosomal recessive cerebral palsy syndrome and clinical expansion of AP-4 deficiency. BMC Med Genet 15, 1–7.

Jamieson, J.D., Palade, G.E., 1967. INTRACELLULAR TRANSPORT OF SECRETORY PROTEINS IN THE PANCREATIC EXOCRINE CELL : I. Role of the Peripheral Elements of the Golgi Complex. J Cell Biol 34, 577.

Jia, S., Wang, Y., You, Z., Liu, B., Gao, J., Liu, W., 2017. Mammalian Atg9 contributes to the post-Golgi transport of lysosomal hydrolases by interacting with adaptor protein-1. FEBS Lett 591, 4027–4038.

Jiang, Wenyan, Chen, Xuechai, Ji, Cuicui, Zhang, Wenting, Song, Jianing, Li, Jie, Wang, Juan, Jiang, W ;, Chen, X ;, Ji, C ;, Zhang, W ;, Song, J ;, Li, J ;, Wang, J, 2021. Key Regulators of Autophagosome Closure. Cells 2021, Vol. 10, Page 2814 10, 2814.

Judith, D., Jefferies, H.B.J., Boeing, S., Frith, D., Snijders, A.P., Tooze, S.A., 2019. ATG9A shapes the forming autophagosome through Arfaptin 2 and phosphatidylinositol 4-kinase IIIβ. Journal of Cell Biology 218, 1634–1652.

Jumper, J., Evans, R., Pritzel, A., Green, T., Figurnov, M., Ronneberger, O., Tunyasuvunakool, K., Bates, R., Žídek, A., Potapenko, A., Bridgland, A., Meyer, C., Kohl, S.A.A., Ballard, A.J., Cowie, A., Romera-Paredes, B., Nikolov, S., Jain, R., Adler, J., Back, T., Petersen, S., Reiman, D., Clancy, E., Zielinski, M., Steinegger, M., Pacholska, M., Berghammer, T., Bodenstein, S., Silver, D., Vinyals, O., Senior, A.W., Kavukcuoglu, K., Kohli, P., Hassabis, D., 2021a. Highly accurate protein structure prediction with AlphaFold. Nature 2021 596:7873 596, 583–589.

Jumper, J., Evans, R., Pritzel, A., Green, T., Figurnov, M., Ronneberger, O., Tunyasuvunakool, K., Bates, R., Žídek, A., Potapenko, A., Bridgland, A., Meyer, C., Kohl, S.A.A., Ballard, A.J., Cowie, A., Romera-Paredes, B., Nikolov, S., Jain, R., Adler, J., Back, T., Petersen, S., Reiman, D., Clancy, E., Zielinski, M., Steinegger, M., Pacholska, M., Berghammer, T., Silver, D., Vinyals, O., Senior, A.W., Kavukcuoglu, K., Kohli, P., Hassabis, D., 2021b. Applying and improving AlphaFold at CASP14. Proteins: Structure, Function, and Bioinformatics 89, 1711–1721.

Kabeya, Y., Mizushima, N., Ueno, T., Yamamoto, A., Kirisako, T., Noda, T., Kominami, E., Ohsumi, Y., Yoshimori, T., 2000. LC3, a mammalian homologue of yeast Apg8p, is localized in autophagosome membranes after processing. EMBO J 19, 5720–5728.

Kabeya, Y., Mizushima, N., Yamamoto, A., Oshitani-Okamoto, S., Ohsumi, Y., Yoshimori, T., 2004. LC3, GABARAP and GATE16 localize to autophagosomal membrane depending on form-II formation. J Cell Sci 117, 2805–2812.

Kadlecova, Z., Spielman, S.J., Loerke, D., Mohanakrishnan, A., Reed, D.K., Schmid, S.L., 2017. Regulation of clathrin-mediated endocytosis by hierarchical allosteric activation of AP2. Journal of Cell Biology 216, 167–179.

Karanasios, E., Walker, S.A., Okkenhaug, H., Manifava, M., Hummel, E., Zimmermann, H., Ahmed, Q., Domart, M.C., Collinson, L., Ktistakis, N.T., 2016. Autophagy initiation by ULK complex assembly on ER tubulovesicular regions marked by ATG9 vesicles. Nature Communications 2016 7:1 7, 1–17.

Kassambara, A., 2021. rstatix: Pipe-Friendly Framework for Basic Statistical Tests.

Kaut, A., Lange, H., Diekert, K., Kispal, G., Lill, R., 2000. Isa1p is a component of the mitochondrial machinery for maturation of cellular iron-sulfur proteins and requires conserved cysteine residues for function. Journal of Biological Chemistry 275, 15955–15961.

Keen, J.H., Willingham, M.C., Pastan, I.H., 1979. Clathrin-coated vesicles: Isolation, dissociation and factor-dependent reassociation of clathrin baskets. Cell 16, 303–312.

Kelly, B.T., McCoy, A.J., Späte, K., Miller, S.E., Evans, P.R., Höning, S., Owen, D.J., 2008a. A structural explanation for the binding of endocytic dileucine motifs by the AP2 complex. Nature 2008 456:7224 456, 976–979.

Kilaru, A., Chapma, K.D., 2020. The endocannabinoid system. Essays Biochem 64, 485–499.

Kimmel, C.B., Ballard, W.W., Kimmel, S.R., Ullmann, B., Schilling, T.F., 1995. Stages of embryonic development of the zebrafish. Developmental Dynamics 203, 253–310.

Kimura, S., Noda, T., Yoshimori, T., 2007. Dissection of the Autophagosome Maturation Process by a Novel Reporter Protein, Tandem Fluorescent-Tagged LC3. Autophagy 3, 452–460.

Kirchhausen, T., Owen, D., Harrison, S.C., 2014. Molecular Structure, Function, and Dynamics of Clathrin-Mediated Membrane Traffic. Cold Spring Harb Perspect Biol 6.

Kirisako, T., Ichimura, Y., Okada, H., Kabeya, Y., Mizushima, N., Yoshimori, T., Ohsumi, M., Takao, T., Noda, T., Ohsumi, Y., 2000. The Reversible Modification Regulates the Membrane-Binding State of Apg8/Aut7 Essential for Autophagy and the Cytoplasm to Vacuole Targeting Pathway. Journal of Cell Biology 151, 263–276.

Klionsky, D.J., Kamal Abdel-Aziz, A., Abdelfatah, S., Abdellatif, M., Abdoli, A., Abel, S., Abeliovich, H., Abildgaard, M.H., Princely Abudu, Y., Acevedo-Arozena, A., Adamopoulos, I.E., Adeli, K., Adolph, T.E., Adornetto, A., Aflaki, E., Agam, G., Agarwal, A., Aggarwal, B.B., Agnello, M., Agostinis, P., Agrewala, J.N., Agrotis, A., Aguilar, P. v, Tariq Ahmad, S., Ahmed, Z.M., Ahumada-Castro, U., Aits, S., Aizawa, S., Akkoc, Y., Akoumianaki, T., Aysin Akpinar, H., Al-Abd, A.M., Al-Akra, L., Al-Gharaibeh, A., Alaoui-Jamali, M.A., Alberti, S., Alcocer-Gómez, E., Alessandri, C., Ali, M., Abdul Alim Al-Bari, M., Aliwaini, S., Alizadeh, J., Almacellas, E., Almasan, A., Alonso, A., Alonso, G.D., Altan-Bonnet, N., Altieri, D.C., C Álvarez, É.M., Alves, S., Alves da Costa, C., Alzaharna, M.M., Amadio, M., Amantini, C., Amaral, C., Ambrosio, S., Amer, A.O., Ammanathan, V., An, Z., Andersen, S.U., Andrabi, S.A., Andrade-Silva, M., Andres, A.M., Angelini, S., Ann, D., Anozie, U.C., Ansari, M.Y., Antas, P., Antebi, A., Antón, Z., Anwar, T., Apetoh, L., Apostolova, N., Araki, T., Araki, Y., Arasaki, K., Araújo, W.L., Araya, J., Arden, C., Arévalo, M.-A., Arguelles, S., Arias, E., Arikkath, J., Arimoto, H., Ariosa, A.R., Armstrong-James, D., Arnauné-Pelloquin, L., Aroca, A., Arroyo, D.S., Arsov, I., Artero, R., Maria Lucia Asaro, D., Aschner, M., Ashrafizadeh, M., Ashur-Fabian, O., Atanasov, A.G., Au, A.K., Auberger, P., Auner, H.W., Aurelian, L., Autelli, R., Avagliano, L., Ávalos, Y., Aveic, S., Alexandra Aveleira, C., Avin-Wittenberg, T., Aydin, Y., Ayton, S., Ayyadevara, S., Azzopardi, M., Baba, M., Backer, J.M., Backues, S.K., Bae, D.-H., Bae, O.-N., Han Bae, S., Baehrecke, E.H., Baek, A., Baek, S.-H., Hee Baek, S., Bagetta, G., Bagniewska-Zadworna, A., Bai, H., Bai, J., Bai, X., Bai, Y., Bairagi, N., Baksi, S., Balbi, T., Baldari, C.T., Balduini, W., Ballabio, A., Ballester, M., Balazadeh, S., Balzan, R., Bandopadhyay, R., Banerjee, Sreeparna, Banerjee, Sulagna, Bánréti, Á., Bao, Y., Baptista, M.S., Baracca, A., Barbati, C., Bargiela, A., Barilà, D., Barlow, P.G., Barmada, S.J., Barreiro, E., Barreto, G.E., Bartek, J., Bartel, B., Bartolome, A., Barve, G.R., Basagoudanavar, S.H., Bassham, D.C., Bast Jr, R.C., Basu, A., Batoko, H., Batten, I., Baulieu, E.E., Baumgarner, B.L., Bayry, J., Beale, R., 2021. Guidelines for the use and interpretation of assays for monitoring autophagy (4th edition). Autophagy 17, 1–382.

Korolchuk, V.I., Saiki, S., Lichtenberg, M., Siddiqi, F.H., Roberts, E.A., Imarisio, S., Jahreiss, L., Sarkar, S., Futter, M., Menzies, F.M., O'Kane, C.J., Deretic, V., Rubinsztein, D.C., 2011. Lysosomal positioning coordinates cellular nutrient responses. Nature Cell Biology 2011 13:4 13, 453–460.

Koshiba, S., Kigawa, T., Kikuchi, A., Yokoyama, S., 2002. Solution structure of the epsin N-terminal homology (ENTH) domain of human epsin. J Struct Funct Genomics 2, 1–8.

Landajuela, A., Hervás, J.H., Antón, Z., Montes, L.R., Gil, D., Valle, M., Rodriguez, J.F., Goñi, F.M., Alonso, A., 2016. Lipid Geometry and Bilayer Curvature Modulate LC3/GABARAP-Mediated Model Autophagosomal Elongation. Biophys J 110, 411–422.

Laulumaa, S., Varjosalo, M., 2021. Commander Complex- A Multifaceted Operator in Intracellular Signaling and Cargo. Cells 2021, Vol. 10, Page 3447 10, 3447.

Lee, Y.K., Lee, J.A., 2016. Role of the mammalian ATG8/LC3 family in autophagy: Differential and compensatory roles in the spatiotemporal regulation of autophagy. BMB Rep 49, 424–430.

Lefran, S., Janvier, K., Boehm, M., Ooi, C.E., Bonifacino, J.S., 2004. An ear-core interaction regulates the recruitment of the AP-3 complex to membranes. Dev Cell 7, 619–625.

Leonhardt, S.A., Purdy, M.D., Grover, J.R., Yang, Z., Poulos, S., McIntire, W.E., Tatham, E.A., Erramilli, S., Nosol, K., Lai, K.K., Ding, S., Lu, M., Uchil, P.D., Finzi, A., Rein, A., Kossiakoff, A.A., Mothes, W., Yeager, M., 2022. CryoEM Structures of the Human HIV-1 Restriction Factor SERINC3 and Function as a Lipid Transporter. bioRxiv 2022.07.06.498924.

Lie, P.P.Y., Nixon, R.A., 2019. Lysosome trafficking and signaling in health and neurodegenerative diseases. Neurobiol Dis 122, 94–105.

Maeda, S., Yamamoto, H., Kinch, L.N., Garza, C.M., Takahashi, S., Otomo, C., Grishin, N. v., Forli, S., Mizushima, N., Otomo, T., 2020. Structure, lipid scrambling activity and role in autophagosome formation of ATG9A. Nat Struct Mol Biol 27, 1194.

Maday, S., Wallace, K.E., Holzbaur, E.L.F., 2012. Autophagosomes initiate distally and mature during transport toward the cell soma in primary neurons. Journal of Cell Biology 196, 407–417.

Majumder, P., Edmison, D., Rodger, C., Patel, S., Reid, E., Gowrishankar, S., 2022. AP-4 regulates neuronal lysosome composition, function, and transport via regulating export of critical lysosome receptor proteins at the trans-Golgi network. Mol Biol Cell 33.

Mallam, A.L., Marcotte, E.M., 2017. Systems-wide Studies Uncover Commander, a Multiprotein Complex Essential to Human Development. Cell Syst 4, 483–494.

Mardones, G.A., Burgos, P. v., Lin, Y., Kloer, D.P., Magadán, J.G., Hurley, J.H., Bonifacino, J.S., 2013. Structural Basis for the Recognition of Tyrosine-based Sorting Signals by the μ3A Subunit of the AP-3 Adaptor Complex. J Biol Chem 288, 9563.

Mari, M., Griffith, J., Rieter, E., Krishnappa, L., Klionsky, D.J., Reggiori, F., 2010. An Atg9-containing compartment that functions in the early steps of autophagosome biogenesis. Journal of Cell Biology 190, 1005–1022.

Maritzen, T., Koo, S.J., Haucke, V., 2012. Turning CALM into excitement: AP180 and CALM in endocytosis and disease. Biol Cell 104, 588–602.

Marshall, R.S., Hua, Z., Mali, S., McLoughlin, F., Vierstra, R.D., 2019. ATG8-Binding UIM Proteins Define a New Class of Autophagy Adaptors and Receptors. Cell 177, 766-781.e24.

Maruyama, T., Alam, J.M., Fukuda, T., Kageyama, S., Kirisako, H., Ishii, Y., Shimada, I., Ohsumi, Y., Komatsu, M., Kanki, T., Nakatogawa, H., Noda, N.N., 2021. Membrane perturbation by lipidated Atg8 underlies autophagosome biogenesis. Nature Structural & Molecular Biology 2021 28:7 28, 583–593.

Matoba, K., Kotani, T., Tsutsumi, A., Tsuji, T., Mori, T., Noshiro, D., Sugita, Y., Nomura, N., Iwata, S., Ohsumi, Y., Fujimoto, T., Nakatogawa, H., Kikkawa, M., Noda, N.N., 2020. Atg9 is a lipid scramblase that mediates autophagosomal membrane expansion. Nat Struct Mol Biol 1–9.

Matsuda, S., Miura, E., Matsuda, K., Kakegawa, W., Kohda, K., Watanabe, M., Yuzaki, M., 2008. Accumulation of AMPA Receptors in Autophagosomes in Neuronal Axons Lacking Adaptor Protein AP-4. Neuron 57, 730–745.

Matsuda, S., Yuzaki, M., 2009. Polarized sorting of AMPA receptors to the somatodendritic domain is regulated by adaptor protein AP-4. Neurosci Res 65, 1–5.

Mattera, R., de Pace, R., Bonifacino, J.S., 2020a. The role of AP-4 in cargo export from the trans-Golgi network and hereditary spastic paraplegia. Biochem Soc Trans.

Mattera, R., de Pace, R., Bonifacino, J.S., 2022. The adaptor protein chaperone AAGAB stabilizes AP-4 complex subunits. Mol Biol Cell.

Mattera, R., Guardia, C.M., Sidhu, S.S., Bonifacino, J.S., 2015. Bivalent Motif-Ear Interactions Mediate the Association of the Accessory Protein Tepsin with the AP-4 Adaptor Complex. Journal of Biological Chemistry 290, 30736–30749.

Mattera, R., Park, S.Y., de Pace, R., Guardia, C.M., Bonifacino, J.S., 2017. AP-4 mediates export of ATG9A from the trans-Golgi network to promote autophagosome formation. Proc Natl Acad Sci U S A 114, E10697–E10706.

Mattera, R., Williamson, C.D., Ren, X., Bonifacinoa, J.S., 2020b. The FTS-Hook-FHIP (FHF) complex interacts with AP-4 to mediate perinuclear distribution of AP-4 and its cargo ATG9A. Mol Biol Cell 31, 963–979.

McCurley, A.T., Callard, G. v., 2008. Characterization of housekeeping genes in zebrafish: Male-female differences and effects of tissue type, developmental stage and chemical treatment. BMC Mol Biol 9, 1–12.

McNally, K.E., Faulkner, R., Steinberg, F., Gallon, M., Ghai, R., Pim, D., Langton, P., Pearson, N., Danson, C.M., Nägele, H., Morris, L.L., Singla, A., Overlee, B.L., Heesom, K.J., Sessions, R., Banks, L., Collins, B.M., Berger, I., Billadeau, D.D., Burstein, E., Cullen, P.J., 2017. Retriever is a multiprotein complex for retromer-independent endosomal cargo recycling. Nat Cell Biol 19, 1214–1225.

Mercer, T.J., Gubas, A., Tooze, S.A., 2018. A molecular perspective of mammalian autophagosome biogenesis. Journal of Biological Chemistry 293, 5386–5395.

Merrifield, C.J., Kaksonen, M., 2014. Endocytic Accessory Factors and Regulation of Clathrin-Mediated Endocytosis. Cold Spring Harb Perspect Biol 6, 1–16.

Mettlen, M., Chen, P.H., Srinivasan, S., Danuser, G., Schmid, S.L., 2018. Regulation of Clathrin-Mediated Endocytosis. Annual Review of Biochemisty 87, 871–896.

Mettlen, M., Stoeber, M., Loerke, D., Antonescu, C.N., Danuser, G., Schmid, S.L., 2009. Endocytic accessory proteins are functionally distinguished by their differential effects on the maturation of clathrin-coated pits. Mol Biol Cell 20, 3251–3260.

Mills, I.G., Praefcke, G.J.K., Vallis, Y., Peter, B.J., Olesen, L.E., Gallop, J.L., Butler, P.J.G., Evans, P.R., McMahon, H.T., 2003. EpsinR an AP1/clathrin interacting protein involved in vesicle trafficking. Journal of Cell Biology 160, 213–222.

Misra, S., Puertollano, R., Kato, Y., Bonifacino, J.S., Hurley, J.H., 2002. Structural basis for acidic-cluster-dileucine sorting-signal recognition by VHS domains. Nature 415, 933–937.

Moreau, K., Ravikumar, B., Renna, M., Puri, C., Rubinsztein, D.C., 2011. Autophagosome precursor maturation requires homotypic fusion. Cell 146, 303–17.

Moreno-De-Luca, A., Helmers, S.L., Mao, H., Burns, T.G., Melton, A.M.A., Schmidt, K.R., Fernhoff, P.M., Ledbetter, D.H., Martin, C.L., 2011. Adaptor protein complex-4 (AP-4) deficiency causes a novel autosomal recessive cerebral palsy syndrome with microcephaly and intellectual disability. J Med Genet 48, 141–144.

Naef, V., Mero, S., Fichi, G., D'Amore, A., Ogi, A., Gemignani, F., Santorelli, F.M., Marchese, M., 2019. Swimming in Deep Water: Zebrafish Modeling of Complicated Forms of Hereditary Spastic Paraplegia and Spastic Ataxia. Front Neurosci 13.

Nair, U., Yen, W.-L., Mari, M., Cao, Y., Xie, Z., Baba, M., Reggiori, F., Klionsky, D.J., 2012. A role for Atg8-PE deconjugation in autophagosome biogenesis. Autophagy 8, 780–793.

Nath, S., Dancourt, J., Shteyn, V., Puente, G., Fong, W.M., Nag, S., Bewersdorf, J., Yamamoto, A., Antonny, B., Melia, T.J., 2014. Lipidation of the LC3/GABARAP family of autophagy proteins relies on a membrane-curvature-sensing domain in Atg3. Nat Cell Biol 16, 415–424.

Nielsen, M.S., Madsen, P., Christensen, E.I., Nykjær, A., Gliemann, J., Kasper, D., Pohlmann, R., Petersen, C.M., 2001. The sortilin cytoplasmic tail conveys Golgi–endosome transport and binds the VHS domain of the GGA2 sorting protein. EMBO J 20, 2180–2190.

Noble, A.J., Stagg, S.M., 2015. COPI gets a fancy new coat: An interconnected scaffolding of proteins bends the membrane to form vesicles. Science (1979) 349, 142–143.

Noda, N.N., 2021. Atg2 and Atg9: Intermembrane and interleaflet lipid transporters driving autophagy. Biochimica et Biophysica Acta (BBA) - Molecular and Cell Biology of Lipids 1866, 158956.

Noda, N.N., Kumeta, H., Nakatogawa, H., Satoo, K., Adachi, W., Ishii, J., Fujioka, Y., Ohsumi, Y., Inagaki, F., 2008. Structural basis of target recognition by Atg8/LC3 during selective autophagy. Genes to Cells 13, 1211–1218.

Noda, T., Kim, J., Huang, W.P., Baba, M., Tokunaga, C., Ohsumi, Y., Klionsky, D.J., 2000. Apg9p/Cvt7p Is an Integral Membrane Protein Required for Transport Vesicle Formation in the Cvt and Autophagy Pathways. Journal of Cell Biology 148, 465–480.

Ohno, H., Fournier, M.C., Poy, G., Bonifacino, J.S., 1996. Structural Determinants of Interaction of Tyrosine-based Sorting Signals with the Adaptor Medium Chains. Journal of Biological Chemistry 271, 29009–29015.

Ohno, H., Stewart, J., Fournier, M.C., Bosshart, H., Rhee, I., Miyatake, S., Saito, T., Gallusser, A., Kirchhausen, T., Bonifacino, J.S., 1995. Interaction of Tyrosine-Based Sorting Signals with Clathrin-Associated Proteins. Science (1979) 269, 1872–1875.

Ohsumi, Y., 2014. Historical landmarks of autophagy research. Cell Res 24, 9.

Olivas, T.J., Wu, Y., Yu, S., Luan, L., Choi, P., Nag, S., de Camilli, P., Gupta, K., Melia, T.J., 2022. ATG9 vesicles comprise the seed membrane of mammalian autophagosomes. bioRxiv 2022.08.16.504143.

Ooi, C.E., Dell'Angelica, E.C., Bonifacino, J.S., 1998. ADP-Ribosylation Factor 1 (ARF1) Regulates Recruitment of the AP-3 Adaptor Complex to Membranes. Journal of Cell Biology 142, 391–402.

Orsi, A., Razi, M., Dooley, H.C., Robinson, D., Weston, A.E., Collinson, L.M., Tooze, S.A., 2012. Dynamic and transient interactions of Atg9 with autophagosomes, but not membrane integration, are required for autophagy. Mol Biol Cell 23, 1860–1873.

Osawa, T., Kotani, T., Kawaoka, T., Hirata, E., Suzuki, K., Nakatogawa, H., Ohsumi, Y., Noda, N.N., 2019. Atg2 mediates direct lipid transfer between membranes for autophagosome formation. Nat Struct Mol Biol 26, 281–288.

Oudin, M.J., Hobbs, C., Doherty, P., 2011. DAGL-dependent endocannabinoid signalling: roles in axonal pathfinding, synaptic plasticity and adult neurogenesis. European Journal of Neuroscience 34, 1634–1646.

Owen, D.J., Collins, B.M., Evans, P.R., 2004. ADAPTORS FOR CLATHRIN COATS: Structure and Function. Annu Rev Cell Dev Biol 20, 153–191.

Owen, D.J., Evans, P.R., 1998. A structural explanation for the recognition of tyrosine-based endocytotic signals. Science (1979) 282, 1327–1332.

Palade, G., 1975. Intracellular aspects of the process of protein synthesis. Science (1979) 189, 347–358.

Palade, G.E., 1955. A SMALL PARTICULATE COMPONENT OF THE CYTOPLASM. J Biophys Biochem Cytol 1, 59–68.

Palade, G.E., Porter, K.R., 1954. STUDIES ON THE ENDOPLASMIC RETICULUM : I. ITS IDENTIFICATION IN CELLS IN SITU. J Exp Med 100, 641.

Patra, S., Patil, S., Klionsky, D.J., Bhutia, S.K., 2022. Lysosome signaling in cell survival and programmed cell death for cellular homeostasis. J Cell Physiol.

Pearse, B.M., Robinson, M.S., 1984. Purification and properties of 100-kd proteins from coated vesicles and their reconstitution with clathrin. EMBO J 3, 1951–1957.

Pearse, B.M.F., 1975. Coated vesicles from pig brain: Purification and biochemical characterization. J Mol Biol 97, 93–98.

Pembridge, O.G., Wallace, N.S., Clements, T.P., Jackson, L.P., 2022. AP-4 loss in CRISPR-edited zebrafish affects early embryo development. Adv Biol Regul 100945.

Popelka, H., Klionsky, D.J., 2015. Analysis of the native conformation of the LIR/AIM motif in the Atg8/LC3/GABARAP-binding proteins. Autophagy 11, 2153–2159.

Popoff, V., Adolf, F., Brügge, B., Wieland, F., 2011. COPI Budding within the Golgi Stack. Cold Spring Harb Perspect Biol 3, a005231.

Popovic, D., Dikic, I., 2014. TBC1D5 and the AP2 complex regulate ATG9 trafficking and initiation of autophagy. EMBO Rep 15, 392–401.

Porter, K.R., 1953. OBSERVATIONS ON A SUBMICROSCOPIC BASOPHILIC COMPONENT OF CYTOPLASM. J Exp Med 97, 727.

Porter, K.R., Claude, A., Fullam, E.F., 1945. A STUDY OF TISSUE CULTURE CELLS BY ELECTRON MICROSCOPY : METHODS AND PRELIMINARY OBSERVATIONS. J Exp Med 81, 233.

Prasad, K., Barouch, W., Greene, L., Eisenberg, E., 1993. A Protein Cofactor Is Required for Uncoating of Clathrin Baskets by Uncoating ATPase. Journal of Biological Chemistry 268, 23758–23761.

Pu, J., Guardia, C.M., Keren-Kaplan, T., Bonifacino, J.S., 2016. Mechanisms and functions of lysosome positioning. J Cell Sci 129, 4329–4339.

Pu, J., Keren-Kaplan, T., Bonifacino, J.S., 2017. A Ragulator-BORC interaction controls lysosome positioning in response to amino acid availability. Journal of Cell Biology 216, 4183–4197.

Pu, J., Schindler, C., Jia, R., Jarnik, M., Backlund, P., Bonifacino, J.S., 2015. BORC, a Multisubunit Complex that Regulates Lysosome Positioning. Dev Cell 33, 176–188.

Puertollano, R., Aguilar, R.C., Gorshkova, I., Crouch, R.J., Bonifacino, J.S., 2001. Sorting of mannose 6-phosphate receptors mediated by the GGAs. Science (1979) 292, 1712–1716.

R Core Team, 2021. R: A language and environment for statistical computing.

Rabanal-Ruiz, Y., Korolchuk, V.I., Rabanal-Ruiz, Y., Korolchuk, V.I., 2018. mTORC1 and Nutrient Homeostasis: The Central Role of the Lysosome. Int J Mol Sci 19, 818.

Rapoport, I., Chen, Y.C., Cupers, P., Shoelson, S.E., Kirchhausen, T., 1998. Dileucine-based sorting signals bind to the β chain of AP-1 at a site distinct and regulated differently from the tyrosine-based motif-binding site. EMBO J 17, 2148–2155.

Ravussin, A., Brech, A., Tooze, S.A., Stenmark, H., 2021. The phosphatidylinositol 3-phosphate-binding protein SNX4 controls ATG9A recycling and autophagy. J Cell Sci 134.

Read, A.D., Bentley, R.E., Archer, S.L., Dunham-Snary, K.J., 2021. Mitochondrial iron–sulfur clusters: Structure, function, and an emerging role in vascular biology. Redox Biol 47, 102164.

Ren, X., Farías, G.G., Canagarajah, B.J., Bonifacino, J.S., Hurley, J.H., 2013. Structural Basis for Recruitment and Activation of the AP-1 Clathrin Adaptor Complex by Arf1. Cell 152, 755–767.

Ren, X., Hurley, J.H., 2010. VHS domains of ESCRT-0 cooperate in high-avidity binding to polyubiquitinated cargo. EMBO J 29, 1045–1054.

Robinson, M.S., 1987. 100-kD coated vesicle proteins: molecular heterogeneity and intracellular distribution studied with monoclonal antibodies. Journal of Cell Biology 104, 887–895.

Robinson, M.S., 2015a. Forty Years of Clathrin-coated Vesicles. Traffic 16, 1210–1238.

Robinson, M.S., Bonifacino, J.S., 2001. Adaptor-related proteins. Curr Opin Cell Biol 13, 444–453.

Robinson, M.S., Pearse, B.M.F., 1986. Immunofluorescent localization of 100K coated vesicle proteins. Journal of Cell Biology 102, 48–54.

Robinson, M.S., Sahlender, D.A., Foster, S.D., 2010. Rapid Inactivation of Proteins by Rapamycin-Induced Rerouting to Mitochondria. Dev Cell 18, 324–331.

Rogov, V. v, Stolz, A., Ravichandran, A.C., Rios-Szwed, D.O., Suzuki, H., Kniss, A., Löhr, F., Wakatsuki, S., Dötsch, V., Dikic, I., Dobson, R.C., McEwan, D.G., 2017. Structural and functional analysis of the GABARAP interaction motif (GIM). EMBO Rep 18, 1382–1396.

Rosenthal, J.A., Chen, H., Slepnev, V.I., Pellegrini, L., Salcini, A.E., di Fiore, P.P., de Camilli, P., 1999. The epsins define a family of proteins that interact with components of the clathrin coat and contain a new protein module. J Biol Chem 274, 33959–33965.

Ross, B.H., Lin, Y., Corales, E.A., Burgos, P. v., Mardones, G.A., 2014. Structural and Functional Characterization of Cargo-Binding Sites on the μ4-Subunit of Adaptor Protein Complex 4. PLoS One 9, e88147.

Roth, T.F., Porter, K.R., 1964. Yolk protein uptake in the oocyte of the mosquito Aedes aegypti L. Journal of Cell Biology 20, 313–332.

Rothnie, A., Clarke, A.R., Kuzmic, P., Cameron, A., Smith, C.J., 2011. A sequential mechanism for clathrin cage disassembly by 70-kDa heat-shock cognate protein (Hsc70) and auxilin. Proc Natl Acad Sci U S A 108, 6927–6932.

Sanger, A., Hirst, J., Davies, A.K., Robinson, M.S., 2019. Adaptor protein complexes and disease at a glance. J Cell Sci 132.

Sarkar, S., Korolchuk, V., Renna, M., Winslow, A., Rubinsztein, D.C., 2009. Methodological considerations for assessing autophagy modulators: A study with calcium phosphate precipitates. Autophagy 5, 307–313.

Sarmah, S., Barrallo-Gimeno, A., Melville, D.B., Topczewski, J., Solnica-Krezel, L., Knapik, E.W., 2010. Sec24D-Dependent Transport of Extracellular Matrix Proteins Is Required for Zebrafish Skeletal Morphogenesis. PLoS One 5, 10367.

Sawa-Makarska, J., Baumann, V., Coudevylle, N., von Bülow, S., Nogellova, V., Abert, C., Schuschnig, M., Graef, M., Hummer, G., Martens, S., 2020. Reconstitution of autophagosome nucleation defines Atg9 vesicles as seeds for membrane formation. Science (1979) 369.

Scarrott, J.M., Alves-Cruzeiro, J., Marchi, P.M., Webster, C.P., Yang, Z.-L., Karyka, E., Marroccella, R., Coldicott, I., Thomas, H., Azzouz, M., 2023. Ap4b1-knockout mouse model of hereditary spastic paraplegia type 47 displays motor dysfunction, aberrant brain morphology and ATG9A mislocalization. Brain Commun 5.

Schmucker, S., Argentini, M., Carelle-Calmels, N., Martelli, A., Puccio, H., 2008. The in vivo mitochondrial two-step maturation of human frataxin. Hum Mol Genet 17, 3521–3531.

Schoppe, J., Mari, M., Yavavli, E., Auffarth, K., Cabrera, M., Walter, S., Fröhlich, F., Ungermann, C., 2020. AP-3 vesicle uncoating occurs after HOPS-dependent vacuole tethering. EMBO J 39, e105117.

Schoppe, J., Schubert, E., Apelbaum, A., Yavavli, E., Birkholz, O., Stephanowitz, H., Han, Y., Perz, A., Hofnagel, O., Liu, F., Piehler, J., Raunser, S., Ungermann, C., 2021. Flexible open conformation of the AP-3 complex explains its role in cargo recruitment at the Golgi. Journal of Biological Chemistry 297, 101334.

Schuermann, J.P., Jiang, J., Cuellar, J., Llorca, O., Wang, L., Gimenez, L.E., Jin, S., Taylor, A.B., Demeler, B., Morano, K.A., Hart, P.J., Valpuesta, J.M., Lafer, E.M., Sousa, R., 2008. Structure of the Hsp110:Hsc70 Nucleotide Exchange Machine. Mol Cell 31, 232–243.

Scott, C.C., Vacca, F., Gruenberg, J., 2014. Endosome maturation, transport and functions. Semin Cell Dev Biol 31, 2–10.

Seaman, M.N.J., Sowerby, P.J., Robinson, M.S., 1996. Cytosolic and Membrane-associated Proteins Involved in the Recruitment of AP-1 Adaptors onto the Trans-Golgi Network. Journal of Biological Chemistry 271, 25446–25451.

Sen, A., Madhivanan, K., Mukherjee, D., Aguilar, R.C., 2012. The epsin protein family: coordinators of endocytosis and signaling. Biomol Concepts 3, 117–126.

Shpilka, T., Weidberg, H., Pietrokovski, S., Elazar, Z., 2011. Atg8: An autophagy-related ubiquitin-like protein family. Genome Biol 12, 226.

Simmen, T., Höning, S., Icking, A., Tikkanen, R., Hunziker, W., 2002. AP-4 binds basolateral signals and participates in basolateral sorting in epithelial MDCK cells. Nature Cell Biology 2002 4:2 4, 154–159.

Simpson, F., Bright, N.A., West, M.A., Newman, L.S., Darnell, R.B., Robinson, M.S., 1996. A novel adaptor-related protein complex. Journal of Cell Biology 133, 749–760.

Singh, S., Kumari, R., Chinchwadkar, S., Aher, A., Matheshwaran, S., Manjithaya, R., 2019. Exocyst Subcomplex Functions in Autophagosome Biogenesis by Regulating Atg9 Trafficking. J Mol Biol 431, 2821–2834.

Solinger, J.A., Spang, A., 2022. Sorting of cargo in the tubular endosomal network. BioEssays 44, 2200158.

Søreng, K., Munson, M.J., Lamb, C.A., Bjørndal, G.T., Pankiv, S., Carlsson, S.R., Tooze, S.A., Simonsen, A., 2018. SNX18 regulates ATG9A trafficking from recycling endosomes by recruiting Dynamin-2. EMBO Rep.

Stamnes, M.A., Rothman, J.E., 1993. The binding of AP-1 clathrin adaptor particles to Golgi membranes requires ADP-ribosylation factor, a small GTP-binding protein. Cell 73, 999–1005.

Stavoe, A.K.H., Holzbaur, E.L.F., 2019. Autophagy in Neurons. Annu Rev Cell Dev Biol 35, 477–500.

Stephens, D.J., Banting, G., 1998. Specificity of interaction between adaptor-complex medium chains and the tyrosine-based sorting motifs of TGN38 and lgp120. Biochemical Journal 335, 567–572.

Suckling, R.J., Poon, P.P., Travis, S.M., Majoul, I. v., Hughson, F.M., Evans, P.R., Duden, R., Owen, D.J., 2015. Structural basis for the binding of tryptophan-based motifs by δ-COP. Proc Natl Acad Sci U S A 112, 14242–14247.

Sun, B., Chen, L., Cao, W., Roth, A.F., Davis, N.G., 2004. The Yeast Casein Kinase Yck3p Is Palmitoylated, then Sorted to the Vacuolar Membrane with AP-3-dependent Recognition of a YXXϕ Adaptin Sorting Signal. Mol Biol Cell 15, 1397.

Suraci, D., Saudino, G., Nasta, V., Ciofi-Baffoni, S., Banci, L., 2021. ISCA1 Orchestrates ISCA2 and NFU1 in the Maturation of Human Mitochondrial [4Fe-4S] Proteins. J Mol Biol 433, 166924.

Takatsu, H., Katoh, Y., Shiba, Y., Nakayama, K., 2001. Golgi-localizing, γ-Adaptin Ear Homology Domain, ADP-ribosylation Factor-binding (GGA) Proteins Interact with Acidic Dileucine Sequences within the Cytoplasmic Domains of Sorting Receptors through their Vps27p/Hrs/STAM (VHS) Domains. Journal of Biological Chemistry 276, 28541–28545.

Tang, B.L., 2019. Syntaxin 16's Newly Deciphered Roles in Autophagy. Cells 8.

Tessa, A., Battini, R., Rubegni, A., Storti, E., Marini, C., Galatolo, D., Pasquariello, R., Santorelli, F.M., 2016. Identification of mutations in AP4S1/SPG52 through next generation sequencing in three families. Eur J Neurol 23, 1580–1587.

Thisse, B., Pflumio, S., Fürthauer, M., Loppin, B., Heyer, V., Degrave, A., Woehl, R., Lux, A., Steffan, T., Charbonnier, X.Q., Thisse, C., 2001. Expression of the zebrafish genome during embryogenesis (NIH R01 RR15402) [WWW Document]. ZFIN Direct Data Submission. URL https://zfin.org/ZDB-PUB-010810-1 (accessed 10.9.22).

Thisse, B., Thisse, C., 2004. Fast Release Clones: A High Throughput Expression Analysis. ZFIN Direct Data Submission. [WWW Document]. URL https://zfin.org/ZDB-PUB-040907-1 (accessed 10.20.22).

Thisse, C., Thisse, B., 2007. High-resolution in situ hybridization to whole-mount zebrafish embryos. Nature Protocols 2008 3:1 3, 59–69.

Traub, L.M., Ostrom, J.A., Kornfeld, S., 1993. Biochemical dissection of AP-1 recruitment onto Golgi membranes. Journal of Cell Biology 123, 561–573.

Travis, S.M., DAmico, K., Yu, I.M., McMahon, C., Hamid, S., Ramirez-Arellano, G., Jeffrey, P.D., Hughson, F.M., 2020. Structural basis for the binding of SNAREs to the multisubunit tethering complex Dsl1. Journal of Biological Chemistry 295, 10125–10135.

Travis, S.M., Kokona, B., Fairman, R., Hughson, F.M., 2019. Roles of singleton tryptophan motifs in COPI coat stability and vesicle tethering. Proc Natl Acad Sci U S A 116, 24031–24040.

Tüysüz, B., Bilguvar, K., Koçer, N., Yalçinkaya, C., Çağlayan, O., Gül, E., Şahin, S., Çomu, S., Günel, M., 2014. Autosomal recessive spastic tetraplegia caused by AP4M1 and AP4B1 gene mutation: Expansion of the facial and neuroimaging features. Am J Med Genet A 164, 1677–1685.

Verkerk, A.J.M.H., Schot, R., Dumee, B., Schellekens, K., Swagemakers, S., Bertoli-Avella, A.M., Lequin, M.H., Dudink, J., Govaert, P., van Zwol, A.L., Hirst, J., Wessels, M.W., Catsman-Berrevoets, C., Verheijen, F.W., de Graaff, E., de Coo, I.F.M., Kros, J.M., Willemsen, R., Willems, P.J., van der Spek, P.J., Mancini, G.M.S., 2009. Mutation in the AP4M1 Gene Provides a Model for Neuroaxonal Injury in Cerebral Palsy. The American Journal of Human Genetics 85, 40–52.

Wan, W., Liu, W., 2019. MTORC1 regulates autophagic membrane growth by targeting WIPI2. Autophagy 15, 742–743.

Wang, B., Yang, R., Tian, Y., Yin, Q., 2022. Reconstituting and Purifying Assembly Intermediates of Clathrin Adaptors AP1 and AP2. Methods in Molecular Biology 2473, 195–212.

Weidberg, H., Shpilka, T., Shvets, E., Abada, A., Shimron, F., Elazar, Z., 2011. LC3 and GATE-16 N Termini Mediate Membrane Fusion Processes Required for Autophagosome Biogenesis. Dev Cell 20, 444–454.

Weidberg, H., Shvets, E., Shpilka, T., Shimron, F., Shinder, V., Elazar, Z., 2010. LC3 and GATE-16/GABARAP subfamilies are both essential yet act differently in autophagosome biogenesis. EMBO J 29, 1792–1802.

Wesch, N., Kirkin, V., Rogov, V. v., 2020. Atg8-Family Proteins—Structural Features and Molecular Interactions in Autophagy and Beyond. Cells 9.

Wickham, H., Averick, M., Bryan, J., Chang, W., D', L., Mcgowan, A., François, R., Grolemund, G., Hayes, A., Henry, L., Hester, J., Kuhn, M., Lin Pedersen, T., Miller, E., Bache, S.M., Müller, K., Ooms, J., Robinson, D., Seidel, D.P., Spinu, V., Takahashi, K., Vaughan, D., Wilke, C., Woo, K., Yutani, H., 2019. Welcome to the Tidyverse. J Open Source Softw 4, 1686.

Wideman, J.G., Leung, K.F., Field, M.C., Dacks, J.B., 2014. The Cell Biology of the Endocytic System from an Evolutionary Perspective. Cold Spring Harb Perspect Biol 6, a016998.

Wirth, M., Zhang, W., Razi, M., Nyoni, L., Joshi, D., O'Reilly, N., Johansen, T., Tooze, S.A., Mouilleron, S., 2019. Molecular determinants regulating selective binding of autophagy adapters and receptors to ATG8 proteins. Nature Communications 2019 10:1 10, 1–18.

Xie, Z., Nair, U., Klionsky, D.J., 2008. Atg8 Controls Phagophore Expansion during Autophagosome Formation. Mol Biol Cell 19, 3290.

Xing, L., Quist, T.S., Stevenson, T.J., Dahlem, T.J., Bonkowsky, J.L., 2014. Rapid and Efficient Zebrafish Genotyping Using PCR with High-resolution Melt Analysis. J Vis Exp.

Xu, P., Hankins, H.M., MacDonald, C., Erlinger, S.J., Frazier, M.N., Diab, N.S., Piper, R.C., Jackson, L.P., MacGurn, J.A., Graham, T.R., 2017. COPI mediates recycling of an exocytic SNARE by recognition of a ubiquitin sorting signal. Elife 6.

Yamamoto, H., Kakuta, S., Watanabe, T.M., Kitamura, A., Sekito, T., Kondo-Kakuta, C., Ichikawa, R., Kinjo, M., Ohsumi, Y., 2012. Atg9 vesicles are an important membrane source during early steps of autophagosome formation. Journal of Cell Biology 198, 219–233.

Yang, J.S., Valente, C., Polishchuk, R.S., Turacchio, G., Layre, E., Branch Moody, D., Leslie, C.C., Gelb, M.H., Brown, W.J., Corda, D., Luini, A., Hsu, V.W., 2011. COPI acts in both vesicular and tubular transport. Nature Cell Biology 2011 13:8 13, 996–1003.

Yap, C.C., Mason, A.J., Winckler, B., 2022. Dynamics and distribution of endosomes and lysosomes in dendrites. Curr Opin Neurobiol 74, 102537.

Yap, C.C., Murate, M., Kishigami, S., Muto, Y., Kishida, H., Hashikawa, T., Yano, R., 2003. Adaptor protein complex-4 (AP-4) is expressed in the central nervous system neurons and interacts with glutamate receptor δ2. Molecular and Cellular Neuroscience 24, 283–295.

Young, A.R.J., Chan, E.Y.W., Hu, X.W., Köchl, R., Crawshaw, S.G., High, S., Halley, D.W., Lippincott-Schwartz, J., Tooze, S.A., 2006. Starvation and ULK1-dependent cycling of mammalian Atg9 between the TGN and endosomes. J Cell Sci 119, 3888–3900.

Yu, L., McPhee, C.K., Zheng, L., Mardones, G.A., Rong, Y., Peng, J., Mi, N., Zhao, Y., Liu, Z., Wan, F., Hailey, D.W., Oorschot, V., Klumperman, J., Baehrecke, E.H., Lenardo, M.J., 2010. Termination of autophagy and reformation of lysosomes regulated by mTOR. Nature 465, 942–946.

Zahoor, M., Farhan, H., 2018. Crosstalk of Autophagy and the Secretory Pathway and Its Role in Diseases. Int Rev Cell Mol Biol 337, 153–184.

Zaremba, S., Keen, J.H., 1983. Assembly polypeptides from coated vesicles mediate reassembly of unique clathrin coats. Journal of Cell Biology 97, 1339–1347.

Zhao, Y.G., Zhang, H., 2019. Autophagosome maturation: An epic journey from the ER to lysosomes. J Cell Biol 218, 757.

Zhou, C., Wu, Z., Du, W., Que, H., Wang, Y., Ouyang, Q., Jian, F., Yuan, W., Zhao, Y., Tian, R., Li, Y., Chen, Y., Gao, S., Wong, C.C.L., Rong, Y., 2022. Recycling of autophagosomal components from autolysosomes by the recycler complex. Nat Cell Biol 24, 497–512.

Zink, S., Wenzel, D., Wurm, C.A., Schmitt, H.D., 2009. A Link between ER Tethering and COP-I Vesicle Uncoating. Dev Cell 17, 403–416.

Zlatic, S.A., Grossniklaus, E.J., Ryder, P. v., Salazar, G., Mattheyses, A.L., Peden, A.A., Faundez, V., 2013. Chemical-genetic disruption of clathrin function spares adaptor complex 3-dependent endosome vesicle biogenesis. Mol Biol Cell 24, 2378–2388.

Zou, S., Kumar, U., 2018. Cannabinoid Receptors and the Endocannabinoid System: Signaling and Function in the Central Nervous System. International Journal of Molecular Sciences 2018, Vol. 19, Page 833 19, 833.

Zouhar, J., Sauer, M., 2014. Helping Hands for Budding Prospects: ENTH/ANTH/VHS Accessory Proteins in Endocytosis, Vacuolar Transport, and Secretion. Plant Cell 26, 4232–4244.

APPENDIX I

SUPPLEMENTAL MATERIALS FROM CHAPTER II

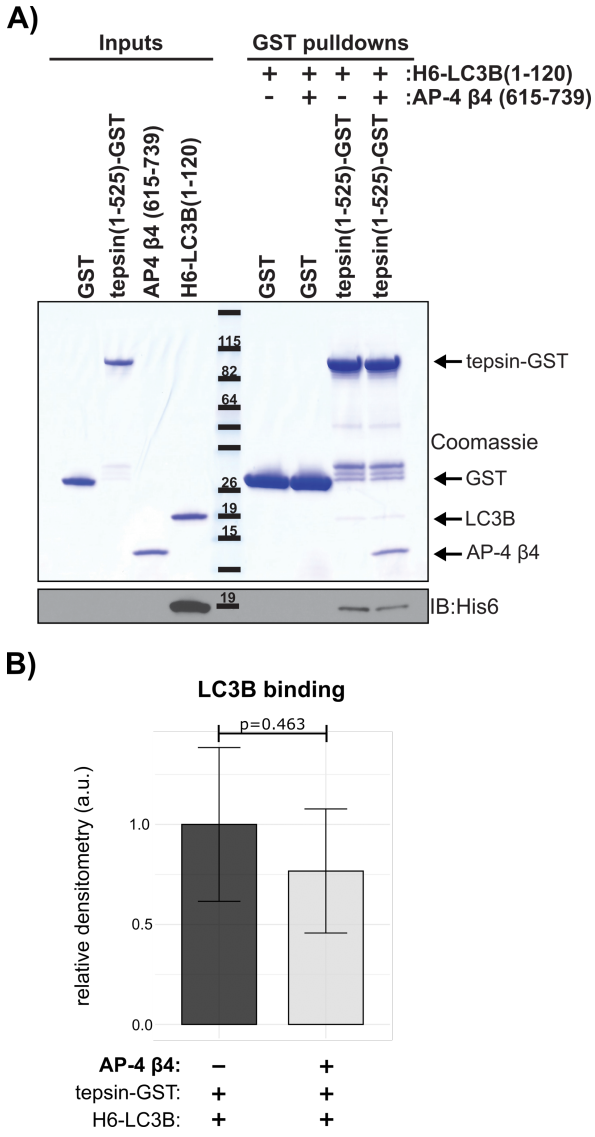

Figure A1-1: Tepsin binds LC3B independently of AP-4-binding *in vitro.* (A) Recombinant full-length tepsin(residues 1-525)-GST pulls down recombinant LC3B (residues 1-120)-His6x in the presence or absence of AP-4 β4 appendage domain. Binding between tepsin and LC3B was detectable on a Coomassie-stained SDS-PAGE gel and further confirmed by Western blot (α-His; Abcam ab184607). (B) Presence of AP-4 β4 appendage domain did not significantly change tepsin/LC3B binding *in vitro*. Bar plots (average ± standard deviation) depict quantification of LC3B binding to tepsin-GST in the presence or absence of AP-4 β4 appendage domain. Statistical analysis by Student's t-test of three independent experiments with p-value indicated (p=0.463).

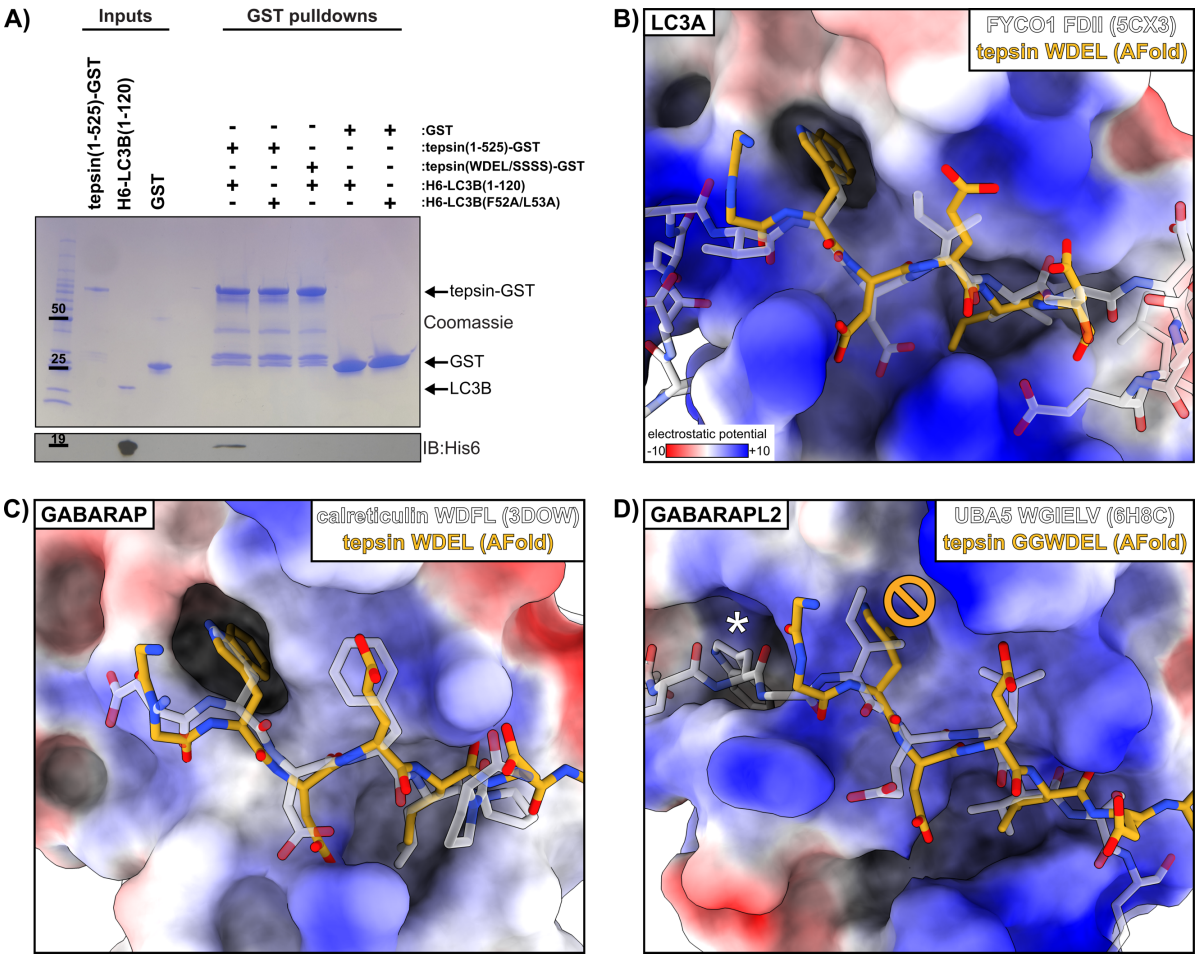

Figure A1-2: Biochemical experiments and computational modelling of the tepsin LIR motif explains binding selectivity among ATG8 family members. (A) Coomassie-stained SDS-PAGE gel and Western blot (α-His; Abcam ab184607) of GST pulldowns. Full-length wild-type tepsin (residues 1-525; WT) does not bind LDS mutant LC3B (F52A/L53A) and LIR mutant (WDEL/SSSS) tepsin does not bind wild-type or LDS mutant LC3B indicating the LIR motif substantially contributes to the tepsin/LC3B interaction *in vitro*. Free GST was used as a negative control. (B-D) AlphaFold Multimer models were generated for mATG8 proteins and superposed with experimental structures: (B) LC3A, (C) GABARAP, (D) GABARAPL2. The hydrophobic residues of the LIR motif dock into hydrophobic pockets of LC3A and GABARAP, although the surface of GABARAP has reduced electrostatic potential compared to LC3; the tepsin Trp residue clashes with the surface in the experimental GABARAPL2 model (indicated) which has an elongated motif to dock the Trp residue in an alternative pocket (*).

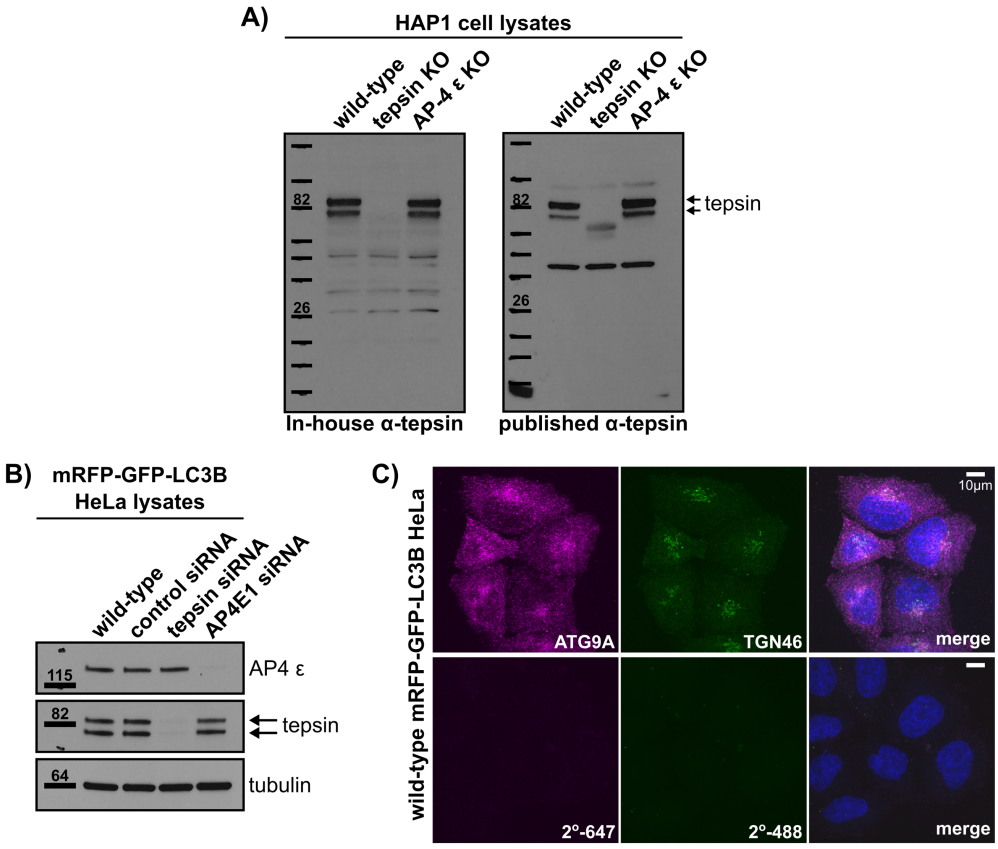

Figure A1-3: Antibody validation in HAP1 AP-4 ε or tepsin knockout cells and staining controls in mRFP-GFP-LC3B HeLa cells. (A) Manufactured tepsin antibody (reported here; described in methods) compared to a published tepsin antibody provided by the Robinson Lab in HAP1 knockout (KO) cells (Borner et al., 2012). Both antibodies predominantly recognize a doublet around 82 kDa which is absent in HAP1 tepsin KO cells. (B) Tepsin or AP-4 ε (gene: AP4E1) siRNA-treated mRFP-GFP-LC3B HeLa cells assayed by Western blot exhibit a corresponding loss of tepsin (α-tepsin; In-house see methods) or AP-4 ε (α-AP-4 epsilon; BD Transduction Labs 612019) respectively. Tubulin is presented as a loading control (α-alpha-tubulin; Proteintech 66031). (C) Exogenous GFP signal from mRFP-GFP-LC3B and TGN46 immunostaining are both visualized by a 520 nm emission peak (see methods). Representative maximum intensity projection confocal images taken from mRFP-GFP-LC3B HeLa cell line demonstrate immunostaining (see methods) effectively quenches exogenous GFP signal from mRFP-GFP-LC3B. Top row: immunostained for ATG9A (α-ATG9A Abcam ab108338; secondary α-Rabbit-647 Thermo Fisher Scientific A32733) and TGN46 (α-TGN46 Bio-Rad AHP500GT; secondary α-Sheep-488 Thermo Fisher Scientific A11015). Bottom row: incubated only with secondary fluorescent antibodies (α-Rabbit-647 Thermo Fisher Scientific A32733; α-Sheep-488 Thermo Fisher Scientific A11015). The GFP signal from exogenous mRFP-GFP-LC3 does not contribute to TGN46 signal, validating analysis of TGN46-positive staining as *trans*-Golgi compartments in these cells. Scale bar: 10 μm.

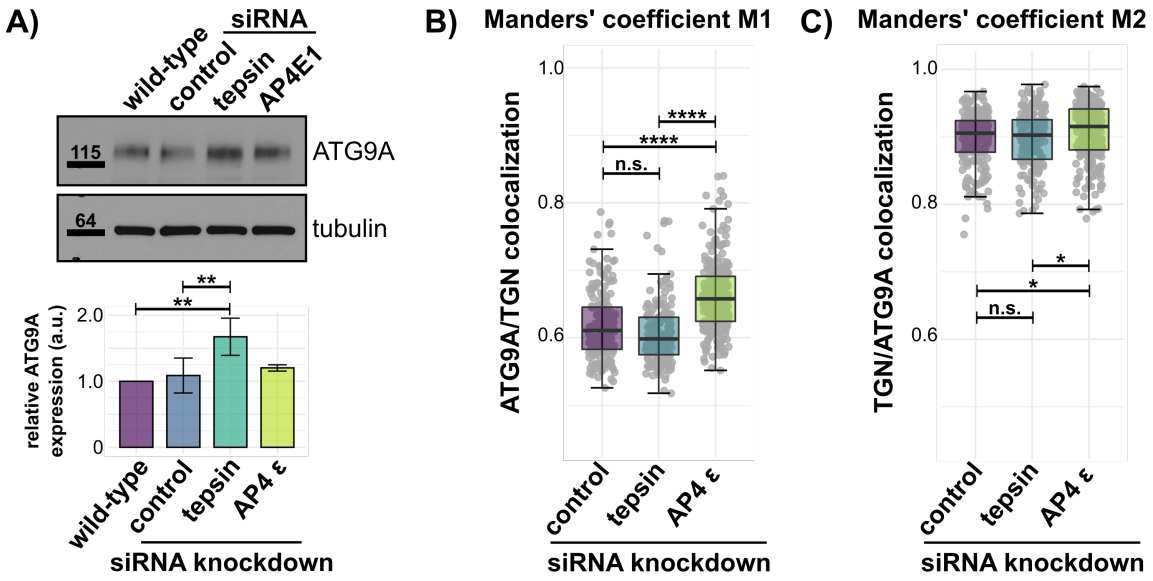

Figure A1-4: Tepsin depletion drives increased ATG9A expression in mRFP-GFP-LC3B HeLa cells. (A) Representative Western blot for ATG9A (α-ATG9A Abcam ab108338) expression in tepsin- or AP-4-depleted lysates. ATG9A expression is significantly increased following tepsin-depletion. Bar plots (average ± SD) depict quantification of the ATG9A expression level relative to wild-type ATG9A expression. One-way ANOVA with Tukey post-hoc test; n=3. Tubulin was used as a loading control (α-alpha-tubulin; Proteintech 66031). (B) Manders' coefficient M1 indicating the fraction of ATG9A signal coincident with *trans*-Golgi marker, TGN46. (C) Manders' coefficient M2 indicating the fraction of TGN46 signal coincident with ATG9A. These M1 and M2 results indicate the majority of ATG9A signal is retained within the TGN of AP-4 ε-depleted cells. The absolute ratio of ATG9A signal within the TGN is not significantly affected in tepsin-depleted cells. Quantification of four independent experiments each with at least 175 total cells per condition. Statistical results from Kruskal-Wallis test, Dunn test with Bonferroni correction; *p≤0.05, **p≤0.01, ***p≤0.001, ****p≤0.0001.

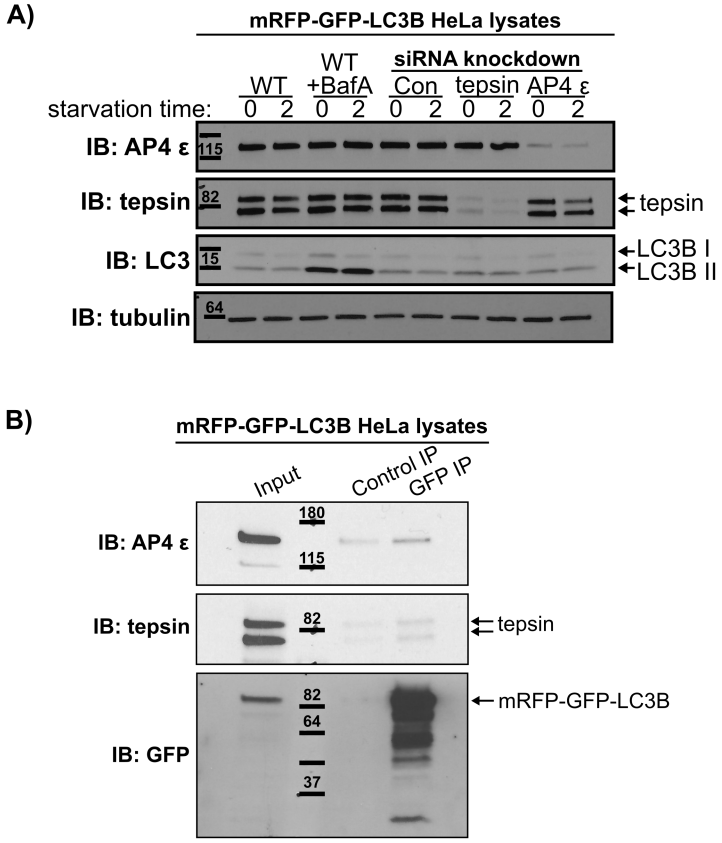

Figure A1-5: Tepsin and AP-4 interact with LC3B in mRFP-GFP-LC3B HeLa cells. (A) Representative Western blots from mRFP-GFP-LC3B HeLa cells treated with tepsin- or AP-4-targeting siRNA indicated effective tepsin or AP-4 knockdown. Western blots show LC3B accumulation following Bafilomycin treatment in wild-type cells confirming starvation conditions induced autophagy. Bafilomycin A treatment at 100 nM in indicated samples. (B) Western blots from co-immunoprecipitation experiments in mRFP-GFP-LC3B HeLa cell lysates. Endogenous tepsin co-immunoprecipitates on GFP-resin but not when using unconjugated resin (control). AP-4 ε also co-immunoprecipitates with mRFP-GFP-LC3B. Representative of 3 replicates. Antibodies: α-AP-4 epsilon, BD Transduction Labs 612019; α-tepsin, In-house (see methods); α-LC3B, Abcam ab48394; α-GFP, Abcam ab6663; α-alpha-tubulin, Proteintech 66031.

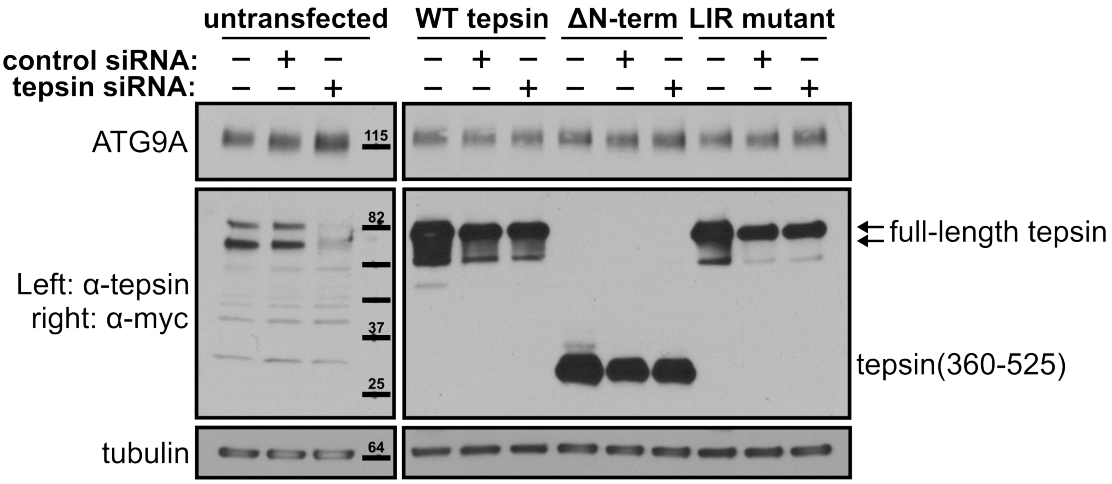

Figure A1-6: Expression of tepsin LIR mutant and ΔN-terminus tepsin constructs in tepsin depleted cells. (A) Representative Western blots from mRFP-GFP-LC3B HeLa cells treated with control or tepsin siRNA followed by transfection of myc-tagged tepsin constructs: wild-type tepsin, tepsin Δ N-terminus (residues 360-525; ΔN-term), or tepsin LIR mutant (WDEL/SSSS) as indicated. Western blots indicate siRNA-resistant transfection of each tepsin construct. Antibodies: α-ATG9A, Abcam ab108338; α-tepsin, In-house (see methods); α-myc-tag, Cell Signaling Technology 2276; α-alpha-tubulin, Proteintech 66031.

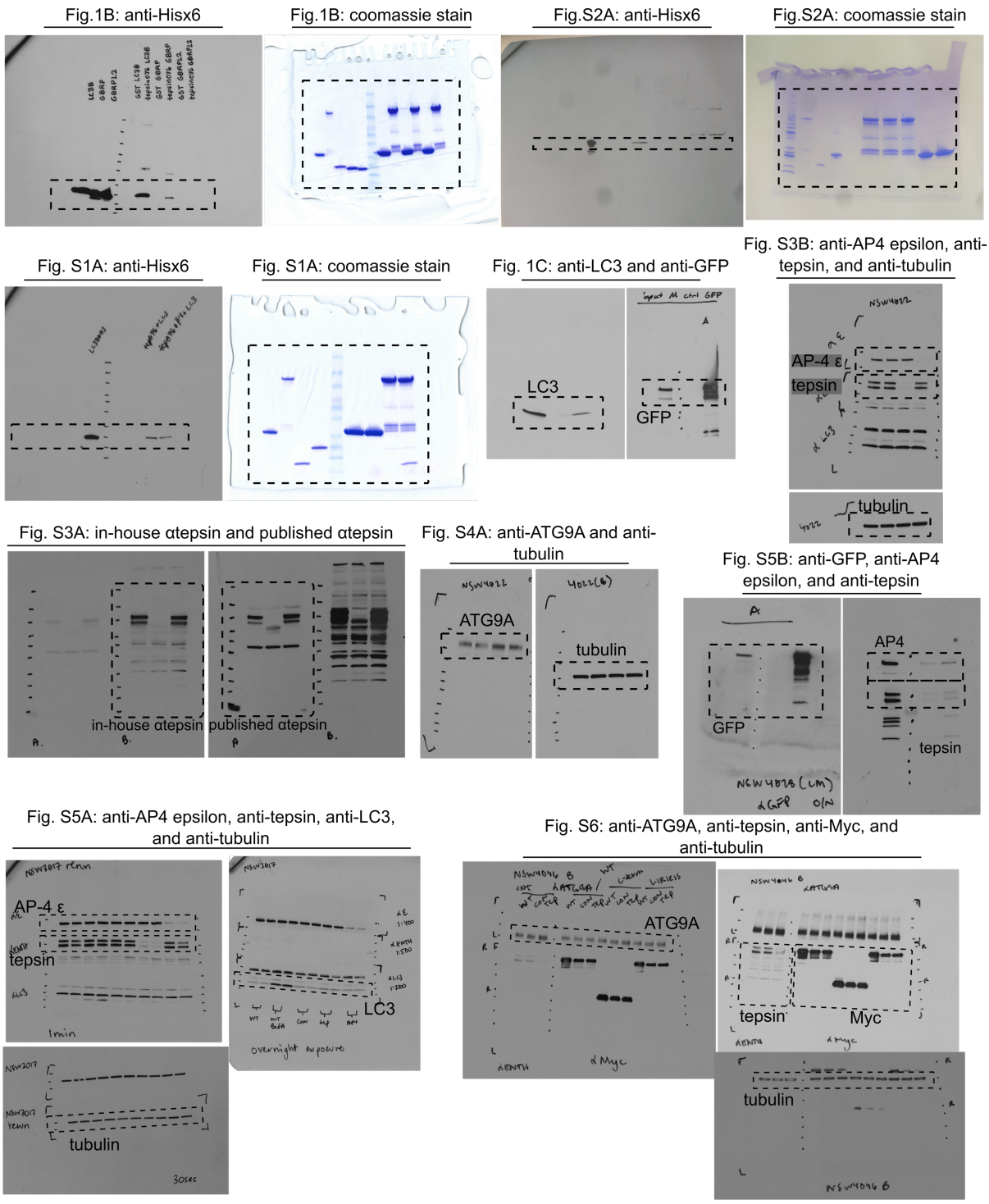

Figure A1-7: Uncropped Western blot films and Coomassie-stained SDS-PAGE gels. Dashed boxes denote regions cropped for the indicated figure.

LC3B	Tepsin LIR peptide	K_D	n
residues 1-120 WT	SGGGWDELS	44.3 μM	0.523
residues 1-120 F52A/L53A	SGGGWDELS	n.b.	n.b.

Table A1-1: Chapter II ITC data summary. This table summarizes representative ITC experiments from Figure 2-2, including protein constructs, relevant mutations, and peptide sequences; calculated K_D values; and stoichiometry (n) values. “WT” denotes wild-type sequence.

Protein	Sequence (5'-3')	Restriction site	Primer use
tepsin(aa1-525)	GGAGCACATATGGCTGCCGCGCC GCCG	*Nde*I	5' human tepsin, starts aa1
tepsin(aa1-525)	TGCCTCGTCGACTCAGGCGTTCAG GAACGCGAA	*Sal*I	3' human tepsin, ends aa525
tepsin LIR mutant (WDEL/SSSS)	GCCGGAGGGGGCTCTAGCTCAAG TGACAGCGGCCCCAGCTC	N/A	5' mutagenesis primer, WDEL/SSSS
tepsin LIR mutant (WDEL/SSSS)	GAGCTGGGGCCGCTGTCACTTGA GCTAGAGCCCCCTCCGGC	N/A	3' mutagenesis primer, WDEL/SSSS
tepsin siRNA resistant	GCAGGCGATGGAGGCCCGAGCGA ATCCCAGGGGGCACG	N/A	5' mutagenesis primer for silent mutation at siRNA binding site
tepsin siRNA resistant	CGTGCCCCCTGGGATTCGCTCGG GCCTCCATCGCCTGC	N/A	3' mutagenesis primer for silent mutation at siRNA binding site
tepsin(aa1-525)-Myc	GGAGCAGGATCCATGGCTGCCGC GCCGCCG	*BamH*I	5' human tepsin, starts aa1
tepsin(aa1-525)-Myc	TGCTCCCTCGAGTCACAGATCCTC TTCTGAGATGAGTTTTTGTTCGGC GTTCAGGAACGC	*Xho*I	3' human tepsin, adds C-terminal Myc tag after aa525
tepsin ΔN-term (aa360-525)-Myc	GGAGCAGGATCCATGGGCACCTC AG	*BamH*I	5' human tepsin, starts at aa360
tepsin ΔN-term (aa360-525)-Myc	TGCTCCCTCGAGTCACAGATCCTC TTC	*Xho*I	3' human tepsin-myc, aa525 and Myc tag
LC3B(aa1-120)	CAGGAGACGTTCGGGTAAGTCGA CTCGAGC	N/A	5' mutagenesis primer to remove aa121-125
LC3B(aa1-120)	GCTCGAGTCGACTTACCCGAACGT CTCCTG	N/A	3' mutagenesis primer to remove aa121-125
LC3B LDS mutant (F52A, L53A)	CAGCTTCCTGTTCTGGATAAAACA AAGGCCGCTGTACCTGACCATGTC AACAT	N/A	5' mutagenesis primer, F52A, L53A
LC3B LDS mutant (F52A, L53A)	ATGTTGACATGGTCAGGTACAGCG GCCTTTGTTTTATCCAGAACAGGA AGCTG	N/A	3' mutagenesis primer, F52A, L53A

Table A1-2: Oligonucleotides used in Chapter II study.

APPENDIX II

SUPPLEMENTAL MATERIALS FROM CHAPTER III

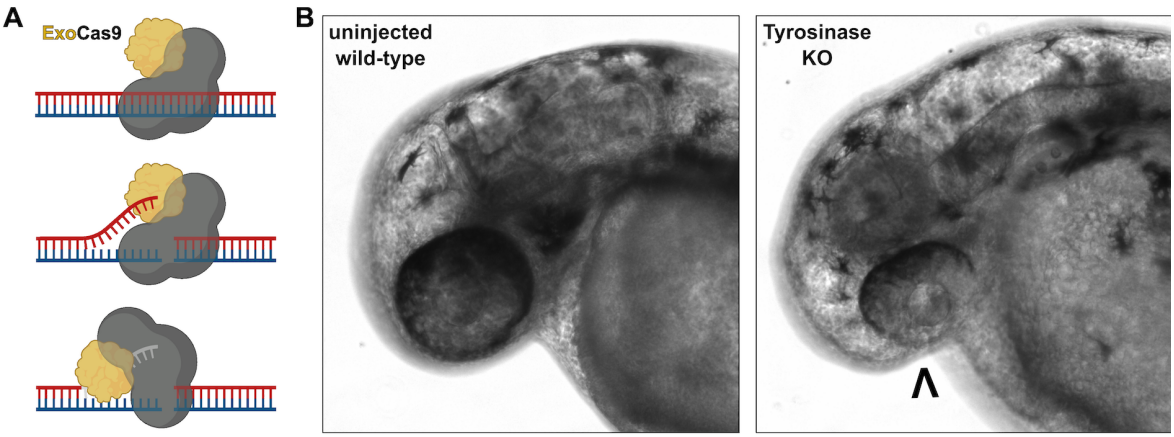

Figure A2-1: CRISPR-ExoCas9 gene editing generates effective tyrosinase knockout embryos. (A) Schematic illustration of the mechanism of CRISPR ExoCas9 (Clements et al., 2017). The Cas9 protein (grey) introduces a double strand break in target DNA (blue and red). The fused 3'-5' ssDNA exonuclease (yellow) then chews back DNA from the break site, leading to longer deletions and increased knockout efficiency. (B) ExoCas9 efficiency was verified by targeting tyrosinase required for melanin production. CRISPR-mediated Tyrosinase knockout (KO) embryos (right; n=46 embryos) have visible eye pigmentation loss (marked by arrowhead) compared to wild-type embryos (left). This establishes the ExoCas9 system is suitable for generating AP-4 and *enthd2* gene knockout models.

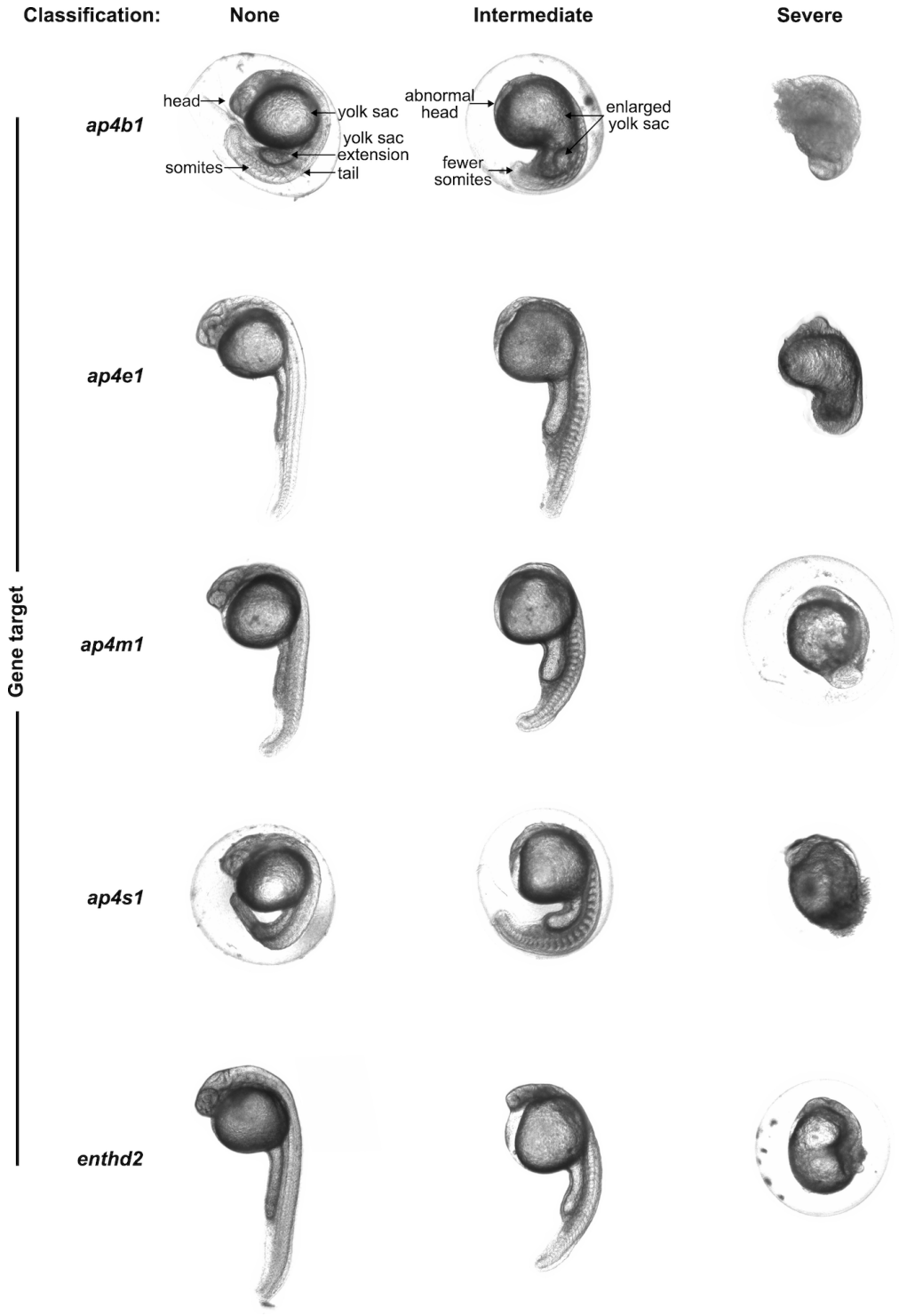

Figure A2-2: Representative phenotypic classes for AP-4 subunit and *enthd2* gene knockout embryos. Representative images of three assigned phenotypic scoring classes (none, intermediate, and severe) for each gene knockout. Rows depict knockout gene targets and columns depict phenotypic classification. Embryos scored into the 'none' category were injected but displayed no phenotypic variation from wild-type embryos. The intermediate category is comprised of the characterized phenotype with abnormal head development and neural necrosis. Embryos in the severe category display no discernible head or tail morphology.

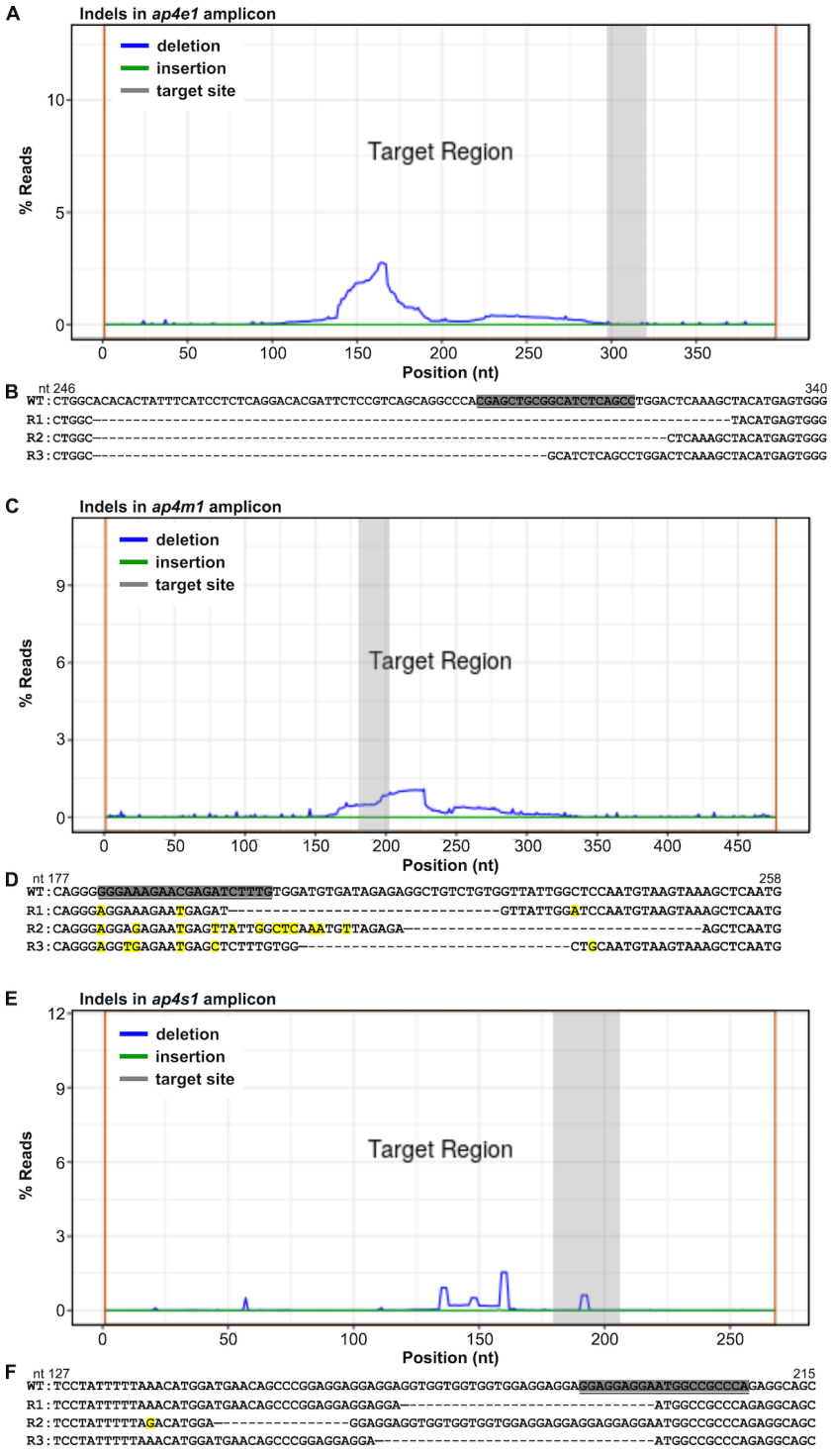

Figure A2-3: Sequencing validates *ap4e1*, *ap4m1*, and *ap4s1* single gene knockout zebrafish embryos. *Ap4e1*, *ap4m1*, and *ap4s1* KO embryos were analyzed by Amplicon EZ deep sequencing (Azenta). Percentage of reads containing insertions (green) or deletions (blue) in the sgRNA target site (gray) are displayed for representative *ap4e1* (A), *ap4m1* (C), and *ap4s1* (E) KO embryos. Sequencing data were obtained from a single representative 24 hpf embryo in the intermediate phenotype category. Three representative reads from sequencing of the *ap4e1* (B), *ap4m1* (D), and *ap4s1* (F) KO embryos are shown together with the WT sequence (underlined target site highlighted in gray with nucleotide numbers marked). Both point mutations (yellow) and deletions (dashes) are observed.

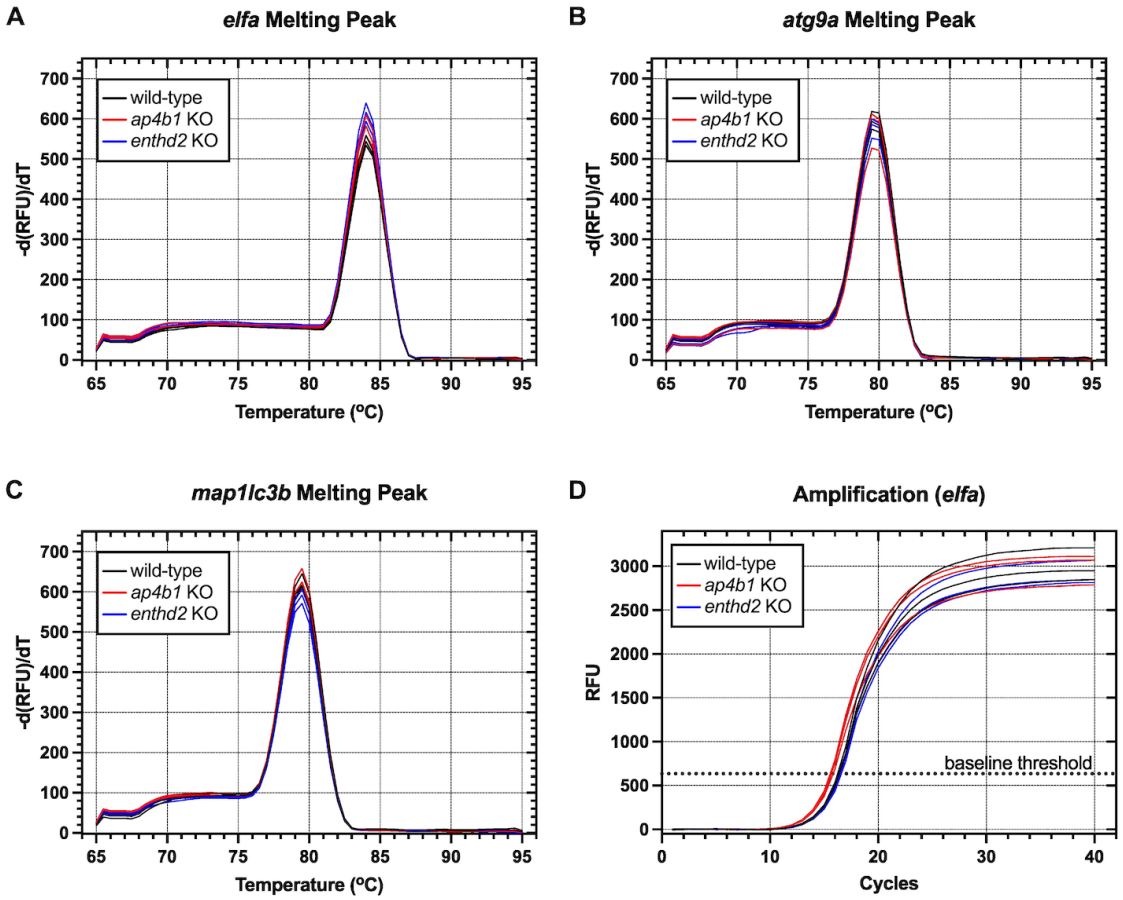

Figure A2-4: RT-qPCR gene target primer validation and normalization. (A-C) Representative melting point peaks of RT-qPCR reaction products. Primers for *elfa* (A), *atg9a* (B), and *map1lc3b* (C) each yield a single sharp melt peak indicating a single gene product is being amplified from both wild-type and KO embryos. (D) Amplification of *elfa* (control gene) is not affected by *ap4b1* or *enthd2* single gene knockout, as indicated by this representative amplification plot. The baseline threshold (dotted line) was calculated using Maestro software (Bio-Rad).

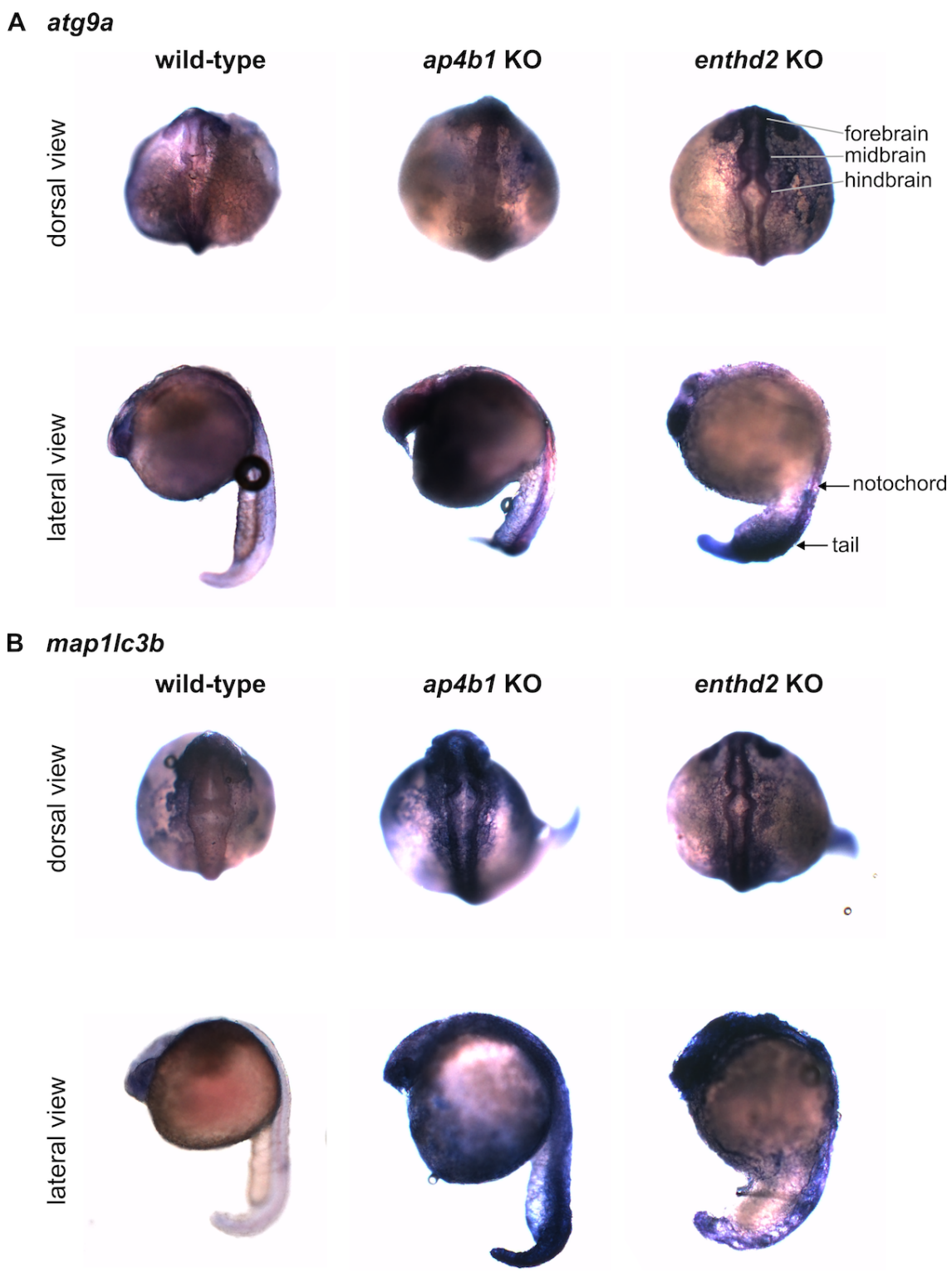

Figure A2-5: *In situ* hybridization profiles of *atg9a* and *map1lc3b* in single gene knockout zebrafish. (A) *atg9a* expression in WT, *ap4b1* KO, and *enthd2* KO embryos shown in dorsal and lateral views. (B) *map1lc3b* expression in WT, *ap4b1* KO, and *enthd2* KO embryos. *Atg9a* (A) and *map1lc3b* (B) primarily express in the brain of WT (column 1) embryos. *Ap4b1* (column 2) and *enthd2* (column 3) single gene knockout embryos exhibit expression of *atg9a* and *map1lc3b* in the brain (forebrain, midbrain, hindbrain), the notochord, and the tail.

APPENDIX III

SUPPLEMENTAL MATERIALS FROM CHAPTER IV

A)

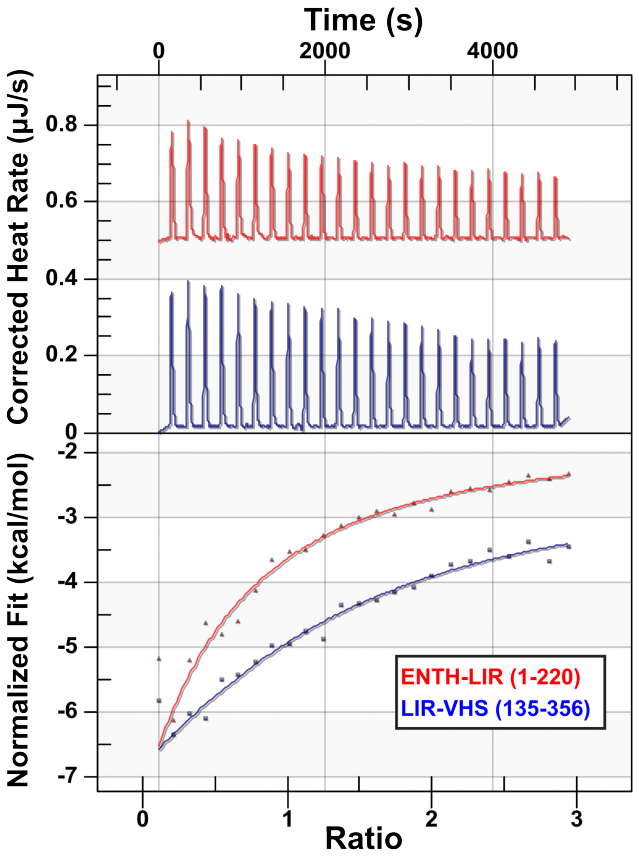

B)

Summary of ITC results			
tepsin	**LC3B**	**K_D ± sd µM**	**n**
ENTH-LIR	LC3B(1-120)	148.7	1
LIR-VHS	LC3B(1-120)	262.9 ± 104.8	>1

Figure A3-1: Preliminary ITC indicates VHS and LIR binding to LC3B is not cooperative. (A) Representative isothermal titration calorimetry experiments. Purified recombinant tepsin and LC3B proteins were used in ITC experiments to quantify binding affinities. ENTH-LIR (residues 1-220) or LIR-VHS (residues 135-356) bind LC3B (residues 1-120) with weak micromolar affinity (K_D ~ 100-300 µM). (B) Summary of ITC results. ENTH-LIR data is from one replicate. LIR-VHS data is from three independent replicates.

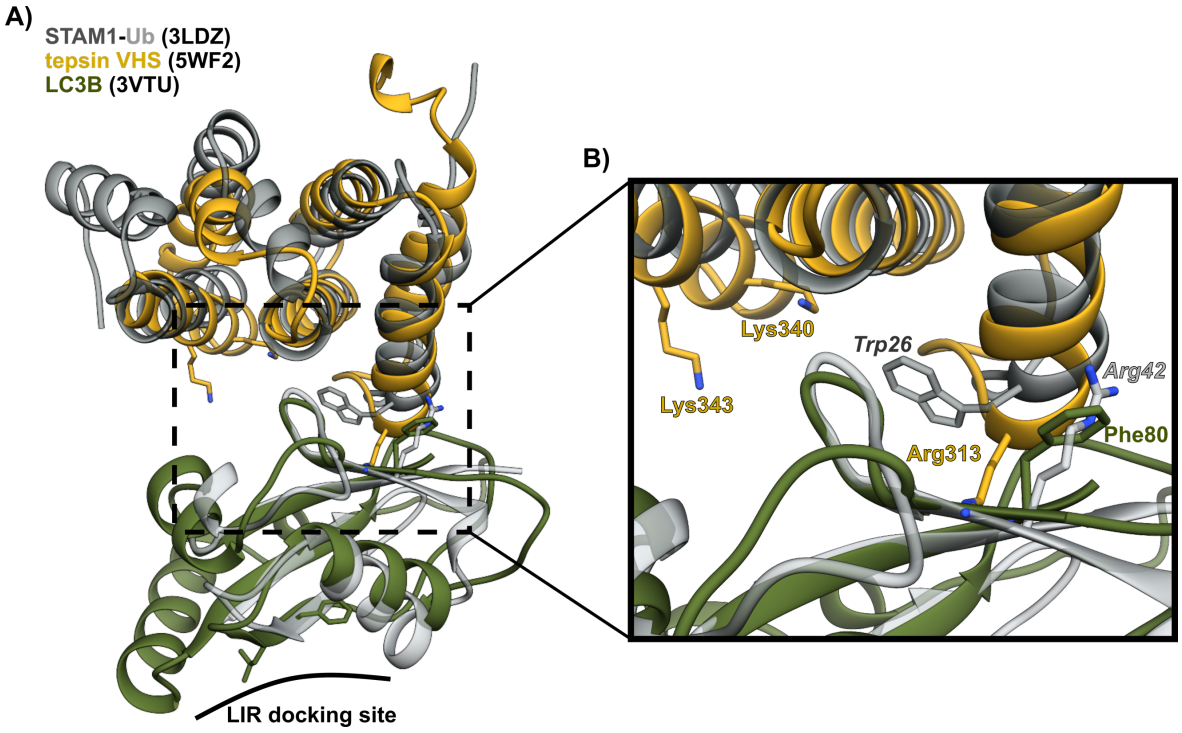

Figure A3-2: Tepsin VHS domain and LC3B clash at the VHS-ubiquitin binding interface. (A) Tepsin VHS domain (PDB: 5WF2) and LC3B (PDB: 3VTU) superposed with the STAM1-Ubiquitin (Ub) x-ray crystal structure (PDB: 3LDZ). The LIR docking site is marked on the opposite face of LC3B from the VHS-ubiquitin interaction. (B) Tepsin VHS domain lacks conserved hydrophobic residues and instead exhibits an obvious clash with Arg313 into the surface of ubiquitin . LC3B also lacks conserved residues for this interaction exhibited here with the residue Phe80 where ubiquitin interacts with STAM1 via Arg42. There are no corresponding acidic residues on this LC3B surface patch to accommodate an interaction with Arg313 of tepsin.

APPENDIX IV

SUPPLEMENTAL MATERIAL FROM CHAPTER V

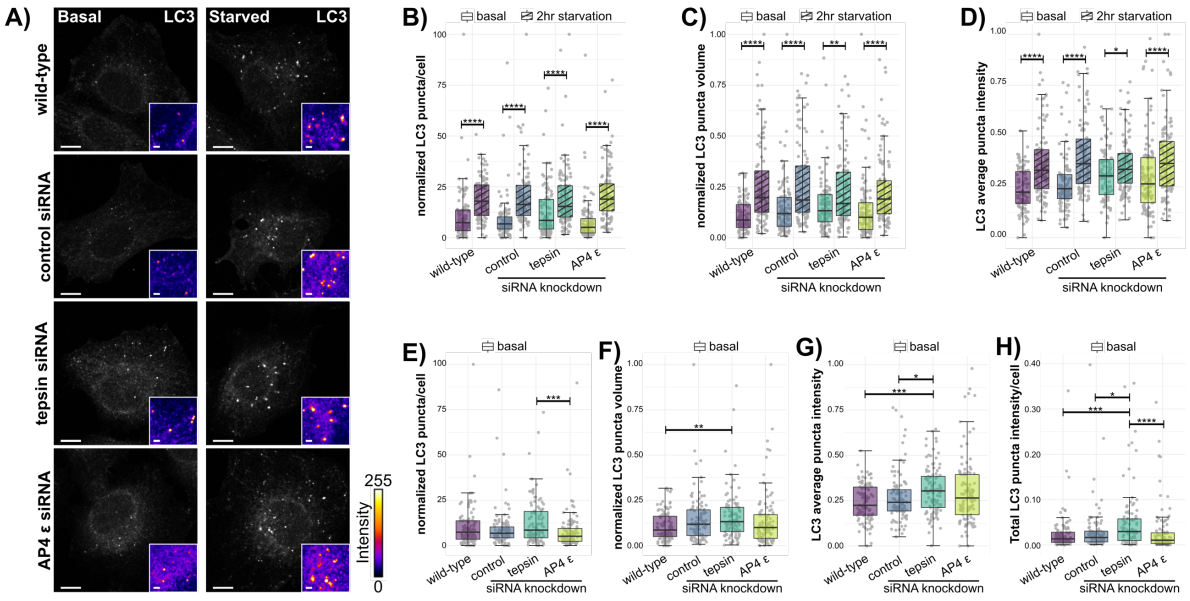

Figure A4-1: Tepsin depletion dysregulates autophagy structure morphology in HeLa cells. HeLa cells were cultured in complete media (basal) or starved in EBSS for 2 hours then immunostained for autophagy marker, LC3 (Molecular Biology Laboratory). (A) Representative single-plane confocal images of wild-type and control (non-targeting) siRNA-, tepsin siRNA-, or AP-4 ε siRNA-treated HeLa cells. Inset is depicted using the Fire look-up table (FIJI) with intensity scale as shown. Scale bar: 10 μm, inset scale bar: 2 μm. (B-D) Comparison of LC3 objects following starvation: LC3-positive objects were quantified by (B) number of puncta per cell or (C) average apparent object volume, (D) average puncta signal intensity. (B) Number of LC3-positive puncta increases in all conditions following starvation. (C and D) Tepsin-depleted cells accumulate larger and brighter LC3-positive puncta in basal conditions, without smaller change following starvation. Statistical results in B-D are from Mann-Whitney U test. (E-H) Comparing LC3-positive objects in basal conditions following tepsin or AP-4 depletion: (E-G) tepsin-depleted cells tend to have more, larger, and brighter LC3 puncta, though spread of the distributions minimizes statistical significance. (H) Total signal intensity from all LC3-positive puncta is elevated in tepsin-depleted cells compared to WT, control, and AP-4 depleted cells. Statistical results from Kruskal-Wallis test, Dunn test with Bonferroni correction. Quantification (B-H): data from three independent biological replicates each with 35 cells per condition was subject to min/max normalization; each data point on the box-and-whisker plots corresponds to one cell; *p≤0.05, **p≤0.01, ***p≤0.001, ****p≤0.0001.